

Lecture Notes in Physics

Pedro L. Garrido Joaquín Marro (Eds.)

Fourth Granada Lectures in
**Computational
Physics**

Proceedings,
Granada,
Spain 1996



Springer

Lecture Notes in Physics

Editorial Board

H. Araki, Kyoto, Japan
E. Brézin, Paris, France
J. Ehlers, Potsdam, Germany
U. Frisch, Nice, France
K. Hepp, Zürich, Switzerland
R. L. Jaffe, Cambridge, MA, USA
R. Kippenhahn, Göttingen, Germany
H. A. Weidenmüller, Heidelberg, Germany
J. Wess, München, Germany
J. Zittartz, Köln, Germany

Managing Editor

W. Beiglböck
Assisted by Mrs. Sabine Lehr
c/o Springer-Verlag, Physics Editorial Department II
Tiergartenstrasse 17, D-69121 Heidelberg, Germany

The Editorial Policy for Proceedings

The series Lecture Notes in Physics reports new developments in physical research and teaching – quickly, informally, and at a high level. The proceedings to be considered for publication in this series should be limited to only a few areas of research, and these should be closely related to each other. The contributions should be of a high standard and should avoid lengthy redraftings of papers already published or about to be published elsewhere. As a whole, the proceedings should aim for a balanced presentation of the theme of the conference including a description of the techniques used and enough motivation for a broad readership. It should not be assumed that the published proceedings must reflect the conference in its entirety. (A listing of abstracts of papers presented at the meeting but not included in the proceedings could be added as an appendix.) When applying for publication in the series Lecture Notes in Physics the volume's editor(s) should submit sufficient material to enable the series editors and their referees to make a fairly accurate evaluation (e.g. a complete list of speakers and titles of papers to be presented and abstracts). If, based on this information, the proceedings are (tentatively) accepted, the volume's editor(s), whose name(s) will appear on the title pages, should select the papers suitable for publication and have them refereed (as for a journal) when appropriate. As a rule discussions will not be accepted. The series editors and Springer-Verlag will normally not interfere with the detailed editing except in fairly obvious cases or on technical matters.

Final acceptance is expressed by the series editor in charge, in consultation with Springer-Verlag only after receiving the complete manuscript. It might help to send a copy of the authors' manuscripts in advance to the editor in charge to discuss possible revisions with him. As a general rule, the series editor will confirm his tentative acceptance if the final manuscript corresponds to the original concept discussed, if the quality of the contribution meets the requirements of the series, and if the final size of the manuscript does not greatly exceed the number of pages originally agreed upon. The manuscript should be forwarded to Springer-Verlag shortly after the meeting. In cases of extreme delay (more than six months after the conference) the series editors will check once more the timeliness of the papers. Therefore, the volume's editor(s) should establish strict deadlines, or collect the articles during the conference and have them revised on the spot. If a delay is unavoidable, one should encourage the authors to update their contributions if appropriate. The editors of proceedings are strongly advised to inform contributors about these points at an early stage.

The final manuscript should contain a table of contents and an informative introduction accessible also to readers not particularly familiar with the topic of the conference. The contributions should be in English. The volume's editor(s) should check the contributions for the correct use of language. At Springer-Verlag only the prefaces will be checked by a copy-editor for language and style. Grave linguistic or technical shortcomings may lead to the rejection of contributions by the series editors. A conference report should not exceed a total of 500 pages. Keeping the size within this bound should be achieved by a stricter selection of articles and not by imposing an upper limit to the length of the individual papers. Editors receive jointly 30 complimentary copies of their book. They are entitled to purchase further copies of their book at a reduced rate. As a rule no reprints of individual contributions can be supplied. No royalty is paid on Lecture Notes in Physics volumes. Commitment to publish is made by letter of interest rather than by signing a formal contract. Springer-Verlag secures the copyright for each volume.

The Production Process

The books are hardbound, and the publisher will select quality paper appropriate to the needs of the author(s). Publication time is about ten weeks. More than twenty years of experience guarantee authors the best possible service. To reach the goal of rapid publication at a low price the technique of photographic reproduction from a camera-ready manuscript was chosen. This process shifts the main responsibility for the technical quality considerably from the publisher to the authors. We therefore urge all authors and editors of proceedings to observe very carefully the essentials for the preparation of camera-ready manuscripts, which we will supply on request. This applies especially to the quality of figures and halftones submitted for publication. In addition, it might be useful to look at some of the volumes already published. As a special service, we offer free of charge L^AT_EX and T_EX macro packages to format the text according to Springer-Verlag's quality requirements. We strongly recommend that you make use of this offer, since the result will be a book of considerably improved technical quality. To avoid mistakes and time-consuming correspondence during the production period the conference editors should request special instructions from the publisher well before the beginning of the conference. Manuscripts not meeting the technical standard of the series will have to be returned for improvement.

For further information please contact Springer-Verlag, Physics Editorial Department II, Tiergartenstrasse 17, D-69121 Heidelberg, Germany

Pedro L. Garrido Joaquín Marro (Eds.)

Fourth Granada Lectures in Computational Physics

Proceedings of the 4th Granada Seminar
on Computational Physics

Held at Granada, Spain, 9–14 September 1996



Springer

Editors

Pedro L. Garrido

Joaquín Marro

Instituto Carlos I de Física Teórica y Computacional

Facultad de Ciencias, Universidad de Granada

Campus Fuentenueva

E-18071 Granada, Spain

Cataloging-in-Publication Data applied for.

Die Deutsche Bibliothek - CIP-Einheitsaufnahme

Fourth Granada lectures in computational physics : proceedings of the 4th Granada Seminar on Computational Physics, held at Granada, Spain, 9 - 14 September 1996 / Pedro L. Garrido ; Joaquín Marro (ed.).

(**Lecture notes in physics ; Vol. 493**)

ISBN 978-3-662-14150-2

ISSN 0075-8450

ISBN 978-3-662-14150-2

ISBN 978-3-662-14148-9 (eBook)

DOI 10.1007/978-3-662-14148-9

This work is subject to copyright. All rights are reserved, whether the whole or part of the material is concerned, specifically the rights of translation, reprinting, re-use of illustrations, recitation, broadcasting, reproduction on microfilms or in any other way, and storage in data banks. Duplication of this publication or parts thereof is permitted only under the provisions of the German Copyright Law of September 9, 1965, in its current version, and permission for use must always be obtained from Springer-Verlag Berlin Heidelberg GmbH

Violations are liable for prosecution under the German Copyright Law.

© Springer-Verlag Berlin Heidelberg 1997

Originally published by Springer-Verlag Berlin Heidelberg New York in 1997

Softcover reprint of the hardcover 1st edition 1997

The use of general descriptive names, registered names, trademarks, etc. in this publication does not imply, even in the absence of a specific statement, that such names are exempt from the relevant protective laws and regulations and therefore free for general use.

Typesetting: Camera-ready by the authors/editors

Cover design: *design & production* GmbH, Heidelberg

SPIN: 10550829 55/3144-543210 - Printed on acid-free paper

GRANADA SEMINAR on COMPUTATIONAL PHYSICS

STEERING COMMITTEE

J. F. Fernández

Instituto de Ciencia de Materiales, C.S.I.C.,
University of Zaragoza, Spain

P. L. Garrido, *Scientific Coordinator*

Instituto Carlos I, and Departamento de Física
Moderna, University of Granada, Spain

H. J. Herrmann

Ecole Supérieure de Physique et Chimie
Industrielle, P.M.M.H, E.S.P.C.I., Paris, France

R. de la Llave

Department of Mathematics, University
of Texas, Austin, Texas, U.S.A.

J. Marro, *Director of Seminar*

Instituto Carlos I, and Departamento de Física
Aplicada, University of Granada, Spain

Preface

The methods developed to deal with the computational aspects of physical problems are useful in an increasing number of situations, from chemistry, biology and geology to engineering, communications and economics. In fact, *computational physics* has evolved into a trans-disciplinary field now concerned with the creative use of computers in scientific research. Moreover, computational methods often help students to develop a deeper understanding of key concepts, and enhance their problem-solving abilities. Therefore, computational physics is recognized as having an important educational value, and educators face the task of outlining appropriate curricula to take advantage of these unique features.

This is an important motivation for the publication of the contents of the Seminar on Computational Physics which is held in Granada every two years. The seminar aims at bringing together small groups of students and active researchers on different aspects of computational physics. It is part of the doctoral programme of the University of Granada. The proceedings of the previous editions were published as *II Granada Lectures in Computational Physics* (World Scientific, Singapore 1993) and *Third Granada Lectures in Computational Physics (Lecture Notes in Physics*, vol. 448, Springer, Berlin 1995) by the same editors. The present book contains the invited lecture notes and a very brief account of contributions by participants at the *4th Granada Seminar on Computational Physics* (Granada, Spain, 9–14 September 1996).

This *Lectures in Computational Physics* series aims to provide a smooth transition from “one-semester course” books to the current literature in specialized journals, which we believe is an important gap to be filled. Therefore, an effort has been made to write the notes pedagogically for the lowest graduate student level, and to give a comprehensive description of each topic. Moreover, some exercises are proposed and some practical computer sessions are illustrated. In this way, the book may introduce the beginner to the world of computational science. In addition, it may serve as a work of reference for teachers, students and researchers looking for a state-of-the-art brief description of specific areas of computational physics. In fact, the series is concerned not only with methods and techniques but also with problems at the frontier that are specially amenable to be investigated by computational means.

We wish to express our gratitude here to all those who have collaborated in making the 1996 edition of the seminar a success. We would first like to mention the invited lecturers who established such a good rapport with the participants and whose personal effort enabled us to accomplish the goals of the seminar, and the other members of the Steering Committee who have effectively helped us to design the format and contents. The smoothness of the organization was ensured by the collaboration of the students C. López, F. de los Santos, J. J. Torres, and J. A. Vacas. Financial support given by the *Dirección General de Enseñanza Superior* of the Spanish Ministry of Education and Culture, as well as the sponsorship of the *Consejería de Educación y Ciencia* of the Andalusian administration *Junta de Andalucía*, of the *Vicerrectorado de Investigación y Relaciones Internacionales*, and of the *Facultad de Ciencias* of the University of Granada is acknowledged.

Granada, April 1997

The Editors

Contents

Part I Invited Lectures

A Variational Approach to Exciton–Phonon Coupling

K. Lindenberg, Y. Zhao, and D.W. Brown	3
1 Introduction	3
2 Exact Benchmarks	6
2.1 $J=0$	7
2.2 $g=0^+$	8
3 Variational Methods	10
3.1 Trial States	12
3.2 Variational Equations	16
3.3 How Results Are Exhibited	18
4 Numerical Aspects	19
5 Typical Results	21
5.1 Exciton and Phonon Amplitudes	22
5.2 More on Phase Diagram and Self-trapping Transition	36
5.3 Energy Bands and Effective Mass	38
6 Solitons	41
7 Conclusion	47

The Power of Cooperation

B.A. Huberman	55
1 Introduction	55
2 Cooperative Search	57
3 Hierarchical Search and Phase Transitions	62
4 Satisficing Searches	65
5 Experiments on Constraint Satisfaction Problems	68
6 Results	69
6.1 Problem Solving by Committee	69
6.2 Problem Solving by Hierarchical Organizations	75
7 Discussion	77

Microscopic Computer Simulation of Fluids	
P. Cordero and D. Risso	83
1 Introduction	83
2 Simulator and Simulations	86
2.1 Background Generalities on Molecular Dynamics	86
2.2 Characteristics of the Simulations	87
2.3 The Simulator	88
2.4 Measurements	93
2.5 Hard Particle Systems	95
2.6 Problems	96
3 Primer on Kinetic Theory	97
3.1 The One-Particle Distribution Function	97
3.2 Mean Free Path and Collision Rate	99
3.3 On Fluxes and Flux Vectors	101
3.4 Boltzmann's Equation	103
3.5 Enskog's Equation	103
3.6 Problems	105
4 Standard and High-Order Balance Equations	106
4.1 Grad's Solution	106
4.2 Application: Thermal Slip	107
4.3 The BBGKY Hierarchy and General Balance Equations	110
4.4 Dilute Systems: Balance Equations and Higher Momenta	112
5 Dilute Gas with Strain Flow	114
5.1 The System and Simulational Conditions	116
5.2 Balance Equations and Boundary Conditions	116
5.3 Expansions	118
5.4 Closed Solution for Uniform Shear Rate	119
5.5 Observations Versus Theory	122
6 Thermal Conductivity	125
6.1 Heat Flux and the Effective Conductivity	126
6.2 Temperature Discontinuity at the Wall	127
6.3 Simulational Conditions	128
6.4 Simulations and Theoretical Predictions	129
6.5 Final Comments	132
Nonequilibrium Potential in Reaction-Diffusion Systems	
H.S. Wio	135
1 Introduction	135
2 Dynamical Systems: Stability	137
2.1 Linear Stability: Two Variable Systems	139
2.2 Bifurcations	142
2.3 Kinetic Potential, Symmetry Breaking	144
2.4 Lyapunov Functional, Global Stability	146
3 Stochastic Processes: A Brief Overview	149

3.1	Langevin Equations	152
3.2	Fokker–Planck Equations	154
3.3	Connection Between LE and FPE	155
3.4	Decay Times: Kramers Result	157
3.5	Notions of Stochastic Resonance	160
4	Spatially Extended Systems	163
4.1	Reaction–Diffusion Systems	164
4.2	Stability for Spatially Extended Systems	166
4.3	Examples of Reaction–Diffusion Systems	168
5	Nonequilibrium Potential	178
5.1	Some Examples of Nonequilibrium Potentials in RD Systems	179
5.2	Stochastic Analysis	184
5.3	Stochastic Resonance	187
6	Conclusions	191

An Introduction to the Mathematical Theory of Neural Networks

S. Albeverio and B. Tirozzi	197	
1	Neural Networks at Dynamical Systems	197
1.1	Introduction	197
1.2	Some Neurobiological Inspiration	197
1.3	Nets Without Back Reaction (Heteroassociative Nets)	198
1.4	Models with Back Reaction (Autoassociative Nets)	200
1.5	Recalling Some Notions of the Theory of Dynamical Systems	202
1.6	The Energy in the Hopfield Model	203
2	Statistical Mechanical Methods	209
2.1	The Case of the Hopfield Dynamics at Temperature Zero	209
2.2	Gibbs Measure for the Positive Temperature Hopfield Model	212
2.3	Stochastic Dynamics Associated with a Probability Measure	214
2.4	The Monte-Carlo Dynamics for the Positive Temperature Hopfield Model	215
2.5	Ergodicity of the Positive Temperature Dynamics	216
2.6	Equilibrium Statistical Mechanical Results for the Positive Temperature Hopfield Model	217

The Statistical Mechanics of Absorbing States

G. Grinstein and M.A. Muñoz	223	
1	Introduction	223
2	Absorbing States and Directed Percolation	223
2.1	Introduction	223
2.2	Directed Percolation and Related Problems	225
2.3	The Langevin Equation	229
2.4	Langevin Representation of Directed Percolation	234
2.5	The Langevin Equation and Universality	235

3	Critical Behavior of DP from Impressionistic RG Analysis	237
3.1	A Brief Technical Digression: RG on the (Very) Cheap	237
3.2	Seed Initial Conditions	245
4	Multiple Absorbing States	246
4.1	Motivation: Models of Catalysis	246
4.2	Langevin Analysis of the Prototypical PCP Model	248
4.3	Numerical Tests	251
4.4	Non-DP Behavior in Conserving Systems	254
5	Multiplicative Noise	255
5.1	An Example from Chemical Reactions	255
5.2	Analysis of the Multiplicative Noise Problem	257
5.3	The Single-Variable Multiplicative Noise Problem	261
5.4	Strong Coupling Exponents: Connection to KPZ	263
5.5	Numerical Verification	266

On the Self-organization of Migrating Individuals

E.	Albano	271
1	Introduction	271
2	Definition of the Model	271
3	Results and Discussion	272
3.1	Dynamics of Population Spreading	272
3.2	The Stationary State	273
4	Conclusions	275

Irreversible Transitions in Reaction Systems

E.	Albano	277
1	Introduction	277
2	The Contact Process with Long Range Correlations	278
3	The Invasion of the Reactive State to Poisoned Phases in the ZGB Model	280
4	Conclusions	282

Part II Contributions

Critical Behavior of an Evolution Model

S. Clar, R.A. Monetti, and F. Schwabl	287
---	-----

Simulation of Phase Behavior of Fluids in Gels

R. Salazar, R. Toral, and A. Chakrabarti	289
--	-----

Mesoscopic Descriptions of Fluids

M. Serrano, P. Espa��ol, and I. Z��niga	291
---	-----

Description of Growth Models with Density Equations	
C. López and P.L. Garrido	293
Langevin Approach to Synthetic Turbulence and Applications	
A.C. Martí, J.M. Sancho, and F. Sagués	294
Irreversible Adsorption of Colloidal Particles	
J. Faraudo and J. Bafaluy	295
Probability Distribution Function for the Random Sequential Adsorption of Aligned and Unaligned Hard-Squares	
F.L. Román, J.A. White, and S. Velasco	297
Resonance Phenomena Induced by Correlated Parametric Noise	
J.L. Cabrera, J. Gorroñogoitia, and F.J. de la Rubia	298
Magnetic Relaxation via Competing Dynamics	
J.A. Vacas and J. Marro	299
Atomic Dynamics in Liquid Alkali Metals. A Theoretical Study	
J. Casas, L.E. González, and D.J. González	300
Electronic Structure of Delta-Doped Quantum Well	
L.M. Gaggero-Sager and R. Pérez-Alvarez	302
Neural Networks with Fluctuating Synapses	
J.J. Torres, P.L. Garrido, and J. Marro	304
Local Field Distribution in Attractor Neural Networks: Effect of the Stimulus	
E. Korutcheva and K. Korutchev	305
A Field Theoretical Study of a Lattice Gas in Two Planes	
F. de los Santos and P.L. Garrido	306
A Regularization of the Nonstationary Two-Body Problem Under the Maneff Perturbing Potential	
I. Aparicio and L. Floría	307

Pattern Formation in Catalytic Processes: Phase-Field Model	
M.N. Kuperman, A.S. Mikhailov, and H.S. Wio	309
Subject Index	311

Part I

Invited Lectures

A Variational Approach to Exciton–Phonon Coupling

K. Lindenberg¹, Y. Zhao², and D.W. Brown³

¹ Department of Chemistry and Biochemistry, University of California, San Diego, La Jolla, California, 92093-0340, U.S.A.

² Rochester Theory Center for Optical Science and Engineering, University of Rochester, Rochester, New York 14627, U.S.A.

³ Institute for Nonlinear Science, University of California, San Diego, La Jolla, California 920093-0402, U.S.A.

1 Introduction

In this set of lectures we revisit from a contemporary perspective a classic problem of polaron theory using a hierarchy of increasingly sophisticated variational methods. Polaron structure is represented by variational surfaces giving the optimal values of the complete set of exciton and phonon amplitudes for every value of the joint exciton-phonon crystal momentum κ . Our variational methods include the approach originally taken by Merrifield, that originally followed by Toyozawa, and a generalization that includes mixed global and local exciton-phonon correlations. Exact results in limiting parameter regimes that serve as benchmarks for variational calculations are presented. We find that the variational solutions include characteristic small polaron, large polaron, and nearly-free phonon structures and we examine in detail the manner in which these compete and/or coexist. Through such examination, the parameter space of the problem is mapped, with particular attention given to problematic areas such as the highly quantum mechanical weak-coupling regime and the highly nonlinear intermediate-coupling regime, and to the self-trapping transition that may be said to mark the onset of the strong-coupling regime. Complete exciton and phonon amplitudes and associated energy bands are presented in illustrative cases, and the principal trends in the ground state energy, polaron band width, and effective mass are identified. The internal structure of our variational Bloch states is examined for qualities that might reflect typical characteristics of solitons. We find that quantitative characteristics typical of solitons do not survive this close scrutiny.

It is our concern to provide an overview of the most complete picture currently available of the lowest energy band for the classic polaron problem , that is, for an electronic excitation or an excess electron (which we will generically call an exciton) coupled to vibrations in a deformable medium such as a molecular crystal (Zhao 1994b, Zhao *et al.* 1996b, Zhao *et al.* 1997a, Brown

& Lindenberg 1997, Brown *et al.* 1997). For a number of reasons the polaron problem has intrigued scientists for decades. From a practical standpoint, excitons in molecular aggregates are important in a variety of physical and biophysical contexts. From a theoretical viewpoint, the challenge lies in understanding the behavior of a system consisting of relatively strongly and nonlinearly coupled exciton and phonon fields. This coupling can in general not be treated perturbatively. The challenge of diagonalizing such a Hamiltonian system, or at the least almost diagonalizing it, that is, of finding optimal polaron states, has attracted some of the keenest minds and has led to the formulation of interesting methodology of broad applicability.

We focus on the traditional Holstein Hamiltonian, given by (Holstein 1959a, Holstein 1959b):

$$\hat{H} = \hat{H}^{\text{ex}} + \hat{H}^{\text{ph}} + \hat{H}^{\text{ex-ph}}, \quad (1)$$

$$\hat{H}^{\text{ex}} = E \sum_n a_n^\dagger a_n - J \sum_n a_n^\dagger (a_{n+1} + a_{n-1}), \quad (2)$$

$$\hat{H}^{\text{ph}} = \omega \sum_n b_n^\dagger b_n, \quad (3)$$

$$\hat{H}^{\text{ex-ph}} = g\omega \sum_n a_n^\dagger a_n (b_n^\dagger + b_n). \quad (4)$$

Here a_n^\dagger creates an exciton of energy E at site n in a rigid lattice, and b_n^\dagger creates a quantum of vibrational energy of the Einstein oscillator of frequency ω located at site n . Since we consider only a single exciton (the Hamiltonian conserves the number of excitons), the commutation properties of the a operators are not important; the b 's are Bose operators, and the a operators commute with the b operators. J is the exciton transfer integral between nearest neighbor sites, g is the local coupling strength between an exciton and the Einstein oscillator at a given site; the exciton-phonon interaction is quadratic in the exciton operators and linear in the phonon operators, and can be thought of as a modulation of the exciton energy by the phonons. A great deal of work in polaron theory focuses on the exciton coupled to an acoustic (dispersive) phonon field rather than to optical phonons; the exciton at site n is in that case coupled to lattice displacements of the neighboring sites $n \pm 1$. Although all of the methods that we discuss here can be applied to other models, including those that involve dispersive phonons and also ones that include off-diagonal coupling in the exciton site index (Zhao *et al.* 1996a) (“nonlocal coupling”), in this chapter we focus on the Holstein Hamiltonian.

In momentum space the Holstein Hamiltonian contributions take the form (with $\hbar \equiv 1$)

$$\hat{H}^{\text{ex}} = \sum_k (E + J_k) a_k^\dagger a_k, \quad (5)$$

$$\hat{H}^{\text{ph}} = \omega \sum_q b_q^\dagger b_q, \quad (6)$$

$$\hat{H}^{ex-ph} = g\omega N^{-1/2} \sum_{kq} a_{k+q}^\dagger a_k (b_q + b_{-q}^\dagger), \quad (7)$$

where $E(k) = E + J_k$ is the energy of an exciton of wave vector k , with

$$J_k = -2J \cos k \quad (8)$$

(throughout we set the lattice constant equal to unity). Note that the exciton portion of the Hamiltonian, (5), has been diagonalized via Fourier transformation, and that the exciton energy ranges from $E - 2J$ to $E + 2J$, that is, the exciton bandwidth is $4J$. The “effective mass” associated with this exciton band is the inverse of the curvature of the band $E(k)$ around $k = 0$:

$$m_0 \equiv \left(\frac{\partial^2 E(k)}{\partial k^2} \right)^{-1} = \frac{1}{2J}. \quad (9)$$

Without loss of generality we set the phonon frequency $\omega \equiv 1$, that is, we measure energies in units of the energy of one optical phonon, and we also set $E \equiv 0$, which conveniently defines the zero of energy.

Above, and throughout this work, we use the Fourier conventions for ladder operators ($c^\dagger = a^\dagger, b^\dagger$) and scalars:

$$c_n^\dagger = N^{-1/2} \sum_p e^{-ipn} c_p^\dagger, \quad c_p^\dagger = N^{-1/2} \sum_n e^{ipn} c_n^\dagger, \quad (10)$$

$$\lambda_n = N^{-1} \sum_q e^{iqn} \lambda_q, \quad \lambda_q = \sum_n e^{-iqn} \lambda_n. \quad (11)$$

To clarify the interpretation of the various formulas to follow, whenever it is possible to separate labels we denote exciton wave vectors by latin k 's, phonon wave vectors by latin q 's, and reserve the greek κ for the total crystal momentum label .

The Holstein Hamiltonian can not in general be diagonalized exactly. It is our purpose to come as close as possible to exact diagonalization. To do this variationally one postulates the form $|\Psi\rangle$ of an eigenstate in terms of unknown parameters, calculates $E = \langle\Psi|\hat{H}|\Psi\rangle$ as a function of these unknown parameters, and then minimizes E with respect to them. The resulting E is then an upper bound for the system energy, and the resulting $|\Psi\rangle$ is assumed to approximate an eigenstate of the system. The quality of the results is of course in large part dependent on the quality of the assumed states, that is, on the flexibility and correct symmetries built into the assumed form of $|\Psi\rangle$.

In carrying out our variational program we recognize from the outset that the Hamiltonian is translationally invariant and therefore so must be its eigenstates (this is one of the “correct symmetries”). In other words, the Hamiltonian commutes with the joint crystal momentum operator

$$\hat{P} = \sum_k k a_k^\dagger a_k + \sum_q q b_q^\dagger b_q. \quad (12)$$

The operator $e^{-i\hat{P}r}$ is easily shown to induce concerted exciton and phonon translations by r lattice sites. The eigenstates of \hat{H} should thus be required to satisfy the Bloch condition

$$e^{-i\hat{P}r}|\Psi\rangle = e^{-i\kappa r}|\Psi\rangle \quad (13)$$

for any lattice vector r . Our trial states therefore carry the crystal momentum label κ ; that is, for each value of the total crystal momentum we postulate a form for the eigenstates of the system, $|\Psi(\kappa)\rangle$. We then use this trial state to compute for each value of the crystal momentum the total energy

$$E(\kappa) = \langle\Psi(\kappa)|\hat{H}|\Psi(\kappa)\rangle. \quad (14)$$

Minimization of $E(\kappa)$ with respect to the variational parameters can be carried out separately for each value of κ since the trial states are eigenfunctions of the total momentum operator. The set of $E(\kappa)$ so produced then constitutes a variational estimate (upper bound) for the polaron energy band (Lee *et al.* 1953, Toyozawa 1961).

The outline of this chapter is as follows. First we discuss the exact solution of the problem in the two limiting cases for which this solution is known: the limiting weak-coupling case ($g = 0^+$) and the “non-adiabatic” limit ($J = 0$). Both of these limiting cases are non-trivial and contain a great deal of information that serves as a benchmark for approximate solutions away from these limits. Then we introduce the variational states that we have used in our work, and discuss the ways in which the output of the variational calculations will be exhibited. We present a detailed picture of polaron structure over essentially all of parameter space: the semiclassical strong coupling small polaron regime, the highly quantum-mechanical weak coupling regime, the large polaron adiabatic regime, and the highly nonlinear intermediate coupling regime. This discussion will introduce notions familiar in the polaron literature: the phase diagram in parameter space, the effective mass, and the so-called “self-trapping transition”. We also present a comparison of our results with those of “soliton theory”. We conclude with a synthesizing summary.

2 Exact Benchmarks

The Holstein Hamiltonian can in general not be diagonalized exactly, nor can it be treated perturbatively in most parameter regimes. It is therefore very helpful and, as it turns out, extremely important, to have available at least some exact results against which one can test approximate work. Furthermore, these exact results offer valuable guidance in the design of approximations.

Here we present two such distinct benchmarks: 1) the exact solution at $J = 0$ for any g , and 2) the exact solution at $g = 0^+$ for any J . While each of

these can be understood straightforwardly, it is a nontrivial matter to demand that a variational solution be consistent with both. Moreover, as will become clear in the sections to follow, though each of these results holds rigorously only in a parametric limit or in a limited portion of the total solution, the characteristics they reveal are reflected in polaron structure well beyond the limiting scenarios.

2.1 J=0

It is well known that in the limit of vanishing exciton transfer integral ($J = 0$) local coupling polaron Hamiltonians are diagonalizable by the well-known “displaced oscillator transformation” (Lang & Firsov 1962). The Bloch eigenstates are

$$|\Psi(\kappa)\rangle = N^{-1/2} \sum_n e^{i\kappa n} a_n^\dagger \exp[-g(b_n^\dagger - b_n)] |0\rangle \quad (15)$$

where $|0\rangle$ represents the exciton and phonon vacuum. The energies are degenerate, that is, they are the same for all κ :

$$E(\kappa) = -g^2. \quad (16)$$

The band is thus completely flat and lowered by an amount g^2 (the “binding energy”) relative to the bare exciton energy. Because of this degeneracy, *all* superpositions of the “small polaron states”

$$\begin{aligned} |\phi\rangle &= a_n^\dagger \exp[-g(b_n^\dagger - b_n)] |0\rangle \\ &= a_n^\dagger \exp[-gN^{-1/2} \sum_q (e^{-iqn} b_q^\dagger - e^{iqn} b_q)] |0\rangle \end{aligned} \quad (17)$$

constitute equally valid eigenstates of the Holstein Hamiltonian in the $J = 0$ limit. It is common for (17) to be regarded as “the” small polaron state since it is often argued that disorder in real materials will favor localized states at small J ’s; however, being concerned here with translationally invariant lattices, the relevant choice is the Bloch superposition that is also an eigenstate of the total crystal momentum operator.

The small polaron state (17) represents an exciton completely localized at site n and the lattice completely undistorted *except* at site n . At site n the phonon component is a product over coherent states that represents the quantum state of each phonon mode; the amplitude of each phonon mode in the small polaron state is given by the coupling constant g . The name “small polaron” for this exciton–phonon structure is clearly appropriate. If one deals with an exciton that is explicitly coupled to the phonon displacements of the nearest neighboring sites, the small polaron involves the site on which the exciton is localized as well as its nearest neighbors. In any case, the phonon distortion is locked tightly to the exciton. Note that although one often speaks

of a “localized state” when speaking about the small polaron, the Bloch state constructed from this state is fully delocalized.

The exact $J = 0$ result is a benchmark against which any variational solution to the problem can be measured in the $J \rightarrow 0$ limit. Although the small polaron solution ceases to be exact when $J \neq 0$, when J is small and/or g is large it is often used as a starting point for perturbative solutions of the problem. The relevant “small parameter” that emerges naturally is the effective polaron transfer parameter $\tilde{J} = Je^{-g^2}$ (the polaron is “heavier” than the original exciton due to the associated phonon distortion and hence the polaron moves more slowly). The effect of \tilde{J} as a perturbation is to cause “hops” between $J = 0$ states, that is, the localized small polaron is often assumed to be the relevant energy transport entity. This approach is also frequently used as a basis for the formulation of finite temperature theories. Here we do not deal with perturbative solutions (nor do we deal with transport processes or with finite temperatures). Instead, we handle deviations from the small polaron limit as J deviates from zero via variational methods.

2.2 $g=0^+$

Let us now consider the Hamiltonian in the *weak coupling limit* of vanishing interaction between the exciton and the phonons. The Hamiltonian in this limit is diagonal,

$$\hat{H} = \sum_k J_k a_k^\dagger a_k + \omega \sum_q b_q^\dagger b_q, \quad (18)$$

with J_k given in (8). What is the lowest energy band for this system? Note that the weak-coupling limit to which we refer is *not* the free-exciton/free-phonon limit in which each subsystem is regarded independently of the other. Rather, we refer to the limiting character of the *joint* but noninteracting exciton-phonon system. That the latter can differ significantly from the separate free-exciton and free-phonon systems turns out to have a strong influence over polaron structure at finite coupling strengths. The question we ask is this: if the joint system has a certain total crystal momentum κ , how should this crystal momentum be distributed among the exciton and the phonons so as to yield the state of lowest joint energy $E(\kappa)$?

The answer depends on the relative values of the exciton transfer rate J and the phonon frequency $\omega \equiv 1$. If $J < 1/4$ then for all crystal momenta the energy is minimized if the exciton carries all of the crystal momentum. The exact energy cost of assigning the full crystal momentum to the exciton is the familiar cosine band over the entire Brillouin zone,

$$E_{g=0^+}(\kappa) - E_{g=0^+}(0) = 2J(1 - \cos \kappa). \quad (19)$$

It would “cost” more energy than this to assign the exciton only a portion (or none) of the crystal momentum and to assign the remainder to the phonons, since the energy of the latter would be at least $\hbar\omega \equiv 1$, which is greater than

the full exciton bandwidth $4J$. This is called the *non-adiabatic* regime. The associated exact eigenstate of the system in the non-adiabatic regime is

$$|\Psi(\kappa)\rangle = a_{k=\kappa}^\dagger |0\rangle. \quad (20)$$

If $J > 1/4$ (*adiabatic* regime) the situation is more complex since the distribution of crystal momentum that minimizes the energy is now more complicated. Now it is “energy effective” for the entire crystal momentum to be associated with the exciton (with no phonons) only up to the value κ_c of the crystal momentum defined by the relation

$$2J(1 - \cos \kappa_c) = 1. \quad (21)$$

The crystal momenta $\pm\kappa_c$ mark the points where the free exciton band penetrates the one-phonon continuum. For $|\kappa| > \kappa_c$ the energy of the system is minimized if the exciton carries no momentum at all and the entire crystal momentum is associated with one phonon. The minimum energy as a function of crystal momentum therefore is

$$\begin{aligned} E_{g=0^+}(\kappa) - E_{g=0^+}(0) &= 2J[1 - \cos(\kappa)] \quad \text{for } |\kappa| < \kappa_c \\ &= 1 \quad \text{for } |\kappa| > \kappa_c \end{aligned} \quad (22)$$

Associated with this energy band are the Bloch states

$$\begin{aligned} |\Psi(\kappa)\rangle &= a_{k=\kappa}^+ |0\rangle \quad \text{for } |\kappa| < \kappa_c, \\ &= b_{q=\kappa}^+ a_{k=0}^+ |0\rangle \quad \text{for } |\kappa| > \kappa_c, \end{aligned} \quad (23)$$

the former being the zero-phonon state in which the exciton carries all the crystal momentum, and the latter being the state in which the exciton is at rest and all the crystal momentum is carried by a single free phonon quantum of momentum κ . The energy band in the adiabatic regime in this weak coupling limit is illustrated in Fig. 1.

These results provide a benchmark against which to measure variational solutions as the exciton-phonon coupling vanishes. As $g \rightarrow 0^+$ in the non-adiabatic regime ($J < 1/4$), an acceptable variational solution must approach a bare exciton of momentum κ . On the other hand, as $g \rightarrow 0^+$ in the adiabatic regime ($J > 1/4$), the variational solution must tend toward an exciton of momentum κ for κ near the zone center, and to a stationary exciton plus an essentially free phonon of momentum κ near the zone boundary.

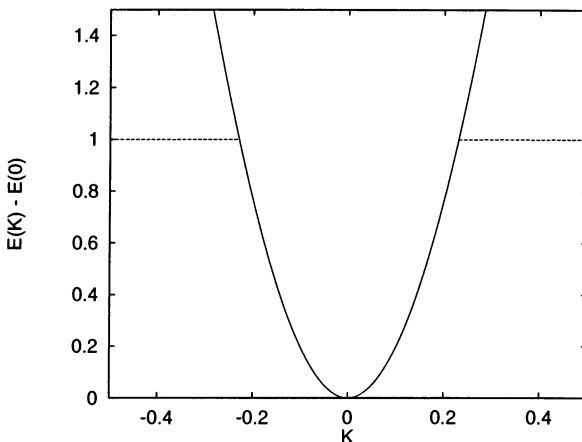


Fig. 1. In the absence of phonons, the free-exciton energy band would be the cosine band throughout the Brillouin zone (solid curve; $J = 2$). When excitons and phonons coexist even in the weak coupling limit, the one-phonon band intersects the exciton band at $|\kappa| = \kappa_c = 0.23\pi$. Thus the polaron band is the cosine band for $|\kappa|/\pi \leq 0.23$ and unity for $0.23 < |\kappa|/\pi \leq 1$, that is, the band consists of the solid curve in the range $(-0.23, 0.23)$ and the dashed line otherwise. $K = \kappa/\pi$, and only half of the Brillouin zone is shown.

3 Variational Methods

The literature on variational approaches to the polaron problem deals with two distinct points of departure. Both begin with the construction of what we call “localized states” $|\phi\rangle$ that carry all the information regarding exciton-phonon correlations. These states need not be localized in the strict sense of the word - they may actually extend over many lattice sites, but in general they do not satisfy the Bloch condition of translational invariance. These states are written in terms of parameters to be determined variationally. In one approach to the problem, which we term the “localized framework,” (Pekar 1946a, Pekar 1946b, Landau & Pekar 1948, Pekar 1954, Rashba 1957a, Rashba 1957b, Davydov 1969, Davydov & Kislyukha 1973, Emin & Holstein 1976, Davydov & Kislyukha 1976, Davydov 1979, Davydov 1980, Holstein 1981, Rashba 1987, Holstein & Turkevich 1988a, Holstein & Turkevich 1988b, Skrinjar *et al.* 1988, Zhang *et al.* 1988, Brown & Ivic 1989, Ivic & Brown 1989, Wang *et al.* 1989, Brown *et al.* 1990), one then applies either a stationary variational principle (e.g. the minimization of the total energy function $E = \langle \phi | \hat{H} | \phi \rangle$) or a time-dependent variational principle to obtain optimal parameter values. In this framework these states are generally understood to describe the internal structure of a quasiparticle whose external dynamics is particle-like. Such approaches, especially in conjunction with a

time-dependent variational principle, are often the starting point for studies of transport properties. We return to an example of the localized framework in Sect. 6. The other approach, which we call the “delocalized framework”, uses the localized states as *form factors* for the construction of Bloch states. The variational procedure (minimization of the energy) is then applied to the delocalized state. It will be evident from the following discussion that the variational results are quite different in the localized and delocalized frameworks even when the localized state and the form factor are formally identical, and even if the localized states are spatially extended.

Our normalized trial Bloch states can be constructed in the form (Brown 1995a)

$$|\Psi(\kappa)\rangle = \frac{|\kappa\rangle}{\langle\kappa|\kappa\rangle^{1/2}}, \quad (24)$$

in which the delocalized vector $|\kappa\rangle$ is generated from the form factor $|\phi\rangle$ through a projection operation

$$|\kappa\rangle = \hat{\Xi}^\kappa |\phi\rangle \quad (25)$$

$((\hat{\Xi}^\kappa)^2 = \hat{\Xi}^\kappa)$. The delocalizing operator $\hat{\Xi}^\kappa$ is given by

$$\hat{\Xi}^\kappa \equiv N^{-1} \sum_n \exp[-i(\hat{P} - \kappa)n], \quad (26)$$

in which N is the number of lattice sites and \hat{P} is the momentum operator (12). The effect of the delocalizing operator is to displace replicas of the localized state $|\phi\rangle$ by all possible lattice translations, weighting each by an appropriate phase, and collecting the entire set of such displaced replicas into a single superposition state. The resulting superposition state satisfies the Bloch condition (13); thus any quantity measured relative to a fixed frame is found to be uniform throughout the lattice.

The delocalizing operator $\hat{\Xi}^\kappa$ contains no variational quantities, and the localized vector $|\phi\rangle$ (which contains all the variational quantities) generally does not bear any dependence on the crystal momentum label κ until *after* a variation is implemented. Every state so constructed is a fitting candidate for energy band calculations regardless of the depth of insight invested in the form factor $|\phi\rangle$. A choice that is too simple yields results of little practical value; one that is too complex yields results of little practical utility.

For the Holstein Hamiltonian we have developed a rather complete picture of the behavior of the full polaron energy band and the states associated with it over a broad range of parameter values J and g (Zhao 1994b, Zhao *et al.* 1996b, Zhao *et al.* 1997a, Brown & Lindenberg 1997, Brown *et al.* 1997, Zhao *et al.* 1996a). In a variational calculation one does not know how close one comes to the “true answer” if this true answer is not known. This is why exact benchmark results are so extraordinarily important. Every variational Ansatz state is constrained by the assumptions built into it from the outset, and one does not know *a priori* if such constraints lead to a serious deviation

from the correct outcome or to a serious truncation of physical reality (again, except for the information provided by the benchmark results). Improvement (as measured by the lowering of the energy) can be achieved by building ever more complex and flexible form factors, and evaluating the changes in the outcome that this increased complexity provides. It is thus a useful exercise to carry out the variational program using a hierarchy of trial states of increasing flexibility. In this section we describe the hierarchy of states that we have analyzed and the way in which the outcome is exhibited; in the next section we present the physical picture of the polaron that emerges from this analysis.

3.1 Trial States

Our form factors can be viewed as complex superpositions of products of exciton and phonon components. In all that we do, the elemental phonon component is a product over coherent states selected to represent the quantum state of each phonon mode. Such coherent state products can be written (Glauber 1963)

$$|\{\zeta_q\}\rangle = \exp[-N^{-1/2} \sum_q (\zeta_q b_q^\dagger - \zeta_q^* b_q)] |0\rangle, \quad (27)$$

in which ζ_q is the complex amplitude characterizing the state of the mode labeled by q . When all $\{\zeta_q\}$ are free to range over the complex numbers, all possible classical lattice configurations are represented as minimum-uncertainty quantum states, making such coherent states natural choices for use in characterizing polaronic lattice distortions at least in the semiclassical (multi-phonon) regime. A hierarchy of trial states can be established based on the characteristics of the phonon coherent state amplitudes and their relationship with the exciton components with which they are paired.

The simplest non-trivial form factor is the small polaron state introduced in Sect. 2:

$$|\phi\rangle = a_m^\dagger |\{ge^{-iqm}\}\rangle \quad (28)$$

[cf. (17)]. This state represents an exciton completely localized at site m , and the lattice completely undistorted *except* at site m , where the Einstein oscillator amplitude is given by the coupling constant g . The delocalized state associated with this form factor is

$$|\Psi(\kappa)\rangle = \sum_m e^{i\kappa m} a_m^\dagger \exp[-gN^{-1/2} \sum_q (e^{-iqm} b_q^\dagger - e^{iqm} b_q)] |0\rangle. \quad (29)$$

Note that there are no variational parameters in this small polaron state, which is the exact Bloch state when $J = 0$.

Next in the hierarchy is the form factor underlying the variational calculation based on the Merrifield method (Merrifield 1964),

$$|\phi\rangle = a_m^\dagger |\{\beta_q\}\rangle. \quad (30)$$

The form factor in this case involves N complex variational amplitudes, β_q for N values of q , for complete specification. This state represents an exciton completely localized at site m , paired with a lattice distortion as given by the set of phonon amplitudes $\{\beta_q\}$. Applying the delocalizing operator to (30) yields the Bloch state (here written explicitly with the phonon amplitudes in site space and equivalently in momentum space)

$$\begin{aligned} |\Psi(\kappa)\rangle &= N^{-1/2} \sum_n e^{i\kappa n} a_n^\dagger \exp[-\sum_{n_b} (\beta_{n_b-n}^\kappa b_{n_b}^\dagger - \beta_{n_b-n}^{\kappa*} b_{n_b})] |0\rangle, \\ &= N^{-1/2} \sum_n e^{i\kappa n} a_n^\dagger \exp[-N^{-1/2} \sum_q (\beta_q^\kappa e^{-iqn} b_q^\dagger - \beta_q^{\kappa*} e^{iqn} b_q)] |0\rangle. \end{aligned} \quad (31)$$

We stress here a point made earlier in passing about the difference between implementation of the variational calculation in the localized and delocalized frameworks. If the variation is implemented in the localized framework directly, that is, on (30), the result is identical to (28), that is, one finds that $\beta_q = ge^{-iqm}$. This complete localization of the exciton component is imposed self-consistently by the variational equations upon the phonon system because $\langle\phi|\hat{H}_{ex}|\phi\rangle = 0$ for this state. On the other hand, the result may be quite different if the variation is implemented in the delocalized framework, that is, on (31). In this case allowance is made through κ and k dependences for the finite mobility of the exciton, allowing spatially-extended polaron structure to be manifested in the phonon amplitudes $\{\beta_q\}$. Thus, although *formally* the Merrifield form factor looks similar to the small polaron, the shape of the self-consistent lattice distortion in the delocalized framework may turn out to be compact, as in the small polaron case, or broad, as is more typical of the “large polaron”. The outcome depends on the parameter values. Our detailed study of polaron structure by the Merrifield method has been presented in Zhao *et al.* (1996b).

An important generalization of both the small polaron and Merrifield states is that associated with Davydov (localized framework) (Pekar 1946a, Pekar 1946b, Landau & Pekar 1948, Pekar 1954, Rashba 1957a, Rashba 1957b, Davydov 1969, Davydov & Kislyukha 1973, Emin & Holstein 1976, Davydov & Kislyukha 1976, Davydov 1979, Davydov 1980, Holstein 1981, Rashba 1987, Holstein & Turkevich 1988a, Holstein & Turkevich 1988b, Skrinjar *et al.* 1988, Zhang *et al.* 1988, Brown & Ivic 1989, Ivic & Brown 1989, Wang *et al.* 1989, Brown *et al.* 1990), and Toyozawa (delocalized framework) (Toyozawa 1961, Toyozawa 1963, Sumi & Toyozawa 1973, Toyozawa 1980, Ueta *et al.* 1986). This form factor abandons the explicit association of the lattice distortion with the site of exciton creation at site m and accounts for the finite mobility of the exciton already in the localized framework by allowing for spatial spreading of the exciton component:

$$|\phi\rangle = |\alpha\rangle \otimes |\{\beta_q\}\rangle, \quad (32)$$

$$|\alpha\rangle = \sum_m \alpha_m a_m^\dagger |0\rangle. \quad (33)$$

This class of states subsumes a wide variety of structures from completely localized to completely delocalized, and has been used as the basis of dynamical theories as well as time-independent analyses; it is here that one first encounters the soliton concept (we return to this in Sect. 6). As in the Merrifield case, the further delocalization which is required by the Bloch state construction has significant consequences for polaron structure, yielding features and trends that cannot be contained in the form factor alone. There are now $2N$ complex variational amplitudes that specify the form factor, the α_m and the β_q . The explicit Bloch state obtained after application of the delocalizing operator, again exhibited in two ways, is

$$|\Psi(\kappa)\rangle = \frac{|\kappa\rangle}{\langle\kappa|\kappa\rangle^{1/2}}, \quad (34)$$

$$\begin{aligned} |\kappa\rangle &= \sum_n e^{i\kappa n} \sum_{n_a} \alpha_{n_a - n}^\kappa a_{n_a}^\dagger \exp[-\sum_{n_b} (\beta_{n_b - n}^\kappa b_{n_b}^\dagger - \beta_{n_b - n}^{\kappa*} b_{n_b})] |0\rangle \\ &= N^{-\frac{1}{2}} \sum_{nk} e^{i(\kappa-k)n} \alpha_k^\kappa a_k^\dagger \exp[-N^{-\frac{1}{2}} \sum_q (\beta_q^\kappa e^{-iqn} b_q^\dagger - \beta_q^{\kappa*} e^{iqn} b_q)] |0\rangle. \end{aligned} \quad (35)$$

Note that the phonon amplitude site index is not connected explicitly to that of the exciton (whereas it is in the Merrifield form (31)). Our detailed study of polaron structure by the Toyozawa method has been presented in Zhao *et al.* (1997a).

An alternate representation of the Merrifield form factor, completely equivalent to (30), would be to write

$$|\phi\rangle = a_m^\dagger |\{\gamma_q e^{-iqm}\}\rangle. \quad (36)$$

The explicit Bloch state written out in detail is identical to (31),

$$\begin{aligned} |\Psi(\kappa)\rangle &= N^{-1/2} \sum_n e^{i\kappa n} a_n^\dagger \exp[-\sum_{n_b} (\gamma_{n_b - n}^\kappa b_{n_b}^\dagger - \gamma_{n_b - n}^{\kappa*} b_{n_b})] |0\rangle, \\ &= N^{-1/2} \sum_n e^{i\kappa n} a_n^\dagger \exp[-N^{-1/2} \sum_q (\gamma_q^\kappa e^{-iqn} b_q^\dagger - \gamma_q^{\kappa*} e^{iqn} b_q)] |0\rangle. \end{aligned} \quad (37)$$

This identity is due to the localization of the exciton component on a single site in the form factor. However, a generalization of (36) to allow for a spreading of the exciton component would lead to exciton-phonon correlations quite distinct from those in (32) provided that the exciton amplitudes exhibit a non-trivial spread in real space. Now we would write

$$|\phi\rangle = \sum_m \alpha_m a_m^\dagger |0\rangle |\{\gamma_q e^{-iqm}\}\rangle. \quad (38)$$

Whereas (32) leads to a single lattice distortion distribution associated with the full distribution of exciton amplitudes, (38) through the additional phase factor e^{-iqm} leads to a replica of a lattice shape function centered upon each exciton creation operator, in effect creating distinguishable lattice distortions

at each site of nonvanishing exciton amplitude. The Bloch state associated with (38) would involve [note the difference in site indices inside the coherent state factors between this form and (35)]

$$|\kappa\rangle = \sum_n e^{i\kappa n} \sum_{n_a} \alpha_{n_a - n}^\kappa a_{n_a}^\dagger \exp[- \sum_{n_b} (\gamma_{n_b - n_a}^\kappa b_{n_b}^\dagger - \gamma_{n_b - n_a}^{\kappa^*} b_{n_b})] |0\rangle. \quad (39)$$

We have not implemented this variational state in our work.

In the following, we refer to correlations carried by site-independent coherent state amplitudes such as the $\{\beta_q\}$ in (32) as *global* correlations, and those carried by m -centered coherent state amplitudes such as the $\{\gamma_q e^{-iqm}\}$ in (38) as *local* correlations.

The *most general* one-exciton state in which the lattice components are represented by phonon coherent state products is

$$|\phi\rangle = \sum_m \alpha_m a_m^\dagger |0\rangle |\{\beta_{qm}\}\rangle, \quad (40)$$

in which the coherent state amplitudes $\{\beta_{qm}\}$ are permitted a general dependence on q and m . This state has received some attention in the localized framework (Davydov 1980, Skrinjar *et al.* 1988, Zhang *et al.* 1988), but has not seen any application as a form factor in a delocalized state. This limited attention is largely due to the vastly larger number of complex variational amplitudes required to express the general spatial dependence of β_{qm} (N^2 β amplitudes plus N α amplitudes), as well as the greater complexity of the formal description required to contain the solution.

It is in this context that Brown and Ivic (Brown & Ivic 1989, Ivic & Brown 1989, Brown *et al.* 1990) attempted to simplify the latter method in such a way that its outstanding feature – a unified description of the principal exciton-phonon correlation channels – would be preserved within a more practical framework. This was done by decomposing the amplitude β_{qm} into a part sensitive to global exciton-phonon correlations as in (32), and a part sensitive to local exciton-phonon correlations as in (38),

$$|\phi\rangle = \sum_m \alpha_m a_m^\dagger |0\rangle |\{\beta_q - \gamma_q e^{iqm}\}\rangle. \quad (41)$$

This form factor requires only $3N$ complex amplitudes. The global amplitude β_q can be related to the spatial average of β_{qm} , and the local amplitude $\gamma_q e^{-iqm}$ can be viewed as an Ansatz for the spatial variation of β_{qm} around this mean value. The latter spatial dependence may appear somewhat *ad hoc*; however, it is motivated by the physical notion of associating a lattice distortion with the site of exciton creation as in (38). Applying the delocalizing operation $\hat{\Xi}^\kappa$ to (41) yields

$$|\kappa\rangle = N^{-\frac{1}{2}} \sum_{nn_a} e^{i\kappa n} \alpha_{n_a - n}^\kappa a_{n_a}^\dagger \exp\{- \sum_{n_b} [(\beta_{n_b - n}^\kappa - \gamma_{n_b - n_a}^\kappa) b_{n_b}^\dagger - H.c.] \} |0\rangle,$$

$$\begin{aligned}
&= N^{-1} \sum_{nn_a k} e^{i\kappa n - ikn_a} \alpha_{n_a - n}^\kappa a_k^\dagger \\
&\times \exp\{-N^{-\frac{1}{2}} \sum_q [(\beta_q^\kappa e^{-iqn} - \gamma_q^\kappa e^{-iqn_a}) b_q^\dagger - H.c.] \} |0\rangle. \tag{42}
\end{aligned}$$

The α 's and β 's relate elementary exciton or phonon components in the global sense discussed above, while the γ 's express a direct relation between elementary exciton and phonon components. This is the most sophisticated state that we have explored. Detailed results for this method that builds in combined global and local exciton-phonon correlations has been presented in Brown *et al.* (1997). We will refer to this as the Global-Local (GL) method.

3.2 Variational Equations

Each of the postulated variational states described above can now be used to compute the total energy function (14). The resulting $E(\kappa)$ is a function of the variational amplitudes that appear in the trial states. Minimization of $E(\kappa)$ with respect to these parameters then leads to a set of coupled nonlinear equations (the number of them determined by the number of variational amplitudes in the trial state and usually somewhat reduced in number by symmetries) that must be solved numerically. We do not present the equations for *each* of the trial states but instead do so only for one as an illustration. The others can be found in the appropriate references. The one we pick to exhibit in detail is that associated with the Toyozawa Ansatz state (35). Those associated with the Merrifield Ansatz state (31) are simpler while those obtained from the GL Ansatz state (42) are more complex.

The expectation values of the several contributions to the Holstein Hamiltonian using the Toyozawa Ansatz state are given by

$$\langle \kappa | \hat{H}^{ex} | \kappa \rangle = -2JN^{-1} \sum_k S_{\kappa-k}^\kappa \cos k |\alpha_k^\kappa|^2, \tag{43}$$

$$\langle \kappa | \hat{H}^{ph} | \kappa \rangle = N^{-2} \sum_{kq} S_{\kappa-k-q}^\kappa |\alpha_k^\kappa|^2 |\beta_q^\kappa|^2, \tag{44}$$

$$\langle \kappa | \hat{H}^{ex-ph} | \kappa \rangle = -gN^{-2} \sum_{kq} \alpha_k^{\kappa*} \alpha_{k+q}^\kappa (S_{\kappa-k-q}^\kappa \beta_q^{\kappa*} + S_{\kappa-k}^\kappa \beta_{-q}^\kappa). \tag{45}$$

$$\langle \kappa | \kappa \rangle = N^{-1} \sum_k S_{\kappa-k}^\kappa |\alpha_k^\kappa|^2. \tag{46}$$

Here S_p^κ is the Fourier transform of the Debye-Waller factor S_n^κ :

$$S_p^\kappa = \sum_n e^{-ipn} S_n^\kappa, \tag{47}$$

$$S_n^\kappa = \langle \{\beta_m\} | \{\beta_{m+n}\} \rangle = \exp[N^{-1} \sum_q |\beta_q^\kappa|^2 (e^{iqn} - 1)], \quad (48)$$

which is to be distinguished from the Franck-Condon factor

$$_{ph} \langle 0 | \{\beta_n\} \rangle = e^{-\frac{1}{2} \sum_n |\beta_n|^2}. \quad (49)$$

The latter is of importance in optical absorption, while the former has a greater role in transport problems since it quantifies the overlap of the polaron lattice distortion with itself displaced by n lattice sites. The nearest-neighbor Debye Waller factors $S_{\pm 1}^\kappa$ appear routinely in the transport terms of effective (small) polaron Hamiltonians, where they are responsible for the renormalization of the effective mass. Longer-range Debye-Waller factors appear in our calculations because the spreading of the exciton amplitudes α_n^κ allows contribution of overlaps between non-nearest-neighbor components. Note, for example, that because $N^{-1} \sum_p S_p^\kappa = S_{n=0}^\kappa = 1$, if the exciton amplitudes contract down to a single site ($\alpha_n^\kappa = \delta_{n0}$, $\alpha_k^\kappa = const.$), all the Debye-Waller factors in Eqs. (44)-(46) disappear, leaving only the nearest-neighbor Debye-Waller factors in the transport term (43).

Minimization of E^κ with respect to $\beta_q^{\kappa*}$ yields

$$\beta_q^\kappa = \frac{L_q^\kappa}{M_q^\kappa + H_q - M_q^\kappa E^\kappa} \quad (50)$$

where

$$L_q^\kappa = gN^{-1} \sum_k S_{\kappa-k-q}^\kappa \alpha_k^{\kappa*} \alpha_{k+q}^\kappa, \quad (51)$$

$$M_q^\kappa = N^{-1} \sum_k S_{\kappa-k-q}^\kappa |\alpha_k^\kappa|^2, \quad (52)$$

and H_q is the sum of three terms:

$$H_q = H_q^{ex} + H_q^{ph} + H_q^{ex-ph}, \quad (53)$$

$$H_q^{ex} = -2JN^{-1} \sum_k S_{\kappa-k-q}^\kappa \cos k |\alpha_k^\kappa|^2, \quad (54)$$

$$H_q^{ph} = N^{-2} \sum_{kq'} S_{\kappa-k-q-q'}^\kappa |\alpha_k^\kappa|^2 |\beta_{q'}^\kappa|^2, \quad (55)$$

$$H_q^{ex-ph} = -gN^{-2} \sum_{kq'} \alpha_k^{\kappa*} \alpha_{k+q'}^\kappa (S_{\kappa-k-q-q'}^\kappa \beta_{q'}^{\kappa*} + S_{\kappa-k-q-q'}^\kappa \beta_{-q'}^\kappa). \quad (56)$$

Similarly, we minimize E^κ with respect to $\alpha_k^{\kappa*}$, obtaining

$$\alpha_k^\kappa = \frac{L_k^\kappa}{M_k^\kappa - (E^\kappa + 2J \cos k) S_{\kappa-k}^\kappa} \quad (57)$$

where

$$L_k^\kappa = g N^{-1} \sum_q \alpha_{k+q}^\kappa (S_{\kappa-k-q}^\kappa \beta_q^{\kappa*} + S_{\kappa-k}^\kappa \beta_{-q}^\kappa) \quad (58)$$

and

$$M_k^\kappa = N^{-1} \sum_q S_{\kappa-k-q}^\kappa |\beta_q^\kappa|^2. \quad (59)$$

These then are the equations that must be solved numerically and self-consistently for each κ . In Sect. 4 we briefly discuss some of the issues associated with this numerical portion of the solution.

3.3 How Results Are Exhibited

We have now established the way in which we approach the polaron problem, the sorts of variational states that we postulate, the numbers of complex amplitudes involved in each type of trial state, and the energy minimization principle that we follow to find the optimal variational amplitudes for each value of the total crystal momentum. The numerical procedure to be followed in solving the variational equations is sketched in the next section, and subsequently we wish to present the results of this effort. An important question that arises at this point is the following: how does one best exhibit these results? Given the large numbers of variational quantities involved in the problem, and the choices of presentation that are available, this bears some comment.

If we were only interested in finding the optimal energy band we would present a graph of the resulting $E(\kappa)$ as a function of κ for some chosen set of parameter values J and g and be done with it. However, we are interested in much more than that: we are interested in the detailed nature of the polaron state, the way in which the exciton and phonons distribute themselves spatially, and the way in which these distributions change as the parameter values change. We have a foretaste of this degree of insight in the benchmark cases presented in the previous section. For example, in the $J = 0$ case not only did we see that the polaron band is lowered from that of a free (but immobile) exciton by an amount determined by the exciton-phonon coupling strength, but we also noted that the polaron form factor in this case consists of an exciton completely localized on one lattice site together with a completely localized lattice distortion of indeterminate phonon number and of amplitude determined by the same coupling strength. In the other benchmark case, that of vanishing exciton-phonon coupling ($g \rightarrow 0^+$), we learned that for sufficiently small J ($J < 1/4$) the polaron band is just the free exciton band, and the polaron is simply the free exciton with no associated phonons. We

saw that if $J > 1/4$, on the other hand, the polaron band is narrowed relative to the free exciton band. We saw that for values of the crystal momentum near the zone center the polaron is again simply the free exciton, but at values of the crystal momentum near the zone edge the polaron consists of an exciton that carries no crystal momentum plus a single free phonon that carries all the momentum. This is the sort of insight that we would like to acquire and present more broadly.

The following are some of the quantities that we will exhibit to convey as much information as possible. We will present exciton and phonon amplitudes so that we may see how the exciton and phonons are spatially distributed in the form factors. This will tell us if the phonons are tightly connected with the exciton (as in a small polaron), or more loosely connected with the exciton (as in a large polaron), or if they are essentially free from one another (as in the weak coupling limit). These amplitudes are complex and multiply indexed, and must thus be presented as surfaces. We can present these surfaces in site space or in Fourier space - the latter challenges the imagination more than the former but sometimes conveys the information in a more useful or complete way. We can present measures of the number of phonons associated with the polaron state so as to get a sense of the “weight” of the polaron. We can present the energy band $E(\kappa)$. We can look at familiar measures associated with the energy band, such as the effective mass of the polaron determined by the curvature of the band around $\kappa = 0$,

$$m_{eff} \equiv \left(\frac{\partial^2 E(\kappa)}{\partial \kappa^2} \right)^{-1}. \quad (60)$$

We can monitor changes in the effective mass with changing parameter values to see if there are any sudden changes such as the rapid increase in the effective mass connected with the “self-trapping transition” often associated with the rapid change from large polaron to small polaron with increasing exciton-phonon coupling strength – more on this later.

Each of these quantities can be analyzed for different parameter values. Indeed, it will be useful to present a parameter space portrait that will summarize many of these results in a compact way.

4 Numerical Aspects

The variational equations associated with the Ansatz states must be solved numerically. It is of course our goal to obtain numerically exact solutions so that our results are only encumbered by the limitations of our assumptions and not by additional numerical uncertainties. Compared with previous work we have imposed no restrictions on the forms of the variational surfaces other than those implicit in each variational Ansatz itself.

Relaxation techniques are efficient iteration methods for identifying energy minima of complex variational systems. The principal difficulties with

this approach lie in the stability of the iteration and the quality of the convergence. Though a proper solution obtained by this or any other variational method must be stable relative to small changes in the variational parameters, and though the search for such solutions relies upon this stability property, it is possible for errors in a fraction of the total solution to spread and destabilize the iteration or otherwise limit the quality of the convergence. Thus, while in principle the same family of solutions should result for randomly-chosen initial data, in practice one finds the best convergence when the search is initialized with input that is already “close” to the solution being sought.

For our problem for the most part the initial guesses for the nonlinear iterative scheme pose no major difficulties because the physical solution is unique over most of parameter space, and because, as discussed earlier, exact solutions are available in certain limits of physical parameters. To achieve efficient and stable iterations toward the variational ground state, one may take advantage of the continuity of the ground state with respect to small changes in system parameters over most of the phase diagram, and may initialize the iteration using a reliable ground state already determined at some nearby point in parameter space. Starting from those limits where exact solutions can be obtained analytically and executing a sequence of variations along well-chosen paths through parameter space using solutions from one step to initialize the next, the whole parameter space can be explored.

Similarities can be drawn between such a step-wise process and calculations involving classical magnetic systems where the external field serves as the control parameter (Zhao & Bertram 1992, Zhao & Bertram 1995). In such systems one may observe hysteresis, that is, a dependence on the path through parameter space along which the physical parameter value of interest is approached. In our calculations we also observe such effects, that is, there are regimes in parameter space where the variational state obtained for a given set of parameter values by iteration depends on the path of approach to those values in parameter space. As we discuss in more detail subsequently, apparent hysteresis may occur because the Ansatzs are not sufficiently flexible to handle correctly rapid changes in the system with respect to physical parameters.

As we have seen, the exact small polaron solution is available in the limit of vanishing bare band width ($J \rightarrow 0$) for any value of the coupling parameter g . Computation typically starts from the region where small polaron theory holds, and the bare band width is gradually increased relative to the small polaron binding energy (g^2) as the computation continues. Reversibility of the computation is tested as the parameter space is mapped; that is, a provisionally convergent solution is used to initialize a new variation at the point in parameter space that provided the initialization for the provisional solution. That particular step of computation is termed reversible if the solution for the previous set of parameters is recovered. Any point in the parameter space can be approached from various points close to it, which we shall call

its “neighbors”. A completely reversible point is one that survives all the reversibility tests of its various neighbors. Most of the regions in our problem are found to be reversible except for a thin tongue (see Fig. 2 and Fig. 14) constituting a “phase boundary” between two types of polaron states. Within that tongue, two solutions are obtained depending on whether those points are reached from above or below the tongue. The significance of this tongue and the choice of solution within it will be discussed subsequently.

Good numerical convergence is achieved for most regions of parameter space. Round-off errors affect computation only in the weak coupling regime; in this regime the polaron energy is increasingly insensitive to round-off errors, allowing errors in the variational parameters themselves to grow. High-momentum states ($|\kappa| > \kappa_c$) are most vulnerable to such inaccuracies.

One of the more subtle signatures of overall improvement as we increase the sophistication of the variational state is a reduction in precision-related sensitivities in numerical computation. Generally speaking, for example, convergence under the GL method is better behaved than under the Toyozawa method, and can be pursued more effectively to weaker exciton-phonon coupling strengths. Also, certain peculiarities of solutions under the Toyozawa method are greatly improved by the GL method, and the growing irregularities of the exciton component in the weak coupling regime are greatly reduced. These findings indicate that those peculiarities are often artifacts of the method and do not represent real physical behavior.

It is possible that algorithmic improvements might allow a more precise resolution of polaron structure at a given machine precision, or that better results might be achieved at higher machine precision. For example, test calculations using the Toyozawa method performed at higher precision on different machines show better convergence for given parameters in the weak coupling region. However, even at higher precision, a small decrease in exciton-phonon coupling in that region greatly increases demands on computational precision, such that increasing precision only slightly reduces the value of the exciton-phonon coupling at which computational reliability is lost.

5 Typical Results

In this section we exhibit and discuss representative results of the variational calculations over most of parameter space. It is not our purpose here (nor is there sufficient space) to present an exhaustive discussion of the comparative improvements brought about by increasing Ansatz state flexibility - this discussion is presented extensively in Zhao *et al.* (1994b, 96b, 97a) and Brown *et al.* (1997). We comment on such comparisons only when they lead to important clarification of the physical picture. Instead, we “mix and match” and present results obtained by convenient any method that makes the point. It is of course true that increasing sophistication always improves the quality

of the energy band and energy states obtained, but it does so non-uniformly, that is, improvement is more pronounced for some parameter regimes than for others, and, for given parameter values, it is more pronounced in some regions of the Brillouin zone than in others. One must decide in any particular case whether increased complexity is worth the improvement.

5.1 Exciton and Phonon Amplitudes

In Fig. 2 we show a number of points representing (J, g) parameter combinations singled out for detailed discussion in the text. The tongue-shaped region will be explained subsequently.

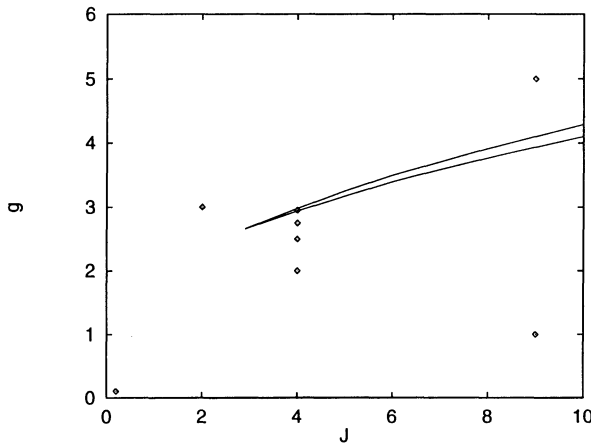


Fig. 2. Phase diagram. The diamonds correspond to parameter values chosen for detailed discussion in the text. The tongue-shaped sector indicates the region in which the variational solutions for the Toyozawa Ansatz are not unique, and lowest energy solutions must be selected explicitly. This tongue-shaped region begins at $J_c = 2.9$, $g_c = 2.66$, and is discussed in detail in the text.

We begin with those regions of parameter space where the polaron states are closest in structure to those presented in the exact benchmark results of Sect. 2. First let us consider the small polaron regime. We mentioned in Sect. 2.1 that departures from small polaron behavior are measured by the magnitude of Je^{-g^2} and that the state of the system is expected to be close to a small polaron as long as this quantity is small. In Fig. 2 the parameter combinations $(J, g) = (2, 3)$ and $(J, g) = (9, 5)$ might be expected to be associated with states that fit this description. Indeed, in this upper large- g region of the phase diagram the polaron is well described as small-polaron-like. A typical set of amplitudes showing this behavior is seen in Fig. 3. These

variational surfaces were obtained using the Toyozawa method and hence there are two surfaces, one for the phonon amplitudes (first panel) and one for the exciton amplitudes (second panel). There are only two surfaces because both amplitudes in Fourier space turn out to be real. We have not proved this analytically, but it turns out this way numerically for all parameter values studied; this is one compelling reason for exhibiting these results in Fourier space. The surfaces shown are typical of the strong-coupling region. The profiles of the β surface in q and of the α surface in k reflect the internal correlations that comprise polaron structure, while the profiles in κ reflect states of motion or polaron dynamics. Consider first the exciton amplitude, and let us perform a “mental inverse Fourier transform” in k to real space. If the exciton surface in Fourier space were completely flat, then in real space the amplitude would be completely localized on one site. Indeed, the exciton amplitude becomes flatter as $J \rightarrow 0$ in our calculations. The small sinusoidal variation in k when transformed to real space implies a slight spatial spreading of the exciton. Note that the exciton form factor shape is essentially independent of (i.e. essentially the same for all values of) the total crystal momentum κ .

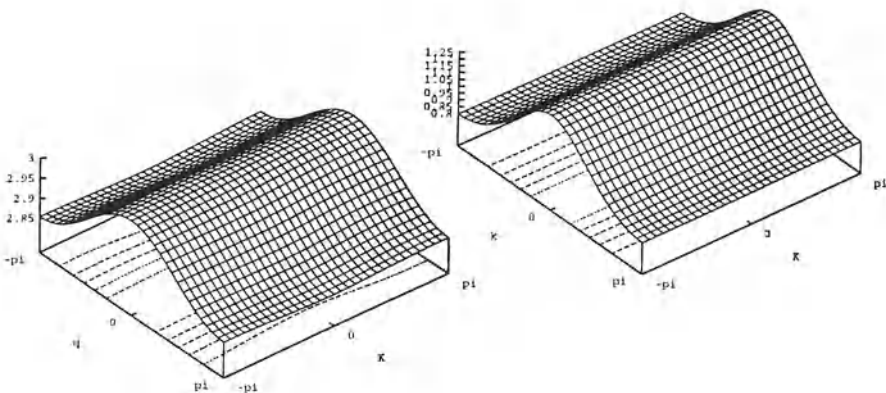


Fig. 3. The phonon displacement β_q^κ (first panel) and the exciton amplitude α_k^κ (second panel) for $g = 3.0$, $J = 2.0$ obtained with the Toyozawa method. Normalization of the latter surface is arbitrary - we have set $\alpha_{k=0}^\kappa = 1$.

Next we observe that β_q^κ and α_k^κ are similar in shape, being nearly independent of the joint crystal momentum κ and being smoothly pulse-shaped around the zone center in both q and k . We describe this condition of strong similarity as a “locking” of the exciton and lattice components. This locking characteristic is reflected in the site-space β_n^κ and α_n^κ as well. Again, if one “mentally” Fourier transforms the surfaces in the figure one finds the lattice

distortion tightly localized and associated with the exciton. These are typical small-polaron-like exciton and phonon amplitudes. Note the small increase in the mean (that is, averaged over q) phonon amplitude with increasing $|\kappa|$: in real space this mean represents the phonon amplitude at the center of the phonon cloud. That this quantity is smaller at the Brillouin zone center than at the zone boundary contributes (along with other measures) to the conclusion that the polaron grows more compact with increasing $|\kappa|$.

The small-polaron-like behavior in this regime of phase space, with deviations from the strict small polaron limit as noted above, is rather well captured by all the variational states introduced earlier. The Merrifield method of course can not capture the slight exciton spreading; the Toyozawa method does, while the improvement provided by the GL method is small for these parameter values. An indication of the improvement, not only for the case just discussed but for other cases as well, can be seen in Fig. 4.

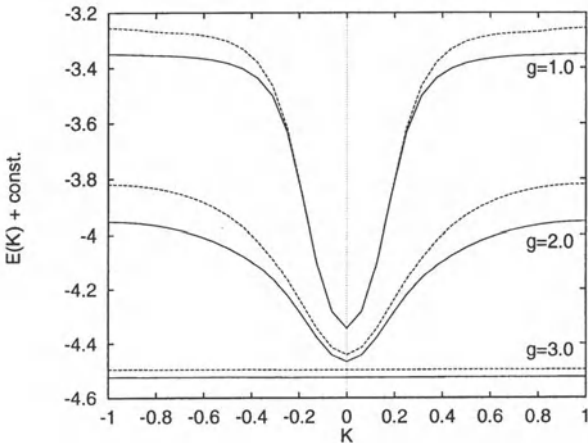


Fig. 4. Energy bands $E(\kappa)$ for $J = 2.0$, $g = 1, 2, 3$ as computed by the GL method (solid lines) and the Toyozawa method (dashed lines). The $g = 2.0$ solid/dashed pair has been shifted by +1.1 and the $g = 3.0$ pair shifted by +4.95 to allow all curves to be compared in a single illustration. $K = \kappa/\pi$.

Confirmation of the polaron structure just described is obtained by looking at the exciton and phonon amplitude surfaces for another set of parameter values in this regime, namely, $J = 9$ and $g = 5$. The associated amplitudes are shown in Fig 5. Note that these results are generated using the GL variational method, and therefore we exhibit three amplitude surfaces. Several features of the figure should be noted. The exciton amplitude is shown in real space rather than in k space; it is therefore complex even though α_k^κ

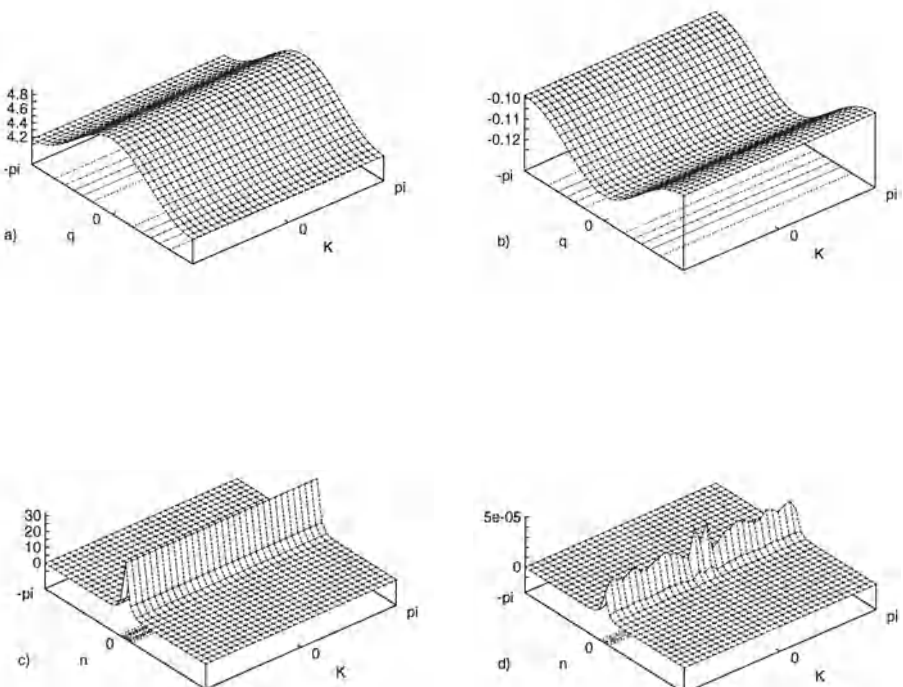


Fig. 5. Complete variational solutions with the GL method for the case $g = 5$ and $J = 9$; a) β_q^κ , b) γ_q^κ , c) $Re\{\alpha_n^\kappa\}$, d) $Im\{\alpha_n^\kappa\}$. The apparently-finite amplitudes in d) are smaller than the error tolerance set for the computation, and so are zero for the purposes of calculation; we note, for example, that $\alpha_{n=0}^\kappa$ is real by construction.

is real. First, we observe the very compact spatial structure of the polaron for all values of the total crystal momentum. The real part of the exciton amplitude is again essentially independent of κ , with most of the amplitude localized on a single site, and most of the remainder concentrated on the nearest neighbors. The imaginary part $Im\{\alpha_n^\kappa\}$ in this case is small beyond the limits of our computation, the apparently-finite amplitudes evident in Fig. 5 being equivalent to zero under the applicable precision criteria. This spatial structure is again mirrored in the phonon amplitudes: both β_q^κ and γ_q^κ are quite flat, essentially independent of κ , with the weak modulation in q being nearly sinusoidal, reflecting a slight spreading of the lattice distortion to nearest neighbors but very little beyond. Note that most of the phonon amplitude is carried by the β amplitude, with only a small portion being

carried by the γ amplitude (which is why the Toyozawa method captures the small-polaron-like regime well even when there is a small amount of spreading of the exciton amplitude).

Next we consider parameter values near our other exact benchmark results, namely, the weak coupling regime. As discussed in Sect. 2.2, the behavior of the system in the weak coupling limit is different in the non-adiabatic ($J < 1/4$) and adiabatic ($J > 1/4$) regimes. In the non-adiabatic regime very near $g = 0$ the system is not very interesting since the polaron is essentially a free exciton with no phonons. More interesting is the behavior in the non-adiabatic regime, especially when g is no longer quite so small, so that one can see the beginnings of the structure that at sufficiently large coupling becomes the small polaron. Also interesting is the behavior in the adiabatic weak coupling regime where in portions of the band one has essentially a free exciton with no phonons, while in other portions of the band the lowest energy state consists of an exciton carrying essentially no momentum and a single phonon carrying essentially the entire crystal momentum.

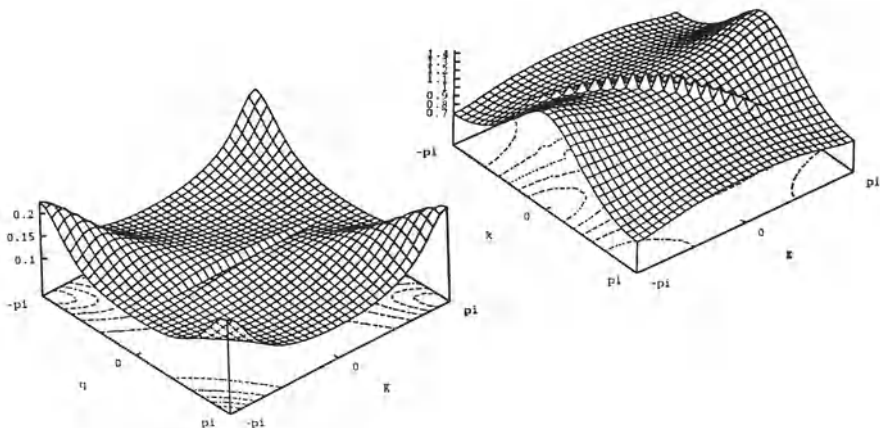


Fig. 6. β_q^κ (first panel) and α_k^κ (second panel) for $g = 0.1$, $J = 0.2$ with the Toyozawa method. $\alpha_{n=0}^\kappa = 1$.

Figure 6 shows the amplitudes (obtained by the Toyozawa method) in the non-adiabatic regime when g is not so very small. The κ -dependence of β_q^κ is relatively strong while that of α_k^κ is weak, suggesting that the phonon cloud is more responsive to dynamics than is the exciton component. Both the exciton and phonon surfaces are characterized by mean values significantly above zero, implying that the real space profiles of both components contain strong central amplitudes. The distortions of the variational surfaces around these mean amplitudes reflect the degree and manner in which the real-space amplitudes extend beyond this central peak. A sinusoidal modulation of any size

in q or k maps into nearest-neighbor real-space amplitudes, and distortions of more anharmonic quality reflect the spreading of the real-space amplitudes beyond nearest neighbors. In the particular case illustrated in Fig. 6, the nearly sinusoidal variation of α_k^κ around a strong, finite background implies a strong central amplitude, small amplitudes on nearest neighbors, and very little amplitude beyond nearest neighbors (as in our previous example). The accompanying phonon surface bears more careful interpretation. The strong, finite background in β_q^κ implies the existence of a strong central amplitude, but the strongly non-sinusoidal excursions near $q = \kappa$ indicate the presence of a broad background component with a prominent modulation of wave vector $q = \kappa$ that reaches its peak amplitude at the Brillouin zone boundary. This growth in the κ -dependent background component is reflective of the increasing strength of exciton-phonon interactions as the “gap” between the free-exciton energy band and the one-phonon continuum decreases. This gap reaches a minimum at the zone boundary, and consequently exciton-phonon interactions are strongest there. This is essentially a level-repulsion phenomenon resulting in the modulation of the multi-phonon cloud by the nearby one-phonon states at a given κ , and is thus a signature of quantum behavior. The appearance of non-negligible asymmetry in the phonon amplitudes is part of this effect, and the absence of any significant related asymmetric feature in the exciton amplitudes may be taken as one indication that the asymmetric phonon structure is in some nontrivial respect “free”.

There are no dramatic changes in the character of variational solutions as J and g are varied within this small- J regime. Overall trends are that the surfaces shown in Fig. 6 flatten as $J \rightarrow 0$ at fixed g and as g either vanishes or diverges at fixed J . The only significant qualitative deviation from the illustrated case is that for J sufficiently small, the zone-edge features seen so prominently in Fig. 6a become insignificant because the energy gap between the free exciton band and the one-phonon continuum is too large for the latter to significantly affect the structure of the phonon cloud. In this *very-small- J* regime, the phonon amplitudes are nearly independent of κ for all coupling strengths, and show “locking” characteristics similar to those discussed earlier.

Next consider weak-coupling behavior in the adiabatic regime, specifically the parameter values $J = 9$ and $g = 1$ (see Fig. 2). The amplitudes for this case, obtained with the GL method, are shown in Fig. 7. In this large J regime the less complex variational states do not adequately capture the quantum aspects of the problem. This solution is marked by a host of features typical of the weak-to-intermediate-coupling regime. The real part of the exciton amplitudes is nearly independent of κ and symmetric about its centroid in real space, spanning a non-trivial number of lattice sites with a rather peaked, pulse-like profile. A deviation from the smooth κ behavior can be seen in the “breaks” in the vicinity of $\kappa = \pm\kappa_c$, the values of κ where the one phonon energy intersects the free exciton band (recall Fig. 1). The imag-

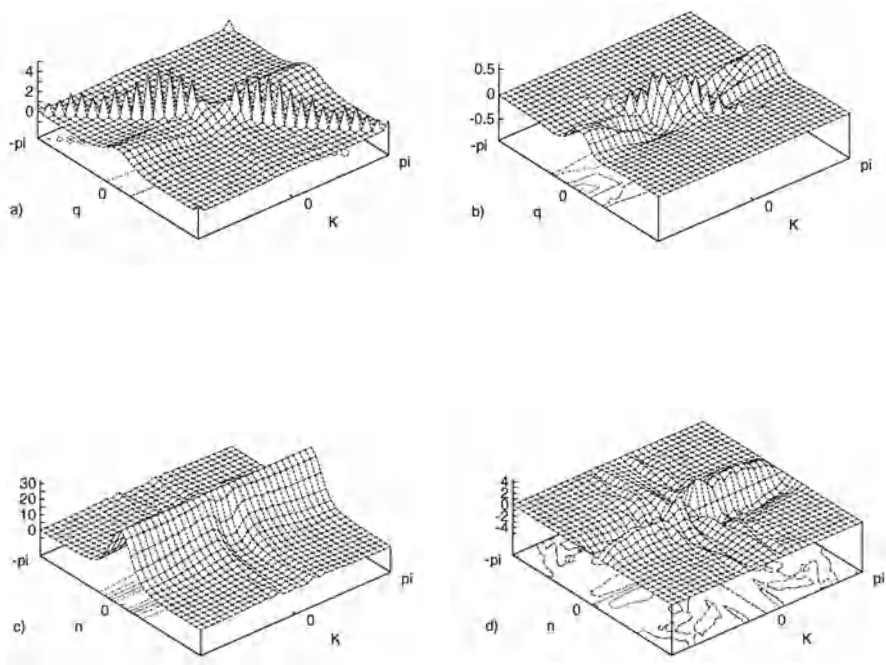


Fig. 7. Complete variational solutions from the GL method for the case $g = 1$ and $J = 9$; a) β_q^κ , b) γ_q^κ , c) $Re\{\alpha_n^\kappa\}$, d) $Im\{\alpha_n^\kappa\}$.

inary part of the exciton amplitudes are small, but finite, accounting for only approximately 0.7% of the total exciton density; however, this small part is antisymmetric about its centroid with its most significant excursions coincident with those of the real part. Moreover, this small imaginary part varies with κ , indicating a momentum sensitivity consistent with the imaginary part of a particle probability amplitude. The β amplitude is characterized by two prominent features, one a rather weak pulse-shaped component that appears to be strongly correlated with the exciton amplitudes (remnants of locking). This portion might be associated with the so-called “large polaron” often mentioned in the polaron literature. The other feature is a strong wave-like component having wave vector $q = \kappa$ that appears to be essentially uncorrelated with the exciton amplitudes and is suggestive of free phonons. With decreasing coupling in this regime the γ amplitudes grow both in absolute and relative strength, and acquire a distinctive shape. The γ amplitudes vary

decidedly in κ , reflecting a momentum sensitivity, but this sensitivity appears in two ways: a feature along the $q = \kappa$ line suggesting involvement with the free phonon component of the β amplitudes, and a κ -dependent pulse-shaped component suggesting involvement with the correlated exciton–phonon pulse already discussed. All components show distinct breaks in the vicinity of $\kappa = \pm\kappa_c$ with distinct structure clearly evident in the inner tenth of the Brillouin zone.

Overall, it must be said that the α and β components of these solutions compare well with the shapes and trends in the corresponding solution components as computed by the Toyozawa method. However, there is no correspondent in the Toyozawa or Merrifield methods to the γ component that by our direct computation has been shown to be qualitatively distinct and of non-trivial magnitude, *at least* in the adiabatic weak-coupling regime.

It is worth noting at this point that the Merrifield method cannot, by construction, capture a single-phonon contribution in a satisfactory way (also see the subsequent discussion surrounding Fig. 9). A single phonon state can be represented as an infinite superposition of coherent states; the following representation, for example, is exact:

$$b^\dagger |0\rangle = \frac{e^{\frac{1}{2}\rho^2}}{\rho} \int_{-\pi}^{+\pi} d\theta e^{i\theta} \exp[-(\rho e^{-i\theta} b^\dagger - \rho e^{i\theta} b)] |0\rangle. \quad (61)$$

The Merrifield form contains only a single coherent state; the Toyozawa form contains a sum and is therefore better able (albeit still approximately) to capture the single phonon behavior; the GL method can do so even more accurately.

A short summation of what has been found so far will help focus our flow of thought. In the strong coupling portion of the parameter phase space (semi-classical regime), “benchmarked” by the exact $J = 0$ small polaron solution, we have found that the polaron form factor is highly localized; both the exciton component and the phonon component are essentially localized on a single lattice site with a small amount of amplitude extending out to nearest neighbors. This is a logical extension of the small polaron solution, which is exact when $J = 0$ and which is seen to be close to the variational solution for nonzero J provided g is sufficiently large. In the weak coupling portion of parameter space (highly quantum mechanical regime), “benchmarked” by the exact weak coupling limit solution, we distinguished between the adiabatic and non-adiabatic regimes. In the latter regime at very weak coupling there is no phonon component at all and the exciton form factor is completely localized. As coupling increases, or as J increases for fixed coupling, the exciton component is still relatively localized. However, the phonon component, in addition to a portion that remains closely correlated with the exciton, now includes an emergent, broad background component. This is the signature of the behavior that becomes apparent once we enter the adiabatic regime. Here there continues to be an exciton–phonon correlated portion in

the polaron, but the free phonon component becomes relatively more prominent with increasing J and/or decreasing g . Distinct structures in the inner and outer portions of the Brillouin zone as defined by κ_c become apparent.

The next question is how the system behaves in the interesting regime of intermediate coupling (highly nonlinear regime), for which we have no benchmark results. To establish this, we will traverse the phase diagram of Fig. 2 downward along the vertical line $J = 4.0$, starting from the strong coupling regime in the upper portion down to the lower portion of the phase diagram. In the polaron literature one often encounters reference to a more-or-less sharp transition, the so-called “self-trapping transition”, between the large polaron region in the lower portion of the phase diagram and the small polaron region in the upper portion of the diagram. It is this regime that we now explore.

On formal grounds, the transition between small and large polaron behavior with changing parameter values is expected to be smooth (Gerlach & Lowen 1987a, Gerlach & Lowen 1987b, Lowen 1988, Gerlach & Lowen 1991) (albeit perhaps very rapid). However, it is common for approximate treatments such as ours to encounter discontinuities where polaron structure changes too rapidly to be represented accurately. Such discontinuities are frequently taken at face value to represent real physical behavior of the system; we stress that they should instead be understood to be artifacts of an insufficiently flexible method. Within this caveat, however, they are convenient “markers” to identify the location of critical points on the phase diagram and thus have at least conceptual utility.

The variational solutions obtained with any of our variational states are found to change incrementally with incremental changes in the parameters J and g over most, but not all, of the phase diagram. The dramatic exception to this smooth behavior occurs in a wedge-shaped region at moderate to large values of J and g . The wedge-shaped region for the Toyozawa method is shown in Fig. 2.

At every point within the wedge-shaped region there exists a κ^* , the particular value of which is dependent upon J and g , at which the variational energy band $E(\kappa)$ is not smooth. More specifically, the variational solutions in a neighborhood around κ^* are not unique, such that the family of solutions continuous with unique solutions at high κ cease to be the minimum energy solutions below κ^* , and the family of solutions continuous with unique solutions at low κ cease to be the minimum energy solutions above κ^* (see Fig. 8). In such cases, the states above κ^* can be interpreted as small polaron states, and the states below κ^* can be interpreted as large polaron states, and the “event” marked by κ^* can be understood as a κ -dependent self-trapping transition at fixed J and g .

The common notion of a self-trapping transition is specifically associated with discrete changes in properties of the ground state, that is, the $\kappa = 0$ state, as J and/or g are varied; for example, the effective mass (60),

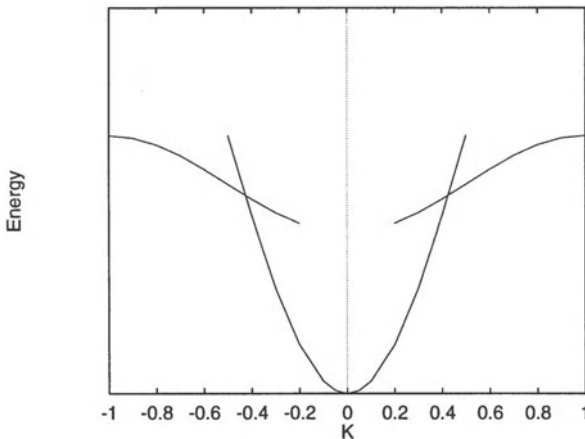


Fig. 8. Schematic illustration of the typical variational situation in the transition region. Two distinct classes of stable solution exist, and *coexist* over a limited range of κ . The variational energy band is arrived at by discarding the higher-energy solutions and joining the resulting branches at their intersection. $K = \kappa/\pi$.

whose rapid change or jump is the traditional hallmark of self-trapping (see Sect. 5.3). Such discrete behavior yields a self-trapping “line” in parameter space separating large and small polaron structures. The κ -dependent self-trapping transition we observe is discrete in a different way: since κ^* ’s exist over a range of J and g , there is not a single transition line, but instead a transition *region* within which the transition *moves* through the band. At every point in this region, the band is interpretable as large-polaron-like at small κ , and small-polaron-like at large κ . The notion of a self-trapping transition is thereby generalized; the usual notion is recovered, however, if from any point within the transition region the coupling parameter is increased sufficiently. In response to increasing coupling strength, κ^* moves toward the center of the Brillouin zone, such that $\kappa^* \rightarrow 0$ at some finite g . At this point, the $\kappa = 0$ solution changes abruptly from being of large polaron character to small polaron character, with properties such as the effective mass experiencing the discrete changes one would expect (see Sect. 5.3).

To clarify how this transition can be at once sharp in κ but broad in J and/or g (or vice versa), we show in Fig. 9 three optimal β_q^κ surfaces representing a transit from strong to weak coupling at fixed J obtained with the Merrifield method (recall that the Merrifield method involves only the β surface); these surfaces do not correspond to points explicitly noted for discussion in Fig. 2 nor is it important for our purposes here (although we will subsequently) to specify what particular value of J and sequence of values of g they correspond to; rather, they are shown because they present in partic-

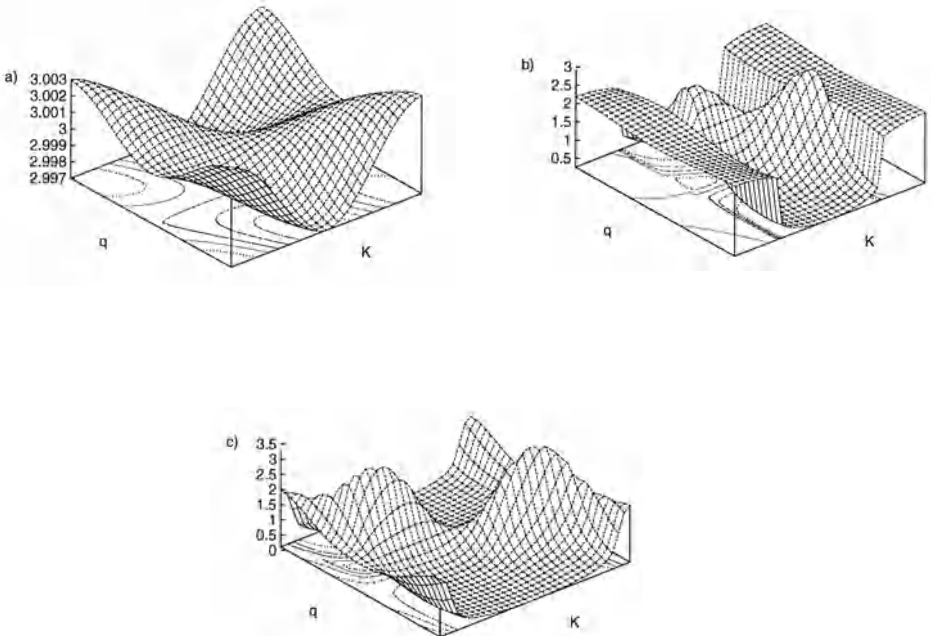


Fig. 9. β^κ obtained with the Merrifield method at fixed J for three different values of g . a) large g , unique solution in the small polaron regime. b) Intermediate g , mixed solution characteristic of the transition region. c) Small g , unique solution in the large polaron regime. Note the differences in scale among these figures and also between these figures and others shown earlier.

ularly clear fashion the nature of the transition. The strong coupling surface (a) is typical of “small polaron” solutions discussed previously. These solutions are characterized by weak undulations around a mean value reflecting a lattice distortion highly localized in real space.

The weak coupling surface (c) is typical of “large polaron” solutions. For small κ , phonon amplitudes are nearly symmetric in q (momentum-poor) and fall off in smooth, pulse-like fashion as q ranges from the zone center to the zone edge, reflecting a pulse-like lattice distortion spanning many lattice sites as is typical of large polarons. At large κ , phonon amplitudes are

strongly asymmetric in q (momentum-rich), imperfectly reflecting the strong one-phonon contribution character of the target solutions at weak coupling as previously discussed (as noted earlier, the Merrifield state, containing only a single phonon coherent state, has difficulty capturing this one-phonon contribution); continued lowering of g from this value would see this asymmetric component narrow toward an arc of delta-functions near the $q = \kappa$ line. At highest κ , near the Brillouin zone boundary, phonon amplitudes again become nearly symmetric in q (momentum-poor) with a mean value significantly greater than at the Brillouin zone center; this reflects a significant contraction of the lattice distortion in real space, and in some respects is more suggestive of small polaron structure.

The intermediate coupling surface is typical of the transition region; the obvious discontinuity marks the location of κ^* for these parameters. The low- κ portion of the surface is strikingly similar to the large-polaron surface at weak coupling, and the high- κ surface is strikingly similar to the small-polaron surface at strong coupling. As one varies parameters so as to cross the transition region, say from weak to strong coupling at fixed J , the discontinuity marked by κ^* moves toward the zone center, consuming the large polaron fraction of the variational solutions until finally, at the traditional self-trapping line (the upper boundary of the transition region), only small polaron contributions remain.

For values of J less than the “critical value” J_c , it is still the case that solutions are “large-polaron-like” at weak coupling, and “small-polaron-like” at strong coupling; however, the transition between these two occurs smoothly.

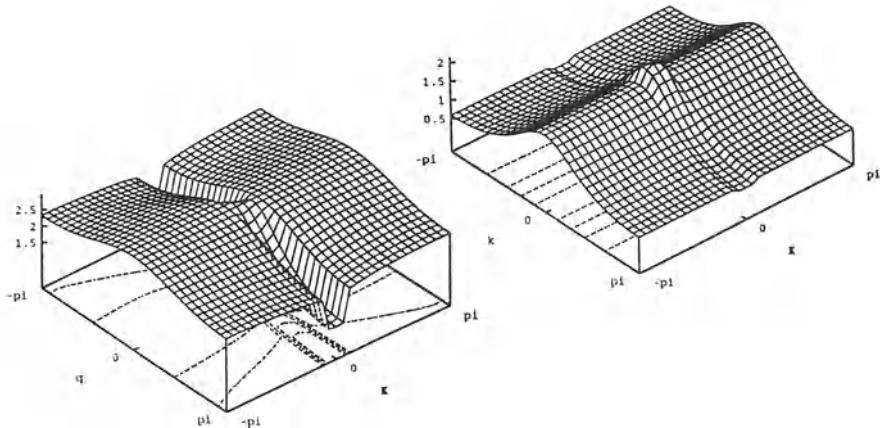


Fig. 10. The phonon displacement β_q^κ (first panel) and the exciton amplitude α_k^κ (second panel) for $g = 2.95$, $J = 4.0$ obtained with the Toyozawa method. $\alpha_{n=0}^\kappa = 1$.

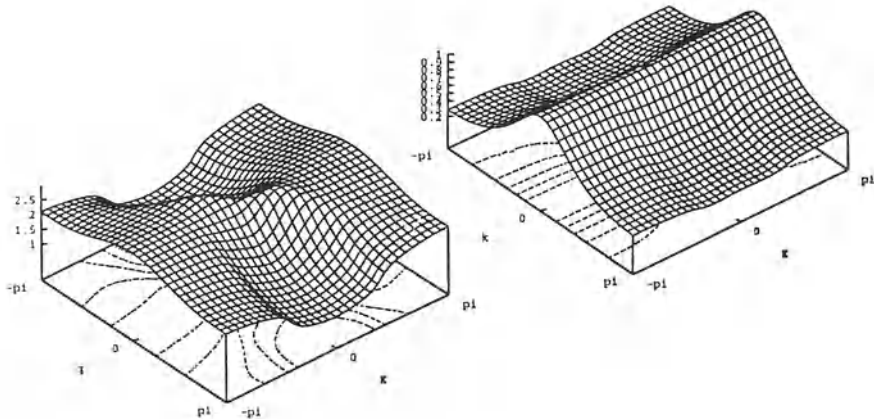


Fig. 11. The phonon displacement β_q^κ (first panel) and the exciton amplitude α_k^κ (second panel) for $g = 2.75$, $J = 4.0$ obtained with the Toyozawa method. $\alpha_{k=0}^\kappa = 1$.

Let us now return to the points indicated explicitly on Fig. 2 and traverse once again the transition region, this time with J fixed at $J = 4$ and using the Toyozawa method. The tongue shown in the figure encloses the region in which the Toyozawa method leads to two variational solutions

Above the transition region, β_q^κ and α_k^κ are “locked”, and are not much different in shape from those in Fig. 3 except that the real-space width of the polaron is increased at comparable values of exciton-phonon coupling strength.

Lowering g through the upper boundary of the transition region causes abrupt changes in the variational amplitudes near $\kappa = 0$, where large-polaron-like structure suddenly appears, bracketed by small-polaron-like structure at higher κ 's (see Fig. 10). When approached from the strong coupling side as we have described, the abrupt change first appears at $\kappa = 0$, identifying the upper edge of the transition region with the traditional notion of a self-trapping transition as widely discussed in the literature. For parameter sets *within* the transition region, variational quantities are smooth within the inner and outer Brillouin zones but vary abruptly at $\pm\kappa^*$. Indeed, while the energy is continuous at $\pm\kappa^*$, most other quantities display jump discontinuities at these points. The polaron structure in the inner zone is in all qualitative respects the same as we have identified with larger polarons, and the structure in the outer zone is likewise the same as we have identified with small polarons; thus, the wave vectors $\pm\kappa^*$ mark momentum-dependent transitions between small and large polarons structure — self trapping — at *fixed J and g*.

When g is lowered below the transition region, clear distinctions remain between different types of correlation structures, though the characteristic

small and large polaron structures are smoothly joined in J , g , and κ . Figure 11 shows such a case for $g = 2.75$, $J = 4.0$. Large κ states remain small-polaron-like, while the zone center states adopt large polaron correlations showing the characteristic increased width of the lattice distortion in real space and a richness of phonon momentum above κ_c . Although the complete solution here is smooth in all respects, a relic of the κ -dependent self-trapping discontinuity of Fig. 10 is clearly evident, though shifted to higher κ as is characteristic of the movement of this feature through the band with changes in coupling strength. As seems typical across much of the phase diagram, away from the transition region the exciton component seems much less sensitive to the crystal momentum label, being nearly independent of κ except for some very weak variations that correlate with the changes in overall polaron structure.

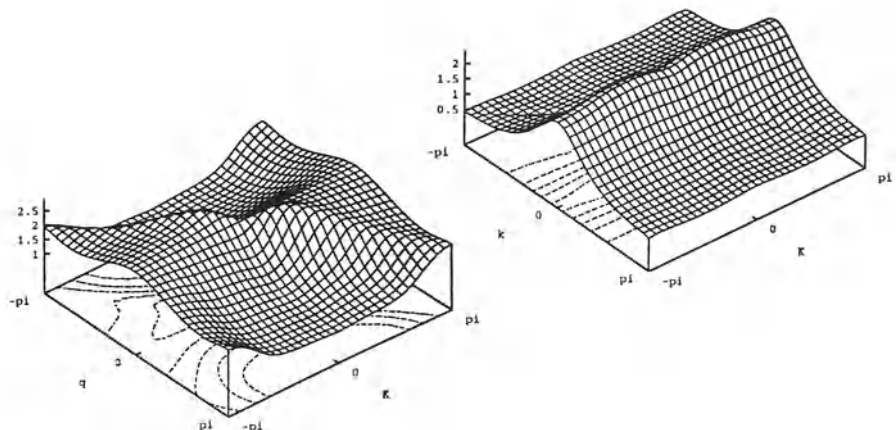


Fig. 12. The phonon displacement β_q^κ (first panel) and the exciton amplitude α_k^κ (second panel) for $g = 2.5$, $J = 4.0$ obtained with the Toyozawa method. $\alpha_{n=0}^\kappa = 1$.

As coupling is decreased further, to $g = 2.5$, the self-trapping related “break” evident at low and intermediate κ in Figs. 10 and 11 respectively reaches the Brillouin zone boundary (see Fig. 12). Though not a sharp transition, we may say that this roughly indicates the value of coupling below which the polaron structure is essentially large-polaron-like for all κ . The ridge in the phonon amplitudes along the line $q = \kappa$ signals the emergence of a one-phonon structure, and the persistence of a “locked” component can still be seen. With a further decrease in coupling to $g = 2.0$, the one-phonon structure is clearly resolved against a background component that is clearly locked with the exciton amplitudes (see Fig. 13). Both the exciton and phonon components of the locked structure show large-amplitude variations in q and k that are strongly anharmonic, reflecting real-space amplitudes that span many lattice sites.

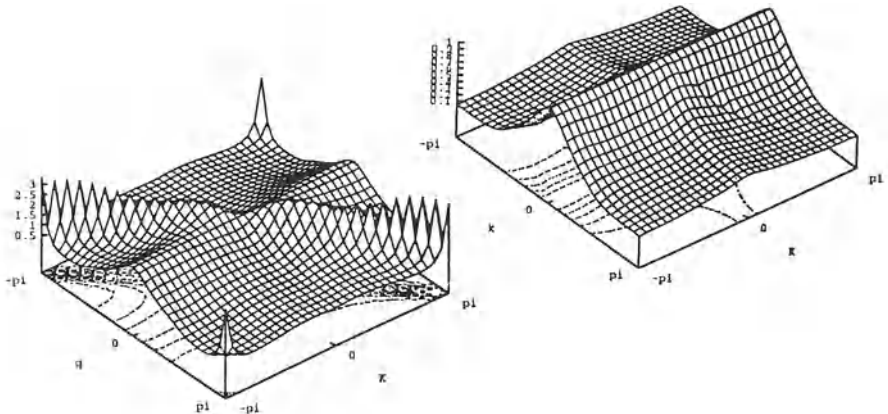


Fig. 13. The phonon displacement β_q^κ (first panel) and the exciton amplitude α_k^κ (second panel) for $g = 2.0$, $J = 4.0$ obtained with the Toyozawa method. The coexistence of a broad, “locked” exciton-phonon structure and “free” one-phonon component is clear. $\alpha_{k=0}^\kappa = 1$.

5.2 More on Phase Diagram and Self-trapping Transition

The specific solutions presented above exemplify the characteristic structures found in varying degrees of resolution and intensity throughout the parameter space of the Holstein Hamiltonian. We have seen that certain features of these structures and/or certain regions of parameter space are well represented even with the less sophisticated variational states (particularly in the strong coupling small-polaron-like semiclassical regime), whereas others (such as the increasingly quantum mechanical behavior in the weak coupling adiabatic regime) require states of increasing sophistication for accurate representation. We have now also discussed the variational solutions in the highly nonlinear intermediate coupling regime. To complete the picture it is important to discuss the progression of the different methods in capturing polaron behavior in this intermediate region.

The phase diagram as presented in Fig. 14 reflects the collected wisdom of each of our three calculations regarding the location of the self-trapping transition. The most prominent feature of the phase diagram at each level of calculation (i.e., by the Merrifield, Toyozawa, or GL method) is the wedge or tongue-shaped region within which the dependence of the variational energy on J , g , and κ is not smooth. As discussed above, the nature of this non-analyticity is such that within the indicated regions there exists a function $\kappa^*(J, g)$, different for each calculation method, such that the minimum-energy states at small κ ($|\kappa| < \kappa^*$) are large-polaron-like, while the minimum-

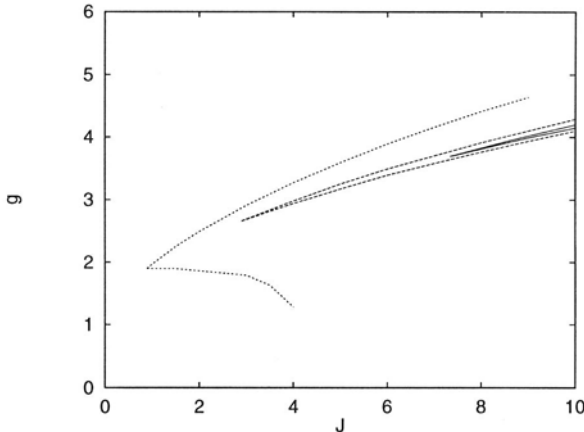


Fig. 14. Phase diagram. Nested wedge- or tongue-shaped sectors indicate those regions in which variational solutions exhibit self-trapping related discontinuities: Outermost tongue - Merrifield method, $J_c = 0.89$, $g_c = 1.90$. Intermediate tongue - Toyozawa method, $J_c = 2.9$, $g_c = 2.66$. Innermost tongue - GL method, $J_c = 7.34$, $g_c = 3.69$.

energy states at high κ ($|\kappa| > \kappa^*$) are small-polaron-like. The traditional self-trapping transition associated with the notion of a discrete jump in the polaron effective mass corresponds to the limit $\kappa^* \rightarrow 0$; i.e., to the point at which the large polaron region $\kappa \in (-\kappa^*, +\kappa^*)$ is squeezed out of existence. The set of points satisfying the condition $\kappa^*(J, g) = 0$ thus corresponds to the traditional notion of a “self-trapping line”. The self-trapping line so defined corresponds to the strong-coupling boundary of the broader κ -dependent transition region associated with each calculation method.

On formal grounds, it is expected that there is no true non-analyticity to be found in the physical system, suggesting that the discontinuous behaviors we associate with self-trapping phenomena are artifacts of insufficiently flexible methodologies (Gerlach & Lowen 1987a, Gerlach & Lowen 1987b, Lowen 1988, Gerlach & Lowen 1991). Our sequence of variational calculations supports this view, showing how incremental refinement of the variational states results in shrinkage of the fraction of the parameter space exhibiting self-trapping related discontinuities; for example, considering the sector of parameter space displayed in Fig. 14, more than half of the displayed area is affected by self-trapping discontinuities under the Merrifield method, shrinking to approximately 1.4% under the Toyozawa method, and to only 0.08% under the GL method. Moreover, this shrinkage is accompanied by a shift of the onset of discontinuities to more extreme parameter values; the values $J_c = 7.34$, $g_c = 3.69$ characterizing the GL method leave a large (J, g) domain free of self-trapping artifacts. It is now meaningful to reveal that the

sequence of amplitudes shown in Fig. 9 correspond to $J = 2$ and $g = 3, 2, 1$; the Toyozawa and GL methods show no discontinuities for this value of J . The amplitudes shown in Fig. 10 correspond to $J = 4$, where the GL method exhibits no discontinuities.

Although self-trapping discontinuities thus appear to be the artifactual results of using insufficiently flexible variational states, the fact nevertheless remains that polaron states in this regime reflect highly nonlinear behavior in the sense that physical quantities may vary very rapidly (albeit continuously) with changing parameter values. This behavior is explored further in the next subsection.

5.3 Energy Bands and Effective Mass

We have seen that the structure of polaron energy bands at general parameter values is strongly influenced by the limiting behaviors at small g and small J .

At zero coupling, the free exciton energy band enters the one-phonon continuum at κ_c , such that the energies of the *joint* ground states of the exciton-phonon system are given by (22),

$$\begin{aligned} E(\kappa) - E(0) &= 2J[1 - \cos(\kappa)] \quad \text{for} \quad |\kappa| < \kappa_c , \\ &= 1 \quad \text{for} \quad |\kappa| > \kappa_c . \end{aligned} \quad (62)$$

with κ_c given by the relation (21). The changes in band structure that occur as the exciton-phonon coupling is turned on display some of the characteristic features of level repulsion. Since the wave vector κ_c marks a crossing of the bare exciton and bare phonon level sets, energies in the vicinity of κ_c respond more strongly to weak exciton-phonon coupling than do energies at higher or lower κ . The first such effect is a rounding of the angular feature at $\pm\kappa_c$, and for a significant interval of coupling strength, the primary effect of increasing coupling is the progressive rounding of this feature and a gradual smoothing of the overall energy band spreading outward to higher and lower κ from these points. Only after reaching a significantly finite value of the exciton-phonon coupling strength does this smoothing of the energy band progress to the point that the band begins to narrow.

Quite distinct from this is the archetypical small polaron energy band, which takes the simple form

$$E(\kappa) = -g^2 - 2Je^{-g^2} \cos(\kappa) . \quad (63)$$

This is the result of applying the displaced-oscillator transformation at small J and neglecting all finite- J corrections (Lang & Firsov 1962). More generally, of course, the dependence of the energy band on the transfer integral J is substantially more complex; however, it is generally expected that the above

small polaron form is recovered at finite J for coupling strengths that are “large enough”.

Qualitatively, then, one expects band shapes similar to (62) at weak coupling to distort into shapes similar to (63) at strong coupling and this is, generally speaking, what we find.

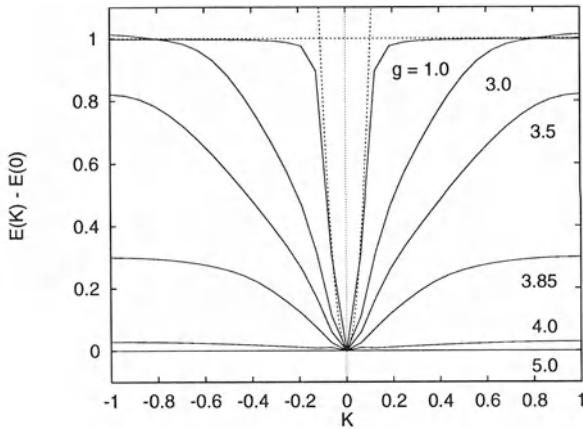


Fig. 15. Shifted energy bands $E(\kappa) - E(0)$ for $J = 9.0$, $g = 1, 3, 3.5, 3.85, 4.0, 5.0$ as computed by the GL method. The dotted, nearly parabolic curve at center is the appropriate portion of the free exciton band $2J[1 - \cos(\kappa)]$. The segmented appearance of some curves is an artifact of finite lattice sizes in our computations. $K = \kappa/\pi$.

Figure 15 shows a sequence of polaron energy bands for $J = 9$ for assorted coupling strengths. This particular sequence clearly shows how the principal effects of the exciton-phonon interaction at weak-coupling are confined to a small region near κ_c , and that only minor changes occur at either large or small κ until the smoothing of the level-crossing feature spreads essentially over the entire band. Consequently, the polaron band width is saturated essentially at unity until $g \approx 3$, then decreases rapidly, encountering the self-trapping transition when $g \approx 4$, after which narrowing continues beyond the resolution of the figure. Above the self-trapping transition the energy band is nearly sinusoidal and strongly narrowed, suggesting a small polaron form; however, non-trivial finite- J corrections remain. Figure 4 shown earlier compares energy bands computed by the GL method with energy bands computed by the Toyozawa method for $J = 2.0$ and various values of g .

Figure 16 shows the dependence of the polaron bandwidth on g for J 's ranging from 2 (see Fig. 4) to 9 (see Fig. 15). Consistent with the discuss-

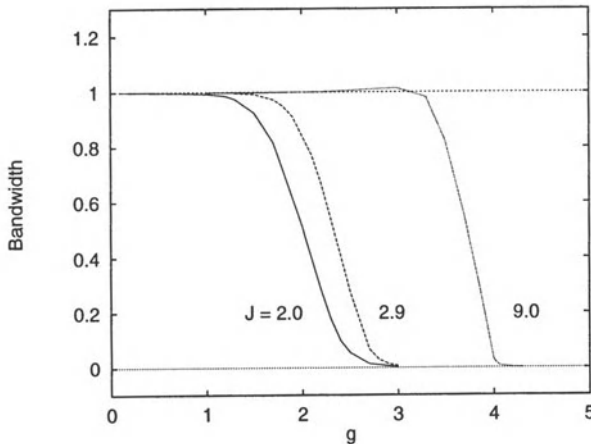


Fig. 16. Polaron bandwidths $E(\kappa = \pi) - E(\kappa = 0)$ as computed by the GL method vs. exciton-phonon coupling strength g ; curves left to right: $J = 2.0$, 2.9 , and 9.0 .

sion above, the bandwidth is near unity up to a finite J -dependent value of g , then it drops rather quickly as the band narrows through the “self-trapping-transition” region, and the continued narrowing beyond that can not be resolved on the scale of this figure.

Considering the role of the one-phonon continuum in determining the structure and energies of the higher-momentum polaron Bloch states, it is expected that the width of the polaron band should always be less than unity at finite exciton-phonon coupling. The Merrifield method fails to meet this criterion over large portions of parameter space (Zhao *et al.* 1996b). The Toyozawa method improves greatly in this respect over the Merrifield results but still fails to a significant extent (Zhao *et al.* 1997a). The GL method does much better; all is not perfect however, since there is still a small overshoot of the expected maximum band width seen for $J = 7.34$ in Fig. 16 (and might be greater for larger J). Still, consistency with the saturation criterion is sufficiently well satisfied to inspire confidence in the picture of band widths so captured.

The polaron effective mass is determined by the curvature of the energy band near $\kappa = 0$, as defined in (60). From Fig. 15 and the discussion surrounding (62) it follows that up to a finite (J -dependent) value of the coupling constant the curvature at the bottom of the band does not change much and one therefore expects the effective mass to be close to m_0 , the effective mass of the bare exciton, cf. (9). On the other hand, for strong coupling the small polaron result (63) yields the greatly increased effective mass $m_{eff} = m_0 e^{g^2}$. The rapid increase in the effective mass is the traditional

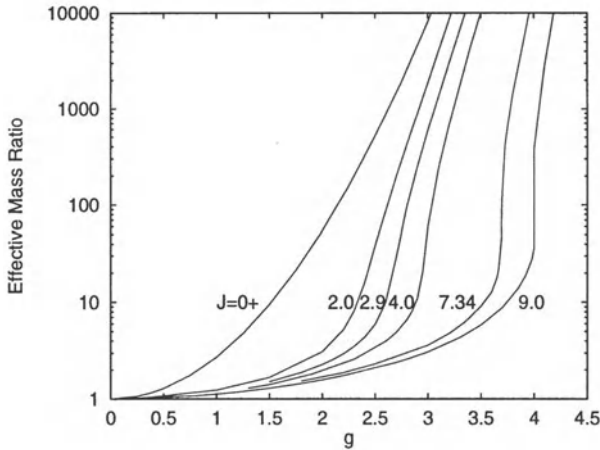


Fig. 17. The ratio of the polaron effective mass to the bare effective mass (m_{eff}/m_0) as obtained with the GL method is plotted against exciton-phonon coupling on a logarithmic scale for $J = 2, 2.9, 4, 7.34$, and 9 .

indicator of the self-trapping transition, the transition being evidenced by an actual jump discontinuity in the effective mass, and the onset of the transition being marked by the parameter values at which such jumps first appear.

The effective mass obtained with the GL method is shown in Fig. 17. As anticipated, for finite J the ratio m_{eff}/m_0 remains near unity up to a finite value of the coupling coefficient and then grows rapidly. This growth is rapid but continuous, and in the real physical system we expect this to be the behavior for any J . The onset of rapid growth marks the parameter regime where the rapid transition from small polaron to large polaron structure takes place. The variational methods are not perfect, however, and the GL method, although better in this sense than the Toyozawa or Merrifield methods, still yields a “critical” value of the exciton transfer integral $J_c \approx 7.34$, such that for any $J < 7.34$ the dependence of the effective mass on the coupling constant g is smooth and continuous, while for $J > 7.34$ the tell-tale jump discontinuity appears. Though still discontinuous at sufficiently large J , the effective mass that results from the GL calculation is considerably more smooth than that which results from either the Merrifield ($J_c \approx 0.89$) or Toyozawa ($J_c \approx 2.9$) method (recall Fig. 14).

6 Solitons

Polaron Hamiltonians such as the one in this chapter, and particularly the analogous Hamiltonian built upon acoustic rather than optical phonons, have

been the basis of a great deal of research relating to the possibility that such systems might support weakly scattered, long-lived collective excitations known as “solitons”. The soliton theories to which we refer are approximate treatments involving dynamical equations based on *localized* Ansatz states such as (32) (“Davydov Ansatz state”). Here we assess some of the essential predictions of soliton theory in the light of our variational results (Brown & Lindenberg 1997, Brown *et al.* 1997).

Soliton theory is usually implemented in the dynamical context, wherein a time-dependent variational principle is used (Brown *et al.* 1990). For the Davydov Ansatz state and the Holstein Hamiltonian, the approximate dynamical equations are

$$i\dot{\alpha}_n = -J(\alpha_{n+1} + \alpha_{n-1}) - g\alpha_n(\beta_n^* + \beta_n), \quad (64)$$

$$i\dot{\beta}_n = \beta_n - g|\alpha_n|^2. \quad (65)$$

The time derivatives of the phonon amplitudes in the latter equation are usually neglected; this leads to the *specific* locking relation

$$\beta_n = g|\alpha_n^2| \quad (66)$$

from which follows a discrete nonlinear Schrödinger equation (DNLS)

$$i\dot{\alpha}_n = -J(\alpha_{n+1} + \alpha_{n-1}) - 2g^2|\alpha_n|^2\alpha_n. \quad (67)$$

With a further continuum approximation, this DNLS yields the continuous nonlinear Schrödinger equation (NLS)

$$i\dot{\alpha}(x, t) = -J\frac{\partial^2\alpha(x, t)}{\partial x^2} - 2J\alpha(x, t) - 2g^2|\alpha(x, t)|^2\alpha(x, t) \quad (68)$$

in which the space variable x is in units of the lattice constant. This is a completely integrable nonlinear wave equation that supports true soliton solutions. The static soliton solution has the profile

$$\alpha(x) = \sqrt{\frac{\lambda}{2}} \operatorname{sech}(x/\lambda) \quad (69)$$

in which the width parameter is given by $\lambda = 2J/g^2$.

A reasonable comparison of soliton theory with our results would appear to be between localized soliton states and our form factors, and the most important features for comparison involve exciton-phonon correlation properties. Comparison is most direct with our results for the Toyozawa method since the variational state in this case is constructed directly from the Davydov Ansatz state. Comparison with the GL method is a bit complicated by the introduction of the additional phonon amplitudes γ , but in so far as these are small it still makes sense to use the β amplitudes for comparison. Furthermore, we have seen that correlations sensitive to the shape of the exciton

profile are exhibited to a greater degree in the β amplitudes. In any case, the conclusions we arrive at in our comparisons are robust, although we recognize that the measures we choose may not be exhaustive nor even necessarily unique. As we make these comparisons, it should be borne in mind that though our calculations are for the optical phonon case only, while most of soliton theory deals with acoustic phonons, we consider only the most general characteristics of solitons that are found in both acoustical and optical formulations. The measures we focus on are:

1. The locking between the exciton and phonon components in the exciton-phonon structures [locking being a characteristic feature of soliton theories via specific relations such as (66)];
2. The actual shapes of exciton-phonon structures [that of the soliton being the characteristic $\text{sech}(x/\lambda)$ shape of (69)];
3. The dependence of the width of exciton-phonon structures on the adiabaticity and coupling parameters J and g (the width in soliton theories being determined by the ratio $2J/g^2$).

The most transparent favorable connection between our results and those of soliton theory is our finding that “locked” exciton-phonon structures appear over significant regions of the polaron parameter space. Locked exciton-phonon structures are found in both NLS and DNLS descriptions, ranging from broad, smooth “true” solitons to highly-discrete “pinned” states essentially localized on a single lattice site. As our presentation shows, we find some similar qualitative trends in our results. We find that locked exciton-phonon structures of considerable breadth in real space appear systematically in the *weak* coupling (small g) region provided that the exciton transfer integral J is sufficiently large, that is to say, provided the system is sufficiently *adiabatic* (recall that this component is actually visible in Fig. 13). This broad, locked component is soliton-like in several ways: 1) it spans multiple sites in real space; 2) striking shape similarities exist among the exciton and phonon components at all κ ; 3) the shape of the locked components is nearly independent of κ , suggesting that the internal structure of this element is relatively insensitive to the external dynamics; 4) the locked element appears to be insensitive to presence of the coexisting one-phonon structure; and 5) the width of the locked structure increases with increasing J and decreasing g .

There is, however, already one important feature of our results that is not captured in soliton theory: in the same adiabatic weak-coupling regime where soliton-like, locked exciton-phonon structures are perhaps identifiable, we *also* find a strong component having the character of a single free phonon quantum (clearly visible in Fig. 13). Such highly quantum mechanical phonon structures are beyond the scope of soliton theory; yet, as we have seen, they are present (and correctly so) in a significant fraction of the total number of Bloch states. In particular, the one-phonon component is located primarily at $|\kappa| > \kappa_c$ (in Fig. 13, $\kappa_c \approx 0.16\pi$) (Zhao *et al.* 1996b, Zhao *et al.* 1997a, Brown

et al. 1997). It would therefore appear that the most favorable comparison with soliton theory would be found in that part of the total polaron solution *least* affected by such highly quantum mechanical features, that is, in the $|\kappa| < \kappa_c$ regime. This region would appear to be favorable as well due to the fact that soliton theories tend to be long-wavelength theories, relying on large excitation widths in real space to justify continuum approximations. Moreover, since the dynamics of solitons in real systems seem even more controversial a matter than the notion of a soliton-like ground state solution, it would appear that the $\kappa = 0$ state in particular should afford the most favorable comparisons. In our quantitative diagnostics we therefore concentrate on the $\kappa = 0$ state. Of course, our $\kappa = 0$ state is delocalized, so the search for correspondences must be based on the amplitudes describing the internal structure of the polaron.

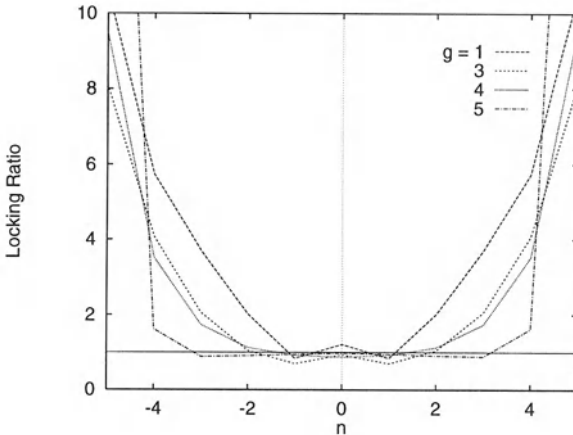


Fig. 18. The locking ratio $\beta_n^{\kappa=0}/(g|\alpha_n^{\kappa=0}|^2)$ for $g = 1, 3, 4$, and 5 obtained with the GL method; a locking ratio equal to unity for all n would indicate consistency with the locking relation typical of soliton theory. $J = 9$ for all curves.

As a means of quantifying the relationship between the exciton and oscillator amplitudes in this illustration, we consider a “locking ratio” motivated by (66). Figure 18 shows the ratio $\beta_n^{\kappa=0}/(g|\alpha_n^{\kappa=0}|^2)$ for $J = 9$ and a number of values of the coupling strength g . Here we have used the β and α amplitudes obtained with the GL method. Were it true that the exciton and lattice components are locked as assumed under soliton theory this ratio would be equal to unity for all n . The figure shows otherwise – it is evident that the quality of the locking is rather poor. A similar set of curves obtained with the Toyozawa method for $J = 4$ (Brown & Lindenberg 1997) leads to even poorer locking results.

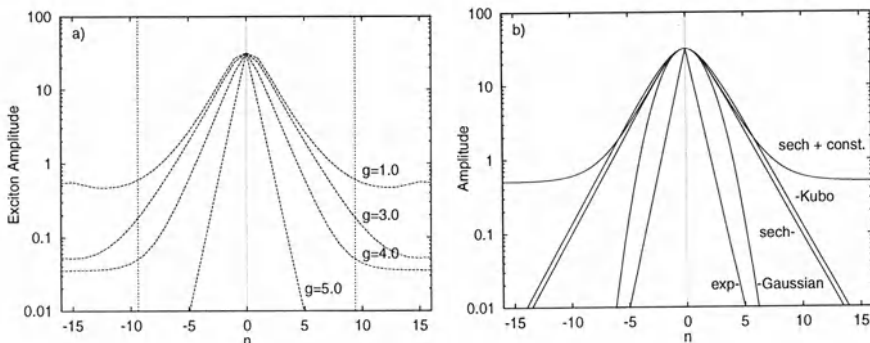


Fig. 19. Exciton amplitudes for $J = 9$, $\kappa_c = 0.1066\pi$. Panel a), $\alpha_n^{\kappa=0}$ plotted on a logarithmic scale for $g = 1, 3, 4$, and 5 obtained with the GL method. Vertical dotted lines indicate the value of π/κ_c , which here is 9.38. Panel b), sample curves showing some quasi-exponential shape functions.

To test the second characteristic feature of soliton theories, namely, the characteristic $\text{sech}(x/\lambda)$ shape of (69), we show in Fig. 19a unnormalized exciton amplitudes $\alpha_n^{\kappa=0}$ from weak to strong coupling at a large fixed value of J ; this scans across the far right of the phase diagram from bottom to top, showing the characteristic contraction of the exciton profile with increasing g . All exciton amplitudes are scaled such that the peaks of all profiles are the same magnitude, and these are then plotted on a logarithmic scale in order better to discriminate distinct quasi-exponential shapes, and to remove the distortions associated with the squaring of the exciton amplitude that is sometimes relevant to shape. Rather than curve fit, we have also plotted in the companion Fig. 19b a family of quasi-exponential shape functions. Some observations are immediately evident – the computed exciton profiles are all plainly *inconsistent* with a Gaussian dependence except over a narrow interval near the peak of the weak-coupling curves, and the strong-coupling curve (*above* the self-trapping transition) is unquestionably exponential. Much more intriguing are the shapes found at weaker values of coupling, at ($g = 4$) or below the self-trapping transition ($g = 1, 3$). These curves are Gaussian over a narrow interval around the peak of the amplitude profile, but quickly turn over into a clear exponential dependence for a decade or two in amplitude before saturating in the wings. (The saturation effect appears to be a mixture of a subtle intrinsic effect and a finite-lattice effect.) This Gaussian-to-exponential turnover is one of the characteristics of a $\text{sech}(x/\lambda)$ profile, and

it appears that a $\text{sech}(x/\lambda)$ describes the situation rather well at weak values of coupling. One of the characteristics of the $\text{sech}(x/\lambda)$, however, is that the same parameter λ controls the curvature of the profile at the peak and the decay of the profile in the wings. Close inspection of all curves suggests that while this one-scale-fits-all dependence may be satisfactory at weak coupling, it does not consistently describe the full set of shapes found. An example of an alternative that exhibits the correct overall trends, but is unrelated to any soliton theory, is the Kubo function (Kubo & Tomita 1954, Kubo 1954, Kubo 1961, Kubo & Toyabe 1967)

$$f(x) = \exp\left\{-\frac{1}{\lambda a}[e^{-a|x|} - 1 + a|x|]\right\}. \quad (70)$$

This function is Gaussian ($\sim \exp\{-ax^2/2\lambda\}$) near the peak and exponential ($\sim \exp\{-|x|/\lambda\}$) in the wings, with the crossover occurring around $|x| \sim 1/a$.

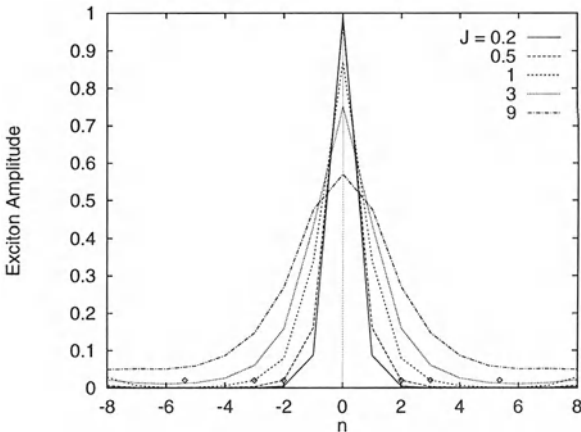


Fig. 20. Exciton amplitude profiles $\alpha_n^{\kappa=0}$ for $g = 1$ obtained with the GL method, subject to the normalization condition $\sum_n |\alpha_n^\kappa|^2 = 1$. Points near the bottom of the figure indicate for $J = 0.5, 1, 3$ the value of the length scale π/κ_c relative to the discrete space variable n . κ_c does not exist for $J = 0.2$ (the free exciton band does not penetrate the one-phonon continuum) and π/κ_c for $J = 9$ falls beyond the edge of the figure.

Our third test focuses on the fact that over much of the regime where soliton theory finds locked exciton-phonon structures, they are characterized by widths that are dependent primarily on the ratio of the tunneling energy to the binding energy, or, in terms of our parameters, the ratio $2J/g^2$. The

widths of the amplitudes in Fig. 19(a) should change by a factor of 25 from $g = 1$ to $g = 5$ if this relation were appropriate; instead only a change by a factor of three is found. In Fig. 20 we show unit-normalized $\alpha_n^{\kappa=0}$ from small to large values of J for a fixed, small value of g ; this scans across the bottom of the phase diagram from left to right, showing the characteristic spreading of the exciton profile with increasing J . When these curves are examined in the same manner as those in Fig. 19(a) and the width measures λ of the quasi-exponential shape function determined, we find that these widths are *not* in proportion to J ; the variation suggests instead a \sqrt{J} dependence.

Our general conclusion on the basis of these three measures (locking ratio, exciton amplitude shape, and exciton amplitude width) is that it is not possible to reconcile our findings with a soliton-theoretic interpretation.

Elsewhere (Zhao *et al.* 1997a) we have given considerable attention to polaron Wannier states, the localized states that energy band theory identifies with the complete set of delocalized Bloch states (Brown 1995a, Wannier 1937, Kohn 1959, Weinreich 1965, Madelung 1978, Brown 1995b). We defer the explicit construction of polaron Wannier states by the GL method to later work (Romero *et al.* 1997); however, certain general properties of Wannier states are immediately worthy of note.

In the weak coupling limit ($g = 0^+$), exact polaron Wannier states can be constructed without appeal to any approximation method. In the non-adiabatic regime ($J < 1/4$), these states are trivially identical to the Wannier states of the rigid lattice, and are completely localized on a single lattice site. In the adiabatic regime, however, the exact polaron Wannier states are generally broad, complex states consisting of a localized component upon a uniform background. The half-width of the localized component can be identified with the length scale π/κ_c . It is reasonable to expect that polaron Wannier states should grow more compact with increasing exciton-phonon coupling strength, and this is, in fact, what we found in our finite- g calculations. These findings suggest that the length scale π/κ_c constitutes an upper bound for the half-width of polaron Wannier states. In Figs. 19(a) and 20 we have included elements that allow the computed $\kappa = 0$ exciton amplitude profiles to be compared with the Wannier length scale π/κ_c ; in every case the bulk of the computed exciton profiles fall within the appropriate Wannier width, and from the scaling of our quasi-exponential width estimates with the transfer integral J ($\lambda \sim \sqrt{J}$), it appears that the Wannier length scale is non-trivially involved in determining the width of the localized component over a substantial range of parameters.

7 Conclusion

We have presented a panoramic view of the classic Holstein polaron problem obtained through our implementation of a hierarchy of increasingly sophisticated variational states. To guide us in our analysis we noted the structure

of the polaron in limiting parameter regimes where this structure is known exactly, and tested our variational solutions against these known limits.

In our studies, polaron structure is represented by variational Bloch states constructed from form factors of increasing complexity. The Bloch state construct insures that the demands of translational invariance are satisfied, while the exciton-phonon correlations are built into the form factors. Our variational analysis includes the methods originally introduced by Merrifield, which incorporates local exciton-phonon correlations, by Toyozawa, which incorporates global exciton-phonon correlations, as well as our generalization (GL method) that includes mixed global and local correlations.

The form factors that we have used to implement the variational calculations all involve coherent state descriptions of the phonon amplitudes. Coherent states provide a fairly straightforward representation of the phonon amplitudes when there are many phonons contained in the polaron - that is, in the strong exciton-phonon coupling limit. As one departs from this limit, however, ever more complex superpositions of coherent states are needed to represent the involvement of fewer and fewer phonons in the polaron. The most general superposition of coherent states involves N^2 phonon amplitudes (N is the number of lattice sites), a number that would tax computational resources well beyond the methods that we have implemented. Our methods require only $O(N)$ amplitudes, but we are confident that these methods, especially the GL method, capture the behavior of the system over essentially all of parameter space.

We presented our results in the context of a parameter phase diagram in which each point represents a pair (J, g) of parameter values (the phonon energy $\hbar\omega$ has been set to unity throughout, so that all energies are measured in units of the phonon energy). The variational solutions lead to a number of characteristic behaviors in various regimes of parameter space. These include the small polaron, the large polaron, and nearly-free phonon structures. We have examined in detail the way in which these compete and/or coexist in the parameter regions that connect these characteristic behaviors.

In the strong coupling portion of the parameter phase space (semi-classical regime) we have found that the polaron form factor is highly localized. The exciton component and the phonon component are both essentially localized on a single lattice site, with a small amount of amplitude extending out to nearest neighbors. This small-polaron-like regime is particularly well suited to a coherent state representation. At the other extreme, when exciton-phonon coupling is weak (highly quantum mechanical regime), we distinguished between adiabatic and non-adiabatic regimes depending on the value of J . In the non-adiabatic regime (small J) at very weak coupling the polaron is essentially just the bare exciton; the form factor is completely localized in this limit. As coupling increases in this non-adiabatic regime the exciton remains essentially localized; the phonon amplitude, in addition to a component closely tied to the exciton, develops a broad background component.

This is an emergent signature of the behavior that becomes more pronounced in the adiabatic regime. In the adiabatic regime there continues to be an exciton-phonon correlated portion of the polaron, but a free phonon component becomes relatively more prominent with increasing J and/or decreasing g . Distinct structures in the inner and outer portions of the Brillouin zone become apparent. The defining momentum scale for these distinct structures is κ_c , the magnitude of the crystal momentum κ where the free exciton band intersects the one phonon band.

The intermediate coupling regime is perhaps the most interesting because it is highly nonlinear and encompasses large changes in polaron structure with small changes in parameter values. This is the regime where the so-called “self-trapping transition” occurs. This transition is traditionally thought of as occurring at a particular J -dependent value of g as one increases g for fixed J , and involves a sudden (discontinuous) increase in the effective mass of the polaron as the curvature of the band near $\kappa = 0$ changes from that characteristic of a large polaron (large curvature) to that associated with a small polaron (small curvature). On formal grounds it is expected that this transition not be discontinuous (although it may be very rapid), and so it should be assumed that any discontinuities are artifacts of the restrictions imposed in the construction of variational states. Our results bear out this conclusion while at the same time broadening the concept of the self-trapping transition. For any specific variational method (Merrifield, Toyozawa, Global-Local) we find a region (rather than just a line) in parameter space within which there is a discontinuous transition in polaron structure from “large” to “small” *at some value of κ* . The traditional self-trapping transition corresponds to the parameter values where this change takes place at $\kappa = 0$, and this marks the upper boundary of the transition regions that we have found. We have thus generalized the notion of self-trapping from $\kappa = 0$ to other values of the crystal momentum.

The clearest indication that a discontinuous transition may indeed be an artifactual manifestation of restrictions imposed by the structure of the assumed variational state is the fact that with increasing flexibility of the state, the parameter space region of discontinuity becomes smaller and that the values of J and g that mark the onset of this region move to larger values.

Although the effective mass m_{eff} probes the curvature of the energy band only near $\kappa = 0$ while we have generalized our analysis to the entire band, the effective mass is useful because it is a familiar measure of the structure of the polaron and because it plays a central role in transport studies. We showed that m_{eff} remains fairly constant (that is, relatively insensitive to changes in g) and small (that is, near in value to the bare exciton mass $1/2J$) below the self-trapping transition region. We showed that m_{eff} increases rapidly through this region as the large polaron collapses to a small polaron, and then it continues to grow with g roughly as predicted by small polaron theory. The growth of the effective mass in the intermediate coupling regime

is rapid and, for sufficiently large J in each of the methods that we have implemented, the effective mass increase is discontinuous with g . However, as indicated above, the onset of discontinuities is moved to ever larger J with increasing state flexibility and is believed to be an artifact. The “exact” solution to the polaron problem is expected to show rapid but continuous growth in the effective mass through this region of parameter space.

In addition to this detailed analysis of the energy band near $\kappa = 0$ we have presented an analysis of the behavior of the entire band. The bare exciton band is the familiar cosine band in which the single parameter J determines the bandwidth ($4J$) and the effective mass ($1/2J$). We have confirmed that in the *non-adiabatic* regime ($J < 1/4$) the energy band essentially retains the cosine form but with an effective transfer parameter \tilde{J} associated with the small polaron and hence decreased from J in the usual small polaron fashion. In the *adiabatic* regime ($J > 1/4$), and especially in the highly adiabatic regime ($J \gg 1/4$) the behavior is considerably more complex. In the limit of vanishingly small coupling the band consists of a cosine portion for small $|\kappa|$ and is equal to unity for large $|\kappa|$, the transition occurring at the points $\pm\kappa_c$ where the single phonon band intersects the exciton band. The bandwidth, which is unity in this limit, is unrelated to the effective mass, which is $1/2J$. The principal effects of the exciton-phonon interaction as coupling increases in the weak coupling regime are confined to small regions near $\pm\kappa_c$ as the level-crossing feature spreads outward from this region. In this regime the curvature at the bottom of the band changes very little (consistent with our above description of the effective mass), and the bandwidth remains near unity. Once the level-crossing feature has spread over essentially the entire band, the band begins to narrow and does so rapidly with increasing g through the self-trapping transition region. Beyond this rapid narrowing regime the band is again nearly sinusoidal and continues to narrow with increasing g , in a way that departs from the small polaron form \tilde{J} via non-trivial finite- J corrections.

Although in this chapter we have not dwelt on the detailed improvements afforded by each degree of increasing flexibility in the variational state, but instead have used the results of any method that clarified the physical picture most unambiguously, we have dealt with this issue carefully in Zhao *et al.* (1996a, 96b, 97a) and Brown *et al.* (1997).

Finally, we have explored the connection between our results and those of soliton theory as applied to the Holstein Hamiltonian. Since soliton theory is an example of a variational approach implemented in the *localized framework* while our work has observed the translational invariance of the problem by implementing the variational approaches in the *delocalized framework* of Bloch states, one must be careful in choosing a “fair” basis for comparison. One natural connection would appear to be between the states obtained from soliton theory and the *form factor* from which the Bloch state is constructed in our approach; this connection is particularly direct with the Toyozawa

method since the form factor of the Bloch state in that method is exactly the localized state that appears in Davydov soliton theory. We analyzed three specific measures that are often used to characterize the results of soliton theory: 1) the locking between the exciton and phonon components, a particular form of locking being a characteristic feature of soliton theories; 2) the actual shape of the exciton-phonon structures, that of the soliton being the characteristic sech shape; and 3) the dependence of the width of the exciton-phonon structures on the adiabaticity and coupling parameters, the width in soliton theories being determined by the ratio $2J/g^2$. For each of these measures we found that the variational solutions in the delocalized framework do *not* support the predictions of soliton theory.

We ended this review with a brief mention of polaron Wannier states, the localized states that energy band theory identifies with the complete set of delocalized Bloch states. Exploration of these states and their utility in the context of transport properties and finite temperature properties of the polaron system is one of our future goals.

Acknowledgment

This work was supported in part by the National Science Foundation under Grant No. DMR 91-18052 and in part by the U.S. Department of Energy under Grant No. DE-FG03-86ER13606.

References

- Brown D. W. (1995a): in *Nonlinear Excitations in Biomolecules*, Centre de physique des Houches **2**, 279-286.
- Brown D. W. (1995b): Proceedings of the SPIE - The International Society for Optical Engineering, **2526**, 40-48.
- Brown D. W., Ivic Z. (1989): Phys. Rev. B **40**, 9876-9887.
- Brown D. W., Lindenberg K. (1997a): in Proceedings of "Fluctuations, Nonlinearity and Disorder", 30 September - 4 October, 1996, Heraclion, Crete, edited by G. P. Tsironis, *et al.*, to appear in Physica D.
- Brown D. W., Lindenberg K., Wang X. (1990): in *Davydov's Soliton Revisited: Self-Trapping of Vibrational Energy in Protein*, NATO ASI Series B: Physics, Vol. 243, edited by Peter Christiansen and Alwyn C. Scott (Plenum Press, New York) pp. 63-82.
- Brown D. W., Lindenberg K., Zhao Y. (1997b): submitted to J. Chem. Phys.
- Davydov A. S. (1969): Phys. Stat. Sol. **36**, 211-219.
- Davydov A. S. (1979): Phys. Scr. **20**, 387-394.
- Davydov A. S. (1980): Zh. Eskp. Teor. Fiz. 51, 789-796 [Sov. Phys. JETP 78, 397-400 (1980)].
- Davydov A. S., Kislyukha N. I. (1973): Phys. Stat. Sol. (b) **59**, 465-470.
- Davydov A. S., Kislyukha N. I. (1976): Zh. Eksp. Teor. Fiz. **71**, 1090-1098 [Sov. Phys.-JETP **44**, 571 (1976)].

- Emin D., Holstein T. (1976): Phys. Rev. Lett. **36**, 323-326.
- Gerlach B., Lowen H. (1987a): Phys. Rev. B **35**, 4291-4296.
- Gerlach B., Lowen H. (1987b): Phys. Rev. B **35**, 4297-4303.
- Gerlach B., Lowen, H. (1991): Rev. Mod. Phys. **63**, 63-90.
- Glauber R. J. (1963): Phys. Rev. **131**, 2766-2788.
- Holstein T. (1959a): Annals Phys. (N.Y.) **8**, 325-342.
- Holstein T. (1959b): Annals of Phys. (N.Y.) **8**, 343-389.
- Holstein T. (1981): Mol. Cryst. Liq. Cryst. **77**, 235-252.
- Holstein T., Turkevich L. (1988a): Phys. Rev. B **38**, 1901-1922.
- Holstein T., Turkevich L. (1988b): Phys. Rev. B **38**, 1922-1937.
- Ivic Z., Brown D. W. (1989): Phys. Rev. Lett. **63**, 426-429.
- Kohn W. (1959): Phys. Rev. **115**, 809-821.
- Kubo R. (1954): J. Phys. Soc. Japan **9**, 935.
- Kubo R. (1961): in *Fluctuation, Relaxation and Resonance in Magnetic Systems*, edited by D. ter Haar (Oliver and Boyd, Edinburgh).
- Kubo R., Tomita, K. (1954): J. Phys. Soc. Japan **9**, 888.
- Kubo R., Toyabe T. (1967): in *Magnetic Resonance and Relaxation*, edited by R. Blinc (North-Holland, Amsterdam).
- Landau L. D., Pekar S. I. (1948): Zh. Eksp. Teor. Fiz. **18**, 419.
- Lang I. G., Firsov Yu. A. (1962): Zh. Eksp. Teor. Fiz. **43**, 1843-1860 [Sov. Phys. JETP **16**, 1301 (1963)].
- Lee T. D., Low F. E., Pines D. (1953): Phys. Rev. **90**, 297-302.
- Lowen H. (1988): Phys. Rev. B **37**, 8661-8667.
- Madelung O. (1978): *Introduction to Solid-State Theory*, (Springer-Verlag, New York).
- Merrifield R. E. (1964): J. Chem. Phys. **40**, 4450-450.
- Pekar S. I. (1946a): Journ. Phys. USSR **10**, 341.
- Pekar S. I. (1946b): Zh. Eksp. Theor. Fiz. **16**, 335.
- Pekar S. I. (1954): *Untersuchungen Über die Elektronentheorie der Kristalle* (Akademie-Verlag, Berlin).
- Rashba E. I. (1957a): Opt. Spektrosk. **2**, 75-87 (in Russian).
- Rashba E. I. (1957b): Opt. Spektrosk. **2**, 88-98 (in Russian).
- Rashba E. I. 1987: in *Excitons*, edited by E. I. Rashba and M. D. Sturge (North-Holland, New York), pp. 273-332.
- Romero A. H., Brown D. W., Lindenberg K. (1997): in preparation.
- Skrinjar M. J., Kapor D. V., and Stojanovic S. D. (1988): Phys. Rev. A. **38**, 6402-6408.
- Sumi A., Toyozawa Y. (1973): J. Phys. Soc. Japan **35**, 137-145.
- Toyozawa Y. (1961): Prog. Theor. Phys. **26**, 29-44.
- Toyozawa Y. (1963): in *Polarons and Excitons*, edited by C. G. Kuper and G. D. Whitfield (Plenum, New York), pp. 211-232.
- Toyozawa Y. (1980): in *Relaxation of Elementary Excitations*, edited by R. Kubo and E. Hanamura (Springer-Verlag, Heidelberg-New York), pp. 3-18.
- Ueta M., Kanzaki H., Kobayashi K., Toyozawa Y., Hanamura E. (1986): *Excitonic Processes in Solids*, (Springer-Verlag, New York).
- Wang X., Brown D. W., Lindenberg K. (1989): Phys. Rev. Lett. **62**, 1796-1799.
- Wannier G. H. (1937): Phys. Rev. **52**, 191-197.

- Weinreich G. (1965): *Solids: Elementary Theory for Advanced Students* (Wiley, New York).
- Zhao Y. (1994b): Doctoral Thesis, University of California, San Diego.
- Zhao Y., Bertram H. N. (1992): J. Mag. Mag. Mat. **114**, 329.
- Zhao Y., Bertram H. N. (1995): J. Appl. Phys. **77**, 6411.
- Zhao Y., Brown D. W., Lindenberg K. (1996a): to appear in J. Chem. Phys.
- Zhao Y., Brown D. W., Lindenberg K. (1996b): to appear in J. Chem. Phys.
- Zhao Y., Brown D. W., Lindenberg K. (1997a): submitted to J. Chem. Phys.
- Zhang Q., Romero-Rochin V., Silbey R. (1988): Phys. Rev. A **38**, 6409-6415.

The Power of Cooperation

B.A. Huberman

Xerox Palo Alto Research Center, Palo Alto, California 94304, U.S.A.

1 Introduction

It is widely believed that a group of cooperating agents engaged in problem solving can solve a task faster than either a single agent or the same group of agents working in isolation from each other. As a matter of fact, that cooperation leads to improvements in the performance of a group of individuals underlies the founding of the firm, the existence of scientific and professional communities, and the establishing of committees charged with solving particular problems. In the realm of computation, the emergence of massively parallel machines underscores the assumed power of concurrency for solving very complex tasks that can be decomposed into smaller pieces, and a large effort is being devoted to the design of parallel algorithms for the solution of computationally hard problems.

Nevertheless, little is known about the quantitative improvements that result from cooperation. While a large body of knowledge has accumulated over the workings of organizations, the evolution of cooperation in the biological world (Axelrod & Hamilton 1981) and the design of parallel computer programs, little is known quantitatively about what ensues from having a collection of agents working cooperatively on problem solving in general situations.

The essential characteristic of distributed cooperative problem solving is that locally programmed agents exchange messages reporting on their partial success towards completion of a goal. Such tasks generally require adaptability to unexpected events, dealing with imperfect and conflicting information from many sources, and acting before all relevant information is available. In particular, incorrect information can arise not only from hardware limitations but also from computations using probabilistic methods, heuristics, rules with many exceptions, or learning procedures that result in overgeneralization. Similarly, delays in receiving needed information can be due to the time required to fully interpret signals in addition to physical communication limitations.

Earlier, we showed that the dynamical behavior of highly-interacting agents in computational ecology exhibits a wide range of behaviors (Huberman & Hogg 1988). By allowing for cooperation between agents engaging in different tasks, one can obtain improved performance of the system as a whole. In many such cases, those agents making the most progress per unit

time are the ones that set the overall performance. For example, consider a concurrent constrained search in a large database in which a number of agents are looking for an item which satisfies the constraints. The overall search time is determined by the agent which arrives at the answer first, thereby terminating all related processes. Thus an interesting question concerns the distribution of performance among the agents, particularly the nature of those performing exceedingly well. This emphasis on the performance distribution highlights the need to study more than just the average behavior of highly interacting systems.

To determine the distribution of performance, one might expect it necessary to know the details of the cooperating processes. Fortunately, however, highly cooperative systems, when sufficiently large, display a universal distribution of individual performance, largely independent of the detailed nature of either the individual processes or the particular problem being tackled. In particular, this predicts an extended tail of high performance and can be expected to apply when such performance requires successful completion of a number of nearly independent steps or subtasks. For instance, this distribution has been observed to describe a wide range of systems (Aitchison & Brown 1957), (Crow & Shimizu 1988) including scientific productivity (Shockley 1957), species diversity in ecosystems (Krebs 1972), and income distributions in national economies (Montroll & Shlesinger 1982). We therefore conjectured that distributed systems operating as computational ecosystems will display the same quantitative characteristics (Huberman & Hogg 1988).

Many problem solving tasks can be viewed as searches in large problem spaces. For realistic problems, where no algorithmic solution is known, heuristic methods are used to prune the search. Recently, a theory that elucidates the performance of cooperative processes searching through a large problem space was developed (Huberman 1990). It showed that cooperative searches, when sufficiently large, can display universal characteristics, independent of the detailed nature of either the individual processes or the particular problem being tackled. This universality manifests itself in two separate ways. First, the existence of a sharp transition from exponential to polynomial time required to find the solution as heuristic effectiveness is improved (Huberman & Hogg 1987). Second, the appearance of a lognormal distribution in individual agent's problem solving effectiveness. The enhanced tail of this distribution guarantees the existence of some agents with superior performance. This can bring about a combinatorial implosion (Kornfeld 1982). In cases where the diversity of problem solving skill increases as the number of agents increases, a superlinear speed-up is observed.

It is important to understand what is meant by cooperation in problem solving. Cooperation involves a collection of agents that interact by communicating information to each other while solving a problem. The method of communication can be of any form, e.g., it may be through broadcasts or

through access to a centralized source of information. The agents may be loosely aggregated as in a committee, or may be more formally organized as in a hierarchy. The information exchanged between the agents may be incorrect, and should sometimes alter the behavior of the agents receiving it. An example of cooperative problem solving is the use of a genetic algorithm (Goldberg 1989) to solve a problem. In a genetic algorithm members of a population exchange pieces of themselves or mutate to create a new population to improve the overall performance of the entire population. Another example is a neural network where the outputs of connected neurons affect the output of the neuron receiving the outputs. An expert system using a knowledge base of facts with a number of processes accessing and *modifying* the knowledge base is also an example of cooperative problem solving. If no modification to the knowledge base takes place then the processes do not interact and there is no cooperation.

In what follows, I will present a theory of the performance increases that result from cooperative problem solving. For a wide class of problems, there is a highly nonlinear increase in performance due to the interactions between agents. In some cases this is further enhanced by sharp phase transitions in the topological structure of the problem. These results will be illustrated in the context of three prototypical search examples. The first considers a general search for a particular goal among a number of states. The second describes the further enhancement of performance due to phase transitions in a hierarchical search problem. The final example concerns a search for a good, but not necessarily optimal, state. Throughout these examples we show how the existence of a diverse society of processes is required to achieve this performance enhancement.

These predictions were tested by running a number of experiments on cooperative problem solving that provided a quantitative assessment of the value of cooperation in problem solving (Clearwater *et al.* 1991), (Huberman *et al.* 1992). The experiments were carried out by having a number of computational agents solve a set of cryptarithmetic problems and measuring their individual and global performance. These results provide a striking example of the improvements in performance from cooperation and suggest an alternative methodology to existing techniques for solving constraint satisfaction problems in computer science and distributed artificial intelligence.

2 Cooperative Search

Consider the case of heuristically guided search, which applies to a wide range of problems (Pearl 1984). A search procedure can be thought of as a process which examines a series of states until a particular goal state is obtained. These states typically represent various potential solutions of a problem, usually obtained through a series of choices. Various constraints on the choices can be employed to exclude undesirable states. Examples range

from well-defined problem spaces as in chess to problems in the physical world such as robot navigation.

As a specific example, consider the case of a d -dimensional vector, each of whose components can take b different values. The search consists of attempting to find a particular suitable value (or goal) among the b^d possible states. It is thus a simple instance of constrained search involving the assignment of values to components of a vector subject to a number of constraints. A random search through the space will, on average, find the goal only after examining one half of the possibilities, an extremely slow process for large problems (i.e. the required time is exponential in d , the number of components to be selected). Other specific approaches can be thought of as defining an order in which the possible states are examined, with the ensuing performance characterized by where in this sequence of states the goal appears. We now suppose that n agents or processes are cooperating on the solution of this problem, using a variety of heuristics and that the problem is completed by the first agent to find the solution. The heuristic used by agent i can be simply characterized by the fraction f_i , between 0 and 1, of unproductive states that it examines before reaching the goal. A perfect heuristic will thus correspond to $f_i = 0$ and one which chooses at random has $f_i = 1/2$.

In addition to their own search effort, agents can exchange information regarding the likely location of the goal state within the space. In terms of the sequence of states examined by a particular agent, the effect of good hints is to move the goal toward the beginning of the sequence by eliminating from consideration states that would otherwise have to be examined. A simple way to characterize a hint is by the fraction of unproductive nodes (and that would have otherwise been examined before reaching the goal) that the hint removes from the search. Since hints need not always be correctly interpreted, they can also lead to an increase in the actual number of nodes examined before the answer is found. For such cases, we suppose that the increase, on average, is still proportional to the amount of work remaining, i.e. bad hints won't cause the agent to nearly start over when it is already near the goal but will instead only cause it to reintroduce a small number of additional possibilities. Note that the effectiveness of hints depends not only on the validity of their information, but also on the ability of recipients to interpret and use them effectively. In particular, the effect of the same hint sent to two different agents can be very different.

A simple example of this characterization of hint effectiveness is given by a concurrent search by many processes. Suppose there are a number of characteristics of the states that are important (such as gender, citations, and subfield in a database). Then a particular hint specifying gender, say, would eliminate one half of all remaining states in a process that is not explicitly examining gender.

To the extent that the fractions of unproductive nodes pruned by the various hints are independent, the fraction of nodes that an agent i will have

to consider is given by

$$f_i = f_i^{\text{initial}} \prod_{j \neq i} f_{j \rightarrow i}^{\text{hint}} \quad (1)$$

where $f_{j \rightarrow i}^{\text{hint}}$ is the fraction of unproductive nodes eliminated by the hint the agent i receives from agent j , and f_i^{initial} characterizes the performance of the agent's initial heuristic. Note that hints that are very noisy or uninterpretable by the agent correspond to a fraction equal to one because they do not lead to any pruning. Conversely, a perfect hint would directly specify the goal and make f_i equal to zero. Furthermore, we should note that since hints will generally arrive over time during the search, the fractions characterizing the hints are interpreted as effective values for each agent, i.e. a good hint received late, or not utilized, will have a small effect and a corresponding hint fraction near one.

The assumption of independence relies on the fact that the agents broadcast hints that are not overlapping, i.e. the pruning of two hints won't be correlated. This will happen whenever the agents are diverse enough so as to have different procedures for their own searches. If the agents were all similar, i.e. the pruning was the same for all of them, the product in (1) would effectively only have one factor. For intermediate cases, the product would only include those agents which differ from each other in the whole population. As additional consideration, the overall heuristic effectiveness f_i must not exceed one, so there is a limit to the number and placement of independent hint fractions larger than one that can appear in (1). We therefore define n_{eff} to be the effective number of diverse agents, which in turn defines the actual number of terms in the product of (1). This leads to a direct dependence of the pruning effectiveness on the diversity of the system. Although the hints that individual agents find useful need not come from the same sources, for simplicity we suppose the number of diverse hints received by each agent is the same.

We now derive the law that regulates the pruning effectiveness among agents. By taking logarithms in (1), one obtains

$$\log f_i = \log f_i^{\text{initial}} + \log f_{1 \rightarrow i}^{\text{hint}} + \dots + \log f_{n_{\text{eff}} \rightarrow i}^{\text{hint}} \quad (2)$$

where we have included only terms arising from diverse hints. If the individual distributions of the logarithms of the fractions satisfy the weak condition of having a finite variance, and if the number of hints is large, then the central limit theorem applies. Therefore, the values of $\log f_i$ for the various agents will be normally distributed around its mean, μ , with standard deviation σ , i.e. according to $N(\mu, \sigma, \log f_i)$. Here μ and σ^2 are the mean and variance of the $\log f_i$ of the various agents, which are given by the sum of the corresponding moments of the individual terms in the sum. In other words, f itself is distributed according to the lognormal distribution (Aitchison &

Brown 1957)

$$\text{Prob}(f) = \frac{1}{\sigma f \sqrt{2\pi}} e^{-\frac{(\log f - \mu)^2}{2\sigma^2}} = \frac{N(\mu, \sigma, \log f)}{f} \quad (3)$$

which gives the probability density for a given agent to have various values of f . The mean value of f is $m = e^{\mu + \sigma^2/2}$ and its variance is given by $m^2(e^{\sigma^2} - 1)$. This distribution is highly asymmetric with a long tail, signifying an enormous range of performance among the individual agents.

To examine the effect of hints, we measure performance for the agents in terms of the speed at which they solve the problem. This is given by

$$S \equiv \frac{\text{size of search space}}{\text{time to reach goal}} = \frac{b^d}{f(b^d - 1) + 1} \quad (4)$$

where the time required to find the goal is just the number of states that were actually examined during the search. For the large search spaces of interest here, this will be approximately given by $1/f$ except for very small values of f . When a variable such as f is lognormally distributed, so is any power of it, in particular $1/f$. Hence the lognormal distribution of f derived above will produce a similar distribution for corresponding values of S . In practice, of course, there is a finite upper limit on performance (given, in this case, by $S_{\max} = b^d$) even though f can be arbitrarily small. This implies an eventual cutoff in the distribution at extremely high performance levels. Nevertheless, the extended tail of the lognormal distribution can be expected to adequately describe the enhancement in performance due to exchange of hints for values well below this maximum.

As a concrete case, we consider the situation in which hints, on the average, neither advance nor hinder performance of the system as a whole, i.e. the mean value of the hint fractions is one, which can be considered a worst case scenario. Thus, any improvement of the overall performance of the system will come from the tail of the distribution. Specifically, we take the $f_{j \rightarrow i}^{\text{hints}}$ values to be normally distributed according to $N(1, 0.02, f)$. We also take the initial performance of the agents (i.e. speed S without hints) to be normally distributed according to $N(4, 0.05, S)$ which corresponds to somewhat better than random search. These choices ensure that there is a negligible chance for S to reach its maximum, so the lognormal distribution will accurately describe the high performance tail in the range of interest. The resulting distributions are compared in Fig.1.

Because of the enhanced performance tail, a collection of cooperating agents is far more likely to have a few high performers than the noninteracting case. This can be seen by examining the tail of the distributions, particularly the top percentiles of performance. In particular, for a system with n agents the expected top performer will be in the top $100/n$ percentile. This can be quantified by specifying the speed reached or exceeded by the top performers. With no hints, the top 0.1 percentile is located at a speed of 4.15. On the

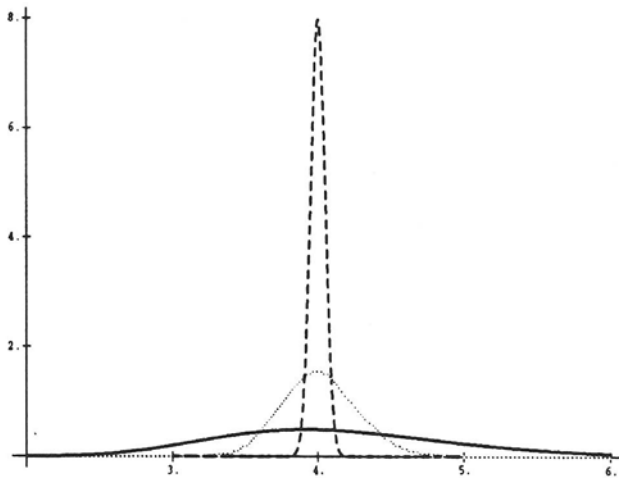


Fig. 1. Distribution of agents according to their performance S in a search with $b = 5$ and $d = 20$. The dashed curve corresponds to the noninteracting case of no hints exchanged during the search. The dotted curve corresponds to $n_{\text{eff}} = 10$, and the solid black one to $n_{\text{eff}} = 100$. Notice the appearance of a long tail in the interacting cases, which results in an improvement in performance. The area under each of the curves is one. The nature of the hints is such that, on the average, they neither enhance nor retard the search procedure.

other hand, this percentile moves up to 4.89 and 7.58 when $n_{\text{eff}} = 10$ and $n_{\text{eff}} = 100$, respectively, where n_{eff} is the effective number of cooperating agents. Note that the top 0.1 percentile characterizes the best performance to be expected in a collection of 1000 cooperating agents. The enhancement of the top performers increases as higher percentiles or larger diversity are considered, and shows the highly nonlinear multiplicative effect of cooperative interactions.

A collection of agents could manage to exchange hints such that on average they *increase* the performance of a system. In this case, in addition to the enhanced tail there will also be a shift of the overall performance curve toward higher values due to the multiplication of a number of factors greater than one. Notice that in such a case high diversity is less important in setting the improved performance than was in the example. We should remark however, that this scenario breaks down for very high performance agents due to the upper bound on the maximum speed $S_{\max} = b^d$.

3 Hierarchical Search and Phase Transitions

A very important class of problem solving involves heuristic searches in tree structures. Thus it is important to elucidate how the above considerations of cooperation apply to this case. In particular, suppose the search takes place in a tree with branching ratio b and depth d , so the total number of nodes in the tree is given by

$$N_{\text{total}} = \frac{b^{d+1} - 1}{b - 1} \quad (5)$$

This can be viewed as an extension of the previous example in that successive levels of the tree correspond to choices for successive components of the desired vector, with the leaves of the tree corresponding to fully specified vectors. The additional tree structure becomes relevant when the heuristic can evaluate choices based on vectors with some components unspecified. These evaluations offer the possibility of eliminating large groups of nodes at once.

The search proceeds by starting at the root and recursively choosing which nodes to examine at successively deeper levels of the tree. At each node of the tree there is one correct choice, in which the search gets one step closer to the goal. All other choices lead away from the goal. The heuristic used by each agent can then be characterized by how many choices are made at a particular node before the correct one is reached. The perfect heuristic would choose correctly the first time, and would find the goal in d time steps, whereas the worst one would choose the correct choice last, and hence be worse than random selection. To characterize an agent's heuristic, we assume that each incorrect choice has a probability p of being chosen by the heuristic before the correct one. Thus, when the branching ratio is 2, the perfect heuristic corresponds to $p = 0$, random to $p = 0.5$, and worst to $p = 1$. For simplicity, we suppose the heuristic effectiveness, as measured by p , is uniform throughout the tree. Alternatively, p can be thought of as the value of the effectiveness averaged over all nodes in the tree. In the latter case, any particular correlations between nodes are ignored, in the spirit of a mean-field theory, which can be expected to apply quite well in large-scale problems. Note that while p specifies the fraction of incorrect choices made before the correct one on average throughout the tree, this probabilistic description allows for variation among the nodes.

The *a posteriori* effect of hints received from other agents can be described as a modification to an agent's value of p . Assuming independence among the hints received, this probability is given by

$$p_i = p_i^{\text{initial}} \prod_{j=1}^{n_{\text{eff}}} f_{j \rightarrow i}^{\text{hint}} \quad (6)$$

where p_i^{initial} characterizes the agent's initial heuristic and the hint fractions are the same as introduced in the previous section, but now averaged over the entire tree. By supposing the various quantities appearing in (6) are random

variables, we again obtain the universal lognormal distribution (over the set of agents) of heuristic effectiveness when there is a large number of agents exchanging hints.

Given this distribution in *local* decision effectiveness, we now need the distribution of performance in the full search problem, i.e. the rate at which the search for the goal is completed. This relationship is more complex than in the unstructured example considered above, and in particular it produces a phase transition in overall agent performance at a critical value of p (Huberman & Hogg 1987). This sharp transition leads to the possibility of an additional enhancement in performance.

Specifically, the overall performance is related to the time T , or number of steps, required to reach the goal from the root of the tree. To quantify the search performance, we consider the search speed given by

$$S \equiv \frac{\text{number of nodes in the tree}}{\text{number of steps to the goal}} = \frac{N_{\text{total}}}{T} \quad (7)$$

To compare trees of different depths, it is convenient to normalize this to the maximum possible speed, namely $S_{\max} = N_{\text{total}}/d$ giving the normalized speed $s \equiv S/S_{\max} = d/T$.

Because of the probabilistic characterization of the heuristic for each agent, T is a random variable. It is determined by two contributions: the length of the correct path to the goal (equal to the depth of the search tree, d), plus the number of nodes visited in every incorrectly chosen subtree along the way to the goal, in itself a random variable. While the actual probability distribution of T values for a given value of p is complicated, one can show that the average number of steps required to reach the goal is given by (Huberman & Hogg 1987) as

$$\langle T \rangle = d + \frac{(\mu - p)(d - \mu - d\mu + \mu^{d+1})}{(\mu - 1)^2} \quad (8)$$

where $\mu = bp$. As the depth of the tree increases, this becomes increasingly singular around the value $\mu = 1$, indicating a sudden transition from linear to exponential search. This is illustrated in Fig.2 which shows the behavior of the average normalized search speed $\bar{s} \equiv d/\langle T \rangle$ as a function of the local decision effectiveness characterized by p . Near the transition, a small change in the local effectiveness of the heuristic has a major impact on the global behavior of large-scale search problems. The existence of such a phase transition implies that, in spite of the fact that the average behavior of cooperative algorithms may be far into the exponential regime, the appearance of an extended tail in performance makes it possible for a few agents to solve the problem in polynomial time. In such a case, one obtains a dramatic improvement in overall system performance by combining these two effects. We should note that other search topologies such as general graphs also exhibit these phase transitions (Bollobas 1985) so these results can apply to a wide range of topologies found in large-scale search problems.

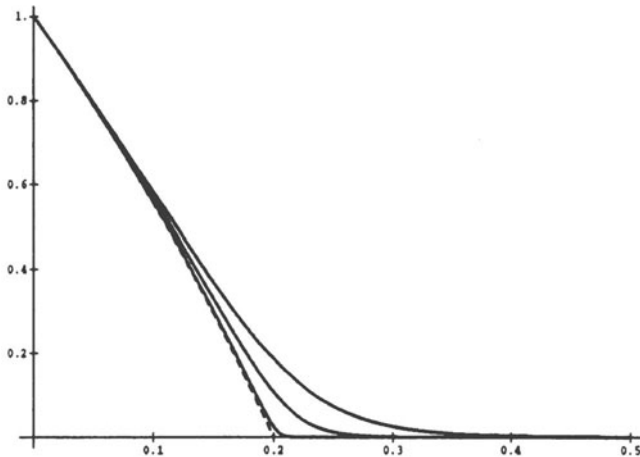


Fig. 2. Plot of \tilde{s} versus local decision effectiveness for trees with branching ratio 5 and depths 10, 20 and 100. The distinction between the linear regime ($p < 0.2$) and the exponential one becomes increasingly sharp as the depth increases. The dashed curve is the limit for an infinitely deep tree and shows the abrupt change at $p = 0.2$ from linear to exponential search.

Finally, to illustrate the result of combining diverse hints with the phase transition in tree searches, we evaluate the distribution of relative global speed s for the agents searching in a tree with a branching ratio $b = 5$ and depth $d = 20$. This combines the distribution of local decision effectiveness with its relation to global speed. As in the previous example, we suppose hints on average neither help nor hinder the agents. In particular, we take the $f_{j \rightarrow i}^{\text{hints}}$ values to be normally distributed according to $N(1, 0.015, f)$. We also take the initial performance of the agents (i.e., p_i^{initial}) to be normally distributed according to $N(0.33, 0.0056, p)$ which corresponds to a bit better than random search. The resulting distributions were evaluated through simulations of the search process and are compared in Fig.3, on a logarithmic scale to emphasize the extended tails.

In this case, the enhancement of the global performance of the system is most dramatic at the higher end of the distribution, not all of which is shown in the figure. In this example, the top 0.1 percentile agents will have an enhancement of global speed over the case of no hints by factors of 2 and 41 for 10 and a 100 hints respectively. This illustrates the nonlinear relation between performance, number of agents, and diversity of hints.

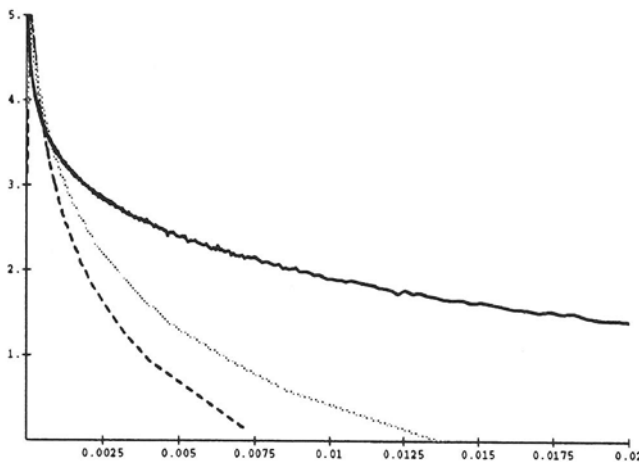


Fig. 3. Distribution of agents (on a log scale) as a function of relative global speed s for a concurrent search in a tree with $b = 5$, and $d = 20$. The dashed line corresponds to the case of no hints being exchanged during the search. The dotted curve corresponds to $n_{\text{eff}} = 10$, and the solid black one to $n_{\text{eff}} = 100$. Note the enhancement of the high performance tail as the diversity of exchanged hints increased.

4 Satisficing Searches

In many heuristic search problems, the exponential growth of the search time with problem size forces one to accept a satisfactory answer rather than an optimal one. In such a case, the search returns the best result found in a fixed amount of time rather than continuing until the optimal value is found. If the search returns have a good value, they can provide acceptable solutions to the problem without the cost involved in obtaining the true optimum. A well-known instance is the traveling salesman problem, consisting of a collection of cities and distances between them and an attempt to find the shortest path which visits each of them. The time required to find this path grows exponentially with the number of cities if $P \neq NP$.

For large instances of the problem, one must settle instead for paths that are reasonably short but not optimal.

In these cases of limited search time, the extended tails of the cooperative distributions discussed above result in a better value returned compared to cases in which hints are not used. To see this we consider an unstructured search problem where the states have various values, v , which we take to be integers between 0 and some maximum V . In the previous examples, one

could view the single goal as having the maximum value while all other states have a value of 0. To allow for the possible usefulness of nonoptimal states, we suppose that their values are distributed throughout the range. In order that a simple random search is unlikely to be effective, we need relatively few states with good values. A simple distribution of values satisfying these requirements is given by the binomial distribution:

$$m_v = \binom{V}{v} 3^{V-v} \quad (9)$$

where m_v is the number of states with value v . Note that this has exactly one state with the maximum value and most states have smaller values clustered around the average $V/4$.

For problems of this kind, the effectiveness of a heuristic is determined by how well it can discriminate between states of high and low value. When faced with selecting among states with a range of values, a good heuristic will tend to pick those states with high value. That is, the likelihood of selecting a state will increase with its value. Moreover, this increase will become more rapid as the heuristic improves. As a concrete example, we suppose that the heuristics used by the various agents in the search are characterized by a discrimination parameter α such that states with value v are selected by the heuristic with relative probability α^v . Large values of α provide excellent discrimination while $\alpha = 1$ corresponds to random selections. In terms of our previous examples, in which only the goal had a nonzero value, the relative selection probabilities were 1 for the goal and p for all other states. Thus we see that this characterization of heuristic discrimination identifies α^V with $1/p$ in the case of only two distinct values.

As in the previous examples, cooperation among diverse agents leads to a lognormal distribution of selection probability values among the agents. Here this means that the α values will themselves be lognormally distributed. Instead of focusing on the time required to find the answer, we can examine the distribution of values returned by the various agents in a given interval of time. As an extreme contrast with the previous examples, which continued until the goal was found, we allow each agent to examine only one state, selected using the heuristic. The value returned by the agent will then correspond to this state. (If additional time were available, the agents would continue to select according to their heuristic and return the maximum value found.) These simplifications can be used to obtain the distribution of returned values resulting from interactions among the agents as a function of the number of diverse agents, n_{eff} .

Since all points are available to be selected, the probability that an agent operating with a heuristic discrimination level of α will select a state with value v is

$$p(\alpha, v) = \frac{m_v \alpha^v}{\sum_{u=0}^V m_u \alpha^u} = \binom{V}{v} \frac{(\alpha/3)^v}{(1 + \alpha/3)^V} \quad (10)$$

To finally obtain the distribution of values returned by the agents, this must be integrated over the distribution of α values. When hints are exchanged, this parameter will be distributed lognormally with a mean μ and standard deviation σ depending on the corresponding values for the hint fractions. The result can be written as

$$P(v) = \frac{1}{\sqrt{2\pi}} \binom{V}{v} e^{v\tilde{\mu} + \frac{(v\sigma)^2}{2}} \int_{-\infty}^{\infty} dt e^{-\frac{t^2}{2}} \left(1 + e^{\tilde{\mu} + v\sigma^2 + \sigma t}\right)^{-V} \quad (11)$$

where $\tilde{\mu} \equiv \mu - \ln 3$.

The distributions are compared in Fig.4 for the case in which the initial agents' heuristic has $\alpha = 1.5$ (i.e. a bit better than random value discrimination) and the hint fractions are distributed according to $N(1, 0.05)$, again giving a case in which the hints, on average, neither help nor hinder the search. In this case, the top 0.1 percentile level is at a value $v = 52$ when $n_{\text{eff}} = 10$ and $v = 70$ when $n_{\text{eff}} = 100$. This compares with the noninteracting case in which this performance level is at $v = 48$.

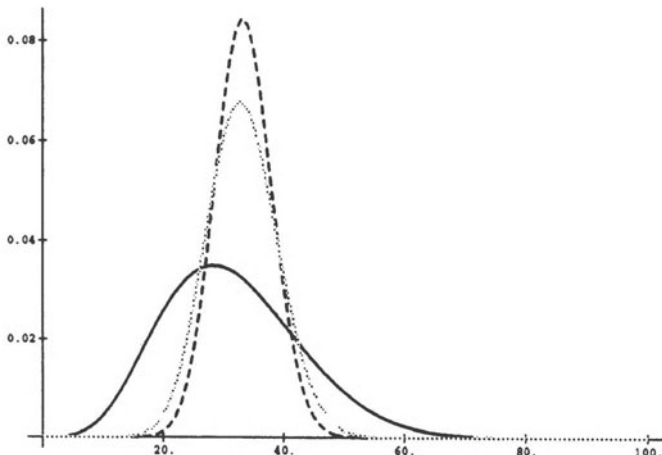


Fig. 4. Distribution of values returned in a satisficing search with $V = 100$. The dashed curve shows the distribution for the noninteracting case. The dotted curve corresponds to $n_{\text{eff}} = 10$, and the solid black one is for $n_{\text{eff}} = 100$. The area under each curve is one.

5 Experiments on Constraint Satisfaction Problems

Constraint satisfaction problems lie at the heart of human and computer problem solving. These are problems in which values must be assigned to a set of variables such that a number of conditions (the constraints) are satisfied in order for the assignment to be a solution. In most cases of interest, no direct solution method is known and one must resort to searching through a large number of possible assignments to find those that satisfy all the constraints. A *state* in the search is a set of assignments for all the variables and a *partial state* has only some of variables assigned. These search problems can be characterized by the total number of states in the search space, T , and the number of solutions, S . Let N be the number of agents or processes involved in the search. In a fully parallel system, each of these can correspond to a separate processor, but they could be simulated by a smaller number of processors as well. To be interesting the problems should be intrinsically difficult so that a single agent can't be expected to solve them in a few steps. This requires that there are many states and that solutions be relatively rare, i.e., $T \gg S$. Moreover, to have any motivation for considering cooperative problem solving, there can't be so many available agents that they could quickly examine all search states independently, i.e., we should have $T \gg N$. Since for typical constraint problems the number of states T grows exponentially with the size of the problem (e.g., the number of variables), these requirements are often satisfied in practice.

As a concrete constraint satisfaction problem for our experiments, we used the familiar problem of solving cryptarithmetic codes. These problems require finding a unique digit assignments to each of the letters of a word addition so that the numbers represented by the words add up correctly. An example is the sum: $DONALD + GERALD = ROBERT$, which has one solution, given by $A = 4, B = 3, D = 5, E = 9, G = 1, L = 8, N = 6, O = 2, R = 7, T = 0$. In general, if there are n letters and the sum uses base b arithmetic then there are b^n possible states. However, not all of these correspond to the requirement that letters represent distinct digits. The requirement of a unique digit for each letter means that there are $\binom{b}{n}$ ways to choose b values and $n!$ ways to assign them to the letters, which reduces the total number of search states to $n! \binom{b}{n} = b!/(b-n)!$. Thus the above example, which has 10 letters and uses base 10 arithmetic, has $10!$ states in its search space. In all our experiments we used base 10 arithmetic.

Solving a cryptarithmetic problem involves performing a search. Although clever heuristics can be used to solve the particular case of cryptarithmetic, our purpose is to address the general issue of cooperation in parallel search using cryptarithmetic as a simple example. Thus we focus on simple search methods, without clever heuristics that can lead to quick solutions by a single agent. This is precisely the situation faced with more complex constraint problems where extremely effective heuristics are not available. The speed at

which an agent can solve the problem depends on the initial conditions and the particular sequence of actions it chooses as it moves through a search space. This sequence relies on the knowledge, or heuristics, that an agent has about which state should be examined next. The better the agent is able to utilize the heuristics, the quicker it will be able to solve the problem. When many agents work on the same problem, this knowledge can include *hints* from other agents suggesting where solutions are likely to be. Our results show that the performance of agents collaborating in constraint satisfaction problems is highly enhanced when compared to that of the same group of agents with no interactions.

More specifically, in our cooperative experiments agents wrote the hints they discovered to a blackboard which could subsequently be read by others. This method for agent interactions differs from a case reported earlier in which the hint blackboard was filled at the start and a search algorithm chose the hints from the blackboard (Engelmore & Morgan 1988). In that analysis, the hint blackboard consisted of orderings of rule antecedents (hints) for use in a rule learning program employing a depth-first search strategy.

6 Results

In this section we present our experiments on the behavior of multiagent search for cryptarithmetic. Although our simulations considered multiple agents, we could just as easily have considered a single agent consisting of many parts. In fact, all the simulations were done on a single processor running a single process. The important point is our observations of the *ratio* of the performance between a cooperative multiagent simulation and a non-cooperative one should not depend on whether we use a single processor or many. What is most important to the increase in performance is the diversity of approaches available by having many agent processes.

6.1 Problem Solving by Committee

In this section we present results from many experiments involving a committee of agents solving cryptarithmetic problems.

Super-linear Speed-ups and Diversity. Amdahl's law predicts at most a linear speed-up in performance with the number of processors. However, this places no restriction on its software equivalent: the speed-up due to adding additional processes with diverse solution methods. One of the most dramatic effects we have seen is a super-linear speed-up due to diverse cooperating agents. While it is difficult to predict what sort of diversity will lead to significant super-linearity it is possible to test the prediction itself. Figure 5 shows a super-linear speed-up as new strategies are added to a collection of cooperating agents along with comparisons to two groups of non-cooperating

agents: those that use the same strategies of interpreting the hints and those that use random generate and test with no hints.

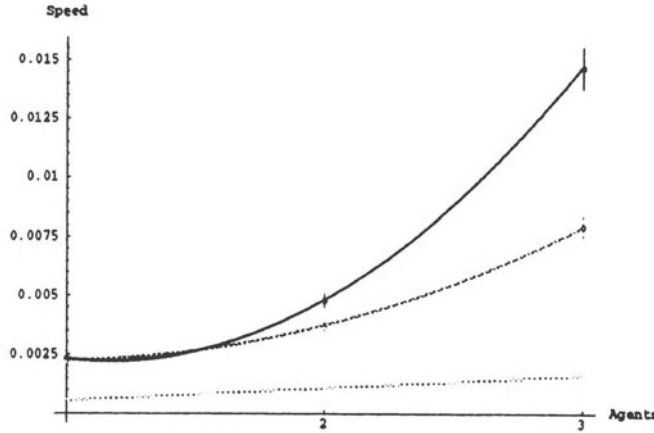


Fig. 5. Adding diversity leads to a super-linear speed-up in solution time. Average speed of the first finisher, defined as the inverse of the average time required until some agent first finds a solution, for 200 runs as a function of the number of agents employed trying to solve $WOW + HOT = TEA$. Steps were related to time by a Poisson process with average rate $\lambda = 1$. The bottom linear line is for the case of non-cooperating agents, each using the same random generate and test strategy with no memory of hints. The two non-linear curves correspond to the case where each agent uses a different strategy for utilizing hints. The middle curve corresponds to the case where the agents were non-cooperating, had their own blackboard and did not revisit states. The dark super-linear curve fits is the cooperating case where the agents shared one blackboard and did not revisit states. Each error bar corresponds to the statistical error of the mean of the measurement.

To illustrate the effect of diverse strategies on problem solving we chose to use the length of the hint for types of diverse strategies, although others could have been used. Three strategies were chosen, corresponding to a non-overlapping partition of hint lengths. In particular, the first strategy used only hints that had length equal to 5. The second strategy used hints of length 4. For a collection of agents using the two strategies, half use the length 5 strategy and half use the length 4 strategy. The third strategy used hints of length two or three. In a collection of agents using all three strategies, each strategy would be used by one-third of the agents. The super-linearity

comes from the fact that agents with a given strategy can contribute hints that it cannot use to agents that can utilize the hints by using a different strategy. This leads to a non-linear increase of the number of hints available. The cooperating agents and the non-cooperating agents with no blackboard or memory of previous states define a performance envelope that corresponds to the extreme cases of performance that may be expected from a collection of agents and strategies. To summarize, for cooperative diverse agents the diversity of problem solving strategies leads to a super-linear speed-up in problem solving.

The Distribution of First Finishing Times. The previous experiment showed the behavior of the average time to first solution. Due to the probabilistic nature of the search, and the exact choice of hints, the time required to find a solution will vary substantially from run to run. Thus while we see that cooperation improves average performance, it is also of interest to examine the distribution of finishing times. A comparison of the distribution of fastest finishers for cooperating agents and non-cooperating agents is shown in Fig.6. It shows that for cooperating agents the probability for finishing sooner is higher so that the benefit is seen for most runs, not only on average.

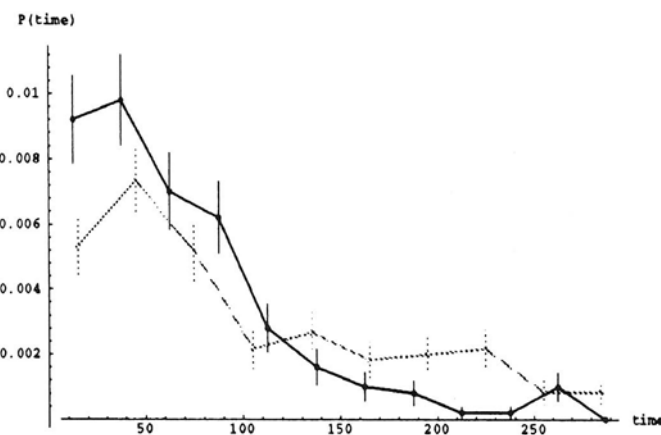


Fig. 6. The distribution of first finishing times is peaked towards faster times for the cooperating case. The data used are the same as in Fig.5 for the three agent case. The dark points connected by black lines correspond to cooperating agents and the gray corresponds to the non-cooperating case.

The Distribution of All Finishing Times. The previous discussion is relevant to the case in which the time to first solution is of most interest. In other kinds of problems, all the agents participate in a series of tasks and the amount of work the entire group can complete in a given amount of time is the relevant performance measure. This leads us to consider the distribution of solution times. Moreover, examining this distribution provides a connection with the theory.

In this set of experiments all the agents used the same strategy but examined different states due to their different initial locations in the state space and their choices from the available hints. Our experiments explored several possible cases of agent interaction. Specifically, the speed distribution for the cases a) noncooperating agents, b) non-cooperating agents with a partitioned search space, and c) cooperating agents, was compiled for agents trying to solve the problem $WOW + HOT = TEA$. The striking overall improvement in performance becomes apparent once we note that the speed is up to 100 times larger for the performance distribution of the cooperating agents than that obtained for the noncooperating case and about 10 times larger than the partitioned case. However, this speed improvement is also partly due to a better search method used by the cooperating agents. The fastest performers, the average performers and even the entire distribution for the cooperating agents is shifted towards higher performance. We should point out that the actual speedup for the cooperative case, when the problem is easy or the hints are very good, can vary greatly from run to run because it is very sensitive to the quality of the first few hints posted to the blackboard. Similar results were obtained on other cryptarithmic problems that used between 5 and 10 different letters and had from 1 to over 100 solutions.

We also consider the effect of diversity on the distribution of all finishers. The speed was fastest when all the agents had access to any hint. Although this corresponded to lower diversity (i.e., all the agents used the same strategy), it was compensated by a much higher average performance. Further, it was observed that by increasing the diversity of the agents' hint interpretation, the mode and median of the speed distribution were reduced. This shows that with greater diversity the higher performers benefit while the lower performers suffer.

The Effectiveness of Hints. It is also worthwhile to note the effect of cooperation as the problems become more difficult. One way of measuring the difficulty of problems is by the complexity ratio, T/S . The table below shows the relative speed for the first finisher of 100 agents for four problems of vastly different complexities, i.e., the ratio of speed of the cooperative to non-cooperative cases. The data for the cooperative case came from simulation runs while the behavior of the non-cooperative case was obtained theoretically. Note that as the problem becomes more difficult the importance of cooperation in speed-up is increased. The relative increase becomes even

more startling when one considers that the fraction of hints posted on the blackboard that are subsets of *any* of the solutions (there may be more than one solution) decreases as the problems become more complex. Thus the high performance is due to some agents finding combinations of hints that lead to solutions.

Problems	Ratio of speeds	T/S	Fraction of hints that are subsets of solutions
$AB + AC = DE$	7	210	0.9 – 1.0
$WOW + HOT = TEA$	45	1844	0.5 – 0.6
$CLEAR + WATER = SCOTT$	145	181440	0.1 – 0.2
$DONALD + GERALD = ROBERT$	315	362880	0.004

Another way of studying the effect of cooperation vs. problem complexity is to vary the effectiveness of the search performed by the agent by itself, without utilizing the hints from the other agents, or the *self-work*. For example, suppose that when the agents are not using hints they perform a depth-first backtrack search, each using a randomly selected ordering for the variables. During the depth-first search the agents have the opportunity to prune partial states which do not lead to any solution. For example, if some columns do not add up correctly there is no point in considering assignments to uninstantiated letters for this state. Whenever a hint comes along it overwrites the current partial state, in the same manner as for the agents using simple generate and test, so that there may be very large jumps through the search space. We can simulate the effect of this pruning by probabilistically pruning partially assigned states that are known not to lead to a solution. (We can do this with cryptarithmetic because we can generate all the solutions.) When the probability of pruning is small this corresponds to difficult problems because the agents must instantiate nearly all the letters before pruning. The results of this study, which are shown in Fig.7, show the greater relative importance of cooperation for harder problems.

Prior Knowledge. In many practical applications the agents start with some prior problem-specific knowledge. We now consider the effect of the quality of the agents' initial knowledge of the search space. This was modelled by the inclusion of hints on the initial blackboard. The effect of a non-empty starting blackboard is to significantly increase the number of unique solutions found. This is because random hints will likely point to different solutions, whereas an empty blackboard implies that the attention of the agents

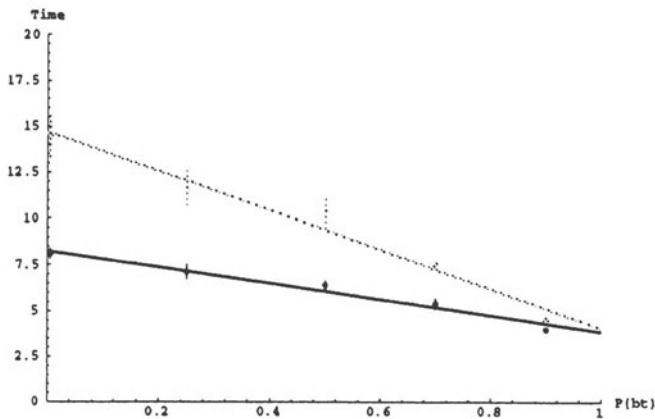


Fig. 7. Cooperation works best for harder problems. Time to first solution as a function of decreasing problem hardness. Specifically, the plot shows the average time to first solution for 100 agents solving $AB + AC = DE$ as a function of the probability of pruning, $P(bt)$, a state that is known not to lead to a solution. The left side of the plot corresponds to “hard” problems where pruning of the search space is very poor, and the right side of the plot corresponds to “easy” problems where pruning is very effective. The light line is for the case of non-cooperating agents, in this case a depth-first search. The dark line is for the case where the agents spend 80% of their time doing depth-first self-work and 20% cooperating, i.e., using hints from the blackboard. The lines show the best linear fits to the data. The data points correspond to the average solution time from 50 – 100 runs. The error bars are the error of the mean.

is highly focused by the first few arriving hints. Also, a non-empty starting blackboard can lead to a smaller diversity because with many hints already available, the importance of hint selection strategy becomes less important.

The initial contents of the blackboard also affect the overall performance of the system. If hints are misleading, the agents will be slowed; if, on the other hand, hints are useful then the overall performance will be improved, especially for the faster agents. In general, as the number of hints present on the initial blackboard was increased, the statistical fluctuations in the effectiveness of the hints decreased and ensuing performance was enhanced.

Fluctuations we have shown that cooperation can lead to a large performance increase, but how consistent are these predictions? By running the same problem numerous times we can get an idea of the fluctuations that can

be expected. With an initially empty blackboard the impact of the quality of the early hints can be easily observed. Figure 8 shows two separate runs of 100 agents solving the problem $CLEAR + WATER = SCOTT$. Although the two runs agree with a lognormal distribution, they are quite different in terms of the speed at which they solved the problem. These fluctuations are amplified by the multiplicative nature of cooperation. We should point out however, that these differences became smaller as the problem became more complex and the number of agents increased.

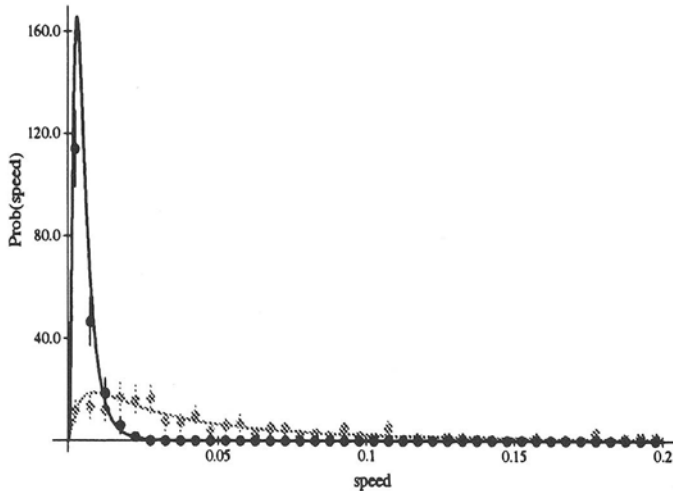


Fig. 8. The quality of hints can lead to vastly different lognormal distribution parameters. The data are speed distributions from two separate runs of 100 agents solving the problem $CLEAR + WATER = SCOTT$. Note that both distributions fit well to a lognormal. The error bars are statistical.

It is possible to study the effect on the overall solution time distribution of making solutions available to the agents on the blackboard. The option of not posting complete solutions had the effect of slowing down the slower finishers. When the solutions were posted for the problems $WOW + HOT = TEA$ and $CLEAR + WATER = SCOTT$, about half the agents found the solution by reading one directly.

6.2 Problem Solving by Hierarchical Organizations

To model the effect of more complex organizations, we considered several alternatives to committees in both the hierarchical structure and the inter-

actions among agents. These alternatives were based on the branching factor between levels, the number of levels, cost of access between and within levels, and other parameters of hierarchies. Under certain conditions a hierarchy can perform poorly. However its performance can be improved by the addition of informal links between members of the organization (Huberman & Hogg 1995). To investigate its applicability to search, we compare behavior in hierarchies, illustrated in Fig. 9, with and without such informal links.

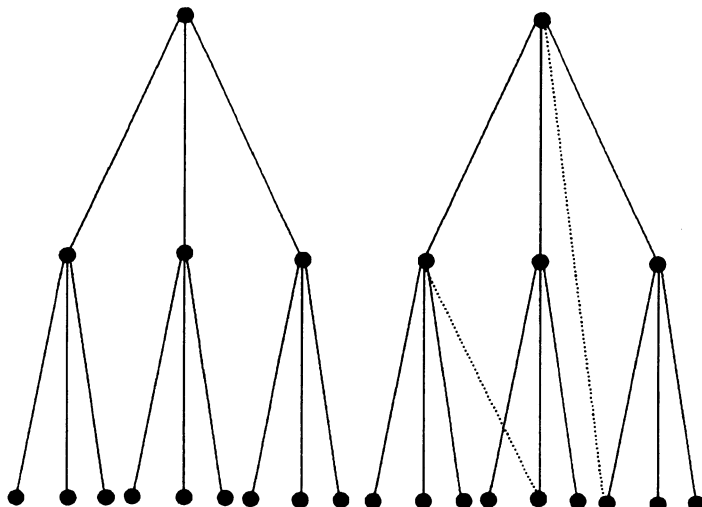


Fig. 9. *Left:* A strict hierarchy with branching factor three and depth three. *Right:* The same tree with two additional “informal” links in dashes. The informal links have little or no communication cost and do not exist in a formal hierarchy.

For search in the hierarchy we associate a blackboard with each agent, but instead of restricting agents to use only their own blackboard (a non-cooperative search), they now can post and read hints from other ones as well. Unlike the committee case involving a single central blackboard, the agents now need to decide where to send and from where to receive their hints. Thus, depending on the particular hierarchy involved different blackboards (agent's individual postings of good columns for the cryptarithmetic problem) were accessible via different costs.

In our experiments the cost of communication increased the greater the distance between the nodes in question, as is the case in real hierarchies. It should be noted that only read access was attributed a cost. Also, although write cost was considered to be free, the likelihood of posting a hint on a

different level blackboard decreased the further away the two blackboards were. This situation only applied for the cases where the better hints were not restricted to higher levels.

Figure 10 shows speed distributions for a purely formal hierarchy and a hierarchy with many informal links. The difference in speed-up between the curves depends on the costs and probability of accessing other nodes as well as the quality of hints at a given level. The speed to solution was found to be greater for organizations that had informal links, i.e., links that violated the strict hierarchy and had zero communication cost. It remains an open question exactly how changes in organizational structure affect the benefit of cooperation.

We also found that hierarchies in which higher quality information was passed only to higher levels achieved a higher performance than those in which information could be posted anywhere. It is interesting to note that with informal links and where no communication among siblings was allowed, the top level agent solved the problem much more frequently than would be expected by its representation in the population. In cases where there was sibling communication or informal links were allowed, the agents at the lowest level solved the problem more frequently than would be expected based simply on their relative occurrence in the organization.

7 Discussion

We have shown how cooperating agents working towards the solution of a constraint satisfaction problem can lead to a marked increase in the speed with which they solve it compared to their working in isolation. In particular, we showed how a diversity of cooperating agents can lead to a super-linear speed-up with agent number in the time to solution. This was compared to the case of non-diverse and non-cooperating agents where linear speed-up was observed.

The effects of diversity are especially important for the fastest and slowest agents. For a sufficiently large number of agents, the group with the highest diversity was able to solve the problem first. Interestingly, high diversity not only leads to very high performers but to very low ones as well.

This work suggests an alternative to the current mode of constructing taskspecific computer programs that deal with constraint satisfaction problems. Rather than spending all the effort in developing a monolithic program or perfect heuristic, it may be better to have a set of relatively simple co-operating processes work concurrently on the problem while communicating their partial results. This would imply the use of “hint engineers” for coupling previously disjoint programs into interacting systems that are able to make use of each others (imperfect) knowledge. Although we have tested our model against only one type of constraint satisfaction problem, we believe that there

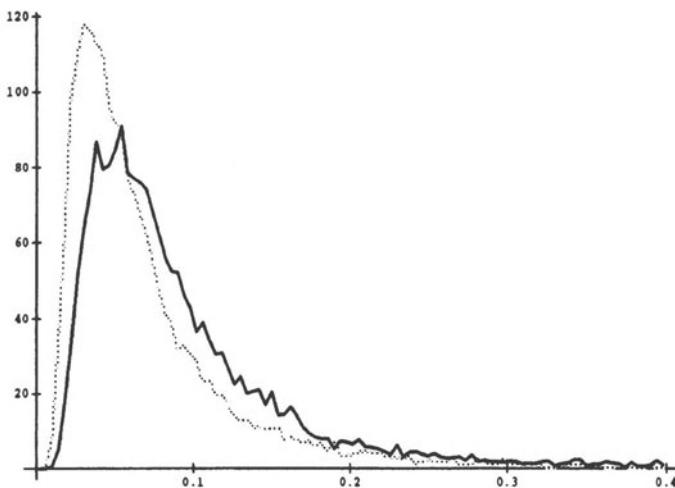


Fig. 10. Speed probability distribution for 100 runs of 111 hierarchical agents trying to solve $WOW + HOT = TEA$. The branching ratio was 10 and depth of the organization 3. The light curve shows the case where there were sibling links but no informal links. The dark curve shows the case where the number of informal links added to each node was equal to the number of its direct descendants, siblings, and all ancestors (except the top node received no informal links).

are more general problem solving settings where we expect cooperation to be beneficial.

In our cryptarithmetic experiments we defined hints in terms of information that moved the agents toward a region of the space that could have a solution. Another possibility is for hints to contain information that tends to move away from regions that can have no solutions. Our theoretical derivation does not depend on which approach is used, only that some part of the search space is pruned, or is more likely to contain a solution. More generally, any search algorithm that agents may use will have parameters that will have an impact on the effectiveness of cooperation. An intrinsic advantage of cooperative search over purely algorithmic search is the former's ability to make large jumps in the search space by opportunistically utilizing shared information. Although in some cases these jumps will prove detrimental, the ability to make large excursions around the search space based on shared information is generally advantageous for at least a few agents. Another consideration is when are the hints most useful for problem solving. At the beginning of a problem the hints provide crucial information for starting the agents off on a plausible course, but will usually be fairly nonspecific. Near the end of the

problem however, there are likely to be many detailed hints but also of less relevance to the agents since they may have already discovered that information themselves. This suggests that typical cooperative searches will both start and end with agents primarily working on their own and that the main benefit of exchanging hints will occur in the middle of the search.

Because our results provide a quantitative relationship between performance, number of agents, and the ability of agents to make use of diverse hints, this new methodology may be particularly useful in areas of artificial intelligence such as design, qualitative reasoning, truth maintenance systems and machine learning. Researchers in these areas are just starting to consider the benefits brought about by massive parallelism and concurrency.

Our discussion focused on the benefits of cooperation among agents that search the space differently (due to different initial states and different hints selected from the blackboard). The most natural way to think of this is a collection of independent processes, possibly running on separate processors. However, it is always possible to have a single computational process that, in effect, multiplexes among the procedures followed by this diverse set of agents. In this way, a single agent could also obtain the benefit of cooperation discussed here. This ability of one computational process to emulate a collection of other processes is quite distinct from other cases of cooperation, e.g., human societies, where individuals have differing skills that are not easily transferred to others.

For computational processes, the issue is not so much cooperation as to what extent partial results from a range of methods are used. That is, the cooperative speed-up is due to applying a diverse set of methods to a problem, each of which fails under different conditions and can sometimes benefit from information provided by other methods. We have shown that even when the individual methods are imperfect and the information exchanged is not always correct, the overall benefit can be very large. This can be contrasted with the usual emphasis on improving individual methods. It is presently an open question as to how to exploit this diversity explicitly in problem solving or to know how to estimate it *a priori*.

Thus we see the emphasis here is on the diversity of methods available to approach a problem, as well as their ability to sometimes benefit from the partial successes of each other. In effect, we observe a huge speed-up as diversity and effectiveness of the exchange of information increases. This contrasts with discussions of the speed-up due to parallel processors in which the speed of a fixed algorithm is measured when running in a number of processors. It is well known from Amdahl's law that the speedup cannot be faster than linear in the number of processors, and is usually less due to communication overheads. There is no such restriction on the speed-up obtainable when additional diversity is introduced, either in the form of new processes running on additional processors, or by having a single algorithm incorporate additional methods.

One of the questions to be addressed is, how “dumb” agents can be yet still benefit from cooperation? If agents are too simple then they will not be able to utilize the information from other agents and thus not benefit from cooperation. For example, a simple random generate and test search that replaces all letter assignments at each step will immediately lose whatever potential benefit a hint gave it. As we saw, simple search methods with some memory can benefit from hints. This issue arises in non-computational examples as well. At the one end of the spectrum consider insect societies, where individuals are very poor problem solvers but when cooperating they are able to solve very complex tasks such as nest building, defense, and food gathering. At the other end of the spectrum the agents of a scientific community are very good at individual problem solving. This is greatly amplified by cooperation through publications and collaborations. Because cooperation appears to improve problem solving at both extremes of individual agent ability, from simple ones as in an insect society to scientists in a technical community, the benefits of cooperation are widely applicable. The agents we considered in our experiments were capable of only very simple interactions and behaviors and yet achieved considerable performance improvement versus isolated agents.

In closing, we comment on the implications of these results for social and biological organizations. In spite of the fact that we studied extremely simple agents (with no learning capabilities, and no specialization) these results may also be relevant to the more complex agents that make human organizations. We base our belief on the established fact that measures of productivity in the scientific community (Shockley 1957), individual problem-solving (Bree 1975), as well as income distributions in a variety of economies, exhibit a log-normal distribution (Aitchison & Brown 1969). Although those distributions have been accounted for in terms of individual probabilities for a given agent to either obtain a certain publishable result or accrue a net worth, cooperative efforts as studied in this paper do give rise to the same performance characteristics, thus suggesting an alternative explanation.

References

- Aitchison J., Brown J.A.C. (1957): *The Lognormal Distribution*. Cambridge University Press, Cambridge.
- Aitchison J., Brown J.A.C. (1969): *The Lognormal Distribution*. Cambridge University Press, Cambridge.
- Axelrod R., Hamilton W. (1981): *The Evolution of Cooperation*, Science, **211** 1390-1396.
- Bollobas B. (1985): *Random Graphs*, Academic Press, NY.
- Bree D.S. (1975): *The Distribution of Problem-Solving Times: An Examination of the Stages Model*, Br. J. Math. Stat. Psychol., **28** 177-200.
- Clearwater S.H., Huberman B.A., Hogg T. (1991): *Cooperative Solution of Constraint Satisfaction Problems*, Sciences **254** 1181-1183.

- Crow E.L., Shimizu K. editors (1988): *Lognormal Distributions: Theory and Applications*, Marcel Dekker, New York.
- Engelmore R., Morgan T. (1988): *Blackboard Systems*, Addison Wesley, Reading.
- Goldberg D.E. (1989): *Genetic Algorithms in Search, Optimization, and Machine Learning*, Addison-Wesley, Reading.
- Huberman B.A., Hogg T. (1987): *Phase Transitions in Artificial Intelligence Systems*, Artificial Intelligence, **33** 155-171.
- Huberman B.A., Hogg T. (1988): *The Behavior of Computational Ecologies*. In *The Ecology of Computation*, B.A. Huberman ed., 77-115. North-Holland, Amsterdam.
- Huberman B.A. (1990): *The Performance of Cooperative Processes*, Physica D, **42** 3847.
- Huberman B.A., Clearwater S.H., Hogg T. (1992): *Cooperative Problem Solving*, Computation: The Micro and the Macro View 33-70.
- Huberman B.A. and Hogg T (1995): *Communities of Practice: Performance and Evolution*, Computational and Mathematical Organization Theory, **1** 73-92.
- Kornfeld W.A. (1982): *Combinatorially Explosive Algorithms*, Communications of the ACM, **25**(10) 734-738.
- Krebs C.J. (1972): *Ecology*, Harper and Row, New York.
- Montroll E.W., Shlesinger M.F. (1982): *On 1/f Noise and other Distributions with Long Tails*, Proc. Natl. Acad. Sci. (USA), **79** 3380-3383.
- Pearl J. (1984): *Heuristics: Intelligent Search Strategies for Computer Problem Solving*, Addison-Wesley, Reading, Mass.
- Shockley W. (1957): *On the Statistics of Individual Variations of Productivity in Research Laboratories*, Proceedings of the IRE, **45** 279-290.

Microscopic Computer Simulation of Fluids

P. Cordero¹ and D. Risso²

¹ Departamento de Física, Facultad de Ciencias Físicas y Matemáticas, Universidad de Chile, Santiago 3, Chile

² Departamento de Física, Facultad de Ciencias, Universidad del Bío Bío, Concepción, Chile

1 Introduction

When studying fluids it is frequently the case that the construction of a reasonable approximate theory becomes an elusive endeavor. The more difficult and interesting these problems are the better it is to have exact results, coming directly from the microscopic kinetics, both to test the existing theoretical approaches and to gain insights into new ones. To progress in the formulation of fluid dynamics it is desirable not to have to undertake the description of a precise and particular realistic fluid. The latter is an interesting but different problem.

Hydrodynamics is the main tool to describe fluids from the macroscopic point of view. The basic assumption of hydrodynamics is that changes in a fluid take place smoothly or slowly so that the system can be assumed to be in a state of local thermodynamic equilibrium. When the condition of smooth/slow variation is not fully satisfied the fluid may be expected to deviate from the predictions of hydrodynamic calculations. If X is a hydrodynamic field (e.g., density, temperature) it can be said that X varies smoothly if $\xi = \ell|\nabla X|/X$ is negligible, ℓ being the mean free path of the particles of the fluid. X varies slowly if $\xi = \frac{\tau}{X} \frac{\partial X}{\partial t}$ is negligible where τ is the mean free flight time. The use of kinetic theory becomes essential if ξ cannot be taken to be zero.

Kinetic theory, on the other hand, gives a more fundamental theory but it has been well developed only for rather dilute systems. The first steps in the formulation of kinetic theory reduces the direct Hamiltonian dynamics first to Liouville's equation and then to an infinite set of integrodifferential equations, known as the BBGKY hierarchy. Since there is no systematic way of applying something like perturbation theory to such system of equations, their analysis has been, and still remains, a patchwork of ingenious techniques that are designed to cover special parameter regimes.

Special mentions deserve Boltzmann's and Enskog's equations. The former can be validated in the so called Boltzmann-Grad limit of low density and finite mean free path, (Grad 1958,60). Enskog's equation has a larger domain of validity and was originally written for a gas of hard spheres, but it can be extended to other cases. For example when the hard spheres interact

\mathbf{c}	molecular velocity
\mathbf{C}	peculiar velocity, $\mathbf{C} = \mathbf{c} - \mathbf{v}$
$f(\mathbf{r}, \mathbf{c}, t)$	distribution function
f_G	Grad's distribution
f_M	Maxwell's distribution
FEL	future event list
Fr	Froude number
$g(r)$	radial distribution function
H	function of the density that appears in the equation of state
k	thermal conductivity
k_B	Boltzmann's constant
ℓ	mean free path
L	length of the side of a cubic (square) box
L_i	box linear dimension in the i direction
MD	molecular dynamics
n	local number density (number of particles per unit volume)
\bar{n}	global number density. In 2D it is $\bar{n} = N/L_X L_Y$
N	number of particles
N_{diff}	number of collisions in one diffusion time
p	hydrostatic pressure
\mathbb{P}	pressure tensor
P_{ij}	components of \mathbb{P}
p_{ij}	traceless part of \mathbb{P} , $P_{ij} = p \delta_{ij} + p_{ij}$
\mathbf{q}	heat current
Ra	Rayleigh number
Re	Reynolds number
t_{diff}	thermal diffusion time
$T(\mathbf{r})$	temperature field
u	specific internal energy per unit mass
u_K	specific kinetic energy per unit mass
\mathbf{v}	hydrodynamic velocity
v_{th}	thermal velocity

Table 1. Glossary of main Latin symbols and acronyms used in the text.

via a square well potential the collision term on the right hand side of the kinetic equation becomes rather involved, but it can be worked out explicitly.

Once one of these kinetic equations is stated the challenge is to find approximate solutions. Perhaps the most widely used method is that of Chapman and Enskog. This method is based on a perturbative expansion about equilibrium where the small parameters are the r th-order spatial derivatives of the density, hydrodynamic velocity and temperature fields. The zeroth order solution is Maxwell's equilibrium distribution; the first order gives Eu-

χ	Enskog's collision factor
η	shear viscosity
γ	adimensional shear rate
Γ	total collision rate, $\Gamma = N\nu/2$
λ	aspect ratio $\lambda = L_X/L_Y$
ν	collision frequency
ρ	mass density, $\rho = m n$
ρ_A	local area density of a two dimensional gas
$\bar{\rho}_A$	global area density of a two dimensional gas, $\bar{\rho}_A = \frac{\pi\sigma^2}{4} n$
σ	diameter of the hard core of a particle
\mathcal{V}	phase space

Table 2. Glossary of main Greek symbols used in the text.

ler's ideal hydrodynamics and the second order provides a version of Navier Stokes equations with linear transport equations and explicit expressions for the transport coefficients. The third order was derived by Burnett in 1935 and will not concern us here.

In hydrodynamics the transport equations are part of the so called *constitutive equations* in the sense that they are needed to make the hydrodynamic equations a closed (self-contained) system of equations.

Harold Grad presented a different way to construct approximate solutions to Boltzmann's (eventually Enskog's) equation, (Grad 1958,60). In his solution he does not expand in gradients of the first five momenta of the velocity distribution (density n , hydrodynamic velocity \mathbf{v} and temperature T) as in the Chapman-Enskog method, but rather uses a self-consistent approach additionally involving higher momenta and no gradients of them. In particular he works out in detail the case when the distribution function f is written in terms of n , \mathbf{v} and T and also the traceless and symmetric part of the pressure tensor, p_{ij} , and the heat flux vector \mathbf{q} . From this method nonlinear transport equations emerge naturally.

Decades ago there was no way to separate the tests of new developments in kinetic theory from the challenge to describe particular fluids. Presently it is possible to get semi-experimental results from microscopic computational simulations using *Molecular Dynamics* (MD) techniques in which the microscopic interactions are part of the data and they are not bound to being realistic.

These lectures give a partial view of the study of the behavior of simple fluids from a microscopic point of view by means of kinetic theory. See Chapman & Cowling (1970), Hansen & McDonald (1986), Lifshitz & Pitaevskii (1993), Résibois & de Leener (1977), Ferziger & Kaper (1972) combined with

the methods of microscopic computational simulations: Allen & Tildesley (1989), Ciccotti & Hoover (1986), Ciccotti *et al.* (1987) taking advantage of recent efficient algorithms and strategies of molecular dynamics, Rapaport (1980), Lubachevsky (1991), Marín *et al.* (1993), Cordero *et al.* (1995).

2 Simulator and Simulations

2.1 Background Generalities on Molecular Dynamics

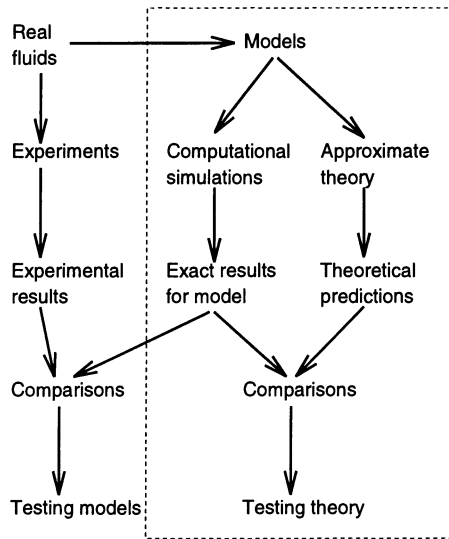


Fig. 1. Diagram adapted from Allen & Tildesley (1989). With realistic interactions it is interesting to compare experiment and simulation results to test a particular model. With *any* suitable interaction the comparison of the theoretical predictions with the simulational results tests the theory itself. Much work is done within the limits of the dashed line rectangular box above.

Molecular Dynamics (MD), in the sense of these lectures, is a computer simulation technique which traces the microscopic *Newtonian* time evolution of a system of N classical particles in the phase space of all of them. In combination with appropriate ensemble or time averaging, the technique gives a solution to the Liouville equation without having to make any assumptions concealed neither behind hydrodynamics nor in the standard formulation of kinetic theory.

MD simulations offer a powerful tool to test hypotheses made about the behavior of fluids particularly because of the intrinsic complexity of kinetic theory.

Making stationary regime MD simulations will usually involve only a few hundred particles and for this reason it is necessary to be careful with size and wall effects. The physics that takes place near the walls may play a non-negligible role. In fact, the fraction of particles that – at any moment – are close to the walls is at least $\mathcal{O}(N^{-1/d})$, where N is the total number of particles in the numeric experiment.

It is perhaps interesting to recall that many important and historical findings were made (by Alder and Wainwright) with systems of about 100 particles mainly at equilibrium. Today many interesting results involving steady state hydrodynamics behavior are commonly made with systems of about 2000 particles as in Mareschall *et al.* (1986,87,88,89).

The fundamental importance of MD simulations rests in the fact that they provide essentially exact, quasi-experimental data on well defined models. As there is no uncertainty about the form of the interaction potential, theoretical results can be tested unambiguously in a manner that is generally impossible with data obtained in experiments with real fluids. It is also possible to obtain information on quantities of theoretical importance that are not readily measurable in the laboratory.

2.2 Characteristics of the Simulations

The type of simulations we deal with in the present lectures have the following common characteristics.

- the only degrees of freedom of the particles are translational
- collisions among particles are perfectly elastic, hence conserving momentum and energy
- the diameter of the particle's hard core is σ : the energy potential is infinite for $r < \sigma$
- the particles may additionally interact among themselves with a square potential of depth $-\epsilon$ in the range $\sigma < r < \alpha\sigma$, ($\alpha > 1$). The parameter α is the adimensional range of the interaction
- the interaction with the walls depends on the case under study. They may be, for example,
 - o specular collisions (adiabatic slip walls)
 - o thermal slip collisions (stress free boundary condition): the particles bounce back conserving their tangential velocity while the normal velocity is sorted out from a Maxwellian distribution characterized by a given temperature T .
 - o thermal nonslip collisions: both components of the velocity are sorted from a heat bath at temperature T and the sign of the tangential component is randomly chosen.
 - o thermal nonslip moving wall: same as the thermal nonslip wall except that a value v_0 is added to the tangential velocity to simulate that that wall is moving orthogonal to its normal.

- o periodic walls: a particle that hits a wall reenters the system through the opposite wall with the same velocity. In this case there can be collisions between particles which are at different sides of a periodic wall.
- o etc
- the basic data to run a simulation are: the number of particles N , the aspect ratios of the box and the bulk density. Other data are needed in each specific class of simulation.

To simulate a fluid one usually wants the mean free path to be significantly smaller than the size of the box, otherwise boundary effects influence the whole system. In the case of a bidimensional system this condition implies that $N \gg 1/\bar{\rho}_A$, where $\bar{\rho}_A$ is the bulk area density. Further, if the simulation is going to be compared with ideal gas results then, loosely speaking, one may say that the mean free path has to be much larger than the size of the particles implying that $\bar{\rho}_A \ll 1$.

Always for a two dimensional gas of disks, the requirement that the equation of state deviates by less than 5% from the ideal gas equation implies that the area density satisfy $\bar{\rho}_A \leq 0.025$. Additionally requiring that, for a system in a $L \times L$ square box, the mean free path satisfies $\ell/L \leq 0.05$, yields that the number of particles has to be $N \geq 1570$.

2.3 The Simulator

In the following there is a description of a strategy to make efficient simulations of systems of several thousand particles interacting via a step potential. A performance of several million collisions per hour is perfectly attainable in present day standard workstations. These algorithms are particularly appropriate for kinetic studies at a microscopic level in situations near or far from thermodynamic equilibrium.

In the case of step potentials the particles move free of each other except at discrete times when they suffer impulsive forces or *events*. The evolution of each particle between events follows Newton's equations of motion with whatever external field (e.g., gravity) may exist but free from interparticle interactions. The events take place whenever a particle hits one of the steps of the potential energy function. Applications of this type of simulations are illustrative and inspiring since the beginning of molecular dynamics till present days. The basic steps of a simulation of this type are sketched in Fig. 2.

A typical action at step 2 could be

$$\begin{aligned} \mathbf{r}_k &\leftarrow \mathbf{r}_k + \mathbf{v}_k \tau_k + \frac{1}{2} \mathbf{g} \tau_k^2, \\ \mathbf{v}_k &\leftarrow \mathbf{v}_k + \mathbf{g} \tau_k, \end{aligned}$$

- 0a) An initial state is given, namely positions and velocities for all particles and
 - 0b) the list of all possible future events, or FEL (*Future Event List*), is initialized.
- 1) The next event is determined from the FEL;
 - 2) if necessary, positions and velocities are updated to the instant of this event;
 - 3) the collision rule that defines the model is applied to the state of the particle(s) involved in the event;
 - 4) new events are predicted for the particles involved in the present event;
 - 5) the new predicted events are inserted (*scheduled*) into the FEL and go back to step (1).

Fig. 2. Basic cycle in an *event driven* simulation.

where τ_k is the time interval between the previous event and the present one and \mathbf{g} is the acceleration of gravity.

This type of dynamics is called *event driven*, because it proceeds by time steps τ_k that are dictated by the dynamics itself instead of proceeding via time steps δt predefined in the algorithm as it is done whenever continuously varying potentials are used. The enormous advantage of event driven simulations is that — because of their efficiency — it is possible to explore significant parts of the evolution of the system.

One of the important bottlenecks of these simulations could be step (1) unless the next event is determined through a carefully written algorithm. A breakthrough in efficiency was given by Rapaport (1980). A different strategy which is efficient in a wider range of densities is found in Marín *et al.* (1993).

The FEL is important because — as it was argued before — these simulations proceed jumping analytically from one collision (or *event*) to the next. And the next event is determined using a binary tree as part of the FEL's structure. But since predictions have to be updated as the simulation proceeds the binary tree is not only called for to pickup the next event but also when new information has to be inserted in it. This may be costly. With this strategy it has been possible to reduce the number of accesses to the binary tree to about one access for every particle involved in each collision (Marín *et al.* 1993). We know of no other algorithm which can attain this performance. Some improvements were introduced in Marín & Cordero (1995).

Cells and a new type of event. To determine the next event without risking the possibility of a mistake it is apparently necessary to know first the times when every possible collision would take place. This means particle-particle as well as particle-wall events. There are $\mathcal{O}(N^2)$ such times and they would have to be compared to get the smallest one. In typical situations most of the predicted events never happen since the particles involved change their direction of movement at previous collisions. In this sense it could be said that many predicted events become *invalidated*.

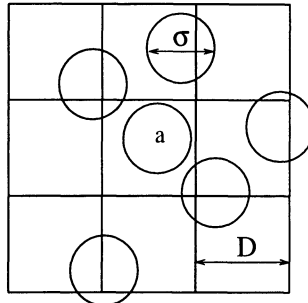
Since the beginning of the history of event driven simulations the convenience of dividing the system in cells was clear (Alder & Wainright 1959). A particle belongs to a cell if its center is inside the cell. The linear size D of the cells is chosen so that a particle cannot interact but with particles which are in its own cell or in the *neighboring cells*. For example, in a bidimensional system broken in square cells a typical cell is surrounded by eight others. The *neighborhood* of a particle k is the cell where k is plus the set of neighboring cells.

For hard disks of diameter σ , for example, the linear size D of a cell has to satisfy, $D > \sigma$ to make the previous concepts consistent.

A new type of event is introduced: *crossing a cell wall*. This event has no physical meaning of course. Their occurrence does not alter the physical evolution of the system but it can be realized that now there is no need to predict events involving a particle i and objects (other particles or a wall) beyond its neighborhood since there is at least one event involving i and an object in its neighborhood prior to any event with objects outside it.

To make this point clear suppose the rare situation where the next *physical event* involves the collision between two particles that are far beyond their respective neighborhoods. From the algorithm's point of view this event is preceded by several cell wall crossings. Each one of these events — artifacts of the algorithm — implies that at step 4 above, new events are predicted for one of these particles. After a sequence of cell wall crossings the two particles will *see* each other and the actual collision will correctly be predicted.

Hence predictions for each particle i at step 4 are made only between objects belonging to the neighborhood of i . After i suffers a collision all predictions for it have to be renewed whereas if i makes a cell wall crossing its neighborhood changes and new predictions are *added*: those involving i and objects in the new cells belonging to the neighborhood of i .



A particle a belongs to the cell where its center is. For a 2D system the neighborhood of a will usually contain 9 cells.

Since each neighborhood contains a number of particles which is independent of the size of the system, the total number of events that have to be predicted for the whole system is $\mathcal{O}(N)$.

The five steps mentioned above suffer some minor obvious modifications because this new type of event is introduced. For example, if the present event is a cell wall crossing there is no need to apply any collision rule.

The future event list (FEL). To search for the next event efficiently one has to keep future events in order. Binary search is a standard strategy, (Knuth 1973). For example when looking for a word in a dictionary one roughly proceeds as follows: cut the dictionary in two equal halves, make a comparison to decide in which half is the target word, then break the chosen part in two again and so forth. The search time is $\mathcal{O}(\ln_2 N)$ if there are N words in the dictionary.

There are many variants of the strategy sketched above. Which strategy should be chosen depends on other aspects of the problem. In the case of our simulations three functions act on the FEL: (a) getting the next event; (b) inserting new predicted events and (c) erasing invalidated events. Binary trees in general allow for efficiently implementing the operations (a) and (b), but erasing is not trivial and it may be time consuming. After a careful assessment of these problems and experimenting with some of the structures put forward in the literature the choice, in Marín *et al.* (1993), was the structure described next. It will be seen that with this algorithm there is no need to make eliminations within the binary tree.

To each particle i is associated a single linked list L_i containing the future events $\mathcal{E}_i(x)$ predicted for particle i with an object x (another particle or a wall). When an event $\mathcal{E}_i(k)$ is predicted for particle i at step 4, it is inserted in the list L_i and it is *not* inserted in the list L_k . Namely, each future event is entered only once to the FEL. These $\mathcal{E}_i(x)$ are structured variables containing the necessary information associated to the specific event. In particular they contain the time when the event is scheduled to happen.

Each one of these N lists has a *local minimum event*, the event in the list that has the lesser schedule time. These N local minima are the only events that enter the binary tree. The determination of the local minimum for particle i and its insertion into the binary tree is performed regardless of the existence of other possible events $\mathcal{E}_\ell(i)$ within the FEL.

The binary tree structure chosen in Marín *et al.* (1993) is that of a *complete binary tree* (Knuth 1973) or CBT. It is a binary tree of K levels. At level 0 is the root, at level 1 are its two children, at level n there are 2^n nodes, children of the nodes at the previous level. K is determined by the number N of particles: $2^{K-1} < N \leq 2^K$, so that the lowest nodes (*leaves*) are exactly N and they are partly at the incomplete level K and the rest at level $K - 1$. Each particle is associated to one and only one of these lowest nodes or *leaves* once and for ever.

Since only the local minima enter the CBT, each particle-label in it has

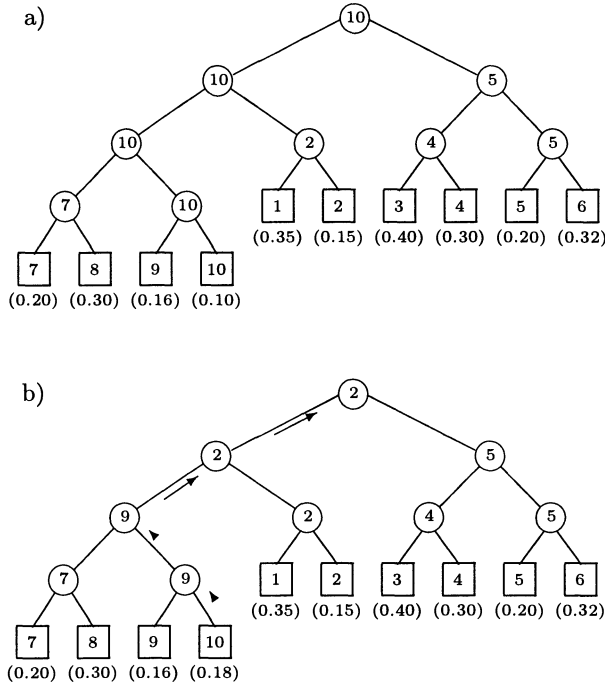


Fig. 3. a) Complete binary tree (CBT) for 10 particles. For N particles the CBT has $2N - 1$ nodes numbered from 0 to $2(N - 1)$. The leaf associated to particle k is the node $q = N + k - 2$. The local minima times are in parenthesis. b) The CBT updated after the local minimum of particle 10 was changed to the value 0.18.

associated the time at which the corresponding local minimum is scheduled to happen. The logic of the CBT is the same one used in many sports tournaments: to each competitor is associated a fixed leaf node. The name of the winner of each individual match (i.e. comparison of the associated times) is transcribed to the parent node. The same rule is recursively applied upwards in the tree and in this way each internal node has the label of the particle with lesser time of its two children. The label of the absolute winner reaches the root of the tree. This is the particle whose local minimum should be the next event. During the simulation the form of the CBT and the labels of the leaves remain unaltered, while the labels at the internal nodes change dynamically.

When a particle i suffers a collision, its list L_i is erased and replaced by the list of new predictions involving i . This is done at step 4. On the contrary, if

particle i crosses a cell wall, then its neighborhood changes. Events involving i with other objects in the new cells are *added* to the list L_i , no events are erased.

In the two situations described in the previous paragraphs it is necessary to reobtain the local minimum for i which is then inserted into the binary tree replacing the old one. Matches are performed along the natural path from leaf i towards the root of the CBT. It is easy to check that $\mathcal{O}(\ln N)$ matches are performed as part of step 5.

At this point it is necessary to clarify that only the labels i identifying the particles associated to the local minima enter the binary tree and not the full structures $\mathcal{E}_i(x)$. Inserting and deleting is efficient because it is an operation over the lists L_i . In fact, in Marín *et al.* (1993) it has been established that the cost of picking the next event and scheduling n new events for each particle are $\mathcal{O}(1)$ and $\mathcal{O}(n - 1 + \ln N)$, respectively. That is, the number of accesses to the binary tree has been reduced to about one access for every particle involved in each collision. As said before, we know of no other algorithm which can attain this performance.

One possible implementation of a CBT could be the following. Let $t[k]$ ($k = 0..M$) be the times that have to be ordered and define the CBT array of integers $B[q]$, $q = 0..2M$ in such a way that 0 is the root node while the children of node p are the nodes $p_- = 2p + 1$ and $p_+ = 2p + 2$. The leaves (nodes with no children) are the nodes from $q = M$ to $q = 2M$, so that $t[k]$ is associated to the leaf node $k + M$. To each internal node p of the tree is associated the same index k (of time $t[k]$) as one of its children according to

$$\text{if } t[B[p_-]] < t[B[p_+]] \quad \text{then } B[p] = B[p_-] \quad \text{else } B[p] = B[p_+]. \quad (1)$$

If a node p' has been updated following the previous rule it is necessary to continue updating upwards. Then p' has to be considered now a child $q = p'$ and its father is node $p = \text{floor}(\frac{q-1}{2})$ with children p_- and p_+ one of which is q . This recursive rule should in principle be applied until the root is reached although it is often possible to stop earlier, Marín & Cordero (1995).

In the case of continuous potentials a totally different strategy has to be followed. Typically they are based on Verlet's algorithm, (Allen & Tildesley 1989). A quite recent reference from which the literature can be traced back is Glikman *et al.* (1996).

2.4 Measurements

The system has to relax before starting measurements in a study of stationary regimes.

To make observations during the simulations the system has to be divided in *cells* to observe its behavior. These cells must not be confused with the cells of the central algorithm. The routines make a careful balance of mass, momentum and energy in each cell (these are densities) and what comes in or

out across each wall of every cell (integrated fluxes). The measured quantities are then averaged in time in every cell or wall depending on whether they are densities or fluxes (Risso 1994).

Nomenclature: We distinguish a *flux vector* \mathbf{J} (which could also be called a *current density*) from an *integrated flux* across a surface \mathcal{S} , $\Phi = \int \mathbf{J} \cdot d\mathcal{S}$. But when no confusion is possible the word flux is used to mean either a flux vector or an integrated flux.

Measuring densities. In principle this means evaluating

$$\bar{\varphi} = \frac{1}{\tau} \int_{t_0}^{t_0 + \tau} \varphi dt \quad (2)$$

during the simulation. Since the simulations are driven by discrete events these averages are in practice evaluated in the form

$$\bar{\varphi} = \frac{1}{\tau} \sum_k \int_{t_{k-1}}^{t_k} \varphi dt, \quad (3)$$

where the t_k are a subset of the event times that will be called the *interesting events* associated to φ . To understand the idea of an *interesting event* two examples follow.

To determine the density in a cell A it is necessary to average the number of particles in A . With this aim the only interesting events are those corresponding to particles crossing from one cell to the next. No collision event is interesting in this case. The integrals appearing in (3) trivially reduce to $m_{k-1}(t_k - t_{k-1})$.

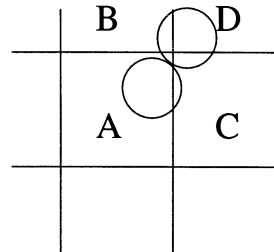
To determine the average kinetic energy in every cell, in the case of a system of bare hard disks, all events are interesting except for the collisions that occur between particles belonging to the same cell.

Measuring fluxes. To get an integrated flux, $\Phi_w = \int_w \mathbf{J} \cdot d\mathcal{S}$, across a cell wall w it is necessary to keep track of every exchange, per unit time, of mass, momentum and energy across the wall w . The instantaneous flux of a quantity φ at the time t_k is given by $\varphi(t_k) \delta(t - t_k)$, where φ is the magnitude of the transferred property. Averaging in time yields

$$\Phi_w(\varphi) = \frac{1}{\tau} \int_{t-\tau}^t \varphi(t_k) \delta(t - t_k) dt = \frac{1}{\tau} \sum_k \varphi(t_k). \quad (4)$$

These exchanges can occur simply because a particle crosses from one cell to the next contributing to the *kinetic transport*, or they occur because there is a collision involving particles which are in different cells (exchanging momentum, for example) contributing to *collisional transport*. The simulation can keep separate track of the kinetic and collisional contributions of every flux vector being studied.

Special care has to be taken when the exchange $\varphi(t_k)$ occurs between two particles that belong to cells which only share a corner as A and D in the figure. This is a problem because fluxes need to be defined through walls and not through corners. The figure represents the collision of two particles belonging to diagonally neighboring cells A and D . These events are rather infrequent and a simple but not totally correct solution is to attribute half the flux to the path $A \rightarrow B \rightarrow D$ and the other half to the path $A \rightarrow C \rightarrow D$.



Collision between two particles that belong to cells that share only a corner.

2.5 Hard Particle Systems

Hard Disks. Attention will often be placed in simple bidimensional systems. These systems will consist of N particles of mass m — either bare hard disks or hard disks interacting with a square well potential. The system will be inside a rectangular box of size $L_X \times L_Z$, aspect ratio λ and *bulk area density* $\bar{\rho}_A$,

$$\lambda = L_X / L_Z, \quad \bar{\rho}_A = \frac{\pi N \sigma^2}{4 L_X L_Z} \quad (5)$$

where σ is the diameter of the hard core of the particles.

The interaction of the particles with the walls was described in §2.2.

The equation of state of a system of hard disks has to have the form

$$p L_X L_Z = N H(\rho_A) k_B T, \quad (6)$$

where $\rho_A = \rho_A(\mathbf{r})$ is the local area density. In general the dependence on T , on the right hand side, is not trivial, but when the interparticle interaction does not introduce an energy scale a dimensional analysis shows that the pressure has to be proportional to the temperature T . The function $H(\rho_A)$ is as much known as the virial coefficients for this system, (Kratky 1978). A practical and simple approximate expression (Henderson 1975, Barker & Henderson 1976) is

$$H(\rho_A) = \frac{1 + \frac{\rho_A^2}{8}}{(1 - \rho_A)^2}. \quad (7)$$

More accurate equations of state are found in Maeso & Solana (1993).

The radial distribution function $g(r)$ at contact, $\chi = g(\sigma^+)$, is a function of the density,

$$\chi(\rho_A) = \frac{H - 1}{2\rho_A} = \frac{1 - \frac{7\rho_A}{16}}{(1 - \rho_A)^2} \quad (8)$$

and the specific heat coefficients are

$$c_v = \frac{k_{\text{B}}}{m}, \quad c_p = \frac{k_{\text{B}}}{m} (1 + H(n) \alpha T). \quad (9)$$

In the last expression α is the thermal expansion coefficient

$$\alpha = -\frac{1}{n} \left(\frac{\partial T}{\partial n} \right)_p^{-1} = \frac{H}{T(nH)'}, \quad (10)$$

where the prime indicates derivative with respect to n .

A time scale to measure the relaxation time of a system comes from an estimation of the thermal diffusion time across the system. The energy equation is $m n \partial u / \partial t = -\nabla \cdot \mathbf{q}$. Accepting Fourier's law of heat conduction: $\mathbf{q} = -k \nabla T$, where k is the thermal conductivity, and remembering that $\partial u / \partial T = c_p$ it is seen that a temperature diffusion time for a system in a $L \times L$ box is

$$t_{\text{diff}} = \frac{m c_p N}{k}. \quad (11)$$

The energy equation mentioned above will be seen later in §4, (55)c.

2.6 Problems

1. Write a program for the 1D movement of two dot particles of masses m_1 and m_2 respectively, moving in a straight line under the effect of gravity g . They have perfectly elastic collisions among themselves and particle 1 hits the floor elastically as well. Normalize your variables so that the total energy of the system is $E = 1$ and $R = m_2/m_1$. Plot x_2 against v_2 every time particle 1 hits the floor. Notice that these points are always within a parabola. Use, for example, $R = 3$. Different initial conditions may lead to different graphs. Carefully explore the graphs for a wide class of initial conditions.
2. Extend the previous program to the case of a system of N hard rods of length a , unit mass, moving inside the box: $[x = 0, x = L]$ and without gravity. Take $N = 20$, $N a/L = 0.75$. i) Make a time average of the local density $n(x)$ within every interval $L/300$ of the box. ii) Determine the average local density relative to the position of a particle up to $4a$ away from it. In other words, make a histogram \mathcal{H}_k of the number of times two particles are found at relative distance between $k\delta$ and $(k+1)\delta$. These densities have a structure. The reason for this is that the probability of having a particle in a given position depends on the positions of the others. This is the basic idea of correlations in position. To write the measurement routines take into consideration what was said under *Measurements* in §2.5. The weakness of the present system is that the velocity distribution does not evolve.

3. Consider just one particle moving in a straight line under the effect of gravity, g . The floor moves following $z(t) = A \cos(\omega t)$ and the particle bounces back from the floor with velocity $v' = (1 + \eta)\dot{z} - \eta v$ where $0 < \eta < 1$ is the restitution coefficient and v is the velocity with which the particle hits the floor. Besides η the other important parameter is $G = \frac{A\omega^2}{g}$. For every value of G take many different initial conditions and see whether asymptotically the particle loses all its energy and sticks to the floor or continues bouncing for ever. For a fixed value of η (e.g., $\eta = 0.6$) plot against G all the possible values of v' when the asymptotic regime is a bouncing particle. You will discover a complex structure; interpret it.
4. Write a program for the evolution of a 2D system of hard disks of diameter σ . To evaluate the time when any two disks a and b will hit each other, define from the positions and velocities at time t_0 the quantities $\mathbf{r} = \mathbf{r}_a - \mathbf{r}_b$, $\mathbf{v} = \mathbf{v}_a - \mathbf{v}_b$ and $b = -\mathbf{r} \cdot \mathbf{v}$. The two disks will hit each other at time t_1 ,

$$t_1 = t_0 + \frac{b - \sqrt{\Delta}}{v^2}. \quad (12)$$

if b and $\Delta = b^2 - v^2(r^2 - \sigma^2)$ are positive, otherwise $t_1 = \infty$. For the rest of the program use the scheme described in Fig. 2.

3 Primer on Kinetic Theory

3.1 The One-Particle Distribution Function

Consider a fluid composed of N unstructured particles. The one-particle state space \mathcal{Y}_1 will be described with position and velocity (\mathbf{r}, \mathbf{c}) . This is a six dimensional space. Divide the space in small cells labeled ξ with volume Δ . Considering many macroscopically equal replicas of the system, call $\mathcal{N}(\xi, t)$ the expected number of particles to be found in cell ξ at time t . For any reasonable fluid these numbers will decrease exponentially as the velocity coordinates increase. If the cells Δ are sufficiently small these occupation numbers, normalized to Δ through $f(\xi, t) = \frac{\mathcal{N}(\xi, t)}{\Delta}$, give much information about the system. In the limit of very small cells $f(\xi, t)$ gives a distribution function $f(\mathbf{r}, \mathbf{c}, t)$ normalized to the number density $n(\mathbf{r}, t)$:

$$\int_{\mathcal{Y}_1} f(\mathbf{r}, \mathbf{c}, t) d\mathbf{c} = n(\mathbf{r}, t),$$

$$\int n(\mathbf{r}, t) d\mathbf{r} = N. \quad (13)$$

Even though f gives much information about the system, it is far from giving a complete description of it. It does not describe, for example, the correlations that usually exist in a fluid. Formally

$$f(\mathbf{r}, \mathbf{c}, t) d\mathbf{r} d\mathbf{c}, \quad (14)$$

X	$\langle X \rangle$	name
\mathbf{c}	$\mathbf{v}(\mathbf{r}, t)$	hydrodynamic velocity
$\frac{1}{2}C^2$	$u_K(\mathbf{r}, t)$	kinetic energy per unit mass
$\rho C_i C_j$	$(\mathbb{P}_K)_{ij}$	kinetic part of the pressure tensor
$\frac{1}{2}\rho C^2 \mathbf{C}$	\mathbf{q}_K	kinetic part of the heat flux vector

Table 3. First momenta of the distribution function

gives the number of particles expected about the point (\mathbf{r}, \mathbf{c}) of Υ_1 at a given instant t . The distribution f is useful to evaluate averages of one-particle quantities. The average is a macroscopic quantity $\langle \varphi \rangle(\mathbf{r}, t)$:

$$\langle \varphi \rangle(\mathbf{r}, t) = \frac{1}{n(\mathbf{r}, t)} \int \varphi(\mathbf{r}, \mathbf{c}, t) f(\mathbf{r}, \mathbf{c}, t) d\mathbf{c}. \quad (15)$$

In this way one defines the hydrodynamic velocity $\mathbf{v}(\mathbf{r}, t)$ and the peculiar velocity $\mathbf{C}(\mathbf{r}, t)$

$$\mathbf{v}(\mathbf{r}, t) = \frac{1}{n(\mathbf{r}, t)} \int \mathbf{c} f(\mathbf{r}, \mathbf{c}, t) d\mathbf{c}, \quad \mathbf{C}(\mathbf{r}, t) = \mathbf{c} - \mathbf{v}(\mathbf{r}, t). \quad (16)$$

For a gas at equilibrium in d dimensions the distribution function is that found by Maxwell

$$f_M(\mathbf{r}, \mathbf{c}, t) = n(\mathbf{r}, t) \left(\frac{m}{2\pi k_B T(\mathbf{r}, t)} \right)^{d/2} e^{-mC(\mathbf{r}, t)^2/2k_B T(\mathbf{r}, t)} \quad (17)$$

but in general the distribution function f deviates from f_M and examples will be seen where this deviation has interesting measurable implications.

From the notion of f it follows, for example, the *histogram* of the number of particles with rapidity about $C \equiv |\mathbf{C}|$ is proportional to $C^{d-1} f_M$. A 2D case at equilibrium is seen in Fig. 4.

Formally the temperature field $T(\mathbf{r}, t)$ is identified with the quasi-equilibrium statistical mechanics concept

$$u_K(\mathbf{r}, t) \equiv \left\langle \frac{1}{2} C^2 \right\rangle = \frac{d}{2m} k_B T(\mathbf{r}, t) \quad (18)$$

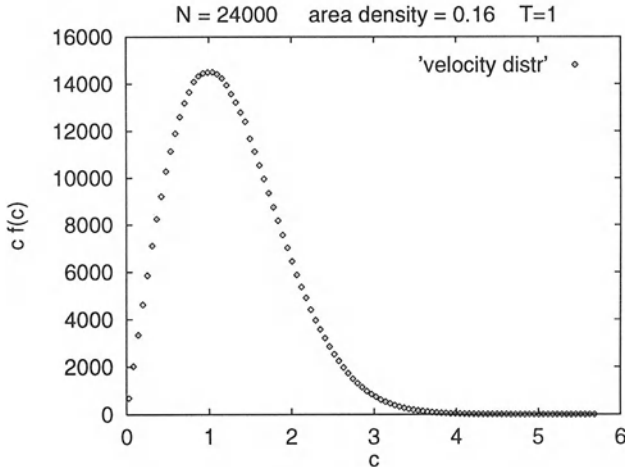


Fig. 4. Histogram of the number of particles having rapidity between C and $C+dC$ in a 2D system at equilibrium. In the present case the figure corresponds to a system of 24000 hard disks and area density 0.16 simulated in a personal computer. Starting with a relaxed system, the figure corresponds to an average over 60 million collisions.

In general the momenta of $f(\mathbf{r}, \mathbf{c}, t)$ define interesting physical quantities, as in Table 3. Since these momenta are local averages — in the sense that \mathbf{r} is kept fixed — they can be thought of as *densities*.

3.2 Mean Free Path and Collision Rate

A textbook illustration of the use of the notion behind (14) consists in deriving a rough estimate of the collision frequency in a gas of spheres of diameter σ . Consider a point $(\mathbf{r}, \mathbf{c}_1)$ of \mathcal{V}_1 . There are $f(\mathbf{r}, \mathbf{c}_1, t) d\mathbf{r} d\mathbf{c}_1$ particles about it and let us think of them as the target. Particles that will collide with this target in the interval $(t, t + dt)$ and having velocity about \mathbf{c}_2 have to be at t inside a cylinder with section $\pi \sigma^2$ and length $|\mathbf{c}_2 - \mathbf{c}_1| dt$. The number of particles about \mathbf{c}_2 inside this cylinder is $\pi \sigma^2 |\mathbf{c}_2 - \mathbf{c}_1| dt f(\mathbf{r}, \mathbf{c}_2, t) d\mathbf{c}_2$. Both distributions are evaluated at the same point because it is being assumed that the mean free path is much larger than σ . For simplicity's sake sometimes it is assumed that the two probabilities are independent, but they are not. As a first approximation Enskog realized that it is necessary to add a corrective factor which, in a reasonable approximation, is the Enskog factor $\chi(\mathbf{r})$, namely, the radial distribution function at contact. Hence, the expected number of collisions per unit time and volume is

$$\pi \sigma^2 \chi(\mathbf{r}) \int f(\mathbf{r}, \mathbf{c}_1, t) f(\mathbf{r}, \mathbf{c}_2, t) |\mathbf{c}_2 - \mathbf{c}_1| d\mathbf{c}_1 d\mathbf{c}_2 \quad (19)$$

and the collision frequency ν per particle is then

$$\nu = \frac{\pi \sigma^2}{n(\mathbf{r}, t)} \chi(\mathbf{r}) \int f(\mathbf{r}, \mathbf{c}_1, t) f(\mathbf{r}, \mathbf{c}_2, t) |\mathbf{c}_2 - \mathbf{c}_1| d\mathbf{c}_1 d\mathbf{c}_2 \quad (20)$$

The mean time between collisions is $\tau = \nu^{-1}$. The mean free path and the total collision rate Γ for a system of N particles are then

$$\ell = \tau v_{\text{th}} \quad \Gamma = \frac{N}{2} \nu = \frac{N}{2} \frac{v_{\text{th}}}{\ell} \quad (21)$$

where $v_{\text{th}} = \langle |\mathbf{c}| \rangle$ is the *thermal velocity*. In case of local thermodynamic equilibrium they can be evaluated with the expressions found in Table 4.

dimension	v_{th}	ℓ
2	$\sqrt{\frac{\pi k_B T}{2m}}$	$\frac{1}{2\sqrt{2}\chi n \sigma} = \frac{\pi \sigma}{8\sqrt{2}\chi \rho_A}$
3	$2\sqrt{\frac{2k_B T}{\pi m}}$	$\frac{1}{\sqrt{2}\chi n \pi \sigma^2} = \frac{\pi \sigma}{6\sqrt{2}\chi \rho_V}$
d	$\sqrt{\frac{2k_B T}{m}} \frac{\Gamma(\frac{d+1}{2})}{\Gamma(\frac{d}{2})}$	$\frac{\Gamma(\frac{d+1}{2})}{\sqrt{2}\chi n \sigma^{d-1} \pi^{(d-1)/2}}$

Table 4. Approximate expressions for the thermal velocity and mean free path for a gas of hard spheres in different dimensions when the distribution is Maxwellian.

The total number of collisions in one thermal diffusion time is the total collisions rate times t_{diff} (which for hard disks was given in (11)),

$$N_{\text{diff}} = \Gamma t_{\text{diff}}. \quad (22)$$

Since the computational time for every collision is $\mathcal{O}(\ln N)$, running a system of hard disks for one diffusion time takes a CPU time $\mathcal{O}(N^2 \ln N)$ making it difficult to go to larger and larger systems.

For a gas ℓ can be $10^5 \sigma$, $\sigma \sim 10^{-8} \text{ cm}$ and the thermal velocity is of the same order as the speed of sound.

3.3 On Fluxes and Flux Vectors

Balance equations connect flux vectors \mathbf{J} with densities. The flux vector associated to a microscopic quantity $\varphi(\mathbf{r}, \mathbf{c}, t)$ can be defined with respect to an absolute frame of reference or with respect to the frame that moves with the hydrodynamic velocity $\mathbf{v}(\mathbf{r}, t)$. The latter is a more interesting quantity but both are trivially related. The *kinetic* contribution to the flux vector associated to a quantity φ in the co-moving frame is

$$\mathbf{J}_\varphi^{(K)}(\mathbf{r}, t) = \int \varphi(\mathbf{r}, \mathbf{c}, t) f(\mathbf{r}, \mathbf{c}, t) \mathbf{C}(\mathbf{r}, t) d\mathbf{c}. \quad (23)$$

In a one component fluid there is no co-moving mass flux. The kinetic contribution to the momentum flux vector is obtained choosing $\varphi = mC_i$ and defining a tensorial quantity that was already mentioned in Table 3,

$$\mathbb{P}_K(\mathbf{r}, t) = m \int \mathbf{C} \mathbf{C} f(\mathbf{r}, \mathbf{c}, t) d\mathbf{c}. \quad (24)$$

For gases usually all flux vectors which are not of kinetic origin can be neglected, and therefore assume, for example, that $\mathbb{P} = \mathbb{P}_K$. The hydrostatic the pressure is

$$p = \frac{1}{3} \text{Tr } \mathbb{P} \quad (25)$$

hence the ideal gas equation of state is satisfied,

$$p = n k_B T \quad (26)$$

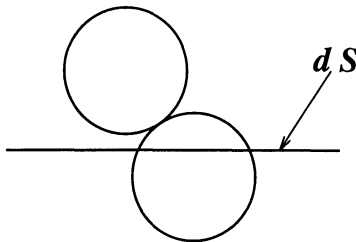
The flux vector of the kinetic energy (choosing $\varphi = \frac{m}{2} C^2$) also defines a quantity already known

$$\mathbf{q}_K = \frac{m}{2} \int C^2 \mathbf{C} f(\mathbf{r}, \mathbf{c}, t), d\mathbf{c} \quad (27)$$

The total macroscopic fluxes have further contributions. Consider, for example, an imaginary surface element $d\mathcal{S}$ cutting the fluid. Whenever a particle crosses that surface element there is a *kinetic* contribution to some fluxes. Parenthetically, it is said that a particle crosses a surface when its center does so.

If two particles — coming from opposite sides of the surface element $d\mathcal{S}$ — hit each other and then continue their flight without crossing $d\mathcal{S}$ there is a contribution to the fluxes, but it is no longer a kinetic contribution but

rather a collisional one. It may also happen that two *bound particles* cross $d\mathcal{S}$. In that case there is a contribution to the *potential energy flux*. It is seen then, that fluxes have contributions which can be either of kinetic origin or due to the interactions. In the case of the energy flux (the heat flux) the interaction implies two contributions: one due to collisions and one that occurs when there are bound particles. In gases at normal pressure the kinetic transport dominates with no competition. Hence they behave as “ideal gases”. In dense gases and liquids the different contributions compete and in solids the kinetic transport is negligible.



Collisional transport through a surface element dS .

The concept of a heat flux vector is perhaps intuitive but the physical idea behind the components of \mathbf{P} is less so. A careful analysis shows that P_{ii} is the force per unit area in the direction i exerted over the plane perpendicular to the direction i . For this reason the P_{ii} are called normal pressures. A non diagonal term P_{ij} is a shear stress in the sense that it represents the force per unit area in the direction i exerted over the plane perpendicular to the direction j .

In hydrodynamics it is usually assumed that the pressure tensor and the heat flux vector obey linear equations called Newton’s law of viscous flow and Fourier’s law of heat conduction,

$$P_{ij} = p\delta_{ij} - \eta \left(\frac{\partial v_i}{\partial x_j} + \frac{\partial v_j}{\partial x_i} - \frac{2}{d}\delta_{ij}\nabla \cdot \mathbf{v} \right) - \zeta\delta_{ij}\nabla \cdot \mathbf{v} \quad (28)$$

$$\mathbf{q} = -k\nabla T \quad (29)$$

where k is the thermal conductivity while η and ζ are the shear and bulk viscosity coefficients.

Low order approximate methods appropriate for low density systems — as the one used in §4.4 — lead to expressions for k and η in dimension $d = 2, 3$,

$$\eta_d = \frac{2+d}{2^{d+1}\sigma^{d-1}} \sqrt{\frac{mk_B T}{\pi}} \quad k_d = \frac{d(d+2)^2 k_B}{2^{d+2}\sigma^{d-1}} \sqrt{\frac{k_B T}{m\pi}} \quad (30)$$

Note that both coefficients, η and k , have the form of a constant times \sqrt{T} . This is a well known property of transport coefficients for low density gases. Using Enskog’s kinetic equation it is possible to get expressions with a wider range of applicability, as seen in §3.5.

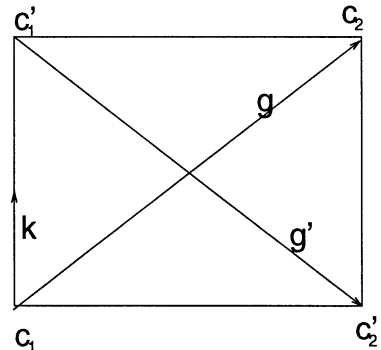
3.4 Boltzmann's Equation

Studying a statistical systems of unstructured particles satisfying a Hamiltonian dynamics it is possible to justify that the equation for the one particle distribution function $f(\mathbf{r}, \mathbf{c}, t)$, in the case of low density, is that of Boltzmann,

$$\left(\frac{\partial}{\partial t} + \mathbf{c}_1 \cdot \nabla_{\mathbf{r}_1} + \mathbf{F} \cdot \nabla_{\mathbf{c}_1} \right) f_1 = \int (f'_1 f'_2 - f_1 f_2) g b db d\epsilon d\mathbf{c}_2 \quad (31)$$

where \mathbf{F} is the net instantaneous external force per unit mass acting on particle 1, b is the impact parameter variable, ϵ is the azimuthal angle of the collision and

$$\begin{aligned} f_1 &= f(\mathbf{r}, \mathbf{c}_1, t) \\ f_2 &= f(\mathbf{r}, \mathbf{c}_2, t) \\ f'_1 &= f(\mathbf{r}, \mathbf{c}'_1, t) \\ f'_2 &= f(\mathbf{r}, \mathbf{c}'_2, t) \\ \mathbf{g} &= \mathbf{c}_2 - \mathbf{c}_1 \\ g &= |\mathbf{g}| \\ \mathbf{c}'_1 &= \mathbf{c}_1 + \mathbf{g} \cdot \hat{k} \hat{k} \\ \mathbf{c}'_2 &= \mathbf{c}_2 - \mathbf{g} \cdot \hat{k} \hat{k} \end{aligned} \quad (32)$$



where \hat{k} is the unit vector in the direction of $\mathbf{c}'_1 - \mathbf{c}_1$.

A list of the – not necessarily independent – assumptions needed to justify Boltzmann's equation: microscopic Hamiltonian dynamics, large number of particles, low density, short range pairwise interactions, absence of bound particles, uncorrelated particle-particle collisions, negligible spatial gradients of the distribution function in the atomic scale, negligible action of the external forces during the collision time. The assumption that the collisions are uncorrelated brings about irreversibility.

3.5 Enskog's Equation

Enskog's theory of transport arises from an extension of Boltzmann's formalism by means of introducing corrections that account for the effects of having a molecular diameter that it is no longer small compared with the mean free path. A major consequence is that the collisional mechanisms of momentum and energy transfer — which is negligible at lower densities — becomes important. In fact, collisional transfer can be as important or even more important than kinetic transfer. The contribution of the collisional transfer, in Enskog's theory, comes into play when the correlations in position are introduced in the basic kinetic equation in an approximate way. In spite of these restrictions, Enskog's formalism — which was developed for the case of hard spheres — is the best systematic description that yields transport coefficients

in the context of kinetic theory (Ferziger & Kaper 1972). Gass (1971) applied it to the 2D case of hard disks.

Enskog's equation perfects Boltzmann's equation (31) by including effects implied by the finite size of the particles and correlations in position among them as it was already described in §3.2. If Boltzmann's equation has the form $\mathcal{D}f = J[ff]$, Enskog starts from an equation having the same left hand side as (31) but the right hand side is different,

$$\begin{aligned} \mathcal{D}f = & \int \left\{ \chi(\mathbf{r} + \frac{\sigma}{2}\hat{k}, t)f(\mathbf{r}, \mathbf{c}_1, t)f(\mathbf{r} + \sigma\hat{k}, \mathbf{c}_2, t) \right. \\ & \left. - \chi(\mathbf{r} - \frac{\sigma}{2}\hat{k}, t)f(\mathbf{r}, \mathbf{c}_1, t)f(\mathbf{r} - \sigma\hat{k}, \mathbf{c}_2, t) \right\} \sigma^2 \mathbf{g} \cdot \hat{k} d^2k d\mathbf{c}_2. \end{aligned} \quad (33)$$

To get Enskog's equation the right hand side is transformed expanding the functions χ and the distributions f about the position \mathbf{r} up to first order in the gradients. *Enskog's collisional operator* then has the form

$$J_E = J_0 + J_1 + J_2. \quad (34)$$

J_0 is Boltzmann's operator J multiplied by χ , $J_0 = \chi J$ while the other two J_k are

$$J_1 = \sigma^3 \int \left\{ \chi \hat{k} \cdot (f'_1 \nabla_r f'_2 + f_1 \nabla_r f_2) + \frac{1}{2} (\hat{k} \cdot \nabla_r \chi) (f'_1 f'_2 + f_1 f_2) \right\} \mathbf{g} \cdot \hat{k} d^2k d\mathbf{c}_2, \quad (35)$$

$$J_2 = \frac{\sigma^3}{2} \int \left\{ \chi \hat{k} \hat{k} : (f'_1 \nabla_r \nabla_r f'_2 - f_1 \nabla_r \nabla_r f_2) + (\hat{k} \cdot \nabla_r \chi) \hat{k} \cdot (f'_1 \nabla_r f'_2 - f_1 \nabla_r f_2) + \frac{1}{4} (\hat{k} \hat{k} : \nabla_r \nabla_r \chi) (f'_1 f'_2 - f_1 f_2) \right\} \mathbf{g} \cdot \hat{k} d^2k d\mathbf{c}_2.$$

where the f_k are to be understood as in (32) and Enskog's equation finally reads

$$\mathcal{D}f = J_0[ff] + J_1[ff] + J_2[ff]. \quad (36)$$

If the system is uniform, the distribution function f does not depend on position and the terms J_1 and J_2 vanish identically, leading to an equation almost equal to Boltzmann's except that now the right hand side is J_0 instead of J .

From a conceptual point of view one should remark though that the hypothesis behind Enskog's equation are almost the same as those made explicit in §3.4 except that for Enskog's equation the size of the particles is considered and the correlations in position are somehow taken into account. The low density hypothesis and small spatial gradients of f hypothesis are not so strongly stated in the present case. This new equation is suitable for describing a gas of hard spheres up to relatively high densities and hence it describes noble gases like Argon relatively well.

Using the Chapman-Enskog method of approximation, the lowest order values predicted for the viscosity and thermal conductivity for a gas of hard spheres are

$$\eta^{(0)} = 1.0160 \frac{5}{16\sigma^2} \left(\frac{mk_B T}{\pi} \right)^{\frac{1}{2}}, \quad k^{(0)} = 2.522 c_v \eta^{(0)}. \quad (37)$$

In terms of these quantities Enskog's theory predicts

$$\eta = \frac{1}{\chi} \left[1 + \frac{4(b\rho\chi)}{5} + 0.7614(b\rho\chi)^2 \right] \eta^{(0)}, \quad (38)$$

$$k = \frac{1}{\chi} \left[1 + \frac{6(b\rho\chi)}{5} + 0.7574(b\rho\chi)^2 \right] k^{(0)} \quad (39)$$

where $b\rho \equiv \frac{2}{3}\pi n\sigma^3$ is the *co-volume* of the molecules and where the virial expansion for χ , in the case of hard spheres, is

$$\chi = 1 + 0.6250b\rho + 0.2869(b\rho)^2 + 0.115(b\rho)^3 + \dots \quad (40)$$

In the 2D case Enskog's theory yields the following thermal conductivity k and shear viscosity η for the hard disk system

$$k = \frac{2.058 k_B}{\sigma \chi} \sqrt{\frac{k_B T}{m \pi}} \left[1 + \frac{3}{2} (2\rho_A \chi) + 0.8718(2\rho_A \chi)^2 \right], \quad (41)$$

$$\eta = \frac{0.511}{\sigma \chi} \sqrt{\frac{mk_B T}{\pi}} [1 + (2\rho_A \chi) + 0.8729(2\rho_A \chi)^2]. \quad (42)$$

3.6 Problems

1. Write a program that defines a large set of N velocity vectors $\{\mathbf{c}_1, \dots, \mathbf{c}_N\}$. In every iteration of a loop the program takes at random two of these vectors, \mathbf{c}_a and \mathbf{c}_b and replaces them by vectors \mathbf{c}'_a and \mathbf{c}'_b using a reasonable collision rule with an impact parameter chosen at random. Study the evolution of the distribution of velocities starting, for example, with every \mathbf{c} a unit vector checking that it converges to a Maxwellian rather fast. You may also study the evolution of Boltzmann's H function.
2. Modify the program for the 1D gas that you wrote in Prob.1.2 so that instead of rods you have point particles with the following particle-particle collision rule: $v'_1 = v_2 \cos \theta + v_1 \sin \theta$ and $v'_2 = v_1 \cos \theta - v_2 \sin \theta$ with a small θ chosen at random every time. The case $\theta = 0$ corresponds to elastic collisions. The collision with the two extremes is specular. Notice that kinetic energy is conserved. *i*) Measure the velocity distribution function. Is it a Maxwell distribution in the limit of a very large system?, *ii*) Make all the measurements of Prob.1.2. *iii*) When measuring the histogram \mathcal{H}_k as in Prob.1.2 simultaneously accumulate in an array \mathcal{S}_k the product of

the velocities $c_a c_b$ of each couple of particles that contribute to \mathcal{H} . If there is any velocity correlation it should be seen in the plot of S_k / \mathcal{H}_k against k .

3. Use the previous program with one variation. The collisions of the particles with the box walls are thermal, namely, particles forget the velocity they had and sort one from a Maxwellian distribution with a given T to bounce back. Put different temperatures in each wall and measure the density and temperature profiles. Measure the energy that is being injected at one extreme and independently measure the energy that is being pumped out of the system in the other extreme. After you have made different simulations with different temperature differences ΔT check the relation between the time average energy flux and ΔT .
4. Starting from the program you wrote solving problem 1.4 write a program for a 2D system with two kinds of disks of diameter σ : A and B . Make each particle interact with others of its own kind as hard disks while an A with a B penetrate each other getting a potential energy $-\varepsilon$ as soon as the distance r between their centers is less than σ . This is a crude model of screened ions and electrons. Working with a small system check that you can get gas, liquid and solid sort of phases.

4 Standard and High–Order Balance Equations

4.1 Grad’s Solution

Harold Grad in 1958 presented an original way of constructing an approximate solution to Boltzmann’s equation, (Grad 1958,60). In his approximate solution he does not expand in gradients of the first five momenta of the velocity distribution (density n , hydrodynamic velocity \mathbf{v} , and temperature T) as in the Chapman-Enskog method, but he rather uses a self-consistent approach involving higher momenta and no gradients of them. In particular he works out in detail the case when the distribution function f is written in terms of n , \mathbf{v} and T and also the traceless and symmetric part of the pressure tensor, p_{ij} , and the heat flux vector \mathbf{q} , which in 3D totals 13 momenta.

Grad’s approximate solution to Boltzmann’s equation, f_G , is obtained assuming that the distribution for a nonequilibrium system gets – in a first approximation – a corrective factor, linear in the the momenta \mathbb{P} and \mathbf{q} , multiplying Maxwell’s distribution:

$$f_G = (1 + \mathcal{A} : \mathbf{p} + \mathcal{B} \cdot \mathbf{q}) f_M, \quad (43)$$

where \mathbf{p} is the symmetric and traceless part of the pressure tensor \mathbb{P} ,

$$P_{ij} = n k_B T \delta_{ij} + \mathbf{p}_{ij}. \quad (44)$$

Grad proved that to have a solution to Boltzmann’s equation consistent with the correct momenta, shown in Table 3, the specific distribution of the

form (43) with $d = 2$ or 3 is

$$f_G = \left[1 + \frac{m}{p k_B T} \left(\frac{m C^2}{(2+d) k_B T} - 1 \right) \mathbf{C} \cdot \mathbf{q} + \frac{m}{2p k_B T} \mathbf{p} : \mathbf{CC} \right] f_M. \quad (45)$$

4.2 Application: Thermal Slip

Consider a gas in a box such that two opposite walls (conventionally called top and bottom as there is no gravity) have different temperature: T_b and T_t respectively and $T_b > T_t$. If the box were infinitely wide the gas would stabilize to a homogeneous temperature profile $T(z)$. To simplify let us assume that the lateral walls have precisely that temperature profile. It will be seen that the gas spontaneously slips parallel to the lateral walls towards the hotter zone, (Ibsen *et al.* 1995). Later on this movement will be quantified and the theoretical predictions compared to the simulational results. It will be seen that the important adimensional parameter for the effect to be noticeable is $\ell |\nabla T| / T$.

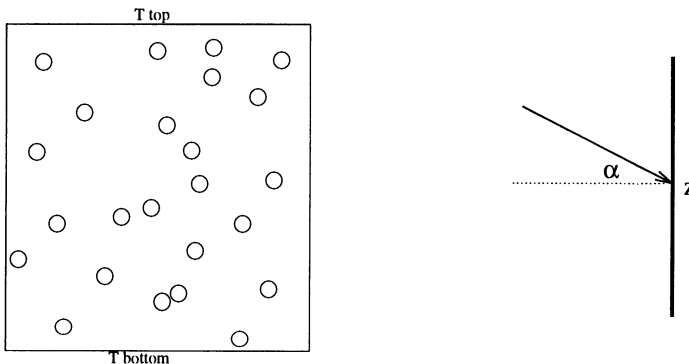


Fig. 5. At left a schematic representation of the system of particles in a square box with temperature T_t at the top and T_b at the bottom. At right a particle hitting the right wall with velocity c forming an angle α with the normal to the wall.

The phenomenon is basically the following. Because there is a heat flux \mathbf{q} across the gas (\mathbf{q} parallel to \hat{z}) the distribution function $f(\mathbf{r}, \mathbf{c}, t)$ is anisotropic. The gas particles hitting a point z (at height z), of a lateral wall are coming from this anisotropic distribution f and, in particular, the mass flux approaching z and forming an angle α with the normal at z (see Fig. 5) has an intensity that depends on α in a non trivial way.

Once the particles hit the wall at z they get in contact with a heat bath at temperature $T(z)$ and the velocity distribution of the out coming flux (from the wall point z) should be nearly Maxwellian. For simplicity's sake it will be assumed that this out coming flux is exactly Maxwellian and hence isotropic.

This situation will be analyzed with the help of Grad's distribution (45) specialized to 2D and neglecting the contribution coming from stress

$$f_G = \left(1 + \frac{m}{p k_B T} \left(\frac{mC^2}{4k_B T} - 1 \right) \mathbf{C} \cdot \mathbf{q} \right) f_M. \quad (46)$$

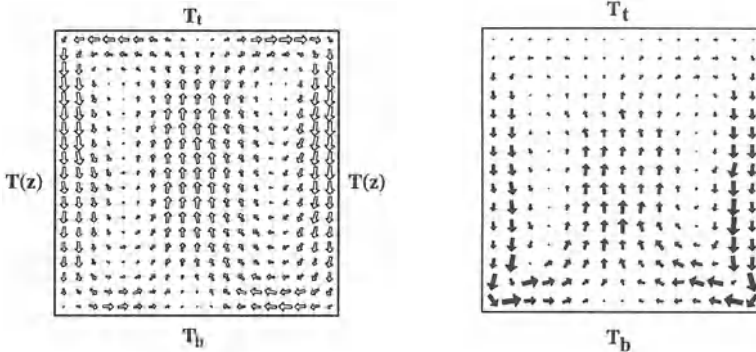


Fig. 6. At left the velocity field in the simulation with $N = 1444$, $n = 0.05$ and $T_t = 0.1$. At right the thermal slip velocity field in a simulation with lateral walls made with particles with their own dynamics.

Accepting that in the bulk of the system the distribution f_G describes well the actual distribution, a natural simple assumption is that the distribution f_{rw} near the right wall is

$$f_{rw} = \begin{cases} f_G & \text{if } C_x > 0 \\ f_M & \text{if } C_x < 0 \end{cases} \quad (47)$$

and an entirely similar distribution near the left wall. Note that (47) defines a distribution only to lowest order as $\int f_{rw} d^2c = n + \mathcal{O}(q)$.

With f_{rw} it is easy to calculate $P_{xz} = \rho \langle C_x C_z \rangle$ and the result is $\frac{q}{8} \sqrt{\frac{2m}{\pi k_B T}}$ which is identified, according to Newton's law, with $-\eta dv_z/dx$, therefore

$$\frac{q}{8} \sqrt{\frac{2m}{\pi k_B T}} = -\eta \frac{dv_z}{dx}. \quad (48)$$

Assuming that the hydrodynamic velocity goes to zero exponentially with the distance to the wall, proportional to $\exp[-x/\ell]$, the right hand side above can be approximated to $-\eta v_z/\ell$ and (48) can be solved for v_z ,

$$v_z = -\frac{\ell}{\eta} P_{xz} = -\frac{1}{8} \frac{q}{p}. \quad (49)$$

To get the last result it was necessary to use the expression for ℓ given in Table 4 and η from (30) with $d = 2$. The minus sign indicates that the gas slips near the lateral walls towards the hotter regions. Figure 6 shows at left the velocity field obtained in a simulation with 1444 particles.

In a preliminary simulation [A], defined below, we determined the temperature profile to be imposed on the lateral walls in the final simulation [B]. This was achieved running simulation [A] with *periodic lateral boundary conditions* and temperatures T_b and T_t . The fluid stabilized in [A] with a vertical temperature profile $T(z)$. This profile was imposed in the final simulation [B] to the hard nonslip thermal lateral walls.

	$ v_z $	$ q/8p $
$N = 1444$		
$n = N/L^2 = 0.05$	0.015 ± 0.002	0.016 ± 0.003
$T_t = 0.1$		
$\ell \approx 7.0 \quad L \approx 170$		
$N = 8100$		
$n = N/L^2 = 0.01$	0.014 ± 0.003	0.020 ± 0.001
$T_t = 0.1$		

Table 5. Units were chosen so that the particle's diameter is $\sigma = 1$, the particle's mass is $m = 1$, the Boltzmann's constant is $k_B = 1$ and the temperature scale is fixed by $T_b = 1$.

The simulations give independently the velocity v_z of the gas in contact with the lateral walls, the pressure p and the heat flux q . The observed results for two simulations are summarized in Table 5.

Equation (47) is the main hypothesis that leads to the quantification of this phenomenon. From the point of view of the simulation the hypothesis is concealed in the collision rule with the lateral wall: particles forget the velocity with which they hit the wall and bounce back with a velocity sorted out from a (isotropic) Maxwellian distribution. In case there is any doubt that the phenomenon exists at all there is a second simulation where no such

hypothesis is introduced (Risso & Cordero 1996c). In this new version there is a realistic wall in the following way. The square box has periodic lateral walls, but between two relatively close parallel vertical lines 420 particles were placed in a nearly close packing. They could not leave the space between the two lines, therefore they formed a vertical wall with its own dynamics. These two lines play the role of the effective surface cohesion between particles forming a solid. The rest of the box contained the usual dilute gas of 1444 particles. The gas particles had no interaction with the vertical lines but they could hit the particles of the vertical wall. For both types of particles the horizontal walls had temperatures T_b and T_t . As before the velocity field of the gas was averaged. The result is seen in the graph at right in Fig. 6.

Replacing in (49) q by $-k\nabla T$, and p by $nk_B T$, and using the expressions given in Table 3 yields

$$v_z = \frac{8}{\pi} \frac{\ell |\nabla T|}{T} v_{th}. \quad (50)$$

showing that this thermal slip is a nonlocal effect.

4.3 The BBGKY Hierarchy and General Balance Equations

None of the densities (15) or flux vectors (like \mathbf{IP} or \mathbf{q}) defined in §3.3 can be evaluated unless the distribution function $f(\mathbf{r}, \mathbf{c}, t)$ is known. A basic problem then is to know how to obtain this distribution. The task can be formulated in many different ways. Directly from Newton's equations for every particle it is possible to derive the Liouville equation for a Hamiltonian system and from there follows a hierarchy of equations for the distributions $f^{(\nu)}(\mathbf{r}_1, \mathbf{c}_1, \dots, \mathbf{r}_\nu, \mathbf{c}_\nu, t)$ normalized to

$$\int f^{(\nu)}(\mathbf{r}_1, \mathbf{c}_1, \dots, \mathbf{r}_\nu, \mathbf{c}_\nu, t) d\mathbf{r}_1 d\mathbf{c}_1 \dots d\mathbf{r}_\nu d\mathbf{c}_\nu = \frac{N!}{(N - \nu)!} \quad (51)$$

that satisfy

$$\begin{aligned} \partial_t f^{(\nu)} + \sum_{a=1}^{\nu} (\mathbf{c}_a \cdot \nabla_{\mathbf{r}_a} + \mathbf{F}_a \cdot \nabla_{\mathbf{c}_a}) f^{(\nu)} = \\ - \sum_{a=1}^{\nu} \int \mathcal{F}_{a,\nu+1} \cdot \nabla_{\mathbf{c}_a} f^{(\nu+1)} dy_{\nu+1} \end{aligned} \quad (52)$$

where \mathbf{F}_a is the net force acting over particle a and

$$\mathcal{F}_{ab} \equiv -\frac{1}{m} \nabla_{\mathbf{r}_a} \phi_{ab} \quad (53)$$

are the interparticle forces and $f^{(\nu)}(\dots) d\mathbf{r}_1 d\mathbf{c}_1 \dots d\mathbf{r}_\nu d\mathbf{c}_\nu$ is the probability of having ν particles of the system of size N about the point $(\mathbf{r}_1, \mathbf{c}_1, \dots, \mathbf{r}_\nu, \mathbf{c}_\nu)$ regardless of where the rest of the particles are. This system of coupled equations is known as the BBGKY hierarchy and it is exact. Naturally $f^{(1)}$ is the distribution f used in previous sections.

Assuming that the particles interact pairwise, making use of the first two equations of the hierarchy and without making any approximation whatsoever it is possible to derive balance equations associated to quantities φ which are additively conserved during binary particle-particle collisions

$$\varphi_1 + \varphi_2 = \varphi'_1 + \varphi'_2 , \quad (54)$$

they are mass, momentum and energy. The exact balance equations that follow have the typical form of the equations of hydrodynamics

$$\begin{aligned} \frac{D\rho}{Dt} &= -\rho\nabla \cdot \mathbf{v} , \\ \rho \frac{D\mathbf{v}}{Dt} &= \rho\mathbf{F} - \nabla \cdot \mathbb{P} , \\ \rho \frac{Du}{Dt} &= -\nabla \cdot \mathbf{q} - \mathbb{P} : \nabla \mathbf{v} , \end{aligned} \quad (55)$$

where

$$\frac{D}{Dt} \equiv \frac{\partial}{\partial t} + \mathbf{v} \cdot \nabla \quad (56)$$

is the convective derivative and the pressure tensor is the sum of kinetic and potential contributions

$$\begin{aligned} \mathbb{P} &= \mathbb{P}_K + \mathbb{P}_\phi , \\ \mathbb{P}_K &= m \int \mathbf{C} \mathbf{C} f(\mathbf{r}, \mathbf{c}, t) d\mathbf{c} , \\ \mathbb{P}_\phi &= -\frac{1}{2} \int_0^1 d\mu \int d\mathbf{r}_{12} \mathbf{r}_{12} \hat{\mathbf{r}}_{12} \phi'_{12} \int n_2(\mathbf{r}_1 - (1-\mu)\mathbf{r}_{12}, \mathbf{r}_1 + \mu\mathbf{r}_{12}, t) \end{aligned} \quad (57)$$

and $\phi_{12} \equiv \phi(r_{12})$ is the interparticle potential that is being assumed to be central and n_2 is

$$n_2(\mathbf{r}_1, \mathbf{r}_2, t) \equiv \int f^{(2)}(\mathbf{r}_1, \mathbf{c}_1, \mathbf{r}_2, \mathbf{c}_2, t) d\mathbf{c}_1 d\mathbf{c}_2 . \quad (58)$$

On the other hand the energy density is

$$\begin{aligned} u &= u_K + u_\phi , \\ u_K &= \frac{1}{2} \int C^2 f(\mathbf{r}, \mathbf{c}, t) d\mathbf{c} , \\ u_\phi &= \frac{1}{\rho} \int \phi(r_{12}) n_2(\mathbf{r}_1, \mathbf{r}_2, t) d\mathbf{r}_2 \end{aligned} \quad (59)$$

while the contributions to the heat flux vector are

$$\begin{aligned}\mathbf{q} &= \mathbf{q}_K + \mathbf{q}_{\phi 1} + \mathbf{q}_{\phi 2} \\ \mathbf{q}_K &= \frac{1}{2} \rho \int C^2 \mathbf{C} f(\mathbf{r}, \mathbf{c}, t) d\mathbf{c}, \\ \mathbf{q}_{\phi 1} &= \frac{1}{2} \int \phi(r_{12}) \mathbf{C}_1 f^{(2)}(\mathbf{r}, \mathbf{c}_1, \mathbf{r}_2, \mathbf{c}_2) d\mathbf{r}_2 d\mathbf{c}_1 d\mathbf{c}_2, \\ \mathbf{q}_{\phi 2} &= -\frac{1}{4} \int \phi'(r_{12}) \hat{\mathbf{r}}_{12} (\mathbf{C}_1 + \mathbf{C}_2) \mathbf{r}_{12}, \\ &\quad \times \int f^{(2)}(\mathbf{r}_1 - (1-\mu)\mathbf{r}_{12}, \mathbf{c}_1, \mathbf{r}_1 + \mu\mathbf{r}_{12}, \mathbf{c}_2, t) d\mu d\mathbf{r}_2 d\mathbf{c}_1 d\mathbf{c}_2 |_{\mathbf{r}_1=\mathbf{r}}.\end{aligned}\tag{60}$$

where again μ is integrated from 0 to 1. The vector $\mathbf{q}_{\phi 1}$ is a contribution to the potential energy flux vector while $\mathbf{q}_{\phi 2}$ contains the derivative of the potential and therefore it is related to the interparticle forces.

The balance equations (55) are hydrodynamic equations. They are an exact and open set of equations in the sense that they are equations for the five fields ρ , \mathbf{v} and u but — in this context — the quantities \mathbb{P} and \mathbf{q} are unknowns in the sense that kinetic theory so far does not give expressions for them in terms of the five hydrodynamic fields as it is necessary to formulate hydrodynamics. The extra expressions are usually referred to as the *constitutive equations* of hydrodynamics and (28) and (29) are examples of them. They have no foundation on first principles.

4.4 Dilute Systems: Balance Equations and Higher Momenta

Starting from Boltzmann's equation it is possible to derive a generic balance equation associated to any quantity φ

$$\begin{aligned}\partial_t(n\langle\varphi\rangle) - n\langle\partial_t\varphi\rangle + \nabla_r \cdot (n\langle\varphi\mathbf{c}\rangle) - n\langle\mathbf{c}\cdot\nabla\varphi\rangle - n\mathbf{F}\cdot\langle\nabla_c\varphi\rangle = \\ \int \varphi(\mathbf{c}_1) (f'_1 f'_2 - f_1 f_2) \sigma^2 \mathbf{g} \cdot \hat{\mathbf{k}} d^2 k d\mathbf{c}_1 d\mathbf{c}_2\end{aligned}\tag{61}$$

In particular if φ is a quantity additively conserved in collisions then it is possible to prove that the right hand side of (61) vanishes identically and the resulting balance equations only contain kinetic contributions. They are

$$\begin{aligned}\frac{D\rho}{Dt} &= -\rho \nabla \cdot \mathbf{v} \\ \rho \frac{D\mathbf{v}}{Dt} &= \rho \mathbf{F} - \nabla \cdot \mathbb{P}_K \\ \rho \frac{Du_K}{Dt} &= -\nabla \cdot \mathbf{q}_K - \mathbb{P}_K : \nabla \mathbf{v}.\end{aligned}\tag{62}$$

But (61) can be used with any quantity. It has been seen that the momenta, higher than the first five ones, namely \mathbb{P} and \mathbf{q} play a significant role.

The choices $\varphi = m(C_i C_j - \frac{1}{3} C^2 \delta_{ij})$ and $\varphi = mC^2 C$ yield balance equations for IP and \mathbf{q} respectively. If it is further assumed that the distribution function is Grad's distribution f_G then the approximate balance equations have explicit forms shown below. These balance equations for the case $d = 3$ are found in Grad's 1958 article, equations (28.19) and (28.20). We have derived them for $d = 2$ in the hard disk case. They can be condensed for $d = 2$ or 3 hard spheres as:

$$\begin{aligned} \frac{\partial p_{ij}}{\partial t} + \frac{\partial}{\partial x_k} (v_k p_{ij}) + \frac{2}{d+2} \left(\frac{\partial q_i}{\partial x_j} + \frac{\partial q_j}{\partial x_i} - \frac{2}{d} \delta_{ij} \frac{\partial q_k}{\partial x_k} \right) + \\ p_{rj} \frac{\partial v_i}{\partial x_r} + p_{ri} \frac{\partial v_j}{\partial x_r} - \frac{2}{d} \delta_{ij} p_{rs} \frac{\partial v_s}{\partial x_r} + \\ p \left(\frac{\partial v_i}{\partial x_j} + \frac{\partial v_j}{\partial x_i} - \frac{2}{d} \delta_{ij} \frac{\partial v_r}{\partial x_r} \right) + \frac{1}{\tau} p_{ij} = 0 \end{aligned} \quad (63)$$

$$\begin{aligned} \frac{\partial q_k}{\partial t} + \frac{\partial}{\partial x_r} (v_r q_k) + \frac{d+4}{d+2} \frac{\partial v_k}{\partial x_r} q_r + \frac{2}{d+2} \frac{\partial v_r}{\partial x_k} v_r + \\ \frac{2}{d+2} \frac{\partial v_r}{\partial x_r} q_k + \frac{k_B T}{m} \frac{\partial p_{kr}}{\partial x_r} + \frac{d+4}{2m} p_{kr} \frac{\partial (k_B T)}{\partial x_r} - \frac{p_{kr}}{\rho} \frac{\partial P_{rs}}{\partial x_s} + \\ \frac{d+2}{2m} p \frac{\partial (k_B T)}{\partial x_k} + \frac{d-1}{d\tau} q_k = 0 \end{aligned} \quad (64)$$

where τ is

$$\tau = \frac{2+d}{2^{d+1}} \frac{1}{\sigma^{d-1} p} \sqrt{\frac{mk_B T}{\pi}}. \quad (65)$$

As Grad has pointed out, in the absence of gradients the above equations are $\tau \partial p_{ij} / \partial t + p_{ij} = 0$ and $\frac{d}{d-1} \tau \partial q_k / \partial t + q_k = 0$ clearly indicating that τ is a relaxation time. But τ is proportional to the mean free flight time, ℓ/v_{th} .

Grad's approximate solution (45) neglects the contribution from higher momenta which becomes important if gradients become sufficiently large. The above higher balance equations are implications of Grad's solution where again the contributions from higher momenta are consistently dropped.

As an illustration of their use consider the first equation, neglect time variations and all gradients except for the velocity gradient. It follows that

$$p_{ij} = -\eta_d \left(\frac{\partial v_i}{\partial x_j} + \frac{\partial v_j}{\partial x_i} - \frac{2}{d} \frac{\partial v_r}{\partial x_r} \delta_{ij} \right) \quad (66)$$

where the shear viscosity η_d for hard spheres in dimension d turns out to be τp which simplifies to (30). Similarly, from (64) the thermal conductivity for hard spheres in dimension d is $d(d+2) k_B p \tau / (2(d-1)m)$ which is equivalent to (30).

The balance equations (63) and (64) written above can take the place of the necessary constitutive equations to have a complete hydrodynamic picture, but they really are dynamic equations. And contrary to the usual

relation for these higher momenta, they do not relate linearly \mathbf{IP} and \mathbf{q} with the gradients of \mathbf{v} and T as (28) and (29) do.

Later in these notes the nonlinear nature of these higher balance equations will be necessary to explain some of the observations.

5 Dilute Gas with Strain Flow

In this section we study a planar Couette flow both analytically and by means of microscopic molecular dynamic techniques for the case of a bidimensional gas of hard disks. The fluid gets warmer in the middle, it has a non Newtonian behavior and there is a heat current which obeys a Fourier law with a *tensorial* shear dependent thermal conductivity. Nonlinear laws of heat transport and of viscous flow are derived from Grad's solution to Boltzmann's equation and it is shown that they describe quite well the observations made with the simulations. Throughout this section the Boltzmann constant has been set to $k_B = 1$.

Several decades ago Green and Kubo introduced a method (GK method from now on) for the calculation of transport coefficients as time integrals of time correlation functions of certain microscopic currents (Green 1952, 53, Kubo 1957). With the advent of computational physics it became possible to apply the GK method to obtain estimates of the transport coefficients for particular interaction laws. These calculations led not only to the conviction that there are long time tails of the GK time correlation functions implying the *divergence* of the *GK transport coefficients in 2D* and, for the 3D case, to numerous specific results for self-diffusion, mutual diffusion, bulk and shear viscosity, and thermal conductivity of model gases and liquids, forming an important basis for the dominant interpretation of both the theory and phenomenology of transport.

In particular the divergence of the 2D transport coefficients has been widely accepted (Ernst *et al* 1978). They are expected to diverge because the corresponding correlation integrals are believed to decay in 2D as $\mathcal{O}(\frac{1}{t})$. On the other hand, recent high-precision simulations as in Hoover & Posch (1995), Posch *et al.* (1995), Gravina *et al.* (1995), Hansen & Evans (1995), Risso & Cordero (1996a) for short range steep repulsive potential (hard disks in Risso & Cordero (1996a) and detailed in §6) produced what looks like size-independent transport coefficients fairly close to the predictions that Gass (1971) derived from the 2D Enskog theory. Namely, no divergence is detected. The reproducible finite nature of viscosity in Hoover & Posch (1995), Gravina *et al.* (1995) and thermal conductivity in Hansen & Evans (1995), Risso & Cordero (1996a) could be made understandable if the coefficients only diverge in a large system limit beyond present computational possibilities. Certainly the GK derivation of divergence fails to hold for *finite systems* with finite steady state nonequilibrium fluxes. One should find a bridge from finite to infinite systems, goal that is beyond our present scope.

Couette flow of a dilute system of Maxwell particles under strong strain has been studied theoretically by different authors (Brey & Santos 1987, Kim *et al.* 1989, Garzó 1994-95). In Brey & Santos (1987) an exact *normal* solution of the BGK equation which includes heat transport (a solution is *normal* if the coordinate dependence comes only through the \mathbf{r} dependence of the hydrodynamic fields (Grad 1958,60)). The momentum flux turns out to be a nonanalytic function of the shear rate and the heat current obeys a Fourier law with a conductivity that depends on the shear rate as well. In Garzó (1994-95) the distribution function is also assumed to obey the BGK equation and, in order to study the rheologic properties of the stationary regime the authors introduce an external nonconservative force that creates the heat flux. There is no temperature gradient, a drag force is included to preserve the stationary state and it is shown that shear affects the heat flux. The authors present explicit expressions for the shear dependent thermal conductivity tensor and the off diagonal terms implies a component of the heat current normal to the temperature gradient as a second order effect not present in the linear constitutive hydrodynamic equations.

MD simulations of Poiseuille or Couette flow in bidimensional dense fluids composed of hard disks exhibit a non-Newtonian behavior (Risso 1994, Risso & Cordero 1996a) and Fourier's law of heat conduction has also been seen to be violated in the sense that heat flux is observed in directions where there is no temperature gradient, temperature being understood as the local average of the kinetic energy in the co-moving frame.

In the present study it is assumed that the gas of hard disks obeys the complete Boltzmann's equation. In the simulations the production of heat has not been inhibited by any means. As expected we observe a heat flux with a component perpendicular to the walls which accounts for the heat being dissipated through the walls (in contact with heat baths) and we also observe a *longitudinal* one.

To be able to make a satisfactory theoretical analysis of this behavior we have (a) performed molecular dynamic simulations of a *dilute* gas, observing the same behavior and (b) compared the simulational results with the implications of Grad's solution to Boltzmann's equation (Risso & Cordero 1997).

The rest of this section presents the case of laminar stationary Couette flow. The flow gets warmer and there is a heat flux from the middle of the channel towards the walls. The predictions coming from Grad's distribution describe quite well our simulational results.

The effect of strain in the case of a Couette flow will be analyzed. In particular, results will be shown from simulations that clearly indicate that the usual linear constitutive equations of hydrodynamics cannot be applied.

5.1 The System and Simulational Conditions

The system of hard disks is inside a $L \times L$ square box. The lateral walls (Y direction) are treated as periodic boundaries, the collisions among particles are perfectly elastic and the collisions with the hard horizontal walls (X direction) are such that they impose a temperature T_0 on the fluid as well as a velocity v_0 at the top wall and $-v_0$ at the bottom wall.

In every simulation the system was relaxed for about 20 thermal diffusion times t_{diff} before local time averages of the main momenta of the distribution ($n, \mathbf{v}, T, p_{ij}, \mathbf{q}$) were taken, in some cases for as long as 4000 t_{diff} .

Units are chosen so that $m = 1$ and $\sigma = 1$ and the temperature T_0 at the horizontal walls is set to $T_0 = 1$. The origin of the Y axis is placed in the middle of the channel to make more evident the symmetry about $y = 0$ so that the y coordinate varies from $-L/2$ to $L/2$.

The control parameters of the simulations were the number of particles, $N = 2539$ or $N = 7680$, v_0 and the bulk number density $\bar{n} = N/L^2$. The tangential velocity v_0 of the walls was in the range $v_0 = 0.25$ to $v_0 = 128.0$.

One has to bear in mind though that, for finite (mesoscopic) systems there are velocity and temperature jumps (see §6.2) which cannot be neglected implying that the limits of $T(y)$ and $v_x(y)$ as $y \rightarrow \pm L/2$ do not give exactly the values externally imposed.

The bulk density $\bar{n} = 4\rho_A/\pi\sigma^2$ was fixed so that the fraction of area covered by the disks was 1% ($\rho_A = 0.01$). With this choice the non-ideal corrections to the equation of state are less than 2%. The number of disks was chosen so that the ratio $c = \ell/L$, where ℓ is the mean free path, be small enough to keep the boundary effects constrained to a small fraction of the system and guarantee that far from the walls the fluid has a hydrodynamic behavior. It is known that for a low density gas of hard disks $\ell = \pi\sigma/(8\sqrt{2}\rho_A)$ and since $L = \sigma\sqrt{N/\bar{n}}$ then $N \sim \pi/(32\rho_A c^2)$. Hence, for $N = 2539$, $c = 0.062$ and for $N = 7680$ it is $c = 0.036$.

5.2 Balance Equations and Boundary Conditions

The hydrodynamic equations for the dilute 2D system of hard disks are the standard balance equations (62) plus (63) and (64) for $d = 2$. The p_{ij} components are eliminated in favor of the complete pressure tensor $P_{ij} = p_{ij} + p\delta_{ij}$.

Under conditions of laminar Couette flow (see values of the Reynolds number below) and times much larger than t_{diff} the system has been able to relax to a stationary regime and the flow presents translation invariance along the channel. All quantities of interest are either uniform or they depend solely on the transversal coordinate y . The hydrodynamic velocity has a unique nonvanishing component, $v_x(y)$. The mass balance equation is identically satisfied.

To fit the simulational results with the theory the following considerations are made. *i*) Grad's solution cannot be expected to be valid near the borders

($y = \pm L/2$), where the interaction with the walls plays an important distorting role, particularly at low densities. *ii)* Assuming that Grad's solution gives the correct behavior for the system in the bulk, the expressions should reproduce the simulational results using corrected values for v_0 and T_0 .

From the two momentum balance equations (55) it follows that both P_{xy} and P_{yy} are uniform. Hence, the balance equations for P_{xx} and P_{yy} , (63), yield

$$p(y) = P_{yy} - \frac{3}{2}\gamma(y)P_{xy}, \quad P_{xx}(y) = P_{yy} - 3\gamma(y)P_{xy} \quad (67)$$

where τ was defined in (65) and γ is an adimensional measure of the shear rate at height y

$$\gamma(y) = \tau(y) v_x(y)' . \quad (68)$$

The rest of the balance equations imply

$$\frac{\tau}{2}q'_x = -P_{xy} - \gamma P_{yy}, \quad (69)$$

$$q_x + 3\gamma q_y = -\frac{6\tau}{m}P_{xy}T', \quad (70)$$

$$\gamma q_x + q_y = -\frac{3\tau}{m}P_{xy}T\gamma' - \frac{\tau}{m}(4P_{yy} + 3\gamma P_{xy})T', \quad (71)$$

$$\tau q'_y = -\gamma P_{xy}. \quad (72)$$

The primes indicate derivatives with respect to y . The above system of equations has as unknowns the fields γ , T , q_x , q_y . The boundary conditions in principle are

$$T(\pm L/2) = T_0, \quad q_x(0) = 0, \quad q_y(0) = 0 \quad (73)$$

plus two integral conditions expressing that the global density \bar{n} and the velocities $\pm v_0$ at the borders are known

$$\int_{-L/2}^{L/2} \frac{p(y)}{T(y)} dy = \frac{N}{L}, \quad (74)$$

$$\int_{-L/2}^{L/2} v_{x,y} dy = 2v_0. \quad (75)$$

The ideal gas equation of state, $p = nT$ ($k_B = 1$), was used in the first integral expression while in the last expression the integrand is $\gamma(y)/\tau(y)$.

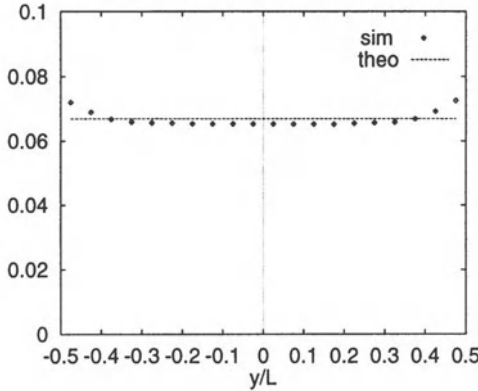


Fig. 7. The diamonds represent the observed values of γ versus the coordinate y/L for a system of $N = 7680$ particles, area density $\rho_A = 0.01$ and imposed lateral velocity $v_0 = 1.4$. The straight line is the theoretical value. The discrepancy away from the borders is about 2%.

5.3 Expansions

At first glance one cannot hope to find an analytic solution of the above system of differential equations and therefore we expand in terms of a small adimensional parameter ε defined in such a way that it would coincide with γ if the shear rate were small and uniform,

$$\varepsilon = \frac{v_0}{2} \sqrt{\frac{m}{\rho_A T_0 N}} \quad (76)$$

$$\gamma(y) = \varepsilon + \varepsilon^3 \eta_3(y) + \varepsilon^5 \eta_5(y).$$

There is a symmetry related to inverting the sign of v_0 (or γ or ε). It is easy to see that T , q_y and P_{yy} have to be even in ε while q_x and P_{xy} have to be odd functions of ε .

The Reynolds number $Re = \frac{v_0 L}{\nu_0}$, where ν_0 is the ideal gas kinematic viscosity, reduces in the present case to $8\bar{\rho}_A N \gamma$ which for the typical values we use amounts to $Re \approx 20$ to 60.

Since q_y vanishes for zero strain its expansion begins with a term $\mathcal{O}(\varepsilon^2)$. Similarly, since T' vanishes when $\varepsilon = 0$ then $T = T_0 + \mathcal{O}(\varepsilon^2)$. From this and (70) it follows that $q_x = \mathcal{O}(\varepsilon^3)$. Finally since for zero shear rate P_{yy} coincides with the hydrostatic pressure and the pressure is nT then the form $P_{yy} = nT_0 + \mathcal{O}(\varepsilon^2)$ was used.

With all the above considerations we have solved the system of equations and their boundary conditions in a consistent way using expansions up to ε^6 . All the algebraic manipulations were done using the symbolic language MAPLE. To our surprise the coefficients η_k that appear in the expansion of γ turn out to be independent of y as if the strain in the bulk of the system

were uniform. The conclusion then is that within the theoretical picture constructed from Grad's 2D eight-momentum distribution function, it is reasonable to assume that the shear rate γ is uniform. The nonuniformity observed in Fig. 7, when the externally imposed strain is high, may be due to boundary effects and not to a deviation of the theory in the bulk where Grad's distribution should be good. Still one should study the range of applicability of Grad's solution mentioned in §4.4.

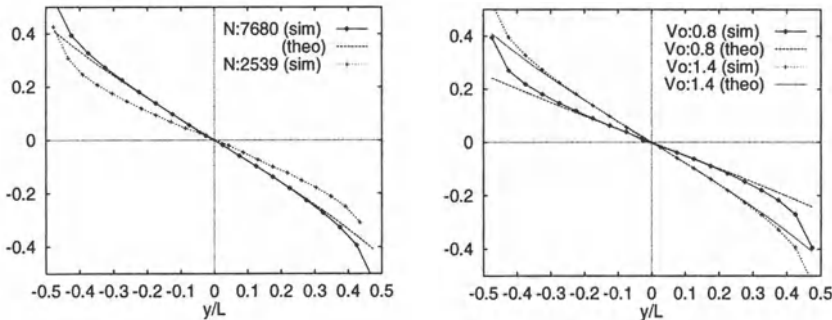


Fig. 8. At left $T'(y)$ for two systems with $\rho_A = 0.01$: $N = 2539$, $\gamma = -0.063$ and $N = 7680$, $\gamma = -0.058$. The first one clearly differs from the theoretical profile. At right two profiles $T'(y)$ for $N = 7680$ but different v_0 . Away from the walls theory and observations coincide.

For given values of v_0 and T_0 , ε or γ are smaller for larger systems. According to (76), $\gamma \sim \mathcal{O}(\frac{1}{\sqrt{N}})$.

5.4 Closed Solution for Uniform Shear Rate

Assuming that γ does not depend on y it is possible to integrate the system of equations and in particular derive that the following ratios do not depend on the temperature field

$$\xi \equiv \frac{P_{xy}}{P_{yy}} = \frac{4 + 3\gamma^2 - \sqrt{\Delta}}{3(4 - 3\gamma^2)\gamma} \approx -\gamma + \frac{9}{4}\gamma^3 \quad (77)$$

$$\frac{q_x}{\gamma q_y} = -\frac{18(2 - \gamma^2)}{-3\gamma^2 + 4 + \sqrt{\Delta}} \quad (78)$$

$$\approx -\frac{9}{2} + \frac{55}{8}\gamma^2 - \frac{489}{16}\gamma^4 + \dots \quad (79)$$

where $\Delta = 16 + 120\gamma^2 - 63\gamma^4$. Observe that (79) implies that there is a heat flux current q_x along the Couette channel.

Minor algebraic manipulation of the equations yield a temperature profile obeying

$$T T'' + \frac{1}{2} T'^2 + K = 0 \quad (80)$$

hence

$$\pm \sqrt{2K} y = T \sqrt{\frac{T_{\max} - T}{T}} + T_{\max} \arctan \sqrt{\frac{T_{\max} - T}{T}} \quad (81)$$

where

$$\sqrt{2K} = f(\gamma) P_{yy} \quad (82)$$

$$\begin{aligned} f(\gamma) &\equiv \sqrt{\frac{81\gamma^4 - 264\gamma^2 + 16 + (15\gamma^2 + 4)\sqrt{\Delta}}{9\gamma^4 - 24\gamma^2 + 16}} \sqrt{\pi} \sigma \gamma \\ &\approx \left(\gamma - \frac{3}{2}\gamma^3 - \frac{9}{8}\gamma^5 - \frac{27}{32}\gamma^7 \right) \sqrt{2\pi} \sigma. \end{aligned} \quad (83)$$

And $\sqrt{2K}$ is real in the interval $0 < \gamma^2 < \frac{1}{3}$.

In practice, to integrate (80) we have imposed that $T(y=0) = T_{\max}$ and $(dT/dy)_{y=0} = 0$. In Fig. 8 there is a comparison of the observed values of T' and the corresponding profiles obtained from the above expressions.

Combining these results and exploiting the boundary conditions it is possible to derive three expressions that link T_{\max} , T_0 and v_0 .

From the condition that the T -profile (81) give $T(\pm L/2) = T_0$ follows that

$$P_{yy} = \frac{2}{f(\gamma)L} \left(T_0 \sqrt{\frac{T_{\max} - T_0}{T_0}} + T_{\max} \arctan \sqrt{\frac{T_{\max} - T_0}{T_0}} \right). \quad (84)$$

The two integral equations combined render

$$\begin{aligned} \sqrt{T_{\max} - T_0} &= \frac{\sqrt{81\gamma^4 - 264\gamma^2 + 16 + (4 + 15\gamma^2)\sqrt{\Delta}}}{4 - 9\gamma^2 + \sqrt{\Delta}} \frac{\sqrt{m} v_0}{2} \\ &\approx \left(1 - 3\gamma^2 + \frac{27}{4}\gamma^4 + \dots \right) \frac{\sqrt{2m}}{4} v_0 \end{aligned} \quad (85)$$

and

$$\sqrt{T_{\max} - T_0} = \frac{v_0}{4\gamma} \sqrt{\frac{m}{N\rho_A}} \arccos \left(\frac{2T_0 - T_{\max}}{T_{\max}} \right). \quad (86)$$

These last two relations connect T_{\max} , T_0 and v_0 . From them it is possible to get that γ does not grow indefinitely with v_0 but saturates to a value $\gamma_{\max} \sim \mathcal{O}(\frac{1}{\sqrt{N\rho_A}})$, see Fig 11.

From the relations $P_{xy} = \xi P_{yy}$ and $p = P_{yy} - 3\gamma P_{xy}/2$ it follows that $P_{xy} = p\xi/(1 - 3\gamma\xi/2)$, where ξ was defined in (77) can formmaly be written as Newton's law of viscous flow even though it is a highly nonlinear expression,

$$\begin{aligned} P_{xy} &= -\eta_\gamma v'_x \\ \eta_\gamma &= -\frac{\xi}{\gamma \left(1 - \frac{3}{2}\gamma\xi \right)} \eta_0 \\ &\approx \left(1 - \frac{15}{4}\gamma^2 + \frac{297}{16}\gamma^4 + \dots \right) \eta_0 \end{aligned} \quad (87)$$

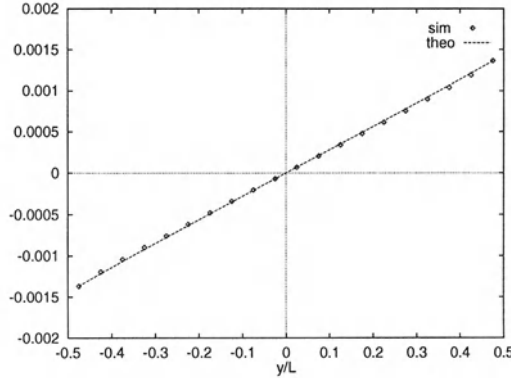


Fig. 9. Predicted and observed values of the transversal heat flux q_y for the system with $N = 7680$ and $v_0 = 1.4$

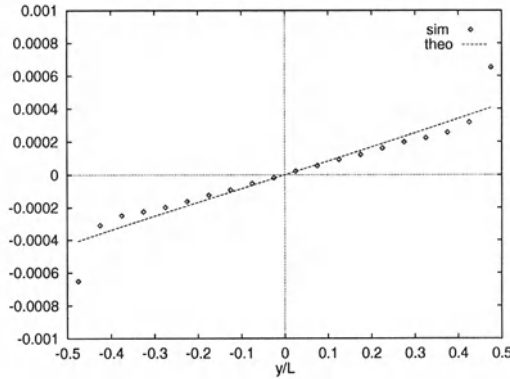


Fig. 10. Predicted and observed values of the longitudinal heat flux q_x for the system with $N = 7680$ and $v_0 = 1.4$. There is no temperature gradient in this direction.

η_0 is the ideal viscosity of (30). The expression above predicts an effective shear thinning which is compared with our observations in Fig. 11. The agreement is excellent.

Equations (70) and (71) can be looked upon as a system of algebraic equations to derive q_x and q_y as combinations of P_{xy} and P_{yy} . Since we already have expressions for the pressure tensor these equations yield

$$\begin{aligned} q_y &= -k_{yy} T' = -\frac{12 - 15\gamma^2 + \sqrt{\Delta}}{2(1 - 3\gamma^2)(4 - 9\gamma^2 + \sqrt{\Delta})} k_0 T' \\ &\approx -\left(1 + \frac{9}{4}\gamma^2 + \frac{153}{16}\gamma^4 + \dots\right) k_0 T'. \end{aligned} \quad (88)$$

This expression can be seen as a Fourier law with an effective thermal con-

ductivity that grows with shear.

$$\begin{aligned} q_x = -k_{xy} T' &= \frac{54\gamma^2 - 27\gamma^4 - 8 + (2 - 3\gamma^2)\sqrt{\Delta}}{(1 - 3\gamma^2)\gamma(4 - 9\gamma^2 + \sqrt{\Delta})} \frac{k_0}{2} T' \\ &\approx \left(\frac{9}{2}\gamma + \frac{9}{8}\gamma^3 + \dots \right) k_0 T'. \end{aligned} \quad (89)$$

The last expression implies a heat current *along* the isotherms and in the same direction as the mass flux. For shears as small as $\gamma = 0.065$ this current is about 30% the size of the transversal heat current q_y .

5.5 Observations Versus Theory

To measure the hydrodynamic behavior of the system, the box was divided in $M_x \times M_y$ rectangular cells. In each cell the time average of the first momenta of the distribution were made. For the system with $N = 7680$ particles the choice was $M_x = M_y = 20$, which corresponds to about 19.2 disks per cell and in the case with $N = 2539$ it was $M_x = M_y = 23$ or about 4.8 disks per cell.

Most quantities show boundary effects. The temperature field shows isotherms parallel to the flow but — as predicted by (89) — the heat flux is not orthogonal to them: it bends in the direction of the mass flow. The equation of state is well satisfied across all the fluid, including the regions near the walls. Observed discrepancies with the ideal gas equation were always below 2% and if Henderson's equation of state (7) is used the discrepancies are below 0.1% for the $N = 7680$ system. The components P_{xy} and P_{yy} of the pressure tensor show no boundary effects but P_{xx} does.

Taking advantage of the translation invariance in the X direction, it was natural to take horizontal averages of the observed cell-results getting in this way smooth vertical profiles for the observed hydrodynamic fields.

As mentioned above (67), P_{xy} and P_{yy} should be uniform. From the horizontal averages of P_{xy} and P_{yy} , for $N = 2539$ particles, their values at each y are obtained with errors of less than 0.6% and less than 0.07% respectively. For the larger system the errors are still smaller. An additional vertical average over each of the previous profiles produce a variance of about 0.1% for P_{xy} and of about 0.008% for P_{yy} when $N = 2539$ and smaller when $N = 7680$. In this sense it can be stated that these two quantities are independent of y as hydrodynamics predicts.

Even though we derived that up to 6th order in ε the adimensional shear rate γ is uniform, the simulations for shear rates as small as $\varepsilon = 0.06$ show a wide region near the boundaries of the channel where γ noticeably varies with y . In the central region γ is quite uniform as seen in Fig. 7.

From these considerations it is clear that the theoretical framework presented in §5.2 needs a reassessment because, even though the differential

equations are expected to be valid in the bulk, this is not true near the boundaries. The closed expressions found in §5.4 should be expected to fit well away from the walls and the values associated to the boundary conditions (T_0 , v_0) should be adjusted to make this fit.

To adjust the observed results we proceeded as follows.

Since both P_{xy} and P_{yy} are independent y within a very small error, vertical averages of these two quantities were taken and from them and (77) an effective value for the shear rate γ is obtained. Figure 7 shows the adjusted γ and the observed shear rate. The figure corresponds to the case $N = 7680$ and $v_0 = 1.4$. Away from the walls the adjusted value of γ is $\gamma = 0.066869 \pm 0.000062$ which differs from the observed value in about 2%. Similar differences are obtained for other values of v_0 . In the extreme case $v_0 = 128.0$ the γ profile is less uniform but still the values in the central part of the box differ by about 4% from the adjusted value.

The constant $\sqrt{2K}$ is then evaluated from (83).

T_{\max} was obtained making a mean square fit of (81) adjusting both, the values of T_{\max} and again the value of $\sqrt{2K}$. Since the temperature profile shows a strong and wide boundary effect different fits were made eliminating one, two, three etc points on each extreme and finally an extrapolation was made. The value for $\sqrt{2K}$ obtained in this way differs from the one obtained from (83) by a few percent.

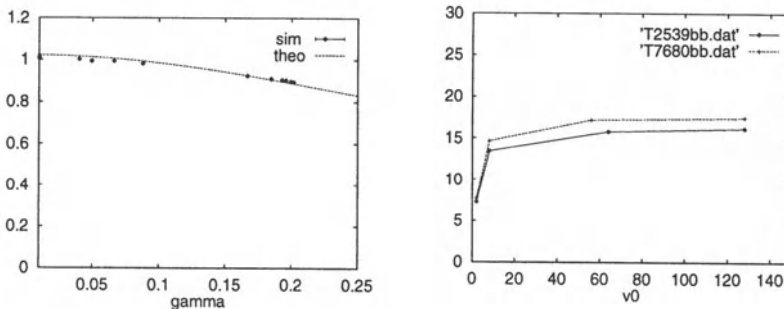


Fig. 11. At left the viscosity η_γ versus γ . At right values of $\sqrt{N} \gamma$ versus v_0 for systems with $N = 2539$ and $N = 7680$.

The previous fit yields what, from now on, we will be calling the theoretical temperature profile $T(y)$. It coincides with the observed T profile only in the central region and fails badly away from it. From the theoretical temperature profile $T(y)$ follows its gradient $T'(y)$. In Fig. 8 there is a comparison of the latter with the observed values. The T' profile agrees quite well away from the walls when the system is larger ($N = 7680$).

Figures 9 and 10 compare the observed heat flux profiles with the theoretical profiles found in the expressions (88), (89). Figure 9 shows the value of

the transversal heat current q_y for the case $N = 7680$, $v_0 = 1.4$. Notice that q_y , as seen in (88) obeys a Fourier type of law with an effective conductivity that depends on the shear rate. The agreement with the theory is excellent. Figure 10 plots the component of the heat flux current q_x along the isotherms for a system with $N = 7680$ and a shear rate about $\gamma \approx 0.067$. It is seen that the agreement is fair. These effects go down as the size of the system is increased, for $N = 2359$ the agreement is rather poor and we did not make the corresponding plot. For q_x the boundary effects propagate deeper into the system.

To check the implications of the integral boundary conditions we proceeded to determine the value of γ that follows from equating the right hand sides of (85) and (86). Taking the system with $N = 7680$, $v_0 = 1.0$ and using for T_0 the value obtained from the theoretical profile, we obtain $\gamma = 0.0495378$ while the value of γ derived from P_{xy}/P_{yy} is $\gamma = 0.0495468$ which is better than what one could expect.

Using the observed values of v'_x and P_{xy} at different points in the channel and in different simulations it is possible to extract a simulational value for the shear viscosity η_γ which turns out to follow quite well the value given in (87) within less than 1% in a range of γ up to $\gamma = 0.2$ (see Fig. 11). We have not enough date to derive error bars but all points are seen to fall close to the theoretical curve.

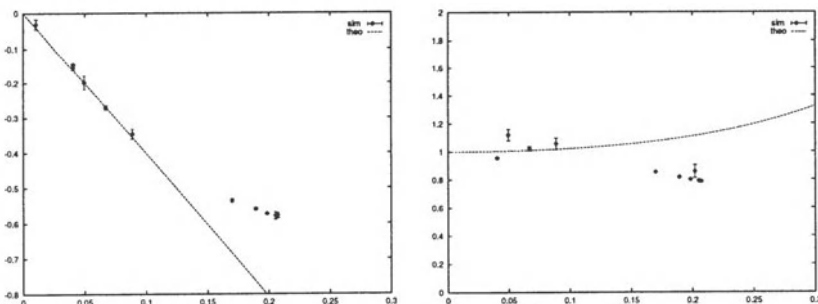


Fig. 12. The predicted conductivities versus γ are compared with the conductivities derived directly from the observations ($N = 7680$). At left is k_{xy}/k_0 and at right k_{yy}/k_0

Similarly, the observed components of the thermal conductivity tensor are compared with the expression implied by (88) and (89). From the observed values for q_x , q_y and T' we have derived profiles for the conductivities $k_{xy} = -q_x/T'$, $k_{yy} = q_y/T'$ after eliminating 2 or 3 data points from the borders and four noisy points from the central part where T' , q_x and q_y are too small. An extrapolation of the profiles of k_{xy}/k_0 and k_{yy}/k_0 at $y = 0$ using a parabolic fit yields the simulational values presented in Fig. 12 for different values of γ .

For k_{xy}/k_0 the agreement is quite good if $v_0 \leq 2$, implying $\gamma = 0.08871$ when $N = 7680$ (see Fig 12). For k_{yy}/k_0 (same figure) the statistics is rather poor. The results show a behavior consistent with the theory for small values of the shear rate, but we do not have enough data to make stronger statements.

Our data is less noisy when the shear rate gets larger ($v_0 > 2.0$) but in that case the discrepancy with theory is substantial both for k_{xy} and k_{yy} . There are many possible sources for these discrepancies. The higher balance equations (63) and (64) are derived, according to Grad, neglecting terms that involve still higher momenta which possibly are no longer negligible at such high shear rates. The boundary effects, on the other hand, are also more complex since the discontinuities of the hydrodynamic fields at the walls are related to their own gradients. This seems particularly relevant in the case of the temperature field.

In summary, it has been shown that a dilute gas of less than 10^4 particles subjected to extreme shear conditions is extraordinarily well described by Grad's solution to Boltzmann's equation.

6 Thermal Conductivity

The behavior of the thermal conductivity k — of a two dimensional system of N hard disks enclosed in a rectangular $L_X \times L_Z$ box — will be studied by means of molecular dynamics when the system has a vanishing hydrodynamic velocity field (a pure conductive regime) and compared with the predictions that stem from Enskog's kinetic equation. Because the system of hard particles has no intrinsic energy, the temperature provides the only energy scale and therefore k has to have the form

$$k(\rho, T) = k_0(\rho) \sqrt{T} \quad (90)$$

if the Fourier law (29) is applicable. The transport coefficients of a system of hard disks are necessary also to analyze in depth simulational results such as, for example, Bénard's convection with hard-disk systems as in Mareschall *et al.* (1986-89), Rapaport (1988,92), Risso & Cordero (1992,93).

During the simulations the collisional and kinetic contributions to the conductivity can be measured separately. Determining the conductivity in this way, however, is lengthy and noisy. Instead it has been preferred to measure the net heat flux q across the system as it would be done in real experiments and define an *effective conductivity* \bar{k} which is the result of the conductivities that the layers of the stratified system have.

An important technical detail comes from a known temperature jump that occurs at the walls when the system is subjected to a temperature difference ΔT . Because of this jump it is necessary to correct the temperatures at the walls by defining a new difference ΔT^* .

The system. The basic parameters that define the system are: the number N of hard disks; their mass m , diameter σ , the size $L_X \times L_Z$ of the box, the acceleration of gravity g , the temperature at the bottom and top walls T_b and $T_t = T_b - \Delta T$. It will be helpful to use the reduced temperature difference

$$C_t \equiv \frac{\Delta T}{T_b} . \quad (91)$$

Due to the important compressibility of this gas a significant density gradient would develop had an acceleration of gravity g not been added in the direction of the temperature gradient.

The hydrostatic momentum balance equation in the \hat{z} direction in the present case reduces to $dp/dz = -mgn$. Using that $p = n H k_B T$ it is easily rewritten, with the help of (10), as $H n'/\alpha = -n H T' - mgn$ where the prime indicates derivation with respect to z . The momentum balance equation is then written in terms of the Froude number Fr as

$$n' = \frac{\alpha n \Delta T}{L_Z} \left(\frac{T' L_Z}{\Delta T} - \frac{Fr}{H} \right) , \quad Fr = \frac{mg L_Z}{k_B \Delta T} \quad (92)$$

If the temperature profile is not too far from being linear then the first term in the parenthesis is approximately one. Hence, the condition that the density profile be as flat as possible reduces to

$$Fr \approx H(n) . \quad (93)$$

A note of warning: in the presence of a temperature gradient and an acceleration of gravity, free thermal convection could be triggered. In Risso & Cordero (1992,93) this phenomenon was analyzed and it can be stated that the simulations connected to this sections where performed far from the convective zone in parameter space.

The disks have elastic collisions among themselves, the vertical walls are perfectly elastic (adiabatic), while the upper and lower walls simulate contact with heat baths at temperatures T_b and T_t . When a particle hits a horizontal wall the tangential component of the velocity is conserved while the normal component is sorted from a Maxwellian distribution associated with the temperature of that wall.

6.1 Heat Flux and the Effective Conductivity

Since the Fourier law of heat conduction (29) states that $\mathbf{q} = -k\nabla T$ an effective *simulational* bulk conductivity can be defined by

$$\bar{k}_{\text{sim}} = \frac{q L_Z}{\Delta T} . \quad (94)$$

Since the system has an important temperature gradient we directly compare the effective conductivity obtained by means of the simulations using

(94) with the effective conductivity \bar{k}_{theo} that stems from Enskog's theory explained in the following paragraph.

Since the thermal conductivity depends on the local values of the density and temperature (see (41)) it is natural to define, in a straightforward manner, a *theoretical effective conductivity* \bar{k}_{theo} for the system as the net effect of the conductivity of all the infinitesimal horizontal slices i , of width δ , in which the system can be thought to be divided

$$\bar{k}_{\text{theo}} = \left(\frac{1}{N_{\text{slices}}} \sum_{i=1}^{N_{\text{slices}}} k_i^{-1} \right)^{-1}. \quad (95)$$

The limit $\delta \rightarrow 0$ is understood. For the present purposes, however, the definition of (95) has been used with slices of finite width to evaluate each $k_i(\rho_A, T)$ from (41) and taking the observed values of ρ_A and T in each slice. The logic behind (95) is the same one used to obtain the effective resistance ($r = 1/k$) of a system of resistors (the horizontal slices with resistance $1/k_i$) connected in series.

6.2 Temperature Discontinuity at the Wall

Once a conductive regime is established, the measured temperature difference in the bulk, ΔT^* , is smaller than the externally imposed difference ΔT . This is a well known effect due to a temperature discontinuity at the walls (Tenenbaum *et al.* 1982, Trozzi & Ciccotti 1984). A similar effect is observed in real, dilute systems (Hirschfelder *et al.* 1954). This temperature discontinuity is related to the collision rate and the temperature difference. In fact, the discontinuity of $T(\mathbf{r})$ near hard walls is an effect of the stochastic thermalization at the walls. A simple derivation of it is now presented for the case of the discontinuity of T for a top wall of a rectangular box. Call T_w the temperature imposed on a wall, T^* the temperature of the fluid in contact with the wall and q the magnitude of the heat flux vector normal to the wall. Particles approaching the wall have $c_y > 0$ and come from a distribution f^* with temperature T^* while particles bouncing back from the wall have $c_y < 0$ and obey a distribution f_w with temperature T_w . The net flux across the wall of a quantity A is

$$G_A = \int_{-\infty}^{\infty} dc_x \left(\int_{-\infty}^0 A c_y f_w(\mathbf{r}, \mathbf{c}) dc_y + \int_0^{\infty} A c_y f^*(\mathbf{r}, \mathbf{c}) dc_y \right). \quad (96)$$

A Maxwellian distribution is used in both integrals. Requiring that the particle net flux ($A = 1$) across the wall is zero, the heat flux ($A = \frac{1}{2}m c^2$) is $q = \pm \frac{3k_B}{2m} (T_w - T^*) G_w$, where

$$G_w = \frac{n^*}{2} \sqrt{\frac{2k_B T^*}{\pi m}} \quad (97)$$

is the number of particles hitting the wall per unit time and unit length (n^* is the density near the wall). There is a \pm in the expression of q above because the right hand side has to be positive.

Since the present context is that of a stationary regime, (55)c yields $\nabla \cdot \mathbf{q} = 0$ implying that the heat flux is the same in all the transversal sections of the fluid, namely, $q_b = q_t = q$, where

$$\begin{aligned} q_b &= \frac{3k_B(T_b - T_b^*)}{2} G_b \\ q_t &= \frac{3k_B(T_t^* - T_t)}{2} G_t \\ q &= \bar{k} \frac{k_B(T_b^* - T_t^*)}{L_Z}. \end{aligned} \quad (98)$$

A bit of algebra then leads to

$$\Delta T^* = (1 + \varepsilon)^{-1} \Delta T \quad \text{where} \quad \varepsilon = \left(\frac{1}{G_b} + \frac{1}{G_t} \right) \frac{2\bar{k}}{3L_Z}. \quad (99)$$

Note that $L_Z \sim \sqrt{N/n}$ implying that $\varepsilon \rightarrow 0$ in the $N \rightarrow \infty$ limit.

For a system of $N = 1521$, $\rho_A = 0.2$, $C_t = 0.5$ and $L_Z = 78\sigma$ the previous result yields $\Delta T^*/\Delta T \approx 0.85$ which is the value observed in the simulations.

From the concept of ΔT^* it is straightforward to define C_t^* and Fr^* and these are the quantities to be used, for example in (94), to make comparisons with the conductivity predicted by Enskog.

6.3 Simulational Conditions

To run these simulations the set of possible control parameters is rather large: g , ΔT , the bulk area density $\bar{\rho}_A$, N and the aspect ratio λ . In the simulations the N range was from 100 to 8100, $\lambda = 1$ and in most simulations $\bar{\rho}_A = 0.2$ and $N = 1521$ while Fr and C_t were used as control parameters.

To make these observations a 15×15 *standard observation mesh* of cells was used. The length of the simulations was determined considering the thermal diffusion time t_{diff} defined in (11). Working all the details (Risso & Cordero 1996a) it turns out that there are about $8\rho_A N$ collisions *per disk* in one diffusion time. Typically the system was relaxed for about $10t_{\text{diff}}$ which, for the case of $N = 1521$ and a density of $\bar{\rho}_A = 0.20$, means about 2250 disk-disk collisions per disk. After relaxing the system measurements were carried out during 10 to 40 diffusion times.

It was checked that the equation of state (6) is satisfied even for large values of g , Fr in the range 0.3–1.7 with C_t up to its maximum value $C_t = 1$. This is illustrated in Fig. 13

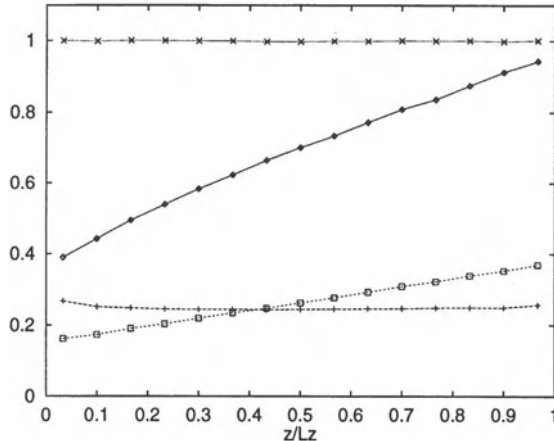


Fig. 13. Profiles of pressure (\square), density (+) and temperature (\diamond) versus the height z for a system with $N = 1521$, $\bar{\rho}_A = 0.2$, $Fr = 1.56$ and $C_t = 0.624$. The ratio $pL_x L_z / NH k_B T$ (\times) is also plotted

6.4 Simulations and Theoretical Predictions

Numerically solving the Navier-Stokes (NS) equations under hydrostatic conditions making use of (a) Henderson's equation of state, (b) Fourier's law, (c) the conductivity $k(\rho_A(z), T(z))$ taken from Enskog's theory, (d) the effective temperature values T_t^* , T_b^* and (e) the condition that $\bar{\rho}_A L_Z = \int \rho_A(z) dz$, it is possible to find the theoretical density, temperature and pressure profiles. Comparing these profiles with those obtained from the simulation for typical values of the imposed Fr and C_t the agreement is excellent. These comparisons are not only made when ρ_A is approximately uniform — namely when $Fr^* \approx H(\bar{\rho}_A)$ — but also when the density varies significantly with height. When comparing the observations with theoretical results (below), some remarks regarding this agreement have been included. Note that near the top and bottom walls ($z = 0$ and $z = L_Z$) the density profile is distorted by boundary effects.

The Effective Conductivity k . Figure 14 shows a comparison of the values of k versus C_t^* obtained from the simulations with $N = 1521$, $\bar{\rho}_A = 0.2$ and $Fr^* \approx 1.56$ using (94) with the theoretical conductivity, (95). To get the results summarized in Fig. 14 seven different simulations for each C_t were used, starting from microscopically different initial conditions but macroscopically equivalent (same density and velocity profiles). Note that because of the statistical fluctuations in the measured values of T_t^* and T_b^* the values of C_t^* show a dispersion for every externally imposed C_t . For $C_t^* < 0.3$ only one simulation was made for every C_t . Note that the observed values of k are systematically larger than the theoretical values.

For a remarkably wide range of values of C_t^* the ratio $\bar{k}_{\text{sim}}/\bar{k}_{\text{theo}}$ is nearly

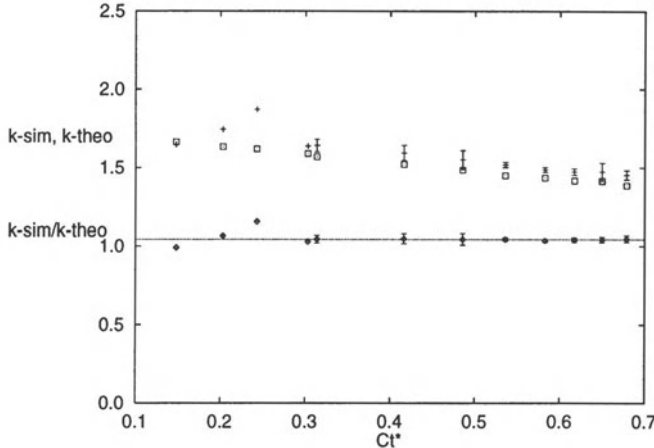


Fig. 14. Conductivities \bar{k}_{sim} (+) and \bar{k}_{theo} (□) and the ratio (\diamond) versus C_t^* for a system with $N = 1521$, $\rho_A = 0.2$, $Fr = 1.56$. The line indicates the mean value 1.044 of the ratio.

constant (Fig. 14) in spite of the large temperature variations across the system. This can be understood from (95) — assuming that the density is about uniform (and equal to $\bar{\rho}_A$) — because one can then derive that

$$\bar{k}_{\text{sim}} \approx \frac{k_0(\bar{\rho}_A)L_Z}{\int \frac{dz}{\sqrt{T(z)}}}. \quad (100)$$

To evaluate the ratio $\bar{k}_{\text{sim}}/\bar{k}_{\text{theo}}$ the same temperature profile is used in the numerator and denominator and therefore this factor cancels out. Only the ratio between the k_0 's remains.

For the case $\bar{\rho}_A = 0.2$, $Fr^* = 1.56$, $N = 1521$ (leaving out cases for which the signal/noise ratio is too small, i.e., $C_t^* < 0.5$), the extrapolation from these simulational results yields $\bar{k}_{\text{sim}}/\bar{k}_{\text{theo}} = 1.044 \pm 0.004$.

Comparison with the theoretical profiles. In the next paragraphs there is an interpretation attempting to explain why the observed profiles fit so well the theoretical predictions while the observed conductivity shows an indisputable difference with Enskog's prediction. In other words, how is it possible to have a discrepancy in the conductivity without having one in the profiles?

From a theoretical point of view it is clear that k has the form (90) and any correction can be written as a corrective factor $C(\rho_A)$ affecting the particular k_0 given in (90).

First let us notice that the local conductivity enters the formalism only through the energy balance equation that in hydrostatics simply is $\nabla \cdot \mathbf{q} = 0$, namely, $\nabla \cdot (k \nabla T) = 0$. Since the only coordinate that matters is z the last equation is

$$(k T')' = 0 \quad \text{or} \quad \frac{T''}{T'} = -\frac{k'}{k}. \quad (101)$$

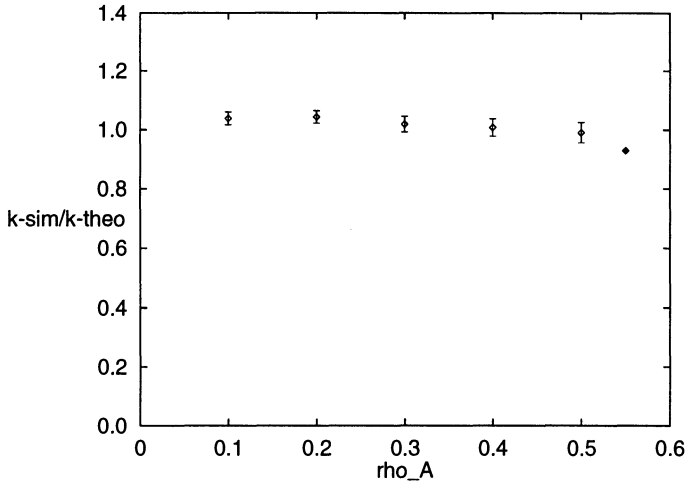


Fig. 15. Observed values for the ration $\bar{k}_{\text{sim}}/\bar{k}_{\text{theo}}$ for the systems with $N = 1521$. The last point represents the value of this ratio reported in Mareschal, Krebs (1995)

Using (90), $k = k_0 \sqrt{T}$, then the T -profile equation is

$$\frac{T''}{T'} + \frac{T'}{2T} = \frac{k'_0}{k_0} = \frac{1}{k_0} \frac{dk_0}{d\rho_A} \rho'_A. \quad (102)$$

Making the change $k_0 \rightarrow C k_0$ in the last expression amounts to changing

$$\frac{1}{k_0} \frac{dk_0}{d\rho_A} \rightarrow C \left(\frac{1}{C} \frac{dC}{d\rho_A} + \frac{1}{k_0} \frac{dk_0}{d\rho_A} \right) \quad (103)$$

adding a term $C^{-1} dC/d\rho_A$ on the right hand side. From the factor k_0 in (41) one can get that $k_0^{-1} dk_0/d\rho_A$ grows smoothly from 3.44 at $\rho_A = 0.15$ to 9.0 at $\rho_A = 0.55$ while, from the data summarized in Fig. 15, one can estimate that about $\rho_A = 0.2$ the value of $C^{-1} dC/d\rho_A$ is about 0.013. Namely, the observed correction to the conductivity would affect the temperature and density profiles by less than 0.3%.

On size effects. Figure 16 shows the ratio $\bar{k}_{\text{theo}}/\bar{k}_{\text{sim}}$ for $N = 100, 300, 900, 1521, 2500$ and 8100 . For $N = 100, 300$ and 2500 only one initial condition was taken while C_t was changed (hence no error bars in these cases). For $N = 8100$ only two initial conditions were considered while for $N = 900$ and 1521 seven different initial conditions were used. The cases $N = 900, 1521$ and 8100 indicate that the ratio is slightly increasing with N but due to the implied computational cost this possibility of making more simulations with $N = 8100$ or simulations with larger N was disregarded. No clear conclusions can then be drawn from here.

Other values for the density. Even though no systematic study of the conductivity as a function of the density was made, we obtained the ratio $\bar{k}_{\text{sim}}/\bar{k}_{\text{theo}}$

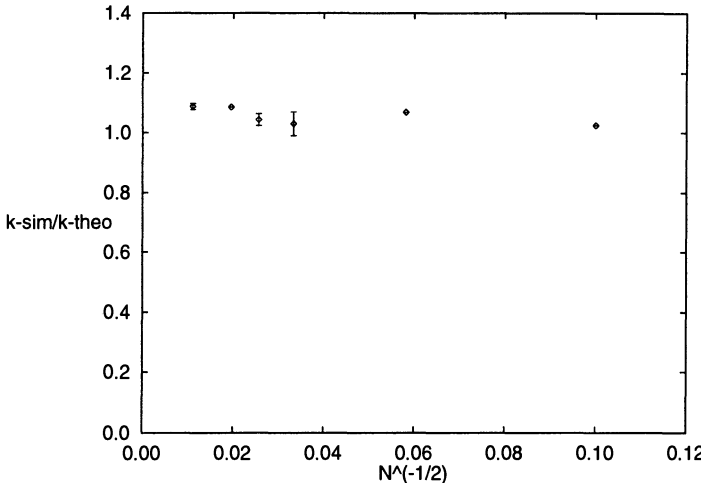


Fig. 16. The ratio between the observed theoretical values for the thermal conductivity do not show detectable size effects.

for different densities ($\bar{\rho}_A = 0.1, 0.2, 0.3, 0.4$ and 0.5) in the case of a system of $N = 1521$ particles with $Fr^* = H(\bar{\rho}_A)$. These ratios are plotted in Fig. 15.

It is seen that the most important discrepancies with Enskog's predictions seem to take place for $\rho_A \approx 0.2$. This may seem strange since one should think that the discrepancies increase with the density. But from our results it seems that the higher order corrections that come in beyond Enskog's theory decrease with the density eventually changing sign. The above results and a recent one by Mareschal & Krebs (1995), where the authors show that for a system at $\bar{\rho}_A = 0.55$ (of particles interacting with a hard, but not infinitely hard, potential) the ratio of conductivities is 0.93, support this point. The result in Mareschal & Krebs (1995) is included in Fig. 15 as the last point. It roughly follows the tendency of the other results.

6.5 Final Comments

- In the above it has been assumed that Fourier's law is valid. First, when the bulk density is $\bar{\rho}_A = 0.2$, an excellent agreement was obtained between theory and simulations regarding the density and temperature profiles.
- Next, an effective conductivity was obtained in such a way that the ratio $\bar{k}_{\text{sim}}/\bar{k}_{\text{theo}}$ is independent of the temperature difference for a wide range of density values ($\bar{\rho}_A$ from 0.1 to 0.5). This independence from the temperature difference validates Fourier's law for the system and justifies extrapolating the value of the conductivity to the limiting case $\Delta T = 0$ for different values of the density $\bar{\rho}_A$.
- The ratio $k_{\text{sim}}/\bar{k}_{\text{theo}}$ however unequivocally differs from unity. For intermediate densities ($\bar{\rho}_A$ about 0.2) the effective conductivity is larger than

the one predicted by the theory while that difference starts to go down for larger values of $\bar{\rho}_A$ and finally the simulational conductivity appears to be slightly smaller than the theoretical value when $\bar{\rho}_A \approx 0.5$.

□ To understand why it is consistent that the profiles (first item above) fit so well while the conductivity does not (third item), it was remarked that the corrective factor $C(\rho_A)$ multiplying Enskog's \bar{k}_{theo} has a sufficiently weak dependence on density — for the case $\bar{\rho}_A = 0.2$ — so that it cannot be detected in the density and temperature profiles.

Acknowledgments

We thank J.M. Pasini for carefully reading the manuscript. This work was supported by *Fundación Andes* grant C-12971 and a *CNRS-Conicyt* grant. One of us (D.R.) is also thankful of the *UBB Diprode* research grants 951005-2 and 960105-2.

References

- Alder B. J. and Wainright T. E. (1959): *J. Chem. Phys.* **31**, 459.
- Allen M. P. and Tildesley D. J. (1989): *Computer Simulation of Liquids*, Oxford Science Pub.
- Barker J. A. and Henderson D. (1976): *What is a liquid?*, Rev. Mod. Phys. **48** 587.
- Brey J. J. and Santos A. (1987): Phys. Rev. A **36** 2842; Kim Ch. S., Dufty J. W., Santos A., Brey J. J. (1989): Phys. Rev. A **40** 7165.
- Chapman S. and Cowling T. G. (1979): *The Mathematical Theory of Nonuniform Gases*, Cambridge University Press, third edition.
- Ciccotti G., Hoover W. G. (eds) (1986): *Molecular Dynamics Simulation of Statistical Mechanical Systems*, North Holland.
- Ciccotti C., Frenkel D. and McDonald I. R. (eds) (1987): *Simulation of Liquids and Solids*, North Holland.
- Cordero P., Marín M. and Risso D. (1995): *Chaos, Solitons and Fractals* **6** 95.
- Ernst M. H., Cichocki B., Dorfman J. R., Sharma J. and van Beijeren H. (1978): Jour. Stat. Phys. **18** 237.
- Hansen D. P. and Evans D. J. (1995): *Molecular Simulation* **14** 409.
- Ferziger J. H. and Kaper H.G. (1972): *Mathematical Theory of Transport Processes in Gases*, North-Holland.
- Garzó V. (1994): J. Chem. Phys. **101** 1423; (1995): Phys. Rev. E **51** 3156; (1995): J. Chem. Phys. **103** 4622.
- Gass D. M. (1971): J Chem Phys **54** 1898.
- Glikman E., Kelson I., Doan N. V. and Tietze H. (1996): Journ. Comp. Phys. **124** 85.
- Grad H. (1958): *Principles of the Kinetic Theory of Gases* in Handbuch der Physik, Vol. XII, edited by S. Flunge, Springer; (1960): *Theory of Rarefied Gases in Rarefied Gas Dynamics*, edited by F. Devienne, Pergamon Press.
- Gravina D., Ciccotti G. and Holian B.L. (1995): Phys. Rev. E **52** 6123.

- Green M. S. (1952): J. Chem. Phys. **20** 1281; (1953):J. Chem. Phys. **22** 398 (1953);
 Kubo R. (1957): J. Phys. Soc. (Japan) **12** 570.
- Hansen J. P. and McDonald I. R. (1986): *Theory of Simple Liquids*, Academic Press.
- Henderson D. (1975): Mol. Phys. **30** 971.
- Hirschfelder J. O., Curtis C. F. and Bird R. B. (1954): *Molecular Theory of Gases and Liquids*, Wiley, New York.
- Hoover Wm. G. (1986): *Molecular Dynamics*, Springer Verlag, Berlin.
- Hoover Wm. G. and Posch H.A. (1995): Phys. Rev. E **51** 273.
- Ibsen J., Soto R. and Cordero P. (1995): Phys. Rev E **52** 4533.
- Knuth D. E. (1973): *The Art of Computer Programming*, Addison-Wesley, Reading, MA.
- Kratky K. W. (1978): J. Chem. Phys. **69** 2251.
- Lifshitz E. M. and Pitaevskii L. P. (1993): *Physical Kinetics* Pergamon Press.
- Lubachevsky B. D. (1991): J. Comp. Phys. **94** 255.
- Maeso M. J. and Solana R. (1993): J. Chem. Phys. **99** 548.
- Mareschal M. and Kestemont E. (1986): Nature **427** 329; Mareschall M. and Kestemont E. (1987): Nature **429** 427; Mareschal M. and Kestemont E. (1987): J. Stat. Phys. **48**, 1187; Puhl A., Malek-Mansour M. and Mareschal M. (1989): Phys. Rev. A **40**, 1999; Mareschal M., Malek-Mansour M., Puhl A. and Kestemont E. (1988): Phys. Rev. Lett. **41**, 2550.
- Mareschal M. and Krebs U. (1995): in *Proceedings of the Eurotherm 36 Conference*.
- Marín M., Risso D. and Cordero P. (1993): J. Comp. Phys. **103** 306.
- Marín M. and Cordero P. (1995): Comp. Phys. Comm. **92** 214.
- Posch H. A. , Hoover Wm. G. and Kum O. (1995): Phys. Rev. E **52** 1711.
- Rapaport D. C. (1980): J. Comp. Phys. **34** 184.
- Rapaport D. C. (1988): Phys. Rev. Lett. **60** 2480; (1992): Phys. Rev. A **46** 1971.
- Résibois P. and de Leener M. (1977): *Classical Kinetic Theory* Wiley.
- Risso D. and Cordero P. (1992): in *Condensed Matter Theories*, A. N. Proto and J. Aliaga, eds., Plenum Press, New York.
- Risso D. and Cordero P. (1992): in *Proceedings of the IV Instability and Nonequilibrium Structures*, E. Tirapegui and W. Zeller, eds., Kluwer, Dordrecht.
- Risso D. (1994): Doctoral thesis, Universidad de Chile, May.
- Risso D. and Cordero P. (1996): J. Stat. Phys. **82** 1452.
- Risso D. and Cordero P. (1996): in *Instabilities and Nonequilibrium Structures V*, E. Tirapegui, W. Zeller eds., Kluwer Acad.
- Risso D. and Cordero P. (1996): *Dilute gas Couette flow: theory and molecular dynamics simulation* preprint.
- Risso D. and Cordero P. (1996): unpublished.
- Tenenbaum A., Ciccotti G. and Gallico R. (1982): Phys. Rev. A **75** 2778.
- Trozzi C. and Ciccotti G. (1984): Phys. Rev. A **29** 916.

Nonequilibrium Potential in Reaction-Diffusion Systems

H.S. Wio

Centro Atómico Bariloche, CNEA, and Instituto Balseiro, UNC, 8400-San Carlos de Bariloche, Argentina and Consejo Nacional de Investigaciones Científicas y Técnicas, Argentina.

1 Introduction

In this set of lectures I present a brief review of the general issue of pattern formation in reaction-diffusion systems emphasizing the point of view of the concept of the nonequilibrium potential. Through some simple examples I discuss the possibilities of exploiting this concept in order to describe the decay of metastable states and introduce an analysis of the stochastic resonance phenomenon in extended systems.

The subject of pattern formation far from equilibrium has captured the attention of researchers for more than a decade, and is by now one of the most active fields in the physics of complex systems (Nicolis & Prigogine 1977, Haken 1978, Prigogine 1980, Fife 1984, Kuramoto 1984, Malchow & Schimansky-Geier 1985, Nicolis 1986, Langer 1987, Cross 1988, Walgraef 1988, Murray 1989, Nicolis 1989, Mikhailov 1990, Meinhardt 1992, Kirkadry 1992, Mikhailov & Loskutov 1992, Cross & Hohenberg 1993, Wio 1994, Nicolis 1995). The extremely rich variety of nonequilibrium systems that one can consider calls for different descriptions. Among them, the reaction-diffusion (RD) approach has shown to be a very fertile source of models for interesting phenomena in the natural and social sciences, where structures can arise and last for longer or shorter periods of time according to their degree of stability (Nicolis & Prigogine 1977, Haken 1978, Prigogine 1980, Fife 1984, Kuramoto 1984, Malchow & Schimansky-Geier 1985, Walgraef 1988, Murray 1989, Mikhailov 1990, Cross & Hohenberg 1993, Wio 1994).

From the equilibrium phenomena point of view, both classical mechanics and reversible equilibrium thermodynamics (the two most prominent branches of macroscopic physics) are characterized by **extremum principles**. In classical mechanics it is the principle of stationary action that determines the classical trajectory, while equilibrium thermodynamics is characterized by the maximum entropy principle in closed systems. Both extremum principles originate as the macroscopic limit of more fundamental theories (quantum mechanics and statistical mechanics respectively) where those principles are violated through the occurrence of fluctuations: quantum fluctuations on one hand (that assign finite probability amplitudes to

nonclassical trajectories) and thermal fluctuations (assigning nonzero probabilities to states with less than the maximum entropy) on the other. It is this deep connection between fluctuation phenomena and extremum principles that allows the system to explore a neighbourhood of the extremizing state and thereby identify the extremum.

The evolution equations governing the nonequilibrium phenomena belong neither to the realm of equilibrium thermodynamics (therefore thermodynamic extremum principles are not applicable) nor to the realm of classical mechanics (implying that the principle of least action is also not applicable). Hence, an extremum principle allowing to characterize time-dependent or time-independent solutions of such evolution equations is not readily available. However, classical fluctuations are also present in nonequilibrium systems, just from thermal origin or due to some stochastic perturbations of general nature. Just as in equilibrium thermodynamics, these fluctuations allow to explore not only the deterministic nonequilibrium trajectory, but also its neighbourhood. Hence, it is expected that some extremum principle must also hold when one is able to identify the minimized potential function, enabling us to characterize stable steady states (or attractors) of the macroscopic evolution equations (as well as the unstable ones or separatrices) by some extremum condition. This is what one seeks in order to understand pattern selection in self-organizing systems and other related phenomena.

The main goal of these lectures is offering an introductory view to the application of the nonequilibrium potential picture into reaction-diffusion systems. We can summarize the main idea behind the nonequilibrium potential approach by saying that the selection of a pattern is strongly influenced by fluctuations. It is only *chance* that could decide through the effect of *fluctuations*. The fluctuations will enable us to explore the **landscape** of the system, and after making some initial unsuccessful attempts finally a particular fluctuation will take over. It is within this framework that the interplay between chance and constraint, or fluctuations and irreversibility, underlying all instability phenomena, is clearly seen (Nicolis & Prigogine 1977, Haken 1978, Prigogine 1980, Malchow & Schimansky-Geier 1985, Nicolis 1989, Mikhailov 1990, Wio 1994, Nicolis 1995).

In the next sections we will review a few concepts on dynamical systems, on stochastic processes and on reaction-diffusion systems as well. Afterwards, we will show a few simple cases where the nonequilibrium potential in reaction-diffusion systems can be evaluated. In the final sections we will show applications of these nonequilibrium potentials in order to analyze the probability of decay of extended metastable states as well as the phenomenon of stochastic resonance in extended systems.

2 Dynamical Systems: Stability

Physics courses have taught us that the evolution of the state variables of a system (for instance, obeying the laws of classical physics) is given by a set of differential equations of first order in time. These may be ordinary differential equations (ODE)-like Hamilton's equations or the chemical kinetic equations in a well stirred reactor; or partial differential equations (PDE)-like the fluid dynamics equations or the nonlinear reaction-diffusion equations. In the latter case, i.e. PDE, which are typical in macroscopic descriptions, one deals with an infinite number of degrees of freedom, corresponding to the values of the state variables or "fields" (for instance, reactant concentrations, order parameters, etc) at each space point as functions of time.

Although in many problems this aspect may constitute the essential characteristic of the phenomenon under study, it is not unusual that the description can be reduced to a finite number of variables. The study of systems with a finite number of variables, that is of ODE's, will give us the chance to learn a few more or less standard techniques to analyze not only systems of ODE's but that are also adequate to deal with some problems describable by PDE's.

Hence we will start considering a set of ODE's assuming that the constraints acting on the system do not depend explicitly on time (i.e. an *autonomous* system), that will have the general form (Nicolis & Prigogine 1977, Nicolis 1986, Cross 1988, Nicolis 1989, Cross & Hohenberg 1993, Wio 1994, Nicolis 1995)

$$\frac{d\mathbf{x}}{dt} = \mathbf{F}(\mathbf{x}, \zeta) \quad (1)$$

with $\mathbf{x} = (x_1, x_2, \dots, x_n)$ and $\mathbf{F}(\mathbf{x}, \zeta) = (F_1(\mathbf{x}, \zeta), F_2(\mathbf{x}, \zeta), \dots, F_n(\mathbf{x}, \zeta))$. Here x_j correspond to the state variables while ζ are some parameters (that we will denote hereafter as *control parameters*) corresponding to the systems' internal structure (diffusion coefficients, viscosities, etc) or to the form of relating with external world (thermal or shear constraints, densities of chemicals pumped in or out of a reactor). The $F_j(\mathbf{x}, \zeta)$'s are in general nonlinear functions of the x_j 's, this nonlinearity being the characteristic that does not allow us to derive explicit solutions for these systems using standard methods.

The evolution of the system described by (1) is embedded in a n-dimensional space spanned by the full set of variables $\mathbf{x} = (x_1, x_2, \dots, x_n)$ which we call the *phase space* Γ . The instantaneous state of the system is given by a particular set of values (x_1, x_2, \dots, x_n) or a unique point \mathbf{P} in phase space. That means a one-to-one correspondence between the system physical states and the phase points.

A succession of states $(\mathbf{x}, \dots, \mathbf{x}_t, \dots)$, attained along the course of time t , will determine a succession of points $(\mathbf{P}, \dots, \mathbf{P}_t, \dots)$ in phase space joined by a curve C , corresponding to a phase trajectory. Repeating the process for all possible sets $(\mathbf{x}', \dots, \mathbf{x}'_t, \dots)$ one generates a continuous family of phase

space trajectories indicating that the evolution of the system corresponds to a mapping of Γ into itself.

The set of points \mathbf{x}_s where

$$F_1(\mathbf{x}_s, \zeta) = F_2(\mathbf{x}_s, \zeta) = \dots = F_n(\mathbf{x}_s, \zeta) = 0, \quad (2)$$

(correspondingly $\dot{x}_1 = \dot{x}_2 = \dots = \dot{x}_n = 0$) are called *singular* or *fixed points* (in autonomous systems singular points remain fixed in phase space). Fixed points correspond to *stationary states* that can eventually be reached after the evolution of the system. The objects embedded in the phase space that are bounded and are mapped into themselves during the evolution generated by (1) are called *invariant manifolds*. For instance, fixed points are invariant manifolds of dimension $d = 0$. The importance of these invariant manifolds arises from the fact that they offer a geometrical view of the dynamical system.

At this point it is worth referring to the conservative or dissipative character of the system under study. Let us consider the probability density $f(x_1, x_2, \dots, x_n, t)$ (Reichl 1980, Kreuzer 1984, Keizer 1987, Wio 1994) that, after multiplying by $dx_1 dx_2 \dots dx_n$, gives the probability of finding the system in the neighbourhood of the phase space point (x_1, x_2, \dots, x_n) . The Liouville or evolution equation for this density is (Reichl 1980, Kreuzer 1984, Keizer 1987, Wio 1994)

$$\frac{\partial f}{\partial t} + \sum \frac{\partial}{\partial x_i} (f F_i) = 0 \quad (3)$$

that can be rewritten as

$$\frac{d \ln f}{dt} = -\nabla \mathbf{F}. \quad (4)$$

We will hence define that a system is conservative if

$$\nabla \mathbf{F} = 0$$

as for a harmonic oscillator; while we define a dissipative system according to

$$\overline{\nabla \mathbf{F}} < 0$$

(where we used the average $\overline{\nabla \mathbf{F}} = T^{-1} \int_0^T \nabla \mathbf{F} dt'$), as for instance, in a damped harmonic oscillator. It is clear that a conservative system will conserve (but perhaps deform) the initial volume $\Delta \Gamma_0$ in phase space. On the other hand, a dissipative system will be such that $\Delta \Gamma_0 \rightarrow \Delta \Gamma_f$ for $t \rightarrow \infty$, where $\Delta \Gamma_f$ is a subset with a lower dimension than the phase space (and with zero volume). Hence, it is in this last case that the system can evolve towards a fixed point that, in this case, is called an *attractor* (Nicolis & Prigogine 1977, Haken 1978, van Kampen 1982, Nicolis 1989, Mikhailov 1990, Wio 1994).

The relevant question here concerns the stability of the indicated solutions (or invariant manifolds) of the system of nonlinear differential equations (NLDE), that is what happens when such a solution is perturbed: does the system return to the fixed point or move away from it?.

2.1 Linear Stability: Two Variable Systems

In order to introduce some basic notions of *linear stability theory*, we will restrict ourselves to a set of two first order NLDE, corresponding to a general second order autonomous system, i.e. :

$$\begin{aligned}\frac{dx_1}{dt} &= F_1(x_1, x_2) \\ \frac{dx_2}{dt} &= F_2(x_1, x_2)\end{aligned}\quad (5)$$

If, for certain values of the coordinates, say (x_1^0, x_2^0) , the functions F_1 and F_2 satisfy very general (Lipschitz) conditions (Nicolis 1995), equations (5) have a unique solution in the neighborhood of the point (x_1^0, x_2^0) . In what follows, we shall assume that these conditions are satisfied.

Through any point (x_1^0, x_2^0) there is a unique phase curve, with the exception of the *singular* or *fixed points* (x_1^s, x_2^s) , where $\dot{x}_1 = \dot{x}_2 = 0$. A fixed point, corresponding to a steady state solution of (5), can always be moved to the origin by the change of variables $x_1 \rightarrow x_1 - x_1^s$ and $x_2 \rightarrow x_2 - x_2^s$. Therefore, we shall assume that the singular point is located at the origin. We then consider a system described by (5) which is in a steady state at $(x_1^s, x_2^s) = (0, 0)$.

If the system is in the steady state, it is important to know how it will behave under the influence of a small perturbation. Here we face several possibilities. The system can leave this steady state and move to another one; it can remain in the neighborhood of the original steady state; or it can decay back to the original state. In order to analyze the different possibilities we use a *linear stability analysis* (Nicolis & Prigogine 1977, Haken 1978, Fife 1978, Cross 1988, Wio 1994, Nicolis 1995). By this procedure we can say something regarding the stability of the system in the neighborhood of the steady state, but nothing about the global stability of the system. To discuss stability in the neighborhood of the steady state we write the solution in terms of the departure from the steady state, i.e. :

$$x_1 = x_1^s + \delta x_1; \quad x_2 = x_2^s + \delta x_2 \quad (6)$$

inserting this into (5), using $x_1^s = x_2^s = 0$, and expanding up to first order in the departures $(\delta x_1, \delta x_2)$ we obtain:

$$\begin{aligned}\dot{x}_1 &= \delta \dot{x}_1 = F_1(0, 0) + \left(\frac{\partial F_1}{\partial x_1}\right)_0 \delta x_1 + \left(\frac{\partial F_1}{\partial x_2}\right)_0 \delta x_2 + O(\delta x_1^2, \delta x_2^2) \\ \dot{x}_2 &= \delta \dot{x}_2 = F_2(0, 0) + \left(\frac{\partial F_2}{\partial x_1}\right)_0 \delta x_1 + \left(\frac{\partial F_2}{\partial x_2}\right)_0 \delta x_2 + O(\delta x_1^2, \delta x_2^2)\end{aligned}\quad (7)$$

Keeping in mind that $F_1(0, 0) = F_2(0, 0) = 0$, calling

$$\left(\frac{\partial F_1}{\partial x_1}\right)_0 = a; \quad \left(\frac{\partial F_1}{\partial x_2}\right)_0 = b; \quad \left(\frac{\partial F_2}{\partial x_1}\right)_0 = c; \quad \left(\frac{\partial F_2}{\partial x_2}\right)_0 = d,$$

and considering very small values of the δx_j , so that we can neglect higher order terms, we reduce the problem to the analysis of the following linear system

$$\begin{pmatrix} \delta \dot{x}_1 \\ \delta \dot{x}_2 \end{pmatrix} = \begin{bmatrix} a & b \\ c & d \end{bmatrix} \begin{pmatrix} \delta x_1 \\ \delta x_2 \end{pmatrix} = \mathbb{M} \begin{pmatrix} \delta x_1 \\ \delta x_2 \end{pmatrix} \quad (8)$$

The solutions of (8) give the parametric forms of the phase curves in the neighborhood of the steady state (at the origin), with time as the parameter.

The general form of the solution of (8) (except when $\lambda_1 = \lambda_2$) is

$$\begin{pmatrix} \delta x_1 \\ \delta x_2 \end{pmatrix} = \alpha \hat{c}_1 e^{-\lambda_1 t} + \beta \hat{c}_2 e^{-\lambda_2 t} \quad (9)$$

where α and β are arbitrary constants, \hat{c}_1 and \hat{c}_2 are the eigenvectors (the *normal modes*) of the matrix \mathbb{M} , associated to the eigenvalues λ_1 and λ_2 respectively. These eigenvalues are determined from the relation

$$\det(\mathbb{M} - \lambda \mathbb{1}) = 0$$

yielding

$$\lambda_{1,2} = \frac{1}{2}(a+d) \pm [(a+d)^2 - 4(ad-bc)]^{1/2}$$

It is thus clear that the temporal behaviour of the system, originally in the steady state $(x_1^s, x_2^s) = (0,0)$, after applying a small perturbation, will depend on the characteristics of the eigenvalues λ_j . We have the following possibilities:

- (i) Both eigenvalues, λ_1 and λ_2 , are real and negative ($\lambda_1 < \lambda_2 < 0$);
- (ii) both eigenvalues are real and positive ($0 < \lambda_1 < \lambda_2$);
- (iii) both eigenvalues are real, but $\lambda_1 < 0 < \lambda_2$;
- (iv) both eigenvalues are pure imaginary;
- (v) both eigenvalues are complex conjugates with $\mathcal{R}e(\lambda_1) = \mathcal{R}e(\lambda_2) < 0$;
- (vi) both eigenvalues are complex conjugates with $\mathcal{R}e(\lambda_1) = \mathcal{R}e(\lambda_2) > 0$.

Some of the situations that could arise, according to the kind of eigenvalues we find, correspond to the phase trajectories depicted in Fig. 1. Case (i) corresponds to a solution that decays for increasing time, and is called a *stable node*. Case (ii) is the opposite situation, and corresponds to an *unstable node*. Case (iii) is intermediate between the two previous situations: it is stable in one direction and unstable in the other, this corresponds to a *saddle point*. Not shown are the cases corresponding to periodic behaviour: with a constant amplitude or *center*, with a decaying amplitude, or *stable focus*, and its opposite or *unstable focus*.

Within this general scheme, even when we extend the results to a larger number of variables, it is possible to identify three basic situations: (a) $\mathcal{R}e(\lambda_j) < 0$ for all j ; (b) at least one $\mathcal{R}e(\lambda_j) > 0$; (c) at least one $\mathcal{R}e(\lambda_j) = 0$. The above analysis yields the following results (remember that all this corresponds to *small perturbations!*):

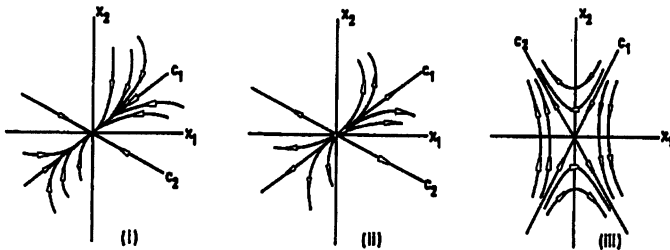


Fig. 1. The phase portrait for the different types of fixed points.

- (a) All $\text{Re}(\lambda_j) < 0$: the steady state is called *asymptotically stable*. Whatever the form of the nonlinear terms in Eq.(3), after a small perturbation the normal modes decay to it. These types of solution are called *attractors*, and the region of phase space including all the points such that any initial state finally tends to the attractor form its *basin of attraction*.
- (b) At least one $\text{Re}(\lambda_j) > 0$: the steady state is *unstable*, that is, the normal mode associated with this eigenvalue will grow with time.
- In either case (a) or (b), the behavior of the individual modes will be oscillatory if $\text{Im}(\lambda_j) \neq 0$, and monotonic otherwise.
- (c) At least one $\text{Re}(\lambda_j) = 0$, all other $\text{Re}(\lambda_k) < 0$: the steady state is *marginally stable* with respect to the mode having $\text{Re}(\lambda_j) = 0$. As a solution of the linearized equation this mode will neither grow nor decay, but could oscillate if in addition it has $\text{Im}(\lambda_j) \neq 0$. Here, the explicit form of the nonlinear terms will determine whether this marginally stable steady state is stable or unstable.

For the case when several fixed points coexist, the basin of attraction of each attractor is separated from the others by curves of *neutral* points, known as *separatrices*.

Besides the cases we have just analyzed, for nonconservative nonlinear equations it is also possible to find another, very important, kind of steady solution, called *limit cycle*, corresponding to stable (and also unstable) *periodic* solutions. If such a periodic solution is stable, all the solutions in its neighborhood will decay to it for long times. We show a typical phase portrait in Fig. 2.

To exemplify this behaviour consider the system

$$\begin{aligned}\dot{x} &= y + x[1 - \rho]\rho^{-1/2} \\ \dot{y} &= -x + y[1 - \rho]\rho^{-1/2}\end{aligned}$$

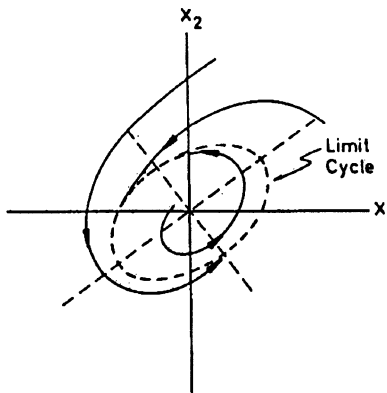


Fig. 2. The phase portrait for a limit cycle.

with $\rho = x^2 + y^2$. It is left to the reader to prove that this system has a limit attractor (hint: use polar coordinates).

2.2 Bifurcations

According to the above classification one might be tempted to conclude that a given system can only be described by a particular kind of fixed point or attractor. But this is not the case. The most interesting aspects of nonequilibrium phenomena arise from the fact that the same system can show a variety of behaviours, each one corresponding to a different attractor. The change from a given state to another is produced by the variation of some of the external constraints (or external parameters) acting on the system, so that the original (or *reference*) state becomes unstable, and subsequently a *bifurcation* to new branches of states occurs (Nicolis & Prigogine 1977, Haken 1978, Wio 1994, Nicolis 1995).

We will analyze two kinds of instabilities which may lead to a stable limit cycle from a fixed point. For our discussion we will refer to Fig. 3. In part (i) of the figure we depict the variation of the eigenvalue λ associated with the unstable original mode. This is usually called *the thermodynamic branch* as it is the direct extrapolation of the equilibrium states, sharing with them the property of asymptotic stability, since in this range the system is able to damp internal fluctuations or external disturbances, and we can still describe the behaviour of the system, essentially, within a thermodynamic approach. The horizontal axis indicates the real part of the eigenvalue and the vertical axis the imaginary part. The real part of λ crosses the imaginary axis, from

the negative to the positive values (left to right), as the control parameter ζ takes a critical value $\zeta = \zeta_c$. In part (ii) and (iii) of the figure, the horizontal axis represents the variation of the control parameter ζ , and the vertical axis schematically indicates a steady state solution of the NLDE describing the system and may represent several different physical or chemical properties (e.g. a concentration of some reactive for a chemical system, an amplitude of oscillation for a mode in a fluid, etc.).

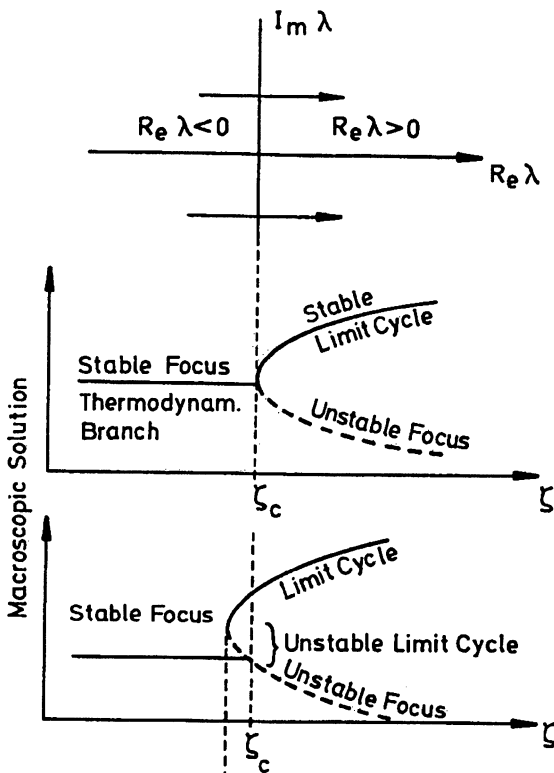


Fig. 3. Schematic picture of the bifurcation process.

As the parameter ζ is varied from left to right (in parts (ii) and (iii) of the figure), a pair of complex eigenvalues λ crosses the imaginary axis (part (i)). Consider the case where, before crossing, the steady state solution (x_1^0, x_2^0) is a *stable focus*. As soon as $R_e(\lambda)$ goes through zero and becomes positive for $\zeta = \zeta_c$, the solution may :

(a) Bifurcate into an *unstable focus* and a *stable limit cycle*. Beyond the bifurcation point ζ_c , the limit cycle is the only stable solution. This kind of

transition, where the limit cycle arises continuously for $\zeta > \zeta_c$, is called a *soft self-excitation*. A bifurcation to the right is called a *supercritical* one.

(b) The bifurcation to a limit cycle may also be subcritical, that is, it may occur to the left of $\zeta = \zeta_c$ as indicated in part (iii). The limit cycle towards which the system bifurcates at ζ_c is unstable, and a stable limit cycle may be reached for $\zeta_a < \zeta < \zeta_c$ but only in response to a finite perturbation that exceeds a certain threshold. For a smaller perturbation, the system will return to the stable steady state. But if the perturbation exceeds the threshold (as indicated in the figure) then it will continue to grow until the system reaches a stable limit cycle. Due to the existence of a threshold this is called a *hard self-excitation*. For small perturbations the system will remain in the stable steady state until $\zeta > \zeta_c$, where the steady state becomes unstable and the system jumps *abruptly* to the limit cycle, in contrast to the *continuous* transition of the previous case. Mathematically both types of instabilities are classified as *Hopf's bifurcations* (Nicolis & Prigogine 1977, Murray 1989, Nicolis 1995).

When discussing the kind of transitions associated with nonequilibrium instabilities, it is usual to adopt the language of equilibrium thermodynamic phase transitions and critical phenomena. For instance, the supercritical bifurcation is analogous to a second-order phase transition, while the subcritical resembles a first-order one.

2.3 Kinetic Potential, Symmetry Breaking

Now, and in order to introduce some notions related to the concept of *symmetry breaking* as well as with *global stability*, we will work out a useful mechanical analogy. Let us analyze the example of a *damped anharmonic oscillator* (Haken 1978, Prigogine 1980). The classical equation of motion of such a system is

$$m \frac{dv}{dt} = -\gamma v + F(x), \quad (10)$$

where x is the position and v is the velocity of a particle of mass m , γ is the friction coefficient and $F(x)$ an external force. Considering that $v = dx/dt$, (10) can be rewritten as

$$m\ddot{x} + \gamma\dot{x} = F(x). \quad (11)$$

We will concentrate on the particular case in which the particle is light (its mass m is very small) while the friction coefficient (γ) is very large. This corresponds to *overdamped motion*, in which the first term on the left hand side, when compared to the second, can be neglected (that is: we assume $\dot{x} \approx 0$), in what is a prototype of *adiabatic elimination procedures* (Haken 1978, van Kampen 1982, Gardiner 1985). Now we can make a change of time scale according to $t \rightarrow \gamma t$, and in this way eliminate the constant γ from the equation, which finally reads

$$\dot{x} = F(x). \quad (12)$$

It has the same form as the equation we have analyzed before (i.e. Eq.(1)). Now, for a one dimensional problem, we have that the force $F(x)$ can always be derived from a potential $V(x)$, according to

$$F(x) = - \frac{\partial}{\partial x} V(x) \quad (13)$$

For instance, in the harmonic case, $V(x) = \frac{1}{2} k_0 x^2$. However, we are interested in the general nonharmonic case. We assume a force that, besides a harmonic linear term has a cubic dependence on the coordinate:

$$F(x) = -k_0 x - k_1 x^3 \quad (14)$$

that derives from a quartic potential

$$V(x) = \frac{1}{2} k_0 x^2 + \frac{1}{4} k_1 x^4. \quad (15)$$

The form of the potential is depicted in Fig.4. In part (i) we show the case $k_0 > 0$, while the case $k_0 < 0$ is shown in part (ii). The equilibrium points will be determined from $F(x) = 0$. From the figure it is clear that in each of these two cases we have a completely different situation.

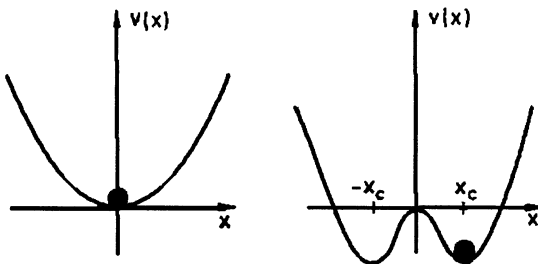


Fig. 4. Schematic quartic potential.

In the first case, for $k_0 > 0$ and $k_1 > 0$, the unique solution is $x = 0$, and is stable; whereas in the second, for $k_0 < 0$ and $k_1 > 0$, we have three solutions, namely, $x = 0$ which is unstable, and two stable symmetric solutions $x = \pm x_c$ (where $x_c = [|\kappa_0| / \kappa_1]^{1/2}$). Here we meet again the *bifurcation* phenomenon discussed above.

It is easy to prove, within linear stability analysis, that both solutions $x = \pm x_c$, are stable. Also, it is simply proven that (12) with $F(x)$ given by (14) is invariant under the transformation $x \rightarrow -x$, that is, (12) is symmetric with respect to this transformation. Also the potential in (15) remains invariant under such a transformation. Although the problem, as described by (12) and (14) is completely symmetric under inversion, the symmetry is now broken as the system will adopt one of the two possible solutions. We then have that, when we slowly change k_0 from positive to negative values, we reach $k_0 = 0$ where the stable equilibrium solution $x = 0$ becomes unstable. This phenomenon is usually described as a *symmetry breaking instability* (Nicolis & Prigogine 1977, Haken 1978, Prigogine 1980, Nicolis 1995).

2.4 Lyapunov Functional, Global Stability

We can extend the previous results to higher dimensional situations to conclude that, when there is a potential function $V(x_1, \dots, x_n)$ from which we can derive the forces

$$F_j(x_1, \dots, x_n) = -\frac{\partial}{\partial x_j} V(x_1, \dots, x_n), \quad (16)$$

we can discuss the stability of the steady state solutions just by looking at the form of the potential. In other words, we have a *global stability criterion*. However, there are a large majority of systems which do not have such a potential. There is a theorem due to *Lyapunov* stating that, if certain conditions are fulfilled, there exists a function which has the desirable properties making it possible to discuss global stability. Such function is not based on the requirement that the forces be derived from a potential, i.e. the system could be *non-variational* (that means: (16) is not fulfilled).

To fix ideas, in the two variable case indicated in (5), Lyapunov's theorem states that: if there exists a function $V(x_1, x_2)$ such that it has a minimum at the fixed point (\bar{x}_1, \bar{x}_2) , in the neighbourhood of this fixed point and both $V(x_1, x_2) > 0$ and $dV(x_1, x_2)/dt \leq 0$, then such a fixed point will be asymptotically stable (Reichl 1980, Kreuzer 1984, Nicolis 1995).

At this point, and with the idea of the Lyapunov function in mind, it is worth to make a brief classification of the different possibilities for the flow in the phase space (Hohenberg & Halperin 1977, Graham 1978, Graham 1987, Cross & Hohenberg 1993, Montagne *et al.* 1996).¹

(i) *Relaxational Gradient Flow*: If there is a potential function $V(x_1, \dots, x_n)$ such that $F_j(x_1, \dots, x_n)$ fulfills (16) (i.e., it is a variational system), implying

$$\dot{x}_j = -\frac{\partial}{\partial x_j} V(x_1, \dots, x_n), \quad (17)$$

¹ I am indebted to Raul Toral for this presentation of the classification of flows in phase space.

where the fixed points will correspond to the extrema of $V(x_1, \dots, x_n)$, the phase space flow will correspond to what is called a *relaxational gradient flow*, and the system will evolve towards the minimum of $V(x_1, \dots, x_n)$ following trajectories that correspond to the line of *steepest descent*. Clearly $V(x_1, \dots, x_n)$ is a Lyapunov functional as it also fulfills

$$\frac{dV}{dt} = \sum \frac{\partial V}{\partial x_j} \frac{dx_j}{dt} = - \sum \left(\frac{\partial V}{\partial x_j} \right)^2 \leq 0. \quad (18)$$

This behaviour is depicted in part (a) of Fig.5.

(ii) *Relaxational non-Gradient Flow*: Consider a system governed by the equation

$$\dot{x}_j = - \sum (\mathbb{T})_{jl} \frac{\partial V}{\partial x_l}, \quad (19)$$

where \mathbb{T} is a real, symmetric, positive definite matrix. The fixed points of the system will still correspond to the extrema of V . However, the trajectories in phase space that will evolve towards the minima of V , will not follow the steepest descent lines. This means that the transient dynamics will not be governed just by V . A, by now, classical example of this situation is the Cahn-Hilliard equation for spinodal decomposition (Langer 1987, Hohenberg & Halperin 1977, Gunton & Droz 1983, San Miguel 1985, Kirkadhy 1992, Cross & Hohenberg 1993), where $(\mathbb{T})_{jl} = -\nabla^2$.

It is clear that V is still a Lyapunov functional as

$$\frac{dV}{dt} = \sum (\mathbb{T})_{jl} \frac{\partial V}{\partial x_j} \frac{\partial V}{\partial x_l} \leq 0. \quad (20)$$

This behaviour is depicted in part (b) of Fig.5.

(iii) *Non-Relaxational Potential Flow*: Here we can consider two situations:

(a) In the first case we assume

$$\dot{x}_j = - \sum (\mathbb{IK})_{jl} \frac{\partial V}{\partial x_l}, \quad (21)$$

Where \mathbb{IK} is an arbitrary, positive definite matrix. We can separate it into a symmetric (\mathbb{S}) and an antisymmetric (\mathbb{F}) part

$$\begin{aligned} \mathbb{IK} &= \mathbb{S} + \mathbb{F} \\ \mathbb{S} &= \frac{1}{2}(\mathbb{IK} + \mathbb{IK}^T) \quad \mathbb{S} = \mathbb{S}^T \\ \mathbb{F} &= \frac{1}{2}(\mathbb{IK} - \mathbb{IK}^T) \quad \mathbb{F} = -\mathbb{F}^T. \end{aligned} \quad (22)$$

The fixed points are again given by the extrema of V . On the other hand we have that V also fulfills

$$\frac{dV}{dt} = \sum (\mathbb{S})_{jl} \frac{\partial V}{\partial x_j} \frac{\partial V}{\partial x_l} - \sum (\mathbb{F})_{jl} \frac{\partial V}{\partial x_j} \frac{\partial V}{\partial x_l} \leq 0, \quad (23)$$

as, clearly, the first term on the rhs is ≤ 0 , while the second one is = 0. Hence V is again a Lyapunov function. The later result implies that the antisymmetric part of \mathbf{IK} induces a flow in the system that keeps the Lyapunov functional constant (that is *without cost*). A typical situation is depicted in part (c) of Fig.5.

(b) In the second case we consider

$$\dot{x}_j = f_j = - \sum_l (\mathbf{T})_{jl} \frac{\partial V}{\partial x_l} + w_j, \quad (24)$$

with $(\mathbf{T})_{jl}$ as in (ii) and w_j an arbitrary function. In the present case, $V(x_1, x_2, \dots)$ will be a Lyapunov functional if the second term on the rhs of

$$\frac{dV}{dt} = - \sum_l (\mathbf{T})_{jl} \frac{\partial V}{\partial x_j} \frac{\partial V}{\partial x_l} + \sum w_j \frac{\partial V}{\partial x_j} \quad (25)$$

is zero. For this to be true, the following orthogonality condition must be fulfilled

$$\sum_l \left(f_l + \sum_j (\mathbf{T})_{jl} \frac{\partial V}{\partial x_j} \right) \frac{\partial V}{\partial x_l} = 0, \quad (26)$$

or

$$(\mathbf{F} + \mathbf{T} \nabla V) \cdot \nabla V = 0, \quad (27)$$

that is analogous to a Hamilton-Jacobi equation. In such a case we have that $\frac{dV}{dt} \leq 0$, and V is a Lyapunov functional.

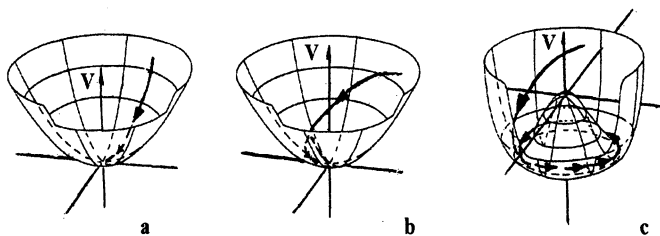


Fig. 5. (a) Case i); (b) case ii) and (c) case iii).

A more general discussion on such a classification of dynamical flows for complex fields can be found in Montagne *et al.* (1996).

At this point it is worth asking about the effect of noise or fluctuations on the dynamical equation (12) as well as on the stability of the fixed points. Before analyzing this problem, we will proceed to make a brief review on some aspects of stochastic processes.

3 Stochastic Processes: A Brief Overview

We start this section by rewriting equation (1) for the one dimensional case:

$$\frac{dx}{dt} = F(x, \zeta) \quad (28)$$

where x corresponds to the state variable while ζ is a control parameter. For instance, such a parameter could be the temperature, an external field, a reactant's controlled flux, etc, indicating the form in which the system is coupled to its surroundings. Experience tells us that it is usually impossible to keep fixed the value of such parameters, and consequently that its fluctuations become relevant. Hence, the original *deterministic* equation will acquire a random or *stochastic* character.

Among the many reasons to justify the increasing interest in the study of fluctuations we can quote that they present a serious impediment to accurate measurements in very sensitive experiments, demanding some very specific techniques in order to reduce their effects. Besides, the fluctuations might be used as an additional source of information about the system. But the most important aspect is that fluctuations can produce macroscopic effects contributing to the appearance of *spatio-temporal patterns* or *dissipative structures* (Horsthemke & Lefever 1984, Nicolis 1986, Nicolis 1989, Doering 1991, Wio 1994).

The general character of equations (1) makes it clear why stochastic methods have become so important in different branches of physics, chemistry, biology, technology, population dynamics, economy, and sociology. In spite of the large number of different problems that arise in all these fields, there are some common principles and methods that are included in a common framework: the theory of stochastic processes. Here we will only briefly review the few aspects relevant for our present needs. For deeper study we refer to van Kampen (1982), Risken (1983), Gardiner (1985), Horsthemke & Lefever (1984), Doering (1991) and Wio (1994).

In order to introduce the presence of fluctuations into our description, we write $\zeta = \zeta_0 + \xi(t)$, where ζ_0 is a constant value and $\xi(t)$ is the random or fluctuating contribution to the parameter ζ . The simplest (or lowest order) form that equation (28) can adopt is

$$\frac{dx}{dt} = \dot{x} = F(x, \zeta_0) + g(x, \zeta_0)\xi(t), \quad (29)$$

The original deterministic differential equation has been transformed into a *stochastic differential equation* (SDE), where $\xi(t)$ is called a *noise term* or stochastic process.

Any stochastic process $x(t)$ is completely specified if we have the information of the complete hierarchy of probability densities. We write

$$P_n(x_1, t_1; x_2, t_2; \dots; x_n, t_n) dx_1 dx_2 \dots dx_n, \quad (30)$$

for the probability that $x(t_1)$ is within the interval $(x_1, x_1 + dx_1)$, $x(t_2)$ in $(x_2, x_2 + dx_2)$, and so on. These P_n may be defined for $n = 1, 2, \dots$, and only for different times. This hierarchy fulfills some properties

- i) $P_n \geq 0$
- ii) P_n is invariant under permutations of pairs (x_i, t_i) and (x_j, t_j)
- iii) $\int P_n dx_n = P_{n-1}$, and, $\int P_1 dx_1 = 1$.

Another important quantity is the *conditional probability density* $P_{n/m}$ that corresponds to the probability of having the value x_1 at time t_1, x_2 at t_2, \dots, x_n at t_n ; given that we have $x(t_{n+1}) = x_{n+1}, x(t_{n+2}) = x_{n+2}, x(t_{n+3}) = x_{n+3}, \dots, x(t_{n+m}) = x_{n+m}$. Its definition is

$$\begin{aligned} P_{n/m}(x_1, t_1; \dots; x_n, t_n | x_{n+1}, t_{n+1}; \dots; x_{n+m}, t_{n+m}) &= \\ &= P_{n+m}(x_1, t_1; \dots; x_n, t_n; x_{n+1}, t_{n+1}; \dots; x_{n+m}, t_{n+m}) \\ &\quad (P_m(x_{n+1}, t_{n+1}; \dots; x_{n+m}, t_{n+m}))^{-1} \end{aligned} \quad (31)$$

Among the many possible classes of stochastic processes, there is one that plays a central role: *Markovian processes* (van Kampen 1982, Risken 1983, Gardiner 1985, Horsthemke & Lefever 1984, Doering 1991, Wio 1994). For a stochastic process $x(t)$, $P(x_2, t_2 | x_1, t_1)$ is the *conditional* or *transition* probability that $x(t_2)$ takes the value x_2 , knowing that $x(t_1)$ has taken the value x_1 . From this definition and (31) results the following identity for the *joint probability* $P_2(x_1, t_1; x_2, t_2)$ (Bayes' rule) :

$$P_2(x_1, t_1; x_2, t_2) = P(x_2, t_2 | x_1, t_1) P_1(x_1, t_1). \quad (32)$$

A process $x(t)$ is called *Markovian* if for every set of successive times $t_1 < t_2 < \dots < t_n$, the following condition holds

$$\begin{aligned} P_n(x_1, t_1, \dots, x_n, t_n) &= P_1(x_1, t_1) P_{n-1}(x_2, t_2, \dots, x_n, t_n | x_1, t_1) \\ &= P_1(x_1, t_1) P(x_n, t_n | x_{n-1}, t_{n-1}) \dots P(x_2, t_2 | x_1, t_1), \end{aligned} \quad (33)$$

From this definition, it results that a Markovian process is completely determined if we know $P_1(x_1, t_1)$ and $P(x_2, t_2 | x_1, t_1)$. It is easy to find a relevant condition to be fulfilled for Markovian processes: specifying the previous equation for the case $n = 3$ and integrating over x_2 , we obtain

$$\int dx_2 P_3(x_1, t_1, x_2, t_2, x_3, t_3) = P_2(x_1, t_1, x_3, t_3)$$

$$\begin{aligned}
&= P_1(x_1, t_1) P(x_3, t_3 | x_1, t_1) \\
&= \int dx_2 P_1(x_1, t_1) P(x_3, t_3 | x_2, t_2) P(x_2, t_2 | x_1, t_1). \quad (34)
\end{aligned}$$

For $t_1 < t_2 < t_3$ we find the identity

$$P(x_3, t_3 | x_1, t_1) = \int dx_2 P(x_3, t_3 | x_2, t_2) P(x_2, t_2 | x_1, t_1), \quad (35)$$

which is the *Chapman-Kolmogorov equation* for Markovian processes. Every pair of non-negative functions $P_1(x_1, t_1)$ and $P(x_2, t_2 | x_1, t_1)$, adequately normalized and satisfying not only (35) but also

$$P_1(x_2, t_2) = \int dx_1 P_1(x_1, t_1) P(x_2, t_2 | x_1, t_1), \quad (36)$$

defines a Markovian process. Some typical (useful) examples of Markov processes are: the *Wiener-Levy*, the *Ornstein-Uhlenbeck* and the *Poisson* processes (van Kampen 1982, Risken 1983, Gardiner 1985, Horsthemke & Lefever 1984, Doering 1991, Wio 1994).

The Chapman-Kolmogorov equation (that is only a property of the solution for Markovian processes) can be recast into a useful form. Returning to (35), we take $t_3 = t_2 + \delta t$ and consider the limit $\delta t \rightarrow 0$. It is clear that we have $P(x_3, t_3 | x_2, t_2) = \delta(x_3 - x_2)$, and it is intuitive to assume that, if $t_3 - t_2 \simeq \delta t$ (very small), the probability that a transition happens must be proportional to δt . According to this we adopt

$$\begin{aligned}
P(x_3, t_2 + \delta t | x_2, t_2) &= \delta(x_3 - x_2) [1 - A(x_2) \delta t] \\
&\quad + \delta t W(x_3 | x_2) + O(\delta t^2), \quad (37)
\end{aligned}$$

where $W(x_3 | x_2)$ is the *transition probability per unit time* from x_2 to x_3 (which in general could also be a function of t_2). The probability normalization tells us that

$$A(x_2) = \int W(x_3 | x_2) dx_3$$

Substitution of the form for $P(x_3, t_2 + \delta t | x_2, t_2)$ into (35) gives

$$\begin{aligned}
P(x_3, t_2 + \delta t | x_1, t_1) &= \int P(x_3, t_2 + \delta t | x_2, t_2) P(x_2, t_2 | x_1, t_1) dx_2 \\
&= [1 - A(x_3) \delta t] P(x_3, t_2 | x_1, t_1) + \delta t \int W(x_3 | x_2) P(x_2, t_2 | x_1, t_1) dx_2 \\
&= P(x_3, t_2 | x_1, t_1) - \delta t \int W(x_2 | x_3) P(x_3, t_2 | x_1, t_1) dx_2 \\
&\quad + \delta t \int W(x_3 | x_2) P(x_2, t_2 | x_1, t_1) dx_2. \quad (38)
\end{aligned}$$

This can be rearranged as

$$\begin{aligned} & [P(x_3, t_2 + \delta t | x_1, t_1) - P(x_3, t_2 | x_1, t_1)]/\delta t = \\ & \int [W(x_3 | x_2)P(x_2, t_2 | x_1, t_1) - W(x_2 | x_3)P(x_3, t_2 | x_1, t_1)] dx_2, \quad (39) \end{aligned}$$

and in the limit $\delta t \rightarrow 0$, we find

$$\begin{aligned} \frac{\partial}{\partial t} P(x, t | x_0, t_0) &= \int [W(x | x') P(x', t' | x_0, t_0) \\ &\quad - W(x' | x) P(x, t | x_0, t_0)] dx', \quad (40) \end{aligned}$$

which corresponds to the *master equation* (van Kampen 1982, Risken 1983, Gardiner 1985, Horsthemke & Lefever 1984, Doering 1991, Wio 1994).

The master equation is a differential form of the Chapman-Kolmogorov equation. It is an equation for the transition probability $P(x, t | x_0, t_0)$, and is more adequate for mathematical manipulations than the Chapman-Kolmogorov equation, and has a direct physical interpretation as a balance equation. At the same time, $W(x | x')\delta t$ is the transition probability during a very short time (δt). It could be evaluated by approximate methods, for instance by time dependent perturbation theory (i.e. : the *Fermi golden rule*) (van Kampen 1982, Gardiner 1985, Wio 1994).

3.1 Langevin Equations

Brownian motion is the oldest and best known physical example of a Markov process. This phenomenon corresponds to the motion of a heavy test particle, immersed in a fluid composed of light particles in random motion. Due to the (random) collisions of the light particles against the test particle, the velocity of the latter varies in a (large) sequence of small, uncorrelated jumps. However, similar ideas can (and have) been applied to a large variety of systems (Weidenmüller 1980, Brink 1980, van Kampen 1982, Kreuzer 1984, Gardiner 1985, Wio 1994). To simplify the presentation we restrict the description to a one dimensional system.

We will give a simple quantitative picture of Brownian motion. We start by writing the Newton equation as :

$$m \dot{v} = F(t) + f(t), \quad (41)$$

where m is the mass of the Brownian particle, v its velocity, $F(t)$ the force due to some external field (i.e. gravitational, electrical for charged particles, etc), and $f(t)$ is the force produced by the collisions of fluid particles against the test particle. Due to the above indicated rapid fluctuations in v , we have two effects. On one hand a *systematic* one, i.e., a kind of *friction* that tends to slow down the particle, and on the other hand, a *random* contribution originated in the random hits of the fluid particle. If the mass of the test particle is much larger than the mass of the fluid particles (implying that the

fluid *relaxes* faster than the test particle, allowing us to assume that it is in equilibrium), we can write

$$\frac{1}{m} f(t) = -\gamma v + \xi(t). \quad (42)$$

In the r.h.s., γ is the friction coefficient, and the minus sign in the first term indicates that this contribution (as a good friction term) opposes the motion. The second term corresponds to the stochastic or random contribution, since we have separated the systematic contribution in the first term, and this random contribution averages to zero : $\langle \xi(t) \rangle = 0$ (where the average is over an *ensemble* of noninteracting Brownian particles). In order to define the so called *Langevin force* (or *white noise*) it is required that

$$\langle \xi(t) \xi(t') \rangle = D \delta(t - t'). \quad (43)$$

We will not consider higher order moments, but it is clear that to fully characterize the fluctuating force, we need the whole hierarchy of moments (van Kampen 1982, Gardiner 1985, Wio 1994).

With the above indicated arguments, and without an external field, (41) adopts the form

$$\dot{v} = -\gamma v + \xi(t), \quad (44)$$

which is known as the *Langevin equation* (van Kampen 1982, Risken 1983, Gardiner 1985, Horsthemke & Lefever 1984, Doering 1991, Wio 1994). This is the simplest example of a SDE (that is, a differential equation whose coefficients are random functions with known stochastic properties). Hence $v(t)$ is a stochastic process, with a given initial condition. For details we refer the reader to van Kampen (1982), Risken (1983), Gardiner (1985), Horsthemke & Lefever (1984), Doering (1991) and Wio (1994).

When an external field is present, we have the pair of equations

$$\begin{aligned} \dot{x} &= v \\ \dot{v} &= \frac{1}{m} F(x) - \gamma v + \xi(t). \end{aligned} \quad (45)$$

After differentiating the first one and replacing the second, it adopts the form

$$\ddot{x} = \frac{1}{m} F(x) - \gamma \dot{x} + \xi(t). \quad (46)$$

In the case of large friction (γ very large), through an *adiabatic elimination* ($\ddot{x} \approx 0$, as in Sect.2.3) (Haken 1978, van Kampen 1982, Gardiner 1985, Doering 1991, Wio 1994), we can rewrite the last equation as

$$\dot{x} = -\frac{\partial}{\partial x} V(x) + \xi(t), \quad (47)$$

where $\frac{\partial}{\partial x} V(x) = -F(x)$, and m and γ have been absorbed into the different terms. The last result corresponds to the problem of *diffusion in a*

field (van Kampen 1982, Risken 1983, Gardiner 1985, Horsthemke & Lefever 1984, Doering 1991, Wio 1994).

The most general form of the SDE that we will consider here is the one indicated by equation (29).

3.2 Fokker–Planck Equations

Let us return to the master equation (40). We assume that x is a continuous variable, and that its changes correspond to *small jumps* (or variations). In this case it is possible to derive, starting from the master equation, a differential equation. The transition probability $W(x | x')$ will decay very fast as a function of $|x - x'|$. We could then write $W(x | x') = W(x', \xi)$, where $\xi = x - x'$ corresponds to the size of the jump. The master equation will take the form

$$\begin{aligned} \frac{\partial}{\partial t} P(x, t | x_0, t_0) = & \int W(x - \xi, \xi) P(x - \xi, t | x_0, t_0) d\xi \\ & - P(x, t | x_0, t_0) \int W(x, -\xi) d\xi. \end{aligned} \quad (48)$$

Following our the assumption of small jumps, and the additional argument that P varies slowly with x , we make a Taylor expansion in ξ that gives

$$\begin{aligned} \frac{\partial}{\partial t} P(x, t | x_0, t_0) = & \int \left[W(x, \xi) P(x, t | x_0, t_0) - \xi \frac{\partial}{\partial x} W(x, \xi) P(x, t | x_0, t_0) \right. \\ & \left. + \xi^2 \frac{\partial^2}{\partial x^2} W(x, \xi) P(x, t | x_0, t_0) - \dots \right] d\xi \\ & - P(x, t | x_0, t_0) \int W(x, -\xi) d\xi. \end{aligned} \quad (49)$$

As the first and the last terms are equal (in the latter changing $-\xi$ by ξ , as well as the integration limits), we get

$$\frac{\partial}{\partial t} P(x, t | x_0, t_0) = \sum_{\nu=1}^{\infty} \frac{(-1)^{\nu}}{\nu!} \frac{\partial^{\nu}}{\partial x^{\nu}} \alpha_{\nu}(x) P(x, t | x_0, t_0), \quad (50)$$

with $\alpha_{\nu}(x) = \int \xi^{\nu} W(x, \xi) d\xi$. This result corresponds to the *Kramers-Moyal expansion* of the master equation (van Kampen 1982, Risken 1983, Gardiner 1985, Horsthemke & Lefever 1984, Doering 1991, Wio 1994). Up to this point we have gained nothing. However, there could be situations where, for $\nu > 2$, the α_{ν} are either zero or very small (even though there are no *a priori* criteria about the relative size of the terms). If this is the case, we have

$$\begin{aligned} \frac{\partial}{\partial t} P(x, t | x_0, t_0) = & - \frac{\partial}{\partial x} \alpha_1(x) P(x, t | x_0, t_0) \\ & + \frac{1}{2} \frac{\partial^2}{\partial x^2} \alpha_2(x) P(x, t | x_0, t_0), \end{aligned} \quad (51)$$

which corresponds to the *Fokker-Planck equation* (van Kampen 1982, Risken 1983, Gardiner 1985, Horsthemke & Lefever 1984, Doering 1991, Wio 1994).

Let us see a couple of examples. For the Wiener-Levy process we find that $\alpha_\nu = 0$ ($\nu > 2$), and then

$$\frac{\partial}{\partial t} P(x, t | x_0, t_0) = \frac{\partial^2}{\partial x^2} P(x, t | x_0, t_0),$$

while for the case of the Ornstein-Uhlenbeck process we get

$$\frac{\partial}{\partial t} P(x, t | x_0, t_0) = - \frac{\partial}{\partial x} x P(x, t | x_0, t_0) + \frac{\partial^2}{\partial x^2} P(x, t | x_0, t_0).$$

Equation (51) corresponds to a *nonlinear Fokker-Planck equation* (due to the dependence of $\alpha_1(x)$ and $\alpha_2(x)$ on x), which is the result of poorly grounded assumptions (i.e., the criteria to decide where to cut the expansion, etc). Even worse, it is **not a systematic** approximation to the master equation. However, there is a procedure due to van Kampen that does make it possible to build up such a systematic procedure, but we will not discuss it here and instead refer the reader to van Kampen (1982), Gardiner (1985) and Wio (1994).

Consider the long time limit, where we expect that the system will reach a stationary behaviour (that is: $\frac{\partial}{\partial t} P(x, t | x_0, t_0) = 0$). In such a case we will have that

$$0 = - \frac{d}{dx} \alpha_1(x) P_{st}(x) + \frac{D}{2} \frac{d^2}{dx^2} P_{st}(x), \quad (52)$$

where in order to simplify we have taken $\alpha_2(x) = \text{ct.} = D$. The stationary distribution turns out to be

$$P_{st}(x) \simeq N e^{- \int dx' \alpha_1(x') / D}. \quad (53)$$

The exponent in the last equation allows us to define the (*nonequilibrium*) potential $U(x)$ through

$$U(x) = - \int dx' \alpha_1(x'). \quad (54)$$

3.3 Connection Between LE and FPE

Here we give a brief and more or less formal (but not completely rigorous from a mathematical point of view) presentation of the relation between *stochastic differential equations* (SDE) of the *Langevin type* (LE), and *Fokker-Planck equations* (FPE). We start considering a general form for the one-dimensional SDE as indicated in (29):

$$\dot{x}(t) = \frac{dx(t)}{dt} = f[x(t), t] + g[x(t), t] \xi(t) \quad (55)$$

where $\xi(t)$ is a *white noise* with

$$\langle \xi(t) \rangle = 0 \quad \text{and} \quad \langle \xi(t) \xi(t') \rangle = \delta(t - t')$$

as in (42) and (43), with $D = 1$. We made the usual assumption that the process is Gaussian. However, $\xi(t)$ is not a well defined stochastic process. In a loose way, it could be considered as the derivative of the well defined *Wiener process*, but such a derivative does not exist at all (van Kampen 1982, Gardiner 1985, Doering 1991, Wio 1994). We now integrate (55) over a short time interval δt

$$x(t + \delta t) - x(t) = f[x(t), t] \delta t + g[x(t), t] \xi(t) \delta t \quad (56)$$

As $x(t)$ is a Markov process, it is well defined if we are able to determine its probability distribution $P_1(x, t)$ as well as its conditional probability distribution $P(x, t | x', t')(t > t')$. In order to obtain an equation for the latter quantity, we define now a *conditional average*, corresponding to the average of a function of the stochastic variable x (say $F(x)$), given that x has the value y at $t' < t$:

$$\langle F(x(t)) | x(t') = y \rangle = \ll F(x(t)) \gg = \int dx' F(x') P(x', t | y, t'). \quad (57)$$

Due to the property $P(x, t | x', t) = \delta(x - x')$, we have

$$\langle F(x(t)) | x(t) = y \rangle = F(y). \quad (58)$$

We use now this definition in order to obtain the first few *conditional moments* of $x(t)$.

$$\begin{aligned} \ll \Delta x(t) \gg &= \langle x(t + \delta t) | x(t) = y \rangle = \\ &= \ll f[x(t), t] \delta t \gg + \ll g[x(t), t] \xi(t) \delta t \gg. \end{aligned} \quad (59)$$

The result shown in (58) indicates that $\ll f[x(t), t] \delta t \gg = f[x(t), t] \delta t$, and also that $\ll g[x(t), t] \xi(t) \delta t \gg = g[x(t), t] \ll \xi(t) \gg \delta t = 0$, resulting in

$$\ll \Delta x(t) \gg = f[x(t), t] \delta t. \quad (60)$$

For the second moment we need to resort to properties of the Wiener process; i.e. using that $\xi(t) \delta t = \int_t^{t+\delta t} dt \xi(t') = \Delta W(t)$, where $W(t)$ is the Wiener process, and $\langle [\xi(t) \delta t]^2 \rangle \simeq \langle (\Delta W(t))^2 \rangle = \Delta t$; to obtain

$$\ll \Delta x(t)^2 \gg = g[x(t), t]^2 \delta t + O(\delta t^2). \quad (61)$$

Let us now consider an arbitrary function $R(x)$, and evaluate its conditional average. Using the Chapman-Kolmogorov equation

$$\begin{aligned} \int dx R(x) P(x, t + \delta t | y, s) &= \int dz P(z, t | y, s) \\ &\quad \int dx R(x) P(x, t + \delta t | z, t), \end{aligned} \quad (62)$$

We can expand $R(x)$ in a Taylor series around z , as for $\delta t \simeq 0$ we know that $P(x, t + \delta t \mid z, t) \simeq \delta(x - z)$, and that only a neighbourhood of z will be relevant. If we also remember the normalization condition for $P(z, t \mid y, s)$, integrate by parts and use (60) and (61) we obtain an equation that, after arranging terms and taking the limit $\delta t \rightarrow 0$, gives

$$\int dx R(x) \left(\frac{\partial}{\partial t} P(x, t \mid y, s) - \left(-\frac{\partial}{\partial x} [f[x, t] P(x, t \mid y, s)] + \frac{1}{2} \frac{\partial^2}{\partial x^2} [g(x, t)^2 P(x, t \mid y, s)] \right) \right) = 0 \quad (63)$$

Due to the arbitrariness of the function $R(x)$, we arrive at the condition

$$\begin{aligned} \frac{\partial}{\partial t} P(x, t \mid y, s) &= - \frac{\partial}{\partial x} \{f[x, t] P(x, t \mid y, s)\} \\ &\quad + \frac{1}{2} \frac{\partial^2}{\partial x^2} \{g(x, t)^2 P(x, t \mid y, s)\} \end{aligned} \quad (64)$$

which is the desired Fokker-Planck equation for the transition probability $P(x, t \mid y, s)$ associated with the stochastic process driven by the SDE (55).

3.4 Decay Times: Kramers Result

Here we want to discuss how, due to the influence of fluctuations, it is possible that transitions from metastable states into more stable states can occur and how to describe this process.

Let us start considering the problem described by the LE (55) or the FPE (64), but assuming the simple case where $g(x, t)^2 = D$ and $f(x, t) = f(x) = -\frac{\partial}{\partial x} U(x)$, with $U(x) = \frac{k}{2}x^2$. The FPE adopts the form

$$\begin{aligned} \frac{\partial}{\partial t} P(x, t \mid y, 0) &= \frac{\partial}{\partial x} \left(\left[\frac{\partial}{\partial x} U(x) \right] P(x, t \mid y, 0) \right) \\ &\quad + \frac{D}{2} \frac{\partial^2}{\partial x^2} P(x, t \mid y, 0). \end{aligned} \quad (65)$$

For $t \rightarrow 0$, we have that $\lim P(x, t \mid y, 0) \rightarrow \delta(x - y)$, and for very long times ($t \rightarrow \infty$) we find the stationary distribution

$$P_{st}(x) = C e^{-U(x)/D} ; \quad C^{-1} = \int dx' e^{-U(x')/D}. \quad (66)$$

When $U(x)$ is not the quadratic potential indicated above but is still monostable (with the minimum in $x = a$) we can approximately write it as in (66)

$$P_{st}(x) \simeq \left(\frac{U''(a)}{2\pi D} \right)^{1/2} e^{-\frac{U''(a)}{2D}(x-a)^2}, \quad (67)$$

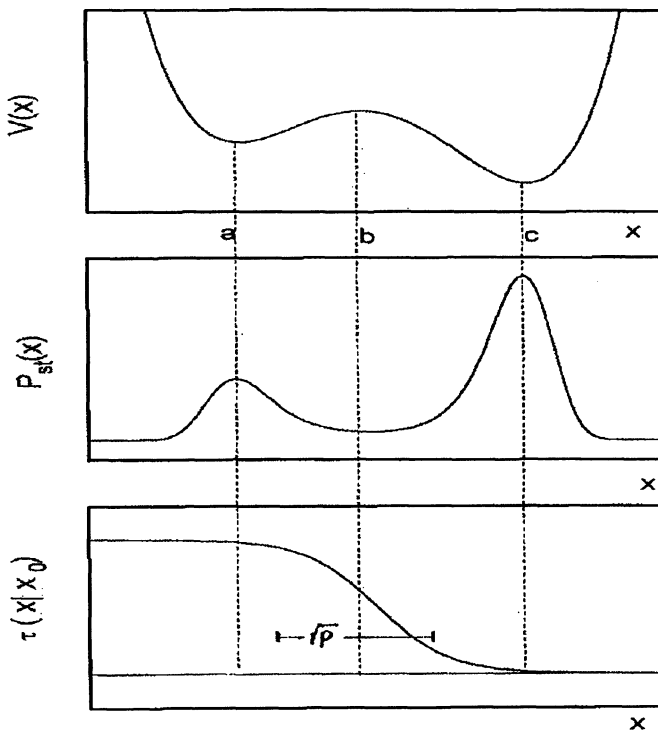


Fig. 6. (i) Bistable potential, (ii) stationary distribution, (iii) decay time.

with $U''(a) = \frac{\partial^2}{\partial x^2} U(x)|_{x=a}$. Clearly, it is also an approximation to the form of $P_{st}(x)$ for a *bistable* potential, near one of the minima. See, as an example, the sketch in Fig.(6)

We can describe the probability of being in the left or in the right well as:

$$\Xi_a(t) = \int_{\Omega(a)} P(x,t) dx \quad (68)$$

$$\Xi_c(t) = \int_{\Omega(c)} P(x,t) dx, \quad (69)$$

where $\Omega(a)$ and $\Omega(c)$ indicates the set of points in the attraction basin of the minimum at $x = a$ and c respectively. Clearly, the probabilities $\Xi_i(t)$ fulfill the normalization condition $\Xi_a(t) + \Xi_c(t) = 1$. Hence, calling τ_{ij} the inverse of the transition probability per unit time from j to i , we can write

the kinetic equations

$$\frac{d}{dt}\Xi_a(t) = -\frac{\Xi_a}{\tau_{ca}} + \frac{\Xi_c}{\tau_{ac}} = -\frac{d}{dt}\Xi_b(t), \quad (70)$$

that have the stationary solutions

$$\begin{aligned} \Xi_a^{st} &= \frac{\tau_{ac}}{\tau_{ac} + \tau_{ca}} \\ \Xi_c^{st} &= \frac{\tau_{ca}}{\tau_{ac} + \tau_{ca}}. \end{aligned} \quad (71)$$

Exploiting the Gaussian approximation (67) we also have

$$\begin{aligned} P_{st}(x) &= \Xi_a^{st} \left(\frac{U''(a)}{2\pi D} \right)^{1/2} e^{-\frac{U''(a)}{2D}(x-a)^2} \\ &\quad + \Xi_c^{st} \left(\frac{U''(c)}{2\pi D} \right)^{1/2} e^{-\frac{U''(c)}{2D}(x-c)^2}, \end{aligned} \quad (72)$$

from which we can obtain the ratio

$$\frac{\Xi_a^{st}}{\Xi_c^{st}} = \frac{\tau_{ac}}{\tau_{ca}} = \left(\frac{U''(c)}{U''(a)} \right)^{1/2} e^{-[U(a)-U(c)]/D}. \quad (73)$$

The exponential factor has the form of an *Arrhenius* factor that arises in the evaluation of reaction probabilities or its inverse, the characteristic decay time, for activation processes (Reichl 1980, van Kampen 1982, Kreuzer 1984, San Miguel 1985, Keizer 1987, Hänggi *et al.* 1990). However, through this procedure we can only obtain the indicated ratio. More elaborate calculations based on Kramers-like approaches (van Kampen 1982, Gardiner 1985, Hänggi *et al.* 1990) yields for the average decay or transition time from the state *a* to the state *c*

$$\tau_{ca} = \left(\frac{2\pi}{U''(a)|U''(b)|} \right)^{1/2} e^{\frac{|U(b)-U(a)|}{D}}, \quad (74)$$

that is known as *Kramers' formula* (or also *Arrhenius law*). However this expression has some constraints that we can summarize in the following points: the large damped limit was used, and the barrier height must be larger than the fluctuations ($U(b) - U(a) \gg D$). A typical behaviour of $\tau(x|x_0)$, that is the escape or decay time from x_0 to x , is depicted in part (iii) of Fig.(6).

For details of the calculation of decay (or *first passage times*) we refer the reader to van Kampen (1982), Risken (1983), Gardiner (1985), Horsthemke & Lefever (1984), Doering (1991) and Hanggi *et al.* (1990).

3.5 Notions of Stochastic Resonance

One of the most fascinating cooperative effects arising out of the interplay between deterministic and random dynamics in a nonlinear system is the phenomenon of *stochastic resonance* (SR). This phenomenon is characterized by the enhancement of the signal-to-noise ratio (SNR) caused by injection of noise into a periodically modulated nonlinear system. The increase in the noise intensity from small initial values induces an increase in the SNR ratio until it reaches a maximum, beyond which there is a decay of SNR for large noise values. Some recent reviews and conference proceedings clearly show the wide interest of this phenomenon and the state of the art (Moss 1992, Moss *et al.* 1993, Wiesenfeld & Moss 1995, Balsara *et al.* 1995, Balsara & Gammaitoni 1996).

The basic picture of SR has been illustrated by means of a mechanical analogy. Consider a particle moving in a double well potential like the one in Fig.6 and subject to friction. Consider a weak signal that periodically modulates the potential alternatively raising and lowering the wells relative to the barrier. Here weak implies that the modulation is too small to deterministically excite the particle over the barrier. Besides modulation, we also consider the effect of noise, that alone is enough to induce irregular switchings between the wells. In the high friction limit the dynamics can be modelled by

$$\dot{x}(t) = -\frac{dU_0(x)}{dx} + \xi(t) + A \cos \Omega_0 t, \quad (75)$$

where $U_0(x)$ is the bare potential, $A \cos \Omega_0 t$ is the *signal* or modulation and $\xi(t)$ is the random contribution. The phenomenon of SR is the nonlinear cooperative effect whereby the small signal entrains the noise inducing hopping in such a way that the transitions becomes surprisingly regular. Even more, the regularity can improve with the addition of more noise, at least up to a point: it is optimally sensitive at some non-zero level of input noise.

The two essential features of SR in the bistable potential are: that it is a threshold phenomenon, and that its statistical properties are nonstationary. Consider the quartic potential

$$U(x) = U_0(x) + cx = -\frac{a}{2}x^2 + \frac{b}{4}x^4 + cx, \quad (76)$$

with $a, b > 0$ and $c = A \cos \Omega_0 t$. Regarding the threshold feature, the threshold c_{th} is the value of c for which the deterministic switching becomes possible, i.e.: the value of c at which the bistability is destroyed ($c_{th} = \pm[4a^3/27b]^{1/2}$). Hence, weak modulation requires $A < c_{th}$ implying that no deterministic switching can occur with the signal alone. The nonstationarity becomes evident when noise is added, and the potential becomes

$$U(x) = -\frac{a}{2}x^2 + \frac{b}{4}x^4 + x[A \cos \Omega_0 t + \xi(t)].$$

The LE that drives the motion of the particle is

$$\dot{x}(t) = ax - bx^3 + [A \cos \Omega_0 t + \xi(t)], \quad (77)$$

and non-stationarity means that the probability density is a (periodic) function of time (Jüng 1993).

Within the indicated picture, the only important dynamical events are the well-to-well switching transitions that can occur whenever

$$|A \cos \Omega_0 t + \xi(t)| \geq c_{th}, \quad (78)$$

indicating that SR is, fundamentally a threshold phenomenon.

To further clarify the mechanism, let us simplify the picture even more and assume that the modulation is such that during the first half period the left well is kept fixed below the right one, while the situation is reversed during the second half period. Hence, considering the Kramers formula (74), it is clear that, during the first half period, the average decay time for jumping from the right well to the left one will be shorter than the reverse transition. The situation is reversed during the second half period. If the noise intensity is such that this decay time is of the order of half the period (while for the reverse less probable transition it is larger), we will meet a *tuning* condition between the random jumps and the modulation that corresponds to the SR phenomenon.

In order to make a more quantitative description of the phenomenon it is necessary to evaluate the power spectrum of the particle motion in the indicated generic bistable potential (76). To do that, we will follow here McNamara and Wiesenfeld's (MNW) calculation (McNamara & Wiesenfeld 1989). We start defining two discrete variables x_{\pm} describing the position of the particle in either the right (+) or left (-) potential well (for instance, in the indicated bistable potential $x_{\pm} = \pm[a/b]^{1/2}$), and the corresponding probabilities $\Xi_{\pm}(t)$ ($\Xi_+(t) = 1 - \Xi_-(t)$). As in the previous section, we can write a rate (or master) equation in terms of W_{\pm} , the transition rates out of the \pm states

$$\frac{d}{dt} \Xi_+(t) = -\frac{d}{dt} \Xi_-(t) = W_- \Xi_-(t) - W_+ \Xi_+(t), \quad (79)$$

which is essentially the same as equation (70) discussed before. Clearly, the only dynamical variables are the particle populations (or probabilities) within the wells, as corresponds to a this approximate two-state dynamics, analogous to the discussion in the previous subsection.

In order to solve (79) at least some approximate form for the W_{\pm} is required. Following MNW we use an expansion in terms of a small parameter $\eta_0 \cos \Omega_0 t$, where $\eta_0 = A/\gamma$ (γ being the noise intensity)

$$W_{\pm} = \frac{1}{2} (\alpha_0 \pm \alpha_1 \eta_0 \cos \Omega_0 t + \dots), \quad (80)$$

where α_0 and $\alpha_1\eta_0$ are treated as parameters of the system. According to what was discussed in the previous subsection, α_0 and α_1 can be related to the unperturbed Kramers rate (with $r_K \simeq \tau_K^{-1}$) in an adiabatic-like approximation

$$r_K \simeq r_{K,0} \left(1 + \frac{A |x_\pm|}{\gamma} \cos \Omega_0 t \right). \quad (81)$$

This allows us to express W_\pm (within a phase factor) in (79), and to solve it finding a solution $\Xi_+(t)$. From this solution we can construct the (conditional) autocorrelation function $\langle x(t)x(t+\tau) | x_0, t_0 \rangle$, that in the asymptotic limit ($t_o \rightarrow -\infty$) yields the desired correlation function $\langle x(t)x(t+\tau) \rangle$. From this last quantity we can obtain the power spectrum through the Wiener-Khinchin theorem (van Kampen 1982, Gardiner 1985, Wio 1994) yielding

$$S(\omega) = \left(1 - \frac{(\alpha_1\eta_0)^2}{2[\alpha_0^2 + \Omega_0^2]} \right) \left(\frac{4\alpha_0 \langle x^2 \rangle}{[\alpha_0^2 + \omega^2]} \right) + \pi \frac{\langle x^2 \rangle (\alpha_1\eta_0)^2}{2[\alpha_0^2 + \Omega_0^2]} \delta(\omega - \Omega_0). \quad (82)$$

This result makes two notable predictions, both borne out by experiment: (i) the shape of the power spectrum is a delta contribution arising from the modulation, riding on a Lorentzian noise background; (ii) the total power -signal plus noise- is a constant. The latter property (that is strictly true only for the bistable model) means that the power in the signal part of the response grows at the expense of the noise power. This result demonstrates that, in such a bistable system, the proper application of noise at the input, can result in more order at the output. This could not be possible with a linear system. Moreover, the nonlinear system must be out of equilibrium.

A quantity that typically has been used to quantify this phenomenon is the *signal-to-noise ratio* (SNR) defined as the ratio between the power from the signal (second term on the rhs of (82)) to the noise power (first term on the rhs of (82), evaluated at $\omega = \Omega_0$). Using the form of the Kramers rate $r_{K,0}$ (inverse of (74)), it is possible to obtain (for the bistable potential) the approximate result

$$\text{SNR} \simeq \left(\frac{A \Delta U_0}{\gamma} \right)^2 e^{-\Delta U_0/\gamma}, \quad (83)$$

where ΔU_0 is the barrier high: $\Delta U_0 = a^2/4b$. The qualitative form of the power spectral density (psd) and the SNR as function of the noise intensity γ is depicted in Fig.7

The maximum of the curve of SNR results for a value of γ that makes the Kramers time (τ_K) roughly equal to half the period of the modulation. For more details on the SR phenomenon we refer to (Moss 1992, Moss *et al.* 1993, Wiesenfeld & Moss 1995, Bulsara *et al.* 1995, Bulsara & Gammaitoni 1996).

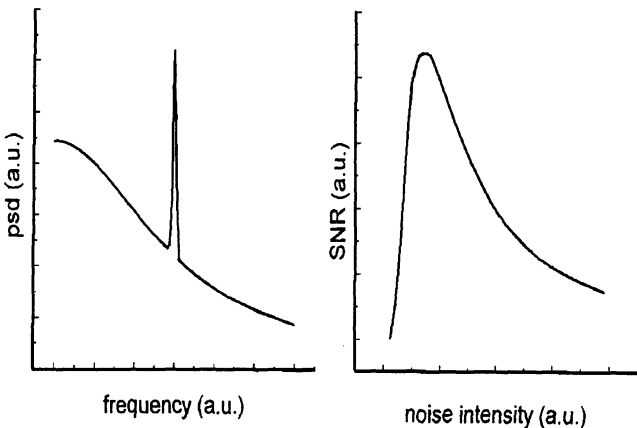


Fig. 7. (i) psd vs. ω and (ii) SNR vs. γ .

4 Spatially Extended Systems

Everywhere around us we find examples of *self-organization* or *cooperative phenomena* in *complex systems*, namely the appearance of a relatively simple (albeit nontrivial) behaviour in systems with many strongly-interacting degrees of freedom. These phenomena occur in far-from-equilibrium situations where, due to the intrinsic nonlinear dynamics, and due to the variation of some *control parameter*, a spontaneous breakdown of the spatiotemporal homogeneity leads to either the formation of stationary (space) or rhythmic (time) patterns or to propagating pulses or fronts.

There are examples of *dissipative structures* for almost all length scales and in almost all sciences:

- (i) mesoscopic: cellular structures in biology, propagation of nerve signals along the neural axon,
- (ii) macroscopic: propagation of electric signals in cardiac tissue, pacemakers and spirals in the Belousov-Zhabotinskii reaction, Bénard convection in fluids, vortex structures in superconductors, social organization in all biological species,
- (iii) global and astronomical: convective motion in the ocean, cloud patterns in planetary atmospheres, nebular structures, etc.

Among the many possible descriptions, the *excitable media* picture is one of the most useful ones in the description of pattern formation and propagation. A distributed excitable medium can be viewed as a set of active elements

(each element being a system with two or more possible steady states) representing small parts of a continuous system interacting among each other. Typically, such interaction is through some transport mechanism, the most common one being diffusion. It is the interplay between the internal nonlinearities of each element with the coupling among them, together with the effect of external control parameters, that can originate the space-temporal structures.

We will focus our discussion on the *reaction-diffusion model*, studying one- and two-component cases, in order to present some of the underlying principles in pattern formation phenomena.

4.1 Reaction-Diffusion Systems

We will consider a *distributed excitable* medium and assume that the interactions between the different elements that compose the medium are local in time and also that the variation in space is not too sharp, implying that we can neglect memory effects, as well as space derivatives of order higher than two. Within the formalism discussed in previous sections, the general form of the system equation, for the case of only one relevant macroscopic state variable ϕ , will be

$$\frac{\partial}{\partial t} \phi(\mathbf{r}, t) = F(\phi; \nabla \phi; \nabla^2 \phi; \dots) \quad (84)$$

For the *reaction-diffusion model*, this equation reduces to

$$\frac{\partial}{\partial t} \phi(\mathbf{r}, t) = F(\phi) + D \nabla^2 \phi. \quad (85)$$

We will not consider a derivation of this equation, but will adopt it as a phenomenological one (Nicolis & Prigogine 1977, Fife 1978, Haken 1978, Fife 1984, Malchow & Schimansky-Geier 1985, Murray 1989, Mikhailov 1990, Wio 1994). For instance, this kind of approach has been found to be adequate for the description of: propagation of electrical signals in cardiac tissue, nervous signals along the neuronal axon, and *target* or *spiral* patterns in the Belousov-Zhabotinskii reaction (Nicolis & Prigogine 1977, Fife 1984, Malchow & Schimansky-Geier 1985, Murray 1989, Mikhailov 1990).

Clearly, the reaction-diffusion equation for one macroscopic variable shown in (85), can be easily extended to several macroscopic variables $\{\phi_1, \phi_2, \dots, \phi_n\}$, resulting in a system of coupled reaction-diffusion equations.

However, and in order to proceed with the analysis we will begin by focussing on the one state variable case as in (85), and also initially consider a one dimensional system (i.e.: $\nabla^2 \rightarrow \partial^2/\partial x^2$).

The first step is to look for stationary solutions, that is to consider $\partial\phi/\partial t = 0$. Equation (85) reduces to

$$0 = D \frac{d^2}{dx^2} \phi + F(\phi). \quad (86)$$

For a one dimensional problem we have seen earlier that the *reaction term* or force $F(\phi)$ can always be derived from a *potential* $V(\phi)$, according to

$$F(\phi) = \frac{\partial}{\partial \phi} V(\phi). \quad (87)$$

In order to fix ideas we resort to an example: the *Schlögl model* (Haken 1978, Malchow & Schimansky-Geier 1985, Mikhailov 1990, Wio 1994), that corresponds to the following reaction scheme



having the associated macroscopic reaction term

$$F(\phi) = \kappa_0 \phi^2 - \kappa_1 \phi^3 - \kappa_2 \phi + \kappa_3, \quad (89)$$

where ϕ is the density of the reactant X , and the constants $\kappa_0, \kappa_1, \kappa_2$ and κ_3 include the reaction rates and the concentration of the reactants A and B . Usually in this model, κ_0 and/or κ_3 , are used as control parameters.

Let us consider the bounded domain case: $x \in [-L, L]$, $2L$ being the system length. In principle, we can consider two different boundary conditions

- (a) Dirichlet boundary conditions: $\phi(-L) = \phi(L) = 0$, with the physical meaning of perfect absorption on the borders,
- (b) Neumann boundary conditions: $\frac{d}{dx}\phi(x = -L) = \frac{d}{dx}\phi(x = L) = 0$, with the physical meaning of zero flux at the boundary.

Another, more general form of boundary condition, that includes both previous cases as limiting ones, is the *albedo* boundary condition. It describes a situation with partial reflectivity at the boundary (Schat & Wio 1992, Wio 1994, Hassan *et al.* 1994, Hassan *et al.* 1994, Hassan & Zanette 1995, Wio *et al.* 1993).

We will focus now on the search of inhomogeneous solutions. We write (87) as

$$V(\phi) = \int_0^\phi F(\phi') d\phi', \quad (90)$$

yielding for the Schlögl model the potential ($V(0) = 0$)

$$V(\phi) = \frac{1}{3} \kappa_0 \phi^3 - \frac{1}{4} \kappa_1 \phi^4 - \frac{1}{2} \kappa_2 \phi^2 + \kappa_3 \phi. \quad (91)$$

The form of equation (86) suggests a mechanical analogy by its interpretation as a particle of mass D , moving under the influence of the potential $V(\phi)$, assimilating the spatial coordinate x to a time variable (varying from $-L$ to L), and ϕ to a spatial coordinate. The first integral of motion yields

$$\frac{D}{2} \left(\frac{d}{dx} \phi \right)^2 + V(\phi) = E, \quad (92)$$

where E , the analogue of the *total mechanical energy*, is conserved. Exploiting this mechanical analogy, the following features of the solutions of (92) (for the potential given in (91) can be easily seen:

- (a) The stationary homogeneous solutions correspond to the extrema of the potential $V(\phi)$.
- (b) If we do not impose the Neumann boundary conditions indicated above, then every value of E corresponds to a solution of (86) in the range of ϕ' s, where $E > V(\phi)$ (for given values of $\phi(-L)$ and $\phi(L)$).
- (c) When we impose Neumann boundary conditions, we require that $\phi(-L)$ and $\phi(L)$ became turning points of the *trajectory*, that is $E = V(\phi(-L)) = V(\phi(L))$. This imposes a constraint on the acceptable solutions, restricting them to those confined to the central *valley*. However, such a valley exists only if $\kappa_0 > \kappa_c$ and $\kappa_3 \in [\kappa_{30}, \kappa_{31}]$, where κ_c and κ_{30}, κ_{31} are some extremum values that can be easily determined (Haken 1978, Malchow & Schimansky-Geier 1985, Mikhailov 1990, Wio 1994). The other case is a trajectory that starts at the origin ($\phi = 0$), bounces back at some value ϕ^* (with $V(\phi^*) \leq V_{max}$) and returns to the origin.

We can resort to known results from classical mechanics, and see how the possible trajectories in phase space can be parametrized with E , etc. But, due to the lack of space we will not do it here but refer the reader to (Haken 1978, Malchow & Schimansky-Geier 1985, Mikhailov 1990, Wio 1994).

In general, it is a difficult (if not impossible) task to find explicit solutions either for the stationary problem indicated in (86), or for the (complete) time dependent one in (85). However, there are situations where one is satisfied just with a qualitative analysis of the behavior of such solutions. Clearly then, the study of the stability becomes of primary importance. In this context, the methods developed in previous sections are of relevance.

4.2 Stability for Spatially Extended Systems

In the present case, we linearize the problem about the stationary solution (say $\phi_s(x)$), considering a small time dependent perturbation, and obtain in this way linear differential equations that contain the needed information. Hence, we consider perturbed solutions of the form

$$\phi(x, t) = \phi_s(x) + \varphi(x) e^{\lambda t} \quad (93)$$

Replacing this into (85), and linearizing in $\varphi(x)$, leads to the following eigenvalue equation

$$D \frac{d^2}{dx^2} \varphi(x) + \left[\frac{\partial}{\partial \phi} F(\phi) \right]_{\phi=\phi_s} \varphi(x) = -\lambda \varphi(x), \quad (94)$$

whose form, for the case of Neumann boundary conditions, suggests solutions of the type

$$\varphi_n(x) \approx \cos \left[\frac{n\pi x}{2L} \right], \quad (95)$$

provided that

$$\left(\frac{\partial}{\partial \phi} F(\phi) \right)_{\phi=\phi_s} - \lambda = D \left(\frac{n\pi}{2L} \right)^2. \quad (96)$$

The last equation shows that there is a tight connection between the eigenvalue λ and the wave vector $k = n\pi/2L$ associated to the perturbation. Hence, it is possible to have cases such that, for a certain range of values of the wave length of the perturbation the system is stable, while for other ranges it becomes unstable.

In order to discuss the emergence of an instability, we will consider the scheme from a more general viewpoint, valid for a wide class of systems. Let us start from (85) for a general (infinite) problem, with a stationary homogeneous solution ϕ_s that is stable. The stability of this solution means that our earlier linear stability analysis will give (for a multicomponent system) a set of eigenvalues λ , all having a negative real part (i.e.: $\text{Re}(\lambda) < 0$). We focus on the one with the largest real part, that we denote by $\lambda(k)$, to make explicit its dependence on the wave vector. Now suppose that there is a control parameter ϵ , whose variation could change the stability of the solution. That is, for $\epsilon < \epsilon_c$ we have $\text{Re}(\lambda(k)) < 0$ (for all k); while for $\epsilon = \epsilon_c$, $\text{Re}(\lambda(k_0)) > 0$ for some $k = k_0$. Here ϵ_c is the *critical value* of the parameter ϵ . Usually, for $\epsilon_c \neq 0$, a *reduced* control parameter is used: $\eta = \frac{\epsilon - \epsilon_c}{\epsilon_c}$. We show in Fig.8 the dependence of $\text{Re}(\lambda(k))$ on η . In part (a), for $\eta < 0$, the reference state ϕ_s is stable and $\text{Re}(\lambda) < 0$, but it becomes unstable for $\eta \geq 0$. For $\eta = 0$, the instability sets in, $\text{Re}(\lambda(k_0)) = 0$, at the wave vector $k = k_0$. For $\eta > 0$, there is a band of wave vectors ($k_1 < k < k_2$) for which the uniform state is unstable. For this situation, when $\eta = 0$, we can have two kinds of instabilities: stationary if $\text{Im}(\lambda) = 0$, or oscillatory when $\text{Im}(\lambda) \neq 0$.

If for some reason (usually a conservation law) it happens that $\text{Re}(\lambda(k=0)) = 0$ for all values of η , another form of instability occurs. It is depicted in part (b) of Fig.8. Here, $k_0 = 0$ is the critical wave vector, and for $\eta > 0$, the unstable band is $0 = k_1 < k < k_2$. It is possible to show that in general $k_2 \approx \eta^{1/2}$, and this indicates that the arising pattern occurs on a long length scale near the threshold $\eta = 0$. Once again we can find steady or oscillatory cases associated with $\text{Im}(\lambda) = 0$ or $\neq 0$.

Finally, in part (c) of the figure, we depict a case where both the instability and the maximum growth rate occur at $k_0 = 0$. This indicates that there is no intrinsic length scale. For this reason the pattern will presumably occur on a scale determined by the system size or by the dynamics. Once again we find steady or oscillatory cases associated with $\text{Im}(\lambda) = 0$ or $\neq 0$ (Cross 1988, Newell 1989, Cross & Hohenberg 1993, Wio 1994).

Another very interesting situation arises, if we have a system of at least two components, when there are two real roots and one of them becomes positive at some critical value of the control parameter. This is a situation leading to a spatially nonuniform steady state that is called a *Turing in-*

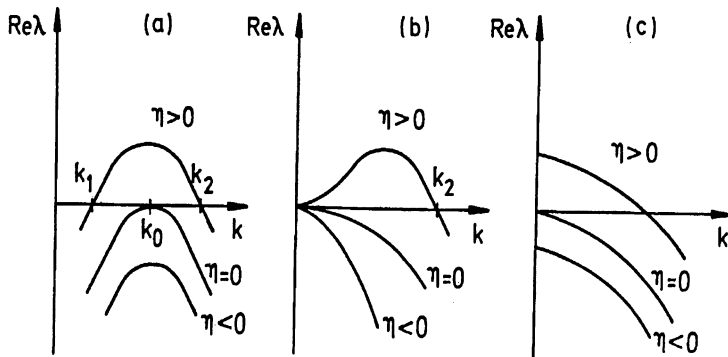


Fig. 8. $\text{Re}(\lambda)$ vs. k .

stability (at variance with the *Hopf instability* discussed before) (Nicolis & Prigogine 1977, Fife 1978, Fife 1984, Murray 1989).

To close this section it is worth remarking that the kind of analysis we have sketched above leads to the determination of the stability regions for particular systems. For instance, it allows us to define the so called Bùsse or stability balloon, to predict the possible appearance of new instabilities such as the Eckhaus instability (associated with a longitudinal or compressional instability), the zig-zag instability (corresponding to a long-wavelength transversal instability), etc (Cross & Hohenberg 1993, Newell 1989, Nicolis 1995).

4.3 Examples of Reaction-Diffusion Systems

Here we will treat two cases of RD models associated to one- and two-component systems. A bistable one-component model corresponding to an electrothermal instability: *the ballast model*; and a two-component model of the *activator-inhibitor* type.

One Component Models: Ballast Resistor. The most commonly used RD model that exemplifies most of the characteristics we have so far discussed is the *Brusselator* (Nicolis & Prigogine 1977, Haken 1978, Murray 1989). This model, introduced by Prigogine and Lefevre, is a simplified version of more elaborate models showing, qualitatively, a behaviour similar to those observed in experiments related to the *Belousov-Zhabotinskii* reaction (Nicolis & Prigogine 1977, Haken 1978, Fife 1984, Malchow & Schimansky-Geier 1985, Murray 1989, Mikhailov 1990, Wio 1994), and in particular the existence of a transition to a limit cycle. However, we will start here considering a different

(one component) model to exemplify the formation of spatial patterns, which is associated with an electrothermal instability: the *ballast resistor* (Mikhailov 1990, Schat & Wio 1992, Wio 1994).

We will adopt a form of the model related to experiments on superconducting microbridges, called the *hot-spot* model (Skocpol *et al.* 1974). We consider a thin wire of a superconductor metal of length $2L$, along which an electric current I is flowing. The wire is immersed in a heat bath with constant temperature T_B . Depending on the values of these parameters, the temperature profile on the wire will be either homogeneous, or inhomogeneous (regions with different temperatures coexisting along the wire). The law of conservation of internal energy per unit length of the wire $u(x, t)$ can be writing as

$$\begin{aligned} \frac{\partial}{\partial t} u(x, t) = & - \frac{\partial}{\partial x} (J(x, t) + h(x, t) I(x, t)) \\ & - Q(x, t) + I(x, t) E(x, t), \end{aligned} \quad (97)$$

where x is the position along the wire ($-L \leq x \leq L$), J is the heat current, h is the enthalpy per unit of charge carrier and unit length, Q is the energy flow dissipated into the gas per unit length, E is the electric field along the wire and IE is the heat generated by the current per unit length. As the Coulomb forces between the charges are very strong, we assume electro-neutrality of the wire, yielding $\frac{\partial}{\partial x} I(x, t) = 0 \Leftrightarrow I(x, t) = I(t)$. However, this assumption will only be valid if one considers a range of time variation that is short when compared with the inverse of the typical plasma frequency of the electrons.

Using the fact that the quantities J , E and Q obey some phenomenological linear laws, as well as Onsager relations between different “transport coefficients” (Peltier and Thompson coefficients, etc), together with the relation between the internal energy of the wire $u(x, t)$ and the local temperature field $T(x, t)$ ($du(x, t) = c dT(x, t)$, with c the heat capacity per unit length) we obtain the system’s equation for the temperature profile on the wire (Schat & Wio 1992, Wio 1994)

$$c \frac{\partial}{\partial t} T(x, t) = \frac{\partial}{\partial x} \lambda \frac{\partial}{\partial x} T - q(T - T_B) + R I^2. \quad (98)$$

Here λ is the heat conductivity of the wire, R the isothermal resistivity per unit length, and q is related to the energy dissipated into the gas due to the difference in temperature between the wire and the gas. All these coefficients may, in principle, depend on the local temperature of the wire, while q may also depend on T_B . In order to further simplify the equation for the temperature profile, we assume that the specific heat c , the heat conductivity λ and the heat transfer coefficient q are all constant along the wire.

As discussed earlier, we are interested in stationary solutions for the temperature field distribution. Hence, our equation has the form

$$0 = \lambda \frac{d^2}{dx^2} T - q(T - T_B) + R I^2. \quad (99)$$

For the resistivity R we will adopt a piecewise-linear approximation of a realistic one (see the l.h.s. of Fig.9), according to $R(T) = R_o \theta[T(x, t) - T_c]$, (with $\theta(z)$ the step function: $\theta(z) = 1$ for $z > 0$, $\theta(z) = 0$ for $z < 0$). The assumption behind of such a form is that for $T < T_c$ the wire is superconducting while it has a finite (constant) resistivity for $T > T_c$. Without loss of generality we take the zero of the temperature scale at the heat bath temperature T_B ($T_B = 0$). We also make a scaling of the parameters in order to have nondimensional coordinates ($y \equiv (q/\lambda)^2 x$, and $y_L = (q/\lambda)^2 L$, with $-y_L \leq y \leq y_L$). In our discussion we will assume that the current I is fixed (the voltage difference depending on I), and we define the following “effective temperature”

$$T_h \equiv I^2 R_o / q$$

With all these assumptions, equation (99) for T adopts the final form

$$\frac{d^2}{dy^2} T(y) - T + T_h \theta[T(y) - T_c] = \frac{d^2}{dy^2} T(y) + \frac{d}{dT} V[T] = 0 \quad (100)$$

where the potential $V(T)$ is defined according to (91) as

$$V(T) = \int_0^T dT' (T_h \theta[T' - T_c] - T'). \quad (101)$$

The shape of the function $F(T) = \frac{\partial}{\partial T} V(T)$, as well as the approximation adopted for the resistivity, are shown in Fig.9.

When we compare the present form of the nonlinear function $F(T)$ with the corresponding term in the Schlögl model of equation (91), we see that the ballast model *mimics* the Schlögl model.

To complete the model, we need to specify the boundary conditions at both borders: $x = \pm L$ (or $y = \pm y_L$). As commented above, we will only consider Dirichlet or Neumann boundary conditions.

To find the form of the stationary solutions one may distinguish two different regions

(i) *Cold regions*, where $T(y) < T_c$, and (100) reduces to

$$\frac{d^2}{dy^2} T(y) - T = 0, \quad (102)$$

with solutions that have the general form $T(y) = A_c e^y + B_c e^{-y}$;

(ii) *Hot regions*, where $T(y) > T_c$, and (100) reduces to

$$\frac{d^2}{dy^2} T(y) - T + T_h = 0, \quad (103)$$

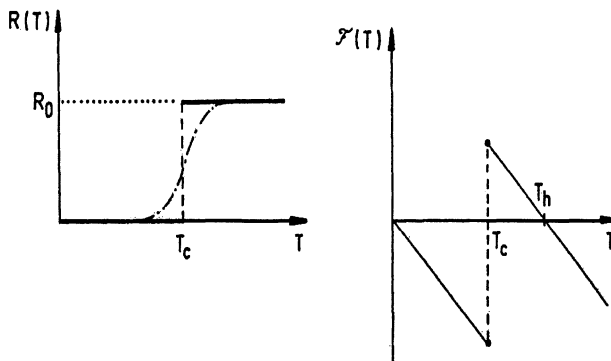


Fig. 9. Approximate forms of $R(T)$ and $F(T)$ for the ballast model.

and with general solutions of the form $T(y) = A_h e^y + B_h e^{-y} + T_h$. The parameters A_c, B_c, A_h and B_h are determined after imposing the boundary conditions. Furthermore, if we have a cold region on the left and a hot region on the right of a certain position coordinate y_c (or vice versa), both solutions should be joined together in such a way that (100) is satisfied at the transition point. This is the case if both T and dT/dy are continuous at $y = y_c$. Using these conditions, it is clear that

$$T(y_c) = T_c$$

allowing us to fix the value of y_c .

Let us now analyze the stationary states. We first consider the homogeneous case. For Neumann B.C. the potential $V(T)$ must have a maximum. This leads to $T(y) = 0$ for all values of T_h (and therefore of the current I). However, if $T_h > T_c$, there is an additional homogeneous solution $T(y) = T_h$. Clearly both satisfy the Neumann boundary conditions. For Dirichlet B.C., there is only one possible homogeneous solution $T(y) = 0$.

We now turn to inhomogeneous stationary temperature profiles. Using the mechanical analogy, it is possible to find inhomogeneous solutions corresponding to several *rebounds* between the *turning points* of the potential. But here we will consider spatial temperature distributions having only one maximum, with two *cold* regions for $-y_L < y < -y_c$ and $y_c < y < y_L$, and one *hot* region for $-y_c < y < y_c$ (with two transition points at $y = \pm y_c$ due to symmetry). Through a linear stability analysis one may prove that solutions with several maxima are always unstable.

Imposing the boundary conditions (Neumann or Dirichlet) on the solutions of the form indicated above, the different constants are determined

yielding the typical shapes indicated in Fig.10; part (a) for Dirichlet and (b) for Neumann b.c.

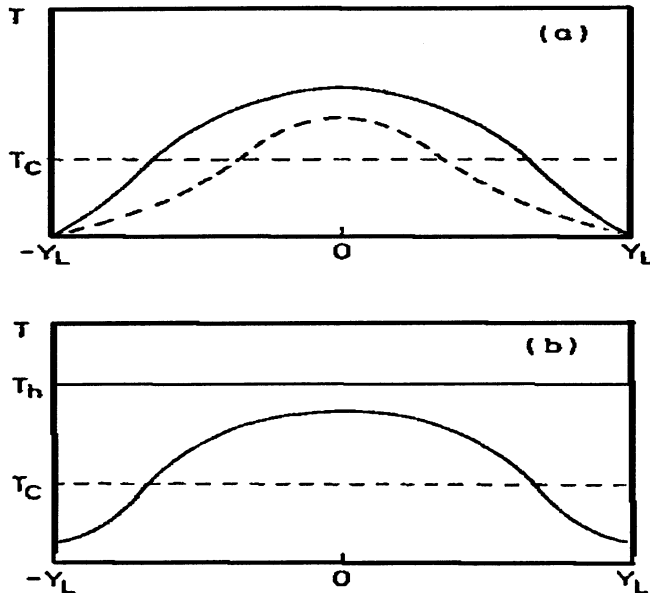


Fig. 10. Patterns in the ballast model: (a) Dirichlet b.c., (b) Neumann b.c.

According to linear stability analysis we can conclude that, for Dirichlet b.c., from the pair of simultaneous solutions, the one with the larger dissipation (i.e. the larger hot region) is stable while the other is unstable. Similarly, for the case of Neumann b.c., indicates that the homogeneous stationary solutions are stable, while inhomogeneous structures are always unstable.

Now, we will briefly discuss how to describe the propagation of structures in one component systems, considering (86) once more in its complete form.

We assume a one dimensional, infinite, system. To complete the description, we need to include some boundary conditions at infinity. Clearly, for a very general form of $F(\phi)$ it is not easy to find an arbitrary solution of (86) fulfilling the chosen b.c. However, there is a particular kind of solutions of great interest called *solitary waves* on which we will now focus our attention. These waves are functions of the spatial (x) and temporal (t) coordinates, not independently, but through the combination $\xi = x - ct$. In terms of the

new variable ξ , (86) adopts the form

$$D \frac{\partial^2}{\partial \xi^2} \phi + c \frac{\partial}{\partial \xi} \phi + F(\phi) = 0. \quad (104)$$

where $\frac{\partial}{\partial t} = -c \frac{\partial}{\partial \xi}$ and $\frac{\partial^2}{\partial x^2} = \frac{\partial^2}{\partial \xi^2}$.

Here we can resort once more to the mechanical analogy used earlier (see Sect. 4.1). We again interpret ϕ as the spatial coordinate of a particle of mass D moving in the force field $F(\phi)$ (derived from the potential $V(\phi)$, i.e. $F(\phi) = \frac{\partial V}{\partial \phi}$), but now in the presence of a *friction force* proportional to the velocity of the particle, i.e. $\frac{\partial \phi}{\partial \xi}$. Hence, c plays the role of the friction coefficient.

Let us concentrate on the situation where the potential $V(\phi)$ has a bistable form, and ask for solutions of (104) with the boundary conditions

$$\phi \rightarrow \phi_2 \quad \text{for} \quad \xi \rightarrow -\infty$$

$$\phi \rightarrow \phi_1 \quad \text{for} \quad \xi \rightarrow \infty$$

with ϕ_1 and ϕ_2 the stationary solutions. The resulting wave, or moving pattern, is called a *trigger* or *front wave*, because its propagation triggers the transition from one stationary state of the system to the other (both minima of V). This kind of waves has been observed, for instance, in chemically reacting media or as electrical activity that propagates without attenuation along the axonal membrane.

In order to analyze qualitatively the behaviour of a bistable system, for instance the dependence of the (unique) front velocity on the potential parameters, we can exploit again the form of the ballast resistor model introduced before. However, and always due to the lack of space, we refer to (Murray 1989, Mikhailov 1990, Schat & Wio 1992, Wio 1994, Hassan *et al.* 1994, Hassan *et al.* 1994, Hassan & Zanette 1995, Castelpoggi *et al.* 1996).

We now turn to discuss the propagation phenomenon in systems with two components.

Many Component Models: Activator–Inhibitor. In order to make a realistic description, for the theoretical representation of travelling waves of chemical, physical or biological activity commonly observed in spatially distributed excitable media, we need to resort to models with more than one component. All excitable media share certain characteristic features. They have a stable rest state, and small perturbations are rapidly damped out. However, perturbations larger than a certain threshold trigger an abrupt and substantial response. After this fast response, the media is typically refractory to further stimulation for some characteristic time before it recovers its full excitability. It is clear that such a sequence of events cannot be represented by a simple one component model of the kind we have discussed so far. On the other hand, the analysis of a model with a large number of components

quickly becomes too cumbersome. Notwithstanding, experience has shown that it is enough to resort to two component models in order to be able to qualitatively (and sometimes quantitatively) reproduce several characteristics of real systems (Fife 1978, Fife 1984, Murray 1989, Mikhailov 1990, Wio 1994).

The set of equations corresponding to a model describing a two component system, with densities $u(x, t)$ and $v(x, t)$, according to (85), (Fife 1978, Fife 1984, Murray 1989, Mikhailov 1990, Wio 1994) has the general form

$$\begin{aligned}\frac{\partial}{\partial t} u(x, t) &= D_u \frac{\partial^2}{\partial x^2} u + f(u, v) \\ \frac{\partial}{\partial t} v(x, t) &= D_v \frac{\partial^2}{\partial x^2} v + g(u, v)\end{aligned}\quad (105)$$

Depending on the actual form of the nonlinear terms $f(u, v)$ and $g(u, v)$, even such an innocent looking pair of equations, can have an extremely complicated behaviour. However, the experience has also shown that a typical and very fruitful form is the one shown in Fig.11. There, we show in the phase plane (u, v) , the form of the nullclines (that is the curves $f(u, v) = 0$ and $g(u, v) = 0$), and the sign of the derivatives of the nonlinear reactive functions in each plane region.

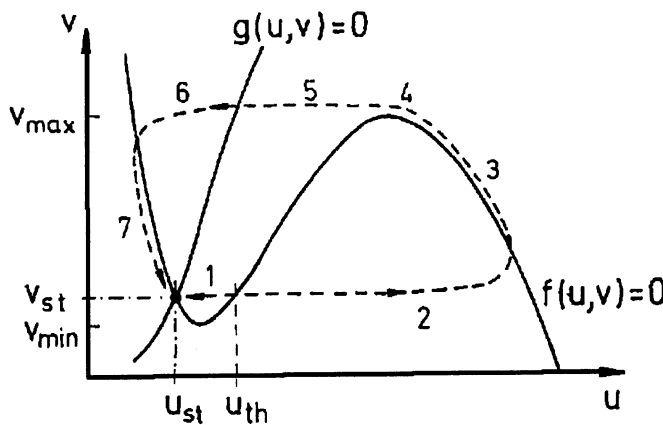


Fig. 11. Nullclines of the activator-inhibitor systems.

We will now qualitatively discuss how it is that such a simple system can

model the sequence of events we have indicated at the begining of this section. We recall that an excitable medium is a spatially distributed system composed of excitable elements. The interaction between neighboring elements through a diffusive coupling makes it possible to produce excitation waves. If a local region of space is disturbed beyond a certain threshold value, then the autocatalytic production of substance u within the excited region causes u to diffuse into the neighboring regions, driving those regions across the threshold and thus making the excitation spread spatially. This corresponds to a front propagation. In order to make a pictorial representation of this process, we refer to Fig.11. There is a unique homogeneous steady state indicated by the point (u_{st}, v_{st}) , that satisfies $f(u_{st}, v_{st}) = 0$ and $g(u_{st}, v_{st}) = 0$, and is locally stable but excitable: while the subthreshold disturbances are rapidly damped (perturbations in the region indicated by 1 in Fig.11), larger disturbances (those driving the system beyond the point u_{th}) provoke an excitation cycle that is governed by the local reaction kinetics before the system returns to the steady state. This cycle is indicated in the figure through the sequence of numbers from 2 to 7, corresponding to differents states of the system. In region 2, u increases by an autocatalytic process, until the phase trajectory reaches the curve $f(u, v) = 0$, where the density of v starts to increase, and the process evolves following the nullcline as indicated by 3. After that the process reaches a maximum value of the density for v in 4, and follows curve 5, where the density of u decreases and after crossing the nullcline $g = 0$, region 6, the other branch of the nullcline $f = 0$ is reached and the system moves along this trajectory (indicated by 7) and reaches the steady state (u_{st}, v_{st}) again.

We have seen that the abrupt overthreshold autocatalytic production of u gives rise to the excitability of the system and the interaction between u and v causes the recovery from the excitation state. For this reason the variable u is sometimes called the *trigger* variable and v the *recovery* variable (or *propagator* and *inhibitor*, respectively). For instance, some examples in real systems are: membrane potential as *propagator* and ionic conductance as *inhibitor* in neuromuscular tissue; bromous acid as *propagator* and ferroin as *inhibitor* in the Belousov-Zhabotinskii reaction; infectious agent as *propagator* and level immunity as *inhibitor* in epidemics.

A typical form of the profile in a one dimensional media for the kind of waves that behave according to the previous description is shown in Fig.12. The transition zone from the resting to the excited state is called the *front*, while the transition zone from the excited to the resting state is the *backfront*.

The process we have so far discussed is clearly not restricted to a one dimensional geometry. In fact, in two dimensional media the same line of argument leads to describing the so called *target structures*, that is perturbations that spread radially originating a sequence of growing rings, such as has been observed in the Belousov-Zhabotinskii reaction. When we look at such structures far from the point where they originated, the curvature has

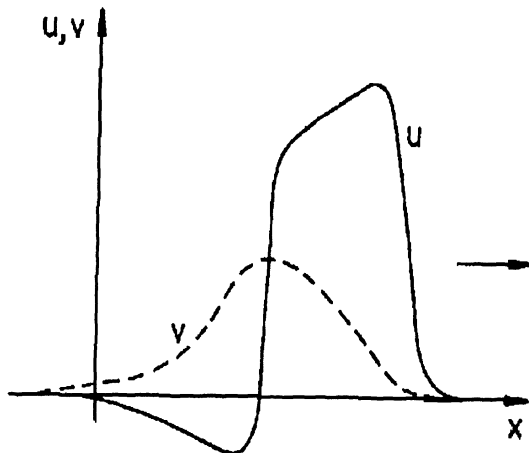


Fig. 12. Activator and inhibitor profiles.

decreased and the structure acquires a one dimensional characteristic, i.e. in the direction of propagation it has the same profile as shown in Fig.12, while it extends “infinitely” in the normal direction.

Let us now qualitatively discuss the origin of a very important type of structure that arises in (two dimensional) *propagator-inhibitor* systems: the *spirals*.

Spirals in Propagator-Inhibitor Systems. A common form of pattern in the reaction-diffusion description of two-dimensional excitable media is the rotating *spiral*. The interest in this kind of pattern is due to its occurrence in chemical (i.e. the Belousov-Zhabotinskii) reactions as well as in biological systems (waves of electrical and neuromuscular activity in cardiac tissue, formation of some bacterial colonies). A complete mathematical description of such structures is extremely difficult. However, within the *propagator-inhibitor* scheme, it is possible to understand intuitively the initial stage in the formation of a spiral wave (Fife 1984, Murray 1989, Mikhailov 1990, Wio 1994). We start considering a thought experiment in a two dimensional medium with a one dimensional solitary wave of the type discussed earlier. That means a propagating straight band, a two-dimensional wave with a profile in the direction of motion like the one shown in Fig.12, and extending indefinitely in the normal direction. Assume that such a band is perturbed in some way (for instance by a light beam incident on a photosen-

sitive reactant). Hence, the pulse-like structure is disturbed in that region, taking the form indicated on the r.h.s. of Fig.13. It is clear that in both branches of the perturbed structure we will see that the points in the front or in the backfront will continue their motion. The only exception will be the point indicated by v^* (that will correspond to the *tip* of the *spiral core*). This point is the boundary between the front and the backfront and, if we consider that the front velocity has to change continuously, it must have zero velocity.

The evolution will develop according to the following steps. We refer our argumentation to Fig.13. On the left, we depict the upper branch of the perturbed band. The points on the front, far from v^* , move at the same original velocity, but when we come closer to v^* , their velocity reduces continuously. The same happens with points on the backfront. This initial situation is indicated by the curve labeled *a*. After a short time has elapsed, the point v^* remains immobile, but all other points have moved into their new positions indicated by the curve labeled *b*. Clearly, the original form of the perturbed band is deformed. After another short time elapses, the same process is repeated and the curve changes to the one labeled *c*; after another short time to *d*, and so on. Carried to its logical extreme, this type of analysis would predict that the front would acquire a growing angular velocity and curvature, a process that finally produces a spiral.

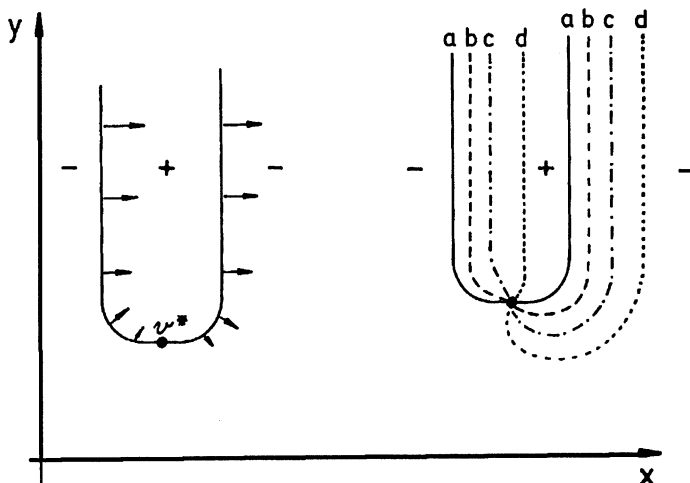


Fig. 13. The genesis of spirals.

The experimental observation of spirals in chemically reactive media, particularly in the Belousov-Zhabotinskii reaction, shows that this kind of pattern appears as pairs of symmetric, counter-rotating spirals. To understand this aspect within the same qualitative picture we must remember that originally there were two branches. However, each one is the specular image of the other, implying that, if the motion in the neighborhood of the upper one is a rotation in the indicated direction, the motion around the one on the bottom will be a rotation in the opposite direction. Hence, the same picture offers a description on the possible origin of spirals as well as their appearance in counter-rotating pairs.

5 Nonequilibrium Potential

Let us now go back to the dynamical system (1) and discuss the *effect of noise* (Graham 1978, Graham 1987, Graham & Tel 1990). We start writing

$$\frac{dx_j}{dt} = F_j(\mathbf{x}) + \sum_l g_{jl}\xi_l(t), \quad (106)$$

where $\xi_l(t)$ are white noise terms of zero mean and correlations $\langle \xi_j(t)\xi_l(t') \rangle = 2\gamma\delta_{jl}\delta(t-t')$. The associated FPE for $P((\mathbf{x}),t) = P(x_1, \dots, x_n, t)$, will be a generalization of (64) given by

$$\frac{\partial}{\partial t}P(\mathbf{x},t) = \sum_j \frac{\partial}{\partial x_j} \left(-[F_j(\mathbf{x})P(\mathbf{x},t)] + \gamma \sum_l \frac{\partial}{\partial x_l} [\mathbf{G}_{jl}P(\mathbf{x},t)] \right) \quad (107)$$

with $\mathbf{G} = \mathbf{g}\mathbf{g}^T$. If we can write that $F_j(\mathbf{x}) = \sum_l (\$)_{jl} \frac{\partial}{\partial x_l} V(\mathbf{x})$, we find again the situation studied in Sect.2.4 where, from a deterministic point of view, we have a *relaxational flow*. Hence, if $\mathbf{G} = \$$, it is possible to derive the expression

$$P_{st}(\mathbf{x}) \simeq e^{-V(\mathbf{x})/\gamma}. \quad (108)$$

Clearly, if $g_{jl} = \delta_{jl}$, the result is trivial.

Let us now consider the case where $F_j(\mathbf{x}) = -\sum_l (\$)_{jl} \frac{\partial V}{\partial x_l} + w_j$, that in analogy with Sect.2.4 corresponds to a *nonrelaxational flow*. We assume that $\$ = \mathbf{g}\mathbf{g}^T$. Hence we will have that the Hamilton-Jacobi like equation (26) that now reads

$$\sum_l \left(F_l + \sum_j (\$)_{jl} \frac{\partial V}{\partial x_j} \right) \frac{\partial V}{\partial x_l} = 0, \quad (109)$$

yields, in the deterministic case, a function $V(\mathbf{x})$ that is a Lyapunov functional of the problem. However, it has been proved by Graham and collaborators (1978,87,90) that in such a case and in the weak noise limit ($\gamma \rightarrow 0$),

the stationary solution of the multivariate FPE (107) associated to the set of SDE (106) is given by

$$P_{st}(\mathbf{x}) \sim e^{-V(\mathbf{x})/\gamma + O(\gamma)}. \quad (110)$$

with $V(\mathbf{x})$ the solution of (109). This functional corresponds to the *nonequilibrium* or *Graham's potential* (Graham 1978, Graham 1987, Graham & Tel 1990).

As discussed in the introduction, we can interpret the effect of noise saying that it induces fluctuations in the system around one of the minima of $V(\mathbf{x})$, fluctuations that allow the system to explore the neighbourhood of such a point and in this way identify it as a minimum.

The knowledge of the potential $V(\mathbf{x})$ offers us, at least in principle, the possibility of getting information about

1. fixed points (extrema of $V(\mathbf{x})$),
2. local stability of the fixed points,
3. global stability of the minima (attractors),
4. barrier heights between different minima,
5. decay times of metastable states.

It is the last point, decay of metastable states, one of the aspects that will be discussed in the following subsections.

5.1 Some Examples of Nonequilibrium Potentials in RD Systems

In relation with pattern formation, boundary conditions (b.c.) have been recently shown to play a relevant role in the appearance and stability as well as on the propagation of spatial structures, for one and two-component systems (Schat & Wio 1992, Wio *et al.* 1993, Hassan *et al.* 1994, Hassan *et al.* 1994). More recently, the role of b.c. in pattern selection, and more particularly the *global stability* of the resulting structures have been analyzed (Izus *et al.* 1995, Izus *et al.* 1996, Izus *et al.* 1996). Such analysis was carried out by exploiting the notion of *nonequilibrium potential* or *Lyapunov functional* (LF) of the system. This kind of approach has not been used in the realm of RD systems because it is usually not possible, insofar as some potential conditions are not fulfilled, to obtain a Lyapunov function for a general problem. However, the results of Graham and collaborators (Graham 1978, Graham 1987, Graham & Tel 1990) point to the possibility of getting information about such functionals as well as about global stability even though the system does not fulfill the above indicated potential conditions.

When the LF exists, such an approach offers an alternative way of confronting a problem that has recently attracted considerable attention, both experimentally and theoretically. Namely, the relative stability of the different attractors, corresponding to spatially extended states, and the possibility of transitions among them due to the effect of (thermal) fluctuations (Kerszberg

et al. 1983, de la Torre & Rehberg 1990, Viñals *et al.* 1991, Hernandez-García *et al.* 1993, Montagne *et al.* 1996).

In this section we will show the results on local and global stability, obtained by means of the nonequilibrium potential, through a couple of simple examples.

Ballast Resistor. The specific model we shall focus on in this section, with a known form of the LF or nonequilibrium potential, corresponds to the same simple one-dimensional, one-component model of an electrothermal instability discussed in Sect.4.3. However, it can be considered as mimicking a broader class of bistable reaction-diffusion models. The particular, nondimensional form that we shall work with is

$$\partial_t T = \partial_{yy}^2 T - T + T_h \theta(T - T_c). \quad (111)$$

In Izus *et al.* (1995), both the global stability of the patterns and the relative change in stability for this model were analyzed, as some b.c. parameter was changed. Here we analyze how those results depend on the threshold parameter.

For the sake of concreteness, we consider here a class of stationary structures $T(y)$ in the bounded domain $y \in (-y_L, y_L)$ with Dirichlet boundary conditions at both ends, $T(y = \pm y_L) = 0$. These are the spatially symmetric solutions to (111) already discussed in Sect.4.3. Such structures can also be seen as a symmetrization of a set of stationary solutions to the Ballast reaction-diffusion model in the interval $(0, y_L)$ with a Neumann boundary condition at $y = 0$, namely, $dT/dy|_{y=0} = 0$.

The explicit forms of the stationary structures are

$$T(y) = T_h \times \begin{cases} \sinh(y_c) \sinh(y_L + y) / \cosh(y_L), & -y_L \leq y \leq -y_c, \\ 1 - \cosh(y) \cosh(y_L - y_c) / \cosh(y_L), & -y_c \leq y \leq y_c, \\ \sinh(y_c) \sinh(y_L - y) / \cosh(y_L), & y_c \leq y \leq y_L, \end{cases} \quad (112)$$

The double-valued coordinate y_c , at which $T = T_c$, is given by

$$y_c^\pm = \frac{1}{2} y_L - \frac{1}{2} \ln \left[z \cosh(y_L) \pm \sqrt{z^2 \cosh(y_L)^2 - 1} \right], \quad (113)$$

with $z = 1 - 2T_c/T_h$ ($-1 < z < 1$).

When y_c^\pm exists and $y_c^\pm < y_L$, the solution (112) represents a structure with a central hot zone ($T > T_c$) and two lateral cold regions ($T < T_c$). For each parameter set there are two stationary solutions, given by the two values of y_c . In Schat & Wio (1992), it has been shown that the structure with the smallest hot region is unstable, whereas the other one is linearly stable. The trivial homogeneous solution $T = 0$ exists for any parameter set and is always linearly stable. These two linearly stable solutions are the only stable stationary structures under the chosen boundary conditions. Therefore,

under suitable conditions, we have a bistable situation in which two stable solutions coexist, one of them corresponding to a cold-hot-cold (CHC) structure and the other one to the homogeneous trivial state. The unstable solution is always a CHC structure, with a relatively small hot region.

For the symmetric solution we are considering here, the nonequilibrium potential or LF reads (Izus *et al.* 1995)

$$\mathcal{F}[T] = 2 \int_0^{y_L} \left\{ - \left(\int_0^T [-T' + T_h \theta(T' - T_c)] dT' \right) + \frac{1}{2} (\partial_y T)^2 \right\} dy. \quad (114)$$

Replacing (112), we obtain the explicit expression

$$\mathcal{F}^\pm = -T_h^2 y_c^\pm z + T_h^2 \sinh(y_c^\pm) \frac{\cosh(y_L - y_c^\pm)}{\cosh(y_L)}. \quad (115)$$

For the homogenous trivial solution $T(y) = 0$, instead, we have $\mathcal{F} = 0$.

In Fig.14 we have plotted the LF $\mathcal{F}[T]$ as a function of $\phi_c = T_c/T_h$ for a fixed system size. The curves correspond to the inhomogeneous structures, \mathcal{F}^\pm , whereas the horizontal line stands for the LF of the trivial solution. The upper branch of each curve is the LF of the unstable structure, where \mathcal{F} attains a maximum. At the lower branch and for $T = 0$, the LF has a local minimum. The curve exists up to a certain critical value of ϕ_c at which both branches collapse. The critical behaviour, around this point (which we will not discuss here) was analyzed in Zanette *et al.* (1995) and Castelpoggi *et al.* (1996).

It is interesting to note that, since the LF for the unstable solution is always positive and, for the stable CHC structure, $\mathcal{F} < 0$ for $\phi_c \rightarrow 0$, and > 0 otherwise, the LF for this structure vanishes for an intermediate value of the parameter: $\phi_c = \phi_c^*$. At that point, the stable inhomogeneous structure and the trivial homogeneous solution interchange their relative stability. In fact, $T(y) = 0$ switches from being a metastable state, to being more stable than the inhomogeneous structure.

Activator–Inhibitor. The importance of activator-inhibitor systems for applications in physics, chemistry and biology is by now very well established (Koga & Kuramoto 1980, Kuramoto 1984, Ohta 1989, Ohta *et al.* 1989, Ohta *et al.* 1990, Wio *et al.* 1993, Petrich & Goldstein 1994, Goldstein *et al.* 1996, Drazer & Wio 1996). Here we shall focus on a specific system belonging to this family of two-component models. We want to present an analysis of the global stability of stationary patterns exploiting the concept of nonequilibrium potential.

We start with a simplified (piecewise linear) version of the activator–inhibitor model sketched in Sect.4.3, which preserves the essential features,

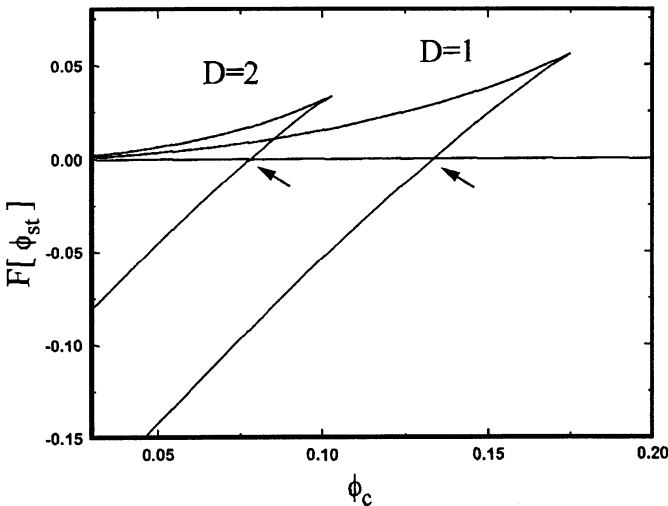


Fig. 14. Nonequilibrium potential \mathcal{F} , for the stationary patterns of the ballast resistor, as a function of ϕ_c , for $L = 1$. The bottom curve corresponds to $\phi_s(y)$ and the top one to $\phi_u(y)$. The points ϕ_c^* , are indicated.

and fix the parameters so as to allow for nontrivial solutions to exist. After scaling the fields, we get a dimensionless version of the model as:

$$\begin{aligned}\partial_t u(x, t) &= D_u \partial_x^2 u - u + \theta[u - a] - v \\ \partial_t v(x, t) &= D_v \partial_x^2 v + \beta u - \gamma v\end{aligned}\quad (116)$$

We confine the system to the interval $-L < x < L$ and impose Dirichlet boundary conditions on both extrema. According to the values of the parameters a , β and γ , we can have a monostable or a bistable situation (Koga & Kuramoto 1980, Ohta *et al.* 1989). In the second case we have two homogeneous stationary (stable) solutions. One corresponds, in the (u, v) plane, to the point $(0, 0)$ while the other is given by (u_0, v_0) with

$$u_0 = \frac{\gamma}{\beta + \gamma}, \quad v_0 = \frac{\beta}{\beta + \gamma}$$

implying that the condition $\frac{\gamma}{\beta + \gamma} > a$ must be fulfilled. Without losing generality we may assume that $0 < a < 1/2$ and $u_0 < 2a$ (Koga & Kuramoto 1980).

The inhomogeneous stationary patterns appear due to the nonlinearity of the system, and ought to have activated regions ($u > a$) coexisting with non-activated regions ($u < a$). This fact, together with the symmetry of

the evolution equations and boundary conditions, implies the existence of symmetric inhomogeneous stationary solutions. We restrict ourselves to the simplest inhomogeneous, symmetric, stationary solutions. That is, a symmetric pattern consisting of a central region where the activator field is above a certain threshold ($u > a$) and two lateral regions where it is below it ($u < a$). As was already discussed, (Koga & Kuramoto 1980, Wio *et al.* 1993), different analytical forms (which are here linear combinations of hyperbolic functions) should be proposed for u and v depending on whether $u > a$ or $u < a$. These forms, as well as their first derivatives, need to be matched at the spatial location of the transition point, which we called x_c . Through that matching procedure and imposing boundary conditions we get the general solution for the stationary case. In order to identify the matching point x_c we have to solve the equation $u(x_c) = a$, resulting in general in a transcendental equation for x_c . In order to avoid the complications arising from the possible spatially oscillatory behaviour of the solutions, we will work in a parameter range where the diffusion coefficient of the activator (D_u) is lower than some critical value (D_u^{osc}), (Koga & Kuramoto 1980, Ohta *et al.* 1989), beyond which the solutions became spatially oscillatory. In particular there are up to four different solutions for x_c , and associated with each one we have different stationary solutions that we will indicate by u_{e1} , u_{e2} , u_{e3} and u_{e4} , with increasing values of the transition point x_c . A linear stability analysis of these solutions indicates that u_{e1} and u_{e3} are unstable while u_{e2} and u_{e4} are locally stable. The stable states will correspond to attractors (minima) of the functional while the unstable ones will be saddle points, defining the barrier height between attractors.

We now write the equations of our system specifying the time scale associated with each field. This allows us to perform an adiabatic approximation and obtain a particular form of the nonequilibrium potential for this system. Measuring the time variable on the characteristic time scale of the slow variable u (i.e.: τ_u), (116) adopt the form

$$\begin{aligned}\partial_t u(x, t) &= D_u \partial_x^2 u(x, t) - u(x, t) + \Theta[u(x, t) - a] - v(x, t) \\ \eta \partial_t v(x, t) &= D_v \partial_x^2 v(x, t) + \beta u(x, t) - \gamma v(x, t)\end{aligned}\quad (117)$$

where $\eta = \tau_v / \tau_u$. At this point we assume that the inhibitor is much faster than the activator (i.e.: $\tau_v \ll \tau_u$). In the limit $\eta \rightarrow 0$, we can rewrite (117) as

$$\begin{aligned}\partial_t u(x, t) &= D_u \partial_x^2 u(x, t) - u(x, t) + \Theta[u(x, t) - a] - v(x, t) \\ 0 &= D_v \partial_x^2 v(x, t) + \beta u(x, t) - \gamma v(x, t)\end{aligned}\quad (118)$$

In the last pair of equations we can eliminate the inhibitor (now *slaved* to the activator) by solving the second equation using the Green function method

$$\begin{aligned}\{-D_v \partial_x^2 + \gamma\}G(x, x') &= \delta(x - x') \\ v(x) &= \beta \int dx' G(x, x') u(x').\end{aligned}\quad (119)$$

This slaving procedure reduces our system to a *nonlocal* equation for the activator only, having the form

$$\partial_t u(x, t) = D_u \partial_x^2 u(x, t) - u(x, t) + \Theta[u(x, t) - a] - \beta \int dx' G(x, x') u(x') \quad (120)$$

From this equation, and taking into account the symmetry of the Green function $G(x, x')$, we can obtain the Lyapunov functional for this system, which has the form

$$\begin{aligned} \partial_t u(x, t) &= -\frac{\delta \mathcal{F}[u]}{\delta u} \\ \mathcal{F}[u] &= \int dx \left\{ \frac{D_u}{2} \{ \partial_x u \}^2 + \frac{u^2}{2} - (u - a) \Theta[u - a] \right. \\ &\quad \left. + \frac{\beta}{2} \int dx' G(x, x') u(x') u(x) \right\} \end{aligned} \quad (121)$$

The spatial nonlocal term in the nonequilibrium potential takes into account the repulsion between activated zones. When two activated zones come near each other, the exponential tails of the inhibitor concentration overlap, increasing its concentration between both activated zones and creating an *effective* repulsion between them, the Green function playing the role of an exponential screening between the activated zones.

We can now exploit this LF in order to discuss the stability of the stationary solutions found earlier. According to the analysis done in Drazer & Wio (1996), we can see that, obtaining the “curvature” of the potential is equivalent to diagonalizing the operator $\mathcal{F}_2[u_e]$ and finding its eigenvalues. Such an analysis is completely analogous to the linear stability one.

A very interesting point is to analyze the stability of the stationary solutions just found, as functions of the activator diffusivity. In Fig.15 we show the dependence of the LF vs. D_u for the different patterns. We see that this dependence of the LF for the different patterns; u_{e1} through u_{e4} , is compatible with the results of a linear stability analysis. A more complete analysis of this problem can be found in Drazer & Wio (1996).

5.2 Stochastic Analysis

We study here the decay of a metastable rest state under the action of external noise. The noise strength is assumed to be weak enough, assuring us that the stability of the patterns without noise is qualitatively not altered. We have previously found that there are locally stable uniform and non-uniform steady states and an unstable non-uniform state with a critical radius, which is a saddle point in the functional space. To obtain the transition probability between metastable and stable states, it is necessary to find the conditional probability for the random field $\phi(\mathbf{r}, t)$ to be in the stable state $\phi_{stable}(\mathbf{r}, t)$ at time t , given that at the initial time $t = 0$ the system was in a metastable state

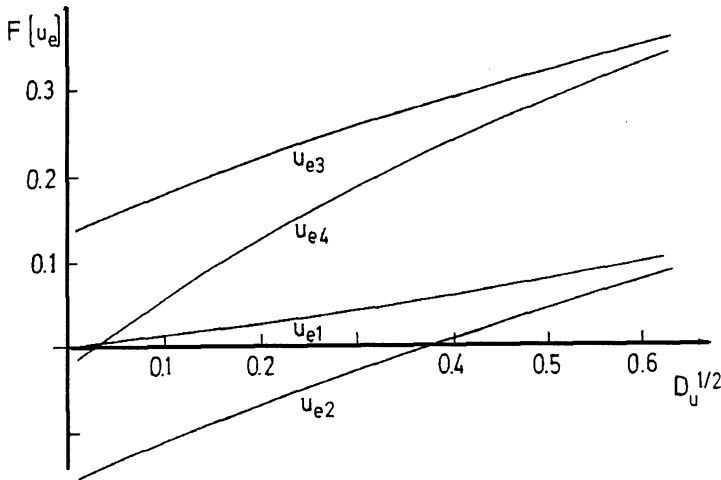


Fig. 15. Nonequilibrium potential as a function of D_u for the activator-inhibitor system with fast inhibitor. The potential for the different stationary states are indicated by its label u_{ei} , $i = 1 - 4$.

$\phi_{meta}(\mathbf{r}, 0)$. This probability can be represented by a path integral (Schulman 1981, Langouche *et al.* 1982, Wio 1990) over those realizations of the random field $\xi(\mathbf{r}, t)$ that satisfy the initial and final conditions, that is:

$$P[\phi_{stable}(\mathbf{r}, t) | \phi_{meta}(\mathbf{r}, 0)] \sim \int Q[\xi] \delta[\phi(\mathbf{r}, t) - \phi_{meta}(\mathbf{r}, 0)] \mathcal{D}\xi(\mathbf{r}, t), \quad (122)$$

where the statistical weight $Q[\xi]$ for a Gaussian white noise is:

$$Q[\xi] = \mathcal{M} e^{-\frac{1}{2\gamma} \int_0^t dt \int d\mathbf{r} \xi^2(\mathbf{r}, t)}, \quad (123)$$

where \mathcal{M} is a normalization constant. In the limit of small noise intensity ($\gamma \rightarrow 0$), the main contribution in (122) comes from those realizations of the field in the neighborhood of the most probable trajectory. Under this conditions, (122) can be estimated by the steepest-descent method.

Due to the tight space, we only outline here the approach developed by Foster & Mikhailov and Fedotov. First, it is convenient in (122) to transform the integration over the random field ξ to an integration over the realizations of the field ϕ (Foster & Mikhailov 1988, Fedotov 1993). In this case, the Lagrangian of the statistical weight results:

$$\mathcal{L}[\phi] = \int d\mathbf{r} \left\{ \frac{\partial \phi}{\partial s} + \frac{\delta F}{\delta \phi} \right\}^2, \quad (124)$$

and we obtain

$$P[\phi_{stable}(\mathbf{r}, t) | \phi_{meta}(\mathbf{r}, 0)] \sim \exp \left\{ -\frac{\mathcal{S}[\phi_{stable}(\mathbf{r}, t) | \phi_{meta}(\mathbf{r}, 0)]}{2\gamma} \right\}, \quad (125)$$

where

$$\mathcal{S}[\phi] = \inf \int_0^t ds \mathcal{L}[\phi], \quad (126)$$

The action functional $\mathcal{S}[\phi]$, taken along the most probable field realization, satisfies the Hamilton–Jacobi equation:

$$\frac{\partial \mathcal{S}}{\partial \tau} + H = 0, \quad (127)$$

where:

$$H = \int \left\{ \frac{1}{2} \left(\frac{\delta \mathcal{S}}{\delta \phi} \right)^2 - \frac{\delta \mathcal{S}}{\delta \phi} \frac{\delta F}{\delta \phi} \right\} d\mathbf{r} \quad (128)$$

with the initial condition $\mathcal{S}[\phi_{meta}(\mathbf{r}, 0), \phi_{meta}(\mathbf{r}, 0)] = 0$. For functional derivation techniques we refer to (Hänggi 1985). The Lagrangian $\mathcal{L}[\phi]$ does not contain the time explicitly, so the functional $\mathcal{S}[\phi]$ may be written as:

$$\mathcal{S}[\phi] = W[\phi] - h t \quad (129)$$

where h is a constant and $W[\phi]$ satisfies:

$$H(\phi, \frac{\delta W}{\delta \phi}) = h \quad (130)$$

with the condition $W[\phi_{meta}(\mathbf{r}), \phi_{meta}(\mathbf{r})] = 0$. As is well known, the expected transition time $\langle \tau \rangle$ is the inverse of the transition probability per unit time p_i . To find p_i it is necessary to minimize the action functional in (126) with respect to t . This gives $h = 0$, and we get for p_i

$$p_i \sim e^{-\frac{1}{2\gamma} W[\phi_{unst}(\mathbf{r}) | \phi_{meta}(\mathbf{r})]} \quad (131)$$

The solution of (126,127) (with $h = 0$) may be written as:

$$W[\phi | \phi_{meta}] = 2\{U[\phi] - U[\phi_{meta}]\} \quad (132)$$

Hence, $\langle \tau \rangle$ results to be

$$\langle \tau \rangle = \tau_0 e^{\frac{1}{\gamma} U[\phi_{unst}(\mathbf{r})] - U[\phi_{meta}(\mathbf{r})]} \quad (133)$$

The factor τ_0 is determined by the curvature of $\mathbf{U}[\phi]$ at its extrema and is negligibly short compared with the average time $\langle \tau \rangle$. This result is a generalization of Kramers formula (see Sect.3.4) for extended systems (Hänggi *et al.* 1990).

Decay Time for the Ballast System. It is of particular interest in RD systems to study the effect of the fluctuations induced by external noise, because they can produce transitions between the different metastable states. As discussed earlier, the linearly stable states correspond to attractors (minima) of the LF while the unstable ones are saddle points, defining the barrier between attractors.

In order to account for the effect of fluctuations in our model, we need to include in our time-evolution equation (111) a fluctuation term, modeled as an additive noise source, yielding a stochastic partial differential equation for the random field $T(y, t)$:

$$\partial_t T(y, t) = \partial_{yy}^2 T - T + T_h \theta(T - T_c) + \xi(y, t). \quad (134)$$

The simplest assumption about the fluctuation term $\xi(y, t)$ is that it is Gaussian white noise with zero mean value and a correlation function given by:

$$\langle \xi(y, t) \xi(y', t') \rangle = 2\gamma \delta(t - t') \delta(y - y'), \quad (135)$$

where γ denotes the noise strength. It is also possible to take into account noise sources yielding a multiplicative noise term, but we shall not consider this possibility here.

Now we will exploit the scheme developed in Sect.5.2. The behavior of $\langle \tau \rangle$ as a function of $\phi_c = T_c/T_h$ for a fixed system size is shown in Fig.16. There is a radical change in the behavior when ϕ_c oversteps a threshold value (ϕ_c^*), as indicated before, due to the change in the relative stability between the homogeneous and nonhomogeneous states. The continuous lines in the figure refer to: the decay of the metastable state towards the absolutely stable one for the line indicated with $\Delta F(\phi_s)$ up to the point ϕ_c^* , while the following line indicates the extention of the lines depicting the value of $\langle \tau \rangle$ from the original state, and viceversa for $\Delta F(\phi_0)$.

The results just obtained will be valid as long as the barrier height between the metastable and the stable states (given by the value of the LF at the unstable state) is large enough, assuring that the Kramers' like formula Eq.(133) applies.

5.3 Stochastic Resonance

We present here a brief analysis of this phenomenon in a spatially extended system by exploiting the results obtained using the notion of the *nonequilibrium potential* (Graham 1978, Graham 1987, Graham & Tel 1990, Izus *et al.* 1995, Izus *et al.* 1996, Izus *et al.* 1996, Zanette *et al.* 1995) in the ballast resistor model, as this model corresponds (to some approximation) to the continuous limit of the coupled system studied by Lindner *et al.* The study of the features of the phenomenon of stochastic resonance in the case of extended systems is still incomplete (Jüng & M.-Kress 1995), with the particularly interesting recent results of numerical simulations of arrays of

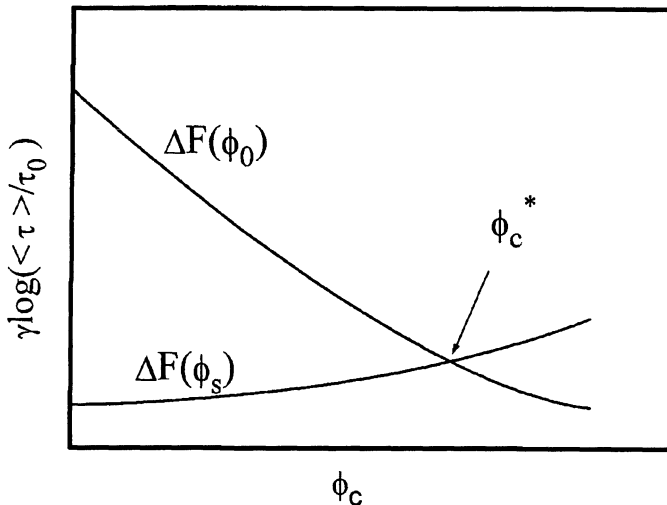


Fig. 16. $\gamma \ln(\langle \tau \rangle / \tau_0)$ vs. ϕ_c for the ballast model with Dirichlet b.c.

coupled nonlinear oscillators (Lindner *et al.* 1995, Bulsara & Gammaitoni 1996, Lindner *et al.* 1996) showing that the coupling enhances the response.

We repeat here the particular form of the (one dimensional) model that we work with

$$\frac{\partial}{\partial t} \phi = D \frac{\partial^2}{\partial x^2} \phi - \phi + \theta(\phi - \phi_c), \quad (136)$$

in the bounded domain $x \in [-L, L]$ and with Dirichlet b.c. at both ends, i.e. $\phi(\pm L, t) = 0$. As discussed earlier, we have the trivial solution $\phi_0(x) = 0$, which is linearly stable and exists for the whole range of parameters, and only one stable nonhomogeneous structure, $\phi_s(x)$, that presents a central excited zone where $\phi_s(x) > \phi_c$. Besides that, we find another similar unstable structure, $\phi_u(x)$, with a smaller central excited zone. This pattern corresponds to the saddle separating both attractors $\phi_0(x)$ and $\phi_s(x)$, see, for instance Fig.14. There are other unstable nonhomogenous solutions, but playing no role in this problem. (Schat & Wio 1992)

The indicated patterns are extrema of the LF or nonequilibrium potential of our system that reads (see Sect.5.1) (Izus *et al.* 1995, Izus *et al.* 1996, Izus *et al.* 1996, Zanette *et al.* 1995)

$$\mathcal{F}[\phi, \phi_c] = \int_{-L}^{+L} \left\{ - \int_0^\phi (-\phi + \theta[\phi - \phi_c]) d\phi + \frac{D}{2} \left(\frac{\partial \phi}{\partial x} \right)^2 \right\} dx. \quad (137)$$

In Fig.14 we show the LF $\mathcal{F}[\phi, \phi_c]$ evaluated at the stationary patterns ϕ_0 ($\mathcal{F}[\phi_0] = 0$), $\phi_s(x)$ ($\mathcal{F}^s = \mathcal{F}[\phi_s]$) and $\phi_u(x)$ ($\mathcal{F}^u = \mathcal{F}[\phi_u]$), for a system size

$L = 1$, as a function of ϕ_c and for two values of D . In the bistable zone, the upper branch of each curve is the LF for $\phi_u(x)$, where \mathcal{F} attains an extremum (as a matter of fact it is a saddle of the nonequilibrium potential). On the lower branch, for $\phi_s(x)$, and also for $\phi_0(x)$, the LF has local minima. For each value of D the curves exist up to a certain critical value of ϕ_c at which both branches collapse. It is interesting to note that, since the LF for $\phi_u(x)$ is always positive and, for $\phi_s(x)$, \mathcal{F}^s is positive for some values of ϕ_c and also $\mathcal{F}^s \rightarrow -\infty$ as $\phi_c \rightarrow 0$, \mathcal{F}^s vanishes for an intermediate value of $\phi_c = \phi_c^*$, where $\phi_s(x)$ and $\phi_0(x)$ exchange their relative stability.

In order to account for the effect of fluctuations, we include in the time-evolution equation of our model (111) a fluctuation term $\xi(x, t)$, as was discussed in Sect.5.2. We denote the noise strength with γ . According to the scheme discussed in Sect.5.2, we have the Kramers' like result for the first-passage-time $\langle \tau \rangle$ indicated in (133) that we repeat here

$$\langle \tau \rangle = \tau_0 \exp \left\{ \frac{\Delta \mathcal{F}[\phi, \phi_c]}{\gamma} \right\}, \quad (138)$$

where $\Delta \mathcal{F}[\phi, \phi_c] = \mathcal{F}[\phi_{unst}(y), \phi_c] - \mathcal{F}[\phi_{meta}(y), \phi_c]$. The prefactor τ_0 is determined by the curvature of $\mathcal{F}[\phi, \phi_c]$ at its extrema. In the Fig.16 we have shown the form of $\Delta \mathcal{F}[\phi_0, \phi_c]$ (line (b)) and $\Delta \mathcal{F}[\phi_s, \phi_c]$ (line(a)), as a function of ϕ_c . It also corresponds to the behavior of $\ln(\langle \tau \rangle / \tau_0)$.

We now assume that, due to an external harmonic variation, the parameter ϕ_c has an oscillatory part $\phi_c(t) = \phi_c^* + \delta\phi_c \cos(\Omega t + \varphi)$. For the spatially extended problem, we need to evaluate the space-time correlation function $\langle \phi(y, t)\phi(y', t') \rangle$. To do this we will use a simplified point of view, based on the two state approach of MNW (McNamara & Wiesenfeld 1989), that allows us to apply almost directly most of their results. To proceed with the calculation of the correlation function we need to evaluate the transition probabilities between our two states ϕ_0 and ϕ_s ,

$$W_{\pm} = \tau_0^{-1} \exp(-\Delta \mathcal{F}[\phi, \phi_c]/\gamma), \quad (139)$$

where

$$\Delta \mathcal{F}[\phi, \phi_c] \approx \Delta \mathcal{F}[\phi, \phi_c^*] + \delta\phi_c \left[\frac{\partial \Delta \mathcal{F}[\phi, \phi_c]}{\partial \phi_c} \right]_{\phi_c^*} \cos(\Omega t + \varphi).$$

This yields for the transition probabilities

$$W_{\pm} \approx \frac{1}{2} \left(\alpha_0 \mp \alpha_1 \frac{\delta\phi_c}{\gamma} \cos(\Omega t + \varphi) \right), \quad (140)$$

with

$$\begin{aligned} \alpha_0 &\approx \exp(-\Delta \mathcal{F}[\phi, \phi_c^*]/\gamma) \\ \alpha_1 &\approx \alpha_0 \frac{d\Delta \mathcal{F}}{d\phi_c} \Big|_{\phi_c^*}. \end{aligned} \quad (141)$$

With this identification, and using the fact that $\phi_0 = 0$, only one term remains. Hence, after averaging over the random phase φ , we end up with an expression similar to their correlation function but in which the position of their minima, $\pm c$, is replaced by $c^2 = \phi_u(x)^2$.

To obtain the generalized susceptibility $S(\kappa, \omega)$, we need to perform the Fourier transform of the correlation function in time as well as in space. Due to the fact that the space and time dependences of the correlation function factorize, $S(\kappa, \omega)$ factorizes too, and it is enough to analyze its time dependence. The Fourier transform of this time dependence yields a function analogous to the usual power spectrum function $S(\omega)$ (McNamara & Wiesenfeld 1989). Finally, the result for the SNR is

$$\text{SNR} \sim (\Lambda \lambda \gamma^{-1})^2 \exp\left(-2\Delta\mathcal{F}[\phi, \phi_c^*]/\gamma\right), \quad (142)$$

where λ is an estimation of the potential curvature at the potential minima (as given by the linear stability eigenvalue), and

$$\Lambda \sim \frac{d\Delta\mathcal{F}}{d\phi_c}|_{\phi_c^*} \delta\phi_c. \quad (143)$$

Equation (142) is analogous to what has been obtained in zero dimensional systems, but $\Delta\mathcal{F}[\phi, \phi_c^*]$ contains all the information regarding the spatially extended character of the system.

In Fig.17 we show the dependence of the present result for the SNR on γ , for typical values of the parameters (same as in Fig.16), and different values of D . It is seen that the response increases for increasing values of D . Also in Fig.16 we show the dependence of the maximum of the SNR as a function of D (that plays here the role of the coupling parameter). These results are in good qualitative agreement with recent numerical results for a system of coupled nonlinear oscillators (Lindner *et al.* 1995, Bulsara & Gammaitoni 1996, Lindner *et al.* 1996, Wio & Castelpoggi 1996).

It is worth remarking here that the present calculation breaks down for large values of D . This is due to the fact that, for increasing D , the curves in Fig.14 shift to the left while the barrier separating the attractors tends to zero. It is also worth noting that, except for the approximation involved in the Kramers' like expression in (138) and the two level approximation used for the evaluation of the correlation function, all the previous results (form of the patterns, nonequilibrium potential) are analytically exact. However, in a more careful analysis of the problem, as indicated by the present rough calculation, it seems reasonable to expect different strengths for the SR phenomena for different wave lengths, as the dependence of the generalized susceptibility $S(\kappa, \omega)$ on κ and ω –that will not necessarily factorize– also imply that $\text{SNR} \sim \text{SNR}(\kappa, \omega)$.

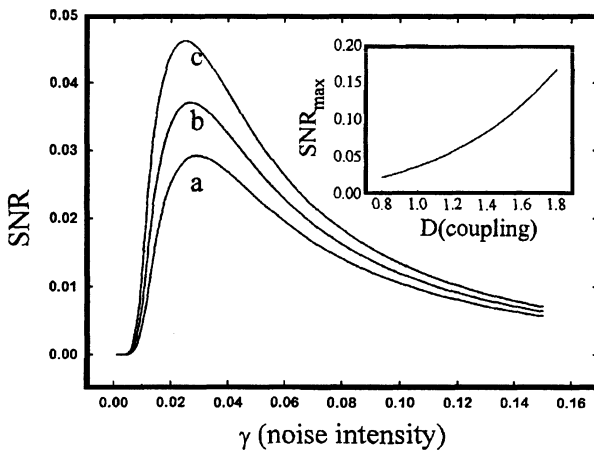


Fig. 17. SNR as a function of the noise intensity γ (Eq.(17)), for (a) $D = 0.9$, (b) $= 1.0$, (c) $= 1.1$. We fixed $\phi_c = \phi_c^*$, $L = 1$, $\delta\phi_c = 0.01$ and $\Omega = 0.01$. The insert shows the maximum of SNR as a function of D .

6 Conclusions

In this set of lectures we have presented some elements of dynamical systems, stochastic processes and reaction-diffusion models, in order to build the necessary background to face the problem of exploiting the notion of the nonequilibrium potential in extended systems. Through the knowledge of such nonequilibrium potential we have studied some simple (piecewise linear) reaction-diffusion models representing bistable systems.

Such nonequilibrium potentials have enabled us to analyze the global stability of the system and the change in the relative stability between attractors as some parameter (threshold parameter, albedo or partial reflectivity at the borders, and/or the system length) is varied. Through this Lyapunov functional, we have also computed the mean lifetime or mean first-passage time for the decay of the metastable stationary state. In this way, we have shown how some parameters or b.c. not only rule the relative stability between attractors, but also the response of the system under the effect of fluctuations.

As a novel aspect we have discussed how to exploit the previous results in order to be able to study the phenomenon of stochastic resonance in extended systems. Such studies are scarce due to the almost unsurmountable difficulties they present (Jüng & M.-Kress 1995, Wio 1996, Marchesoni *et al.* 1996, Wio & Castelpoggi 1996).

We are fairly certain that the present form of analysis could be extended to the general activator-inhibitor system and other multicomponent systems. There is strong evidence of the possibilities of obtaining the nonequilibrium potential for more general situations as shown in some recent papers (Descalzi & Graham 1992, Descalzi & Graham 1994, Izus *et al.* 1996). The possible applications in chemical and biological systems (Moss 1992, Bezrukov & Vodyanoy 1995, Collins *et al.* 1995, Wiesenfeld & Moss 1995), and their relation with spatio-temporal synchronization problems (Kuramoto 1984), are very well known.

Acknowledgements. The author thanks R. Graham, D.H. Zanette, R. Deza, E. Tirapegui, R. Toral, G. Izús, M. Kuperman, G. Drazer, F. Castelpoggi for discussions and/or collaborations, V. Grunfeld for a critical reading of the manuscript and A. Sánchez, M. Kuperman and F. Castelpoggi for their help with the figures. Partial support from CONICET, Argentina, and from Fundación Antorchas, is also acknowledged.

References

- Bulsara A.R., Chilleni S., Kiss L., McClintock P.V.E., Mannella R., Marchesoni F.V., Nicolis G., Wiesenfeld K., editors (1995): *Proc. 2nd. Int. Workshop on Fluctuations in Physics and Biology: Stochastic Resonance, Signal Processing and Related Phenomena*, Il Nuovo Cim. **D** **17**.
- Bulsara A. and Gammaconi L. (1996): Physics Today **49**, 39.
- Bezrukov S.M. and Vodyanoy I. (1995): Nature **378**, 362.
- Brink D.M., (1980): Prog. Part. & Nucl. Phys. **4**, 323.
- Castelpoggi F., Wio H.S. and Zanette D.H. (1996): Int. J. Mod. Phys. B (in press).
- Collins J.J., Chow C.C. and Imhoff T.T. (1995): Nature **376**, 236.
- Cross P.C. (1988): *Theoretical Methods in Pattern Formation in Physics, Chemistry and Biology*, in *Far From Equilibrium Phase Transitions*, Ed.L.Garrido (Springer-Verlag, Berlin).
- Cross P.C. and Hohenberg P. (1993): Rev.Mod.Phys. **65**, 851.
- Descalzi O. and Graham R. (1992): Phys. Lett. A **170**, 84.
- Descalzi O. and Graham R. (1994): Z.Phys.B **93**, 509.
- Doering C.R. (1991): *Modeling Complex Systems: Stochastic Processes, Stochastic Differential Equations and Fokker-Planck Equations*, in *Lectures in Complex Systems*, vol.III, Ed.L.Nadel and D.Stein, (Addison-Wesley, N.Y.).
- Drazer G. and Wio H.S. (1996): *Nonequilibrium potential for an activator-inhibitor model with fast inhibition*, submitted to Physica A.
- Fedotov S.P. (1993): Phys. Lett. A **176**, 220.
- Fife P.C. (1978): *Mathematical Aspects of Reacting and Diffusing Systems*, (Springer-Verlag, Berlin).
- Fife P.C. (1984): *Current Topics in Reaction-Diffusion Systems*, in *Nonequilibrium Cooperative Phenomena in Physics and Related Fields*, Ed.M.G.Velarde (Plenum, N.Y.).
- Foster A., Mikhailov A.S. (1988): Phys. Lett. A **126**, 459.

- Gardiner C.W. (1985): *Handbook of Stochastic Methods*, 2nd Ed. (Springer-Verlag, Berlin).
- Goldstein R.E., Muraki D.J. and Petrich D.M. (1996): Phys. Rev. E., to appear.
- Graham R. (1978): in *Lecture Notes in Physics*, vol. 84 (Springer-Verlag, Berlin).
- Graham R. (1987): *Weak Noise Limit and Nonequilibrium Potentials of Dissipative Dynamical Systems*, in *Instabilities and Nonequilibrium Structures*, Eds. E.Tirapegui and D.Villaroel (D.Reidel, Dordrecht).
- Graham R. and Tel T. (1990): Phys. Rev. A **42**, 4661.
- Gunton J.D. and Droz M. (1983): *Introduction to the theory of metastable and unstable states*. Lecture notes in physics vol 183, (Springer-Verlag, Berlin).
- Haken H. (1978): *Synergetics: An Introduction*, 2nd Ed. (Springer-Verlag, N.Y.).
- Hänggi P. (1985): *The Functional Derivative and its use in the Description of Noisy Dynamical Systems*, in *Stochastic Processes Applied to Physics*, Eds. L.Pesquera and M.A.Rodriguez (World Scientific, Singapore).
- Hänggi P., Talkner P. and Borkovec M. (1990): Rev. Mod. Phys, **62**, 251.
- Hassan S.A., Kuperman M.N., Wio H.S. and Zanette D.H. (1994): Physica A **206**, 380.
- Hassan S.A., Zanette D.H. and Wio H.S. (1994): J.Phys. A **27**, 5129.
- Hassan S.A. and Zanette D.H. (1995): Physica A **214**, 435.
- Hernandez-García E., Viñals J.R., Toral R. and San Miguel M. (1993): Phys. Rev. Lett. **70**, 3573.
- Hohenberg P.C. and Halperin B.I. (1977): Rev. Mod. Phys. **49**, 535.
- Horsthemke W. and Lefever R. (1984): *Noise-Induced Transitions*, (Springer-Verlag, Berlin).
- Inchiosa M.E. and Bulsara A. (1996): Phys. Rev. E **53**, R2021.
- Izús G., Deza R., Ramírez O., Wio H.S., Zanette D.H. and Borzi C. (1995): Phys. Rev. E **52**, 129.
- Izús G., Wio H.S., Reyes de Rueda J., Ramírez O. and Deza R. (1996): Int. J. Mod. Phys. B **10**, 1273.
- Izús G., Wio H.S., Zanette D.H., Deza R. and Von Haeften B. (1996): *Evolution of bistable reaction-diffusion systems within a Lyapunov functional framework*, submitted to Physica A.
- Izús G., Deza R., Wio H.S. and Borzi C. (1996): Phys. Rev. E, (in press).
- Jüng P. (1993): Phys. Reports **234**, 175.
- Jüng P. and Mayer-Kress G. (1995): Phys. Rev. Lett. **74**, 208.
- Keizer J. (1987): *Statistical Thermodynamics of Nonequilibrium Processes*, (Springer-Verlag, Berlin).
- Kerszberg M. (1983): Phys. Rev. A **28**, 1198.
- Kirkady J.S. (1992): Rep.Prog.Phys. **55**, 723.
- Koga S. and Kuramoto Y. (1980): Prog.Theor.Phys. **63**, 106.
- Kreuzer H.J. (1984): *Nonequilibrium Thermodynamics and its Statistical Foundations*, (Clarendon P., Oxford).
- Kuramoto Y. (1984): *Chemical Oscillations, Waves, Turbulence*, (Springer-Verlag, Berlin).
- Langer J.S. (1987): *Lectures in the Theory of Pattern Formation*, in *Chance and Matter*, Eds. Souletie J., Vannimenus J., Stora R. (North-Holland, Amsterdam).
- Langouche F., Roekaerts D. and Tirapegui E.(1982): *Functional Integration and Semiclassical Expansions* (D.Reidel Pub.Co., Dordrecht).

- Lindner J.F., Meadows B.K., Ditto W.L., Inchiosa M.E. and Bulsara A. (1995): Phys. Rev. Lett. **75**, 3.
- Lindner J.F., Meadows B.K., Ditto B.K., Inchiosa M.E. and Bulsara A. (1996): Phys. Rev. E **53**, 2081.
- Marchesoni F., Gamaitoni L. and Bulsara A.R. (1996): Phys. Rev. Lett. **76**, 2609.
- McNamara B. and Wiesenfeld K. (1989): Phys. Rev. A **39**, 4854.
- Malchow H. and Schimansky-Geier L. (1985): *Noise and Diffusion in Bistable Nonequilibrium Systems*, (Teubner, Berlin).
- Meinhardt H. (1992): Rep. Prog. Phys. **55**, 797.
- Mikhailov A.S. (1990): *Foundations of Synergetics I*, (Springer-Verlag, Berlin).
- Mikhailov A.S. and Loskutov A.Yu. (1992): *Foundations of Synergetics II*, (Springer-Verlag, Berlin).
- Montagne R., Hernández-García E. and San Miguel M. (1996): Physica D, **96**, 47.
- Moss F. (1992): in *Some Problems in Statistical Physics*, edited by G. Weiss (SIAM, Philadelphia).
- Moss F., Bulsara A. and Shlesinger M., editors (1993): *Proceedings of the NATO Advanced Research Workshop on Stochastic Resonance in Physics and Biology*, J. Stat. Phys. **70** No. 1/2.
- Murray J.D. (1989): *Mathematical Biology* (Springer-Verlag, Berlin).
- Newell A.C. (1989): *The Dynamics and Analysis of Patterns*, in *Complex Systems*, Ed.D.Stein, (Addison-Wesley, N.Y.).
- Nicolis G. (1986): Rep. Prog. Phys. **49**, 873.
- Nicolis G. (1989): *Physics of Far-from-Equilibrium Systems and Self-Organization*, in *The New Physics*, Ed.P.Davis, (Cambridge U.P., Cambridge).
- Nicolis G. (1995): *Introduction to Nonlinear Science*, (Cambridge U.P., Cambridge).
- Nicolis G. and Prigogine I. (1977): *Self-Organization in Nonequilibrium Systems*, (Wiley, N.Y.).
- Ohta T. (1989): Prog.Theor.Phys. **99**, 33.
- Ohta T., Mimura M. and Kobayashi K. (1989): Physica D **34**, 115.
- Ohta T., Ito A. and Tetsuka A. (1990): Phys. Rev. A **42**, 3225.
- Petrich D.M. and Goldstein R.E. (1994): Phys. Rev. Lett. **72**, 1120.
- Prigogine I. (1980): *From Being to Becoming* (W.H.Freeman, San Francisco).
- Reichl L.E. (1980): *A Modern Course in Statistical Physics*, (Univ.Texas Press. Austin).
- Risken H. (1983): *The Fokker-Planck Equation*, (Springer-Verlag, Berlin).
- San Miguel M. (1985): *Stochastic Methods and Models in the Dynamics of Phase Transitions*, in *Stochastic Processes Applied to Physics*, Eds. L.Pesquera and M.A.Rodriguez (World Scientific, Singapore).
- Schat C.L. and Wio H.S. (1992): Physica A **180**, 295.
- Schulman L.S. (1981): *Techniques and Applications of Path Integration* (Wiley, New York).
- Skocpol W.J., Beasley M.R. and Tinkham M. (1974): J. Appl. Phys. **45**, 4054.
- de la Torre M. and Rehberg I. (1990): Phys. Rev. A **42**, 2096 and 5998.
- van Kampen N. (1982): *Stochastic Processes in Physics and Chemistry*, (North Holland).
- Viñals J., Hernandez-García E., San Miguel M. and Toral R. (1991): Phys. Rev. A **44**, 1123.

- Walgraef D. (1988): *Structures Spatiales loin de l'équilibre*, (Mason, Paris).
- Weidenmüller H.A., (1980): Prog. Part. & Nucl. Phys. **4**, 123.
- Wiesenfeld K. and Moss F. (1995): Nature **373**, 33.
- Wio H.S. (1990): *Introducción a las Integrales de Camino* (Univ.Iles Balears, Palma de Mallorca, Spain).
- Wio H.S. (1994): *An Introduction to Stochastic Processes and Nonequilibrium Statistical Physics*, (World Scientific, Singapore).
- Wio H.S. (1996): Phys. Rev. E **54**, R3075.
- Wio H.S. and Castelpoggi F. (1996): *Stochastic Resonance in a Reaction-Diffusion System: Enhancement due to Coupling*, Proc.Conf.UPoN'96, Szeged, September 1996, C.R. Doering, L.B. Kiss and M. Shlesinger Editors (World Scientific, Singapore).
- Wio H.S, Izús G., Deza R., Ramírez O. and Borzi C. (1993): J.Phys.A: Math.Gen. **26**, 4281.
- Zanette D.H., Wio H.S. and Deza R. (1996): Phys. Rev. E **53**, 353.

An Introduction to the Mathematical Theory of Neural Networks

S. Albeverio^{1,2} and B. Tirozzi³

¹ Department of Mathematics, Ruhr–Universität, D 44780 Bochum (Germany).

² SFB 237, BiBoS; CERFIM (Locarno), Acc. Arch., USI (Mendrisio).

³ Dipartimento di Fisica, Università di Roma (“La Sapienza”), Piazzale Aldo Moro, I-00185 ROMA (Italy).

1 Neural Networks at Dynamical Systems

1.1 Introduction

In this lecture we present a short introduction to the theory of neural networks, in which the mathematical aspects are given special consideration. Static and dynamic aspects of models for pattern retrieval are discussed as well as a statistical mechanical treatment of the Hopfield model in the case where the number of patterns and neurons is large. As a motivation for the study of neural networks we mention the contrast between the fact that von Neumann’s type of sequential or parallel computers are quick in algorithmic computations but slow in performing recognition of patterns, whereas brains (not necessarily human brains) are comparatively slow in algorithmic computations but much quicker in performing pattern recognition. Neural networks (as “caricatures” of biological neuronal networks) are attempts to understand operationally such features of quick recognition of patterns (or signals). In fact they show some efficiency in performing “associative, adaptive memory” (as manifested in retrieval of memories and recognition of simple patterns). The methods used for their study stem from statistical mechanics and the theory of stochastic processes. This is particularly evident in the study of the Hopfield model (Hopfield 1982) to which we shall dedicate most attention in these lectures.

1.2 Some Neurobiological Inspiration

A simplified scheme for the functioning of the brain is as follows:

- 1) there is an “input”, which consists of stimuli (sounds, colours, pressure, temperature, ...)
- 2) this input is registered by the “sensors” (organs of sense: ears, eyes, skin, ...)
- 3) the sensors transmit “coded” signals in correspondence with the stimuli through electro-chemical impulses which run through the nerves

- 4) the brain (resp. the neurocontex) receives these signals, puts them in connection with “modified patterns” and transmits a response through the nerves
- 5) this response reactivates the “effectors” (e.g. muscles ...), which then yield an “output”

It should be remarked that the neurocontex is extremely folded (it corresponds to a volume of ca $0.2\text{m}^2 \cdot 0.002\text{m}$ when unfolded in space) and contains a large number (ca 10^{10}) of elementary units or neurons. Each of these present on the average ca 10^4 connections to its neighbours (which put on a line would yield a total of ca $5 \cdot 10^5\text{km}$ of connections for the entire neuron net) (cfr. e. g. Kinnebrock (1992)).

Another estimate yields $6 \cdot 10^4$ neurons on average in 1mm^2 , the dendrites in such a surface constituting a total length of ca. 8–9km.

The connections between a neuron and the “dendrites” are provided by a system of “synapses” (input into the neuron), the output of each neuron being given by a unique “axon”, which bifurcates into several dendrites which then connect with the system of synapses of the “next neuron”.

Moreover we should keep in mind the following facts:

- a) Synapses reinforce resp. inhibit the signals. The “firing/non firing” of a given neuron occurs according to “thresholds”
- b) There is a certain “localisation” and “continuity” of signals
- c) One observes the presence of certain “associative possibilities” in the whole system ...

For basic information on neuronal systems see, e. g., Amit (1989), Peretto (1992), Rojas (1993), Hecht-Nielsen (1990), Kinnebrock (1992), Ritter *et al.* (1994) and Taylor (1993).

1.3 Nets Without Back Reaction (Heteroassociative Nets)

In models of this type one imagines to have a system of two layers of neurons, the input layer and the output layer. The input layer has M neurons labeled with the index $i = 1, \dots, M$ and the output layer has N neurons with indices $j = 1, \dots, N$. To each neuron there is associated an “activity variable” e , taking only 2 values, ± 1 , +1 for “firing” and -1 for “non firing”. The action of the i -th synapse ($i = 1, \dots, M$) on the j -th neuron ($j = 1, \dots, N$) is given by multiplication by the real factor w_{ij} (“synaptic potential” between neurons j and i). To the synapse i there is also associated a real number θ_i , the “threshold number”. So to the input M -tuple (vector) $e = (e_1, \dots, e_M) \in \{\pm 1\}$ there is associated by the action of the synapses an output “ N -tuple (vector)” $we \in \mathbb{R}^N$ s. t. $(we)_j = \sum_{k=1} w_{jk} e_k$, $i = 1, \dots, N$. We introduce an output vector $a = (a_1, \dots, a_N) \in \{\pm 1\}^N$ determined by the input and the threshold vector $\theta = (\theta_1, \dots, \theta_M)$, by the prescription that $a_j = 1$ (interpreted as i is

“firing”) if $we > \theta$ (in the sense that $(we)_j > \theta_j \forall j = 1, \dots, N$) and $a_j = -1$ (interpreted as j is “non firing”) if $we \leq \theta$.

Thus we have (for the passage from time n to time $n + 1$, i. e. for e the configuration of activities of the neurons of the input layer at time n and for a the configuration of activities of the output layer at time $n + 1$)

$$a = f(we - \theta) \quad (1)$$

in the sense that

$$a_j = f\left(\sum_{k=1} w_{j,k} e_k - \theta_j\right), \quad j = 1, \dots, N$$

$$f(x) \equiv \text{sign}x \equiv \begin{cases} 1 & x > 0 \\ -1 & x \leq 0 \end{cases}$$

f is called the “binary transfer function”.

Remarks

a) We have $\frac{1}{2}(f + 1) = H$, with H the Heaviside function:

$$H(x) = \begin{cases} 1 & x > 0 \\ 0 & x \leq 0 \end{cases}$$

b) f is sometimes more conveniently replaced by $f_{\text{sign}}(x) \equiv \frac{2}{1+e^{-cx}} - 1$, $c > 0$. We observe that $|f_{\text{sign}}| \leq 1$, $f_{\text{sign}}(0) = 0$, $f_{\text{sign}}(x) \rightarrow 1$ as $x \rightarrow +\infty$, $f_{\text{sign}}(x) \rightarrow -1$ as $x \rightarrow -\infty$.

We also remark that (1) can be written as

$$a = f(\tilde{w}(\tilde{e})) \quad (1)'$$

when we introduce $\tilde{e} \equiv (e_0, e)$, $e_0 = 1$, $\tilde{w}_{i,j} = w_{i,j}$, $i = 1, \dots, M$, $j = 1, \dots, N$, $\tilde{w}_{0,j} \equiv -\theta_j$, $j = 1, \dots, N$. The general problem one is faced when studying such models is to find w (or, equivalently, \tilde{w}) to obtain a wanted output a starting from a given input e (and threshold θ). Variations of w are seen as “learning rules” for w .

Some brief historical notes. Precursors of the models mentioned above are the “mathematical neurons” as “logical threshold elements” (with no variation of w) by W. S. McCulloch, W. Pitts and N. Wiener (ca. 1943, at MIT). The psychologist D. Hebb introduced in 1949 the “learning rule” (now called “Hebbian rule”) $\delta w_{i,j} = \sigma e_i a_j$, $\sigma > 0$ (variation δw of w proportional to the “presynaptic activity” e_i and the “postsynaptic activity” a_j) This is more often modified, in applications, into the “delta rule” (of Widrow-Hoff):

$$\delta w_{i,j} = \sigma e_i \delta a_j.$$

(which thus replaces a_j by its variation δa_j).

In 1954 B. C. Cragg and H. V. Temperley realized that there is an analogy of above systems of neurons with systems of “magnetic moments”.

In 1958 F. Rosenblatt introduced a random version of above setting (1) (resp. (1)'), accompanied with the “delta rule”, as the “perceptron model” of “supervised learning”. In this model one starts with a random input vector e , one introduces random couplings w , getting random outputs a , to be compared with the wanted outputs a^{wanted} .

If $a = a^{\text{wanted}}$ the procedure ends, if $a \neq a^{\text{wanted}}$, w is corrected according to the δ rule (with $\delta a_j = a_j^{\text{wanted}} - a_j$).

In 1969 Minsky and Papert showed that not all logical functions are representable by such methods; but if a logical function is representable by such methods, then convergence of the procedure to the wanted result happens in finitely many steps. In fact one shows that $\Phi(w) \equiv \frac{1}{2} \sum_i (\delta a_i)^2$ acts as a Ljapunov function; for $f = f_{\text{sign}}$, one has $\delta \Phi \leq 0$, with an absolute minimum of Φ for $\delta a_i = 0$.

Incidentally there is no difficulty in representing any logical function if instead of “one layer” (e, a) one considers “multilayers configurations” (see e. g. Kinnebrock (1992)).

E.g. for the a 2-steps back propagation algorithm $\delta w_{i,j}^1 = \alpha \delta a_i h_j$ (with an “hidden level” h_1, \dots, h_N , between e and a), $\delta w_{i,j}^2 = \alpha \sum_m e_m w_{m,i}^1 e_j$, $\alpha > 0$, see Kinnebrock (1992), one can show that $\delta \Phi \leq 0$ with Φ as above.

Other types of neural networks will be discussed in the next subsection.

1.4 Models with Back Reaction (Autoassociative Nets)

Such models were introduced by W. A. Little (1974) and J. J. Hopfield (1982) (the latter in analogy with the “spin glass” models in statistical mechanics).

In models with back reaction there is no longer an input/output distinction (variables e, a) but rather a “feedback” for the input variable e . Thus $N = M$ and the vector of neural activities is the collection of $z_i = \pm 1$ for $i = 1, \dots, N$. The matrix (w_{ij}) , $i, j = 1, \dots, N$ is then interpreted as connection matrix, the element w_{ij} describing the connection between e_i and e_j . One usually extends the indices in w to $0, \dots, N$, by setting $w_{ll} = 0$, $\forall l = 0, \dots, N$, $\theta_0 \equiv -1$, $w_{i0} = 0$, $i = 1, \dots, N$, $w_{0j} = -\theta_j$, $j = 0, \dots, N$ and one assumes the important symmetry condition

$$w_{ij} = w_{ji}, \quad i, j = 0, \dots, N.$$

One introduces the synchronous (φ_s) resp. asynchronous (φ_{as}) dynamics (in the sense of discrete dynamical systems) given through

$$t \in \mathbb{N}_0 \equiv \mathbb{N} \cup \{0\}$$

$$t = 0 \quad : \quad z(0) \equiv z \in E$$

$$t \in \mathbb{N} : z(t) \equiv \varphi(z(t-1))$$

with

$$\varphi = \varphi_s \text{ resp. } \varphi = \varphi_{as},$$

with

$$\varphi_s(z) \equiv (f(wz)_1, \dots, f(wz)_n);$$

$$\varphi_{as}^{(a)} \equiv (z_1, \dots, z_{a_{n-1}}, f(wz)_{a_n}, z_{a_{n+1}}, \dots, z_N)$$

with

$$f = \text{sign.}$$

$a \equiv (a_n)_{n \in \mathbb{N}}$, with $a_n = k$, infinitely often, $\forall k = 1, \dots, N$ stands for a given sequence of numbers (on which the asynchronous dynamics depends). Explicitly we have thus for the synchronous dynamics:

$$z_i(t) = f\left(\sum_{j=1}^N w_{ij} z_j(t-1) - \theta_i\right), \quad i = 1, \dots, N$$

and for the asynchronous dynamics

$$z_i(t) = z_i(t-1) \quad \text{for } i \leq a_{n-1}, \quad \text{and } i \geq a_{n+1}$$

$$z_{a_n}(t) = f\left(\sum_{j=1}^N [w_{a_n j} z_j(t-1) - \theta_j]\right)$$

Remark

- a) This way of describing the asynchronous dynamics has been introduced in Ay (1996), where a_n is called an “actualization sequence”. If there exists an i. i. d. system (independent, identically distributed) random variables $X_n(\omega), n \in \mathbb{N}$ s.t. $a_n = X_n(\omega)$ (ω being a point in a probability space), and $P(X_n = k) > 0 \forall k = 1, \dots, N$ then one has (using the Borel-Cantelli-Lemma) that $a_n = k$ infinitely often.
- b) Recently Malyshev & Spieksma (1997) generalized the approach described above, and discussed in Procesi & Tirozzi (1989), introducing a stochastic dynamic instead of the deterministic one defined in (1), the randomness being introduced by setting $a_j = \pm 1$ with probability $(1/2, 1/2)$ in the case $(we)_j = \theta_j$, they were able to prove that also in this case the dynamics obtained in the limit $N = M$ large is deterministic.

A network with such connections and dynamics is called an *Hopfield-type model* (with synchronous resp. asynchronous dynamics)

Exercise: Compute $z(t)$ under the synchronous dynamics for

$$w = \begin{pmatrix} 0 & 1 & 1 \\ 1 & 0 & 1 \\ 1 & 1 & 0 \end{pmatrix}, \quad z(0) = \begin{pmatrix} 1 \\ -1 \\ 1 \end{pmatrix}, \quad \theta = 0.$$

Solution: $z(1) = f(wz(0))$, with $wz(0) = \begin{pmatrix} 0 \\ 2 \\ 0 \end{pmatrix}$ i. e. $z(1) = (f(0), f(2), f(0)) = (-1, 1, -1)$ (where we need the definition of f) In a similar way we get $z(2) = (-1, -1, -1)$. From this we then obtain easily

$$z(3) = f \left(w \begin{pmatrix} -1 \\ -1 \\ -1 \end{pmatrix} \right) = f \begin{pmatrix} -2 \\ -2 \\ -2 \end{pmatrix} = \begin{pmatrix} -1 \\ -1 \\ -1 \end{pmatrix} = z(2)$$

and similarly $z(n) = z(2) \forall n \geq 2$.

1.5 Recalling Some Notions of the Theory of Dynamical Systems

Let E be a “state space”, $z \in E$ be a “state”. A family of maps $\varphi_t : E \rightarrow E$, $t \in I \equiv \mathbb{N}_0 \equiv \mathbb{N} \cup \{0\}$ (or $I = \mathbb{Z}$) is called a “discrete time dynamical system”.

$z \equiv (z(t), t \in I)$, with $z(t)$ determined in terms of the initial value $z(0) \equiv z$ and φ_t by $z(t) \equiv \varphi_t(z(t-1))$, $t \in I \setminus \{0\}$, is called a “process” or “dynamical system”. $z(t)$ is the state of the process “at time t ”. If $z(t) = z(0) = z \forall t \in I$ one says that z is a stable or invariant point.

Remark: If $\varphi_t = \varphi_1 \forall t \in \mathbb{N}$ we have $z(t) = (\varphi_1 \circ \dots \circ \varphi_1) z \equiv \varphi_1^t z$, $t \in \mathbb{N}$. $\varphi_1^0 = \text{identity}$, $\varphi_1^t \equiv \Phi(t)$ is a semigroup indexed by $I = \mathbb{N}_0 \equiv \mathbb{N} \cup \{0\}$ in the sense that $\Phi(t) \circ \Phi(s) = \Phi(t+s) \forall s, t \in I$. One has z stable $\iff \varphi_1 z = z$ i. e. z is a fixed point of φ_1 (or Φ).

In the general theory of dynamical systems one studies the behaviour of $z(t)$ for $t \rightarrow \infty$, trying to determine the “attractors”. E. g. one says that there exists a “one point attractor” $z(\infty) \in E$ if $z(t) \rightarrow z(\infty)$ as $t \rightarrow \infty$, independently of the initial condition $z(0)$ (this is e. g. the case when the dynamics is given by the classical mechanics of a “damped pendulum”).

One says that one has a k -points attractor if $z(t)$, $t \rightarrow \infty$, converges to $z^j(\infty)$, $j = 1, \dots, k$, where $z^j(\infty)$ depends on the initial point $z(0)$.

By definition one calls basin of attraction $B(\infty)$ of the attractor a subset $B(a)$ of E such that $z(0) \in B(a)$ implies $z(t) \rightarrow a$ for $t \rightarrow \infty$

1.6 The Energy in the Hopfield Model

In this section we closely follow Ay (1996). One shows that the attractors in Hopfield models (as defined in section I.4) possess an interesting structure which makes such models suitable for modelling “associative features”, at least below a certain threshold (there exists thus a “critical capacity” which makes that the requirement of too much association for the models brings about its collapse). To discuss this, let us introduce some definitions: one calls *fixed points of the Hopfield dynamics* the solutions of $e = \varphi(we)$, $e \in \theta$. Let \mathcal{F} be the set of all fixed points.

Remark: If $\theta = 0$ and $e \in \mathcal{F}$ then also $-e \in \mathcal{F}$ (since $-e = -\varphi(we) = \varphi(-we)$, by the definition of φ : but

$$\varphi(-we) = \varphi(w(-e)) \quad \text{qed.}$$

By I.15 we have thus that \mathcal{F} coincides with the set of stable points of the Hopfield dynamics.

One interprets the points of \mathcal{F} as “patterns to be learned” (by adjustments of the w)

One has the following characterization of \mathcal{F} , for the synchronous dynamics:

Proposition 1:

$$z \in \mathcal{F} \Rightarrow z_i \sum_j w_{ij} z_j \geq \theta_i z_i \quad \forall i = 1, \dots, N \quad (2)$$

If $z \notin \mathcal{E} \equiv \{y \in E | wy = \theta, y > 0\}$ then the converse also holds, i. e. (2) implies $z \in \mathcal{F}$

Proof: “ \Rightarrow ” Let $z \in \mathcal{F}$ then $\varphi(z) = z$ By the definition of $\varphi = \varphi_s$ this means that $z_i = +1 \rightarrow \sum_j w_{ij} z_j > \theta_i$ and $z_i = -1 \rightarrow \sum_j w_{ij} z_j \leq \theta_i$, hence 2) holds, which proves \Rightarrow .

Assume conversely that (2) holds for some $z \notin \mathcal{E}$. This implies $z_i = 1 \rightarrow \sum_j w_{ij} z_j \geq \theta_i$ and since $z \notin \mathcal{E}$ this implies $\sum_j w_{ij} z_j > \theta_i$. If however $z_i = -1$ then by 2) we get $\sum_j w_{ij} z_j \leq \theta_i$, hence, since $z \notin \mathcal{E}$, $\sum_j w_{ij} z_j < \theta_i$, thus in both cases:

$$\begin{aligned} z_i &= f(\sum_j w_{ij} z_j - \theta_i) \quad \text{i.e.} \\ z &= \varphi(z) \text{ i.e. } z \in \mathcal{F}. \end{aligned}$$

□

Definition 1: One calls energy function for the Hopfield models we consider the functional $H : E \rightarrow \mathbb{R}$ given by

$$\begin{aligned} H(z) &= -\frac{1}{2} \sum_{i,j} w_{ij} z_i z_j + \sum_i \theta_i z_i \\ &= -\frac{1}{2} z \cdot w z + \theta z. \end{aligned}$$

Definition 2: The *Hamming distance* on E is defined by

$$d(z^1, z^2) \equiv \frac{1}{2} \sum_{j=1}^N |z_j^1 - z_j^2|,$$

$$z^1, z^2 \in E$$

One shows that it satisfies the axioms of a distance function, hence it defines a metric on E .

Remark: z and $\hat{z}^{(k)} \equiv (z_1, \dots, z_{k-1}, -z_k, z_{k+1}, \dots, z_N)$ are nearest neighbours in this metric, since

$$d(z, \hat{z}^{(k)}) = \frac{1}{2} |2z_k| = |z_k| = 1.$$

Definition 3: $z \in E$ is said to be “ k -place local minimum” of H if

$$H(z) \leq H(\hat{z}^{(k)}),$$

z is said to be a “ k -place isolated local minimum” of H if

$$H(z) < H(\hat{z}^{(k)}).$$

Proposition 2: Let H be defined as above then for any $z \in E$, $k \in \{1, \dots, N\}$

$$H(\hat{z}^{(k)}) - H(z) = 2z_k \sum_j w_{kj} z_j - 2\theta_k z^k. \quad (3)$$

Proof: Let $\delta H(z) \equiv H(\hat{z}^{(k)}) - H(z)$. From the definition of H , $\hat{z}^{(k)}$ we see that

$$\begin{aligned} \delta H(z) &= -\frac{1}{2} \sum_{\substack{i,j \\ i,j \neq k}} w_{ij} z_i z_j \\ &\quad - \sum_j w_{kj} (-z_k) z_j - \sum_i w_{ik} z_i (-z_k) \\ &\quad + \sum_{i \neq k} \theta_i z_i - \theta_k z_k \end{aligned}$$

$$\begin{aligned}
& + \frac{1}{2} \sum_{\substack{i,j \\ i,j \neq k}} w_{ij} z_i z_j + \sum_j w_{kj} z_k z_j \\
& + \sum_i w_{ik} z_i z_k - \sum_{i \neq k} \theta_i z_i - \theta_k z_k,
\end{aligned}$$

which is equal to the right hand side of (3) \square

Corollary 1: z is a k -place local minimum of H

$$\iff z_k \sum_i w_{kj} z_j \geq \theta_k z_k \quad (4)$$

One can add “isolated” local minimum iff $>$ holds in (4).

Proof: This follows easily from the definition of (isolated) local minimum and Prop. 2. \square

Definition 4: A solution of the Hopfield Φ -dynamics

$$z(t) = \Phi(t)z(0)$$

is said to be “ k th place stable” if $z_k(1) = z_k(0)$.

Corollary 2: z is k th place stable with respect to the synchronous Hopfield dynamics \Rightarrow

$$z_k(0) \sum_j w_{kj} z_j(0) \geq \theta_k z_k(0) \quad (5)$$

Conversely (5) and $z(0) \notin \mathcal{E}$ imply that z is k th place stable with respect to the synchronous Hopfield dynamics.

Remark: Corollary 2 holds also for a_n asynchronous dynamics with k -stable replaced by stable and (5) holding for all k .

Proof of Corollary 2: k th place stable $\iff z_k(1) = z_k(0)$ (by definition). This means $z_k(0) = \pm 1 \implies z_k(1) = \pm 1 \implies (5)$ (by the definition of the dynamics

$$z_k(1) = \Phi(z_k(0)) = f \left(\sum_j w_{kj} z_j(0) - \theta_k \right),$$

Vice versa (5) implies for $z_k(0) = -1$ that $\sum_j w_{kj} z_j(0) \leq \theta_k$, hence $z_k(1) = -1$. In case $z_k(0) = +1$, we have by (5) $\sum_j w_{kj} z_j(0) \geq \theta_k$ and since $z(0) \notin \mathcal{E}$ for this it follows $z_k(1) = 1$. Thus z is k th place stable as for the asynchronous dynamics, it suffices to take $k = a_n$ and then proceed as above. \square

Remark: One has: z stable respect to *some* $(a_n)_{n \in \mathbb{N}}$ asynchronous dynamics $\iff z$ stable resp. *all* asynchronous dynamics \implies (5) holds for all k . Viceversa if (5) holds for all k and $z(0) \notin \mathcal{E}$, then z is stable resp. all asynchronous dynamics.

Proof: Exercise. □

Remark: Since the range of values of any sequence $\{a_n\}_{n \in \mathbb{N}}$ is, by definition, the whole set $\{1, \dots, N\}$, one has that the set of values of $\Phi_{as}^{(a_n)}$ is also $\{1, \dots, N\}$. This implies that the set \mathcal{F} of stable points for an asynchronous dynamics is independent of the chosen sequence $(a_n)_{n \in \mathbb{N}}$.

From Corollary 1 and Corollary 2 we have then

Theorem 1 If a solution $z(t)$, $t \in \mathbb{N}$ of the Hopfield synchronous dynamics is k th place stable then $z(0)$ is a k th place local minimum of H . Viceversa: If $z(0)$ is k th place local minimum of H and $z(0) \notin \mathcal{E}$ then the corresponding $z(t)$, $t \in \mathbb{N}$ is k th place stable.

The corresponding statements hold for any a_n -asynchronous dynamics where k -place stable is replaced by stable and then $z(0)$ is k th place local minimum of H for all k . ■

For the a_n -asynchronous dynamics we also have

Theorem 2: If there exists an $n \in \mathbb{N}$ so that $z(n) = \Phi_{as}^{(a)}(z(n-1)) \neq z(n-1)$ then $H(z(n)) < H(z(n-1))$ except for $z_{a_n}(n-1) = +1$ and

$$\sum_j w_{a_n j} z_j(n-1) = \theta_{a_n}.$$

Proof: $z(n) \neq z(n-1)$ implies, by the definition of $\Phi_{as}^{(a)}$

$$f \left(\sum_j w_{a_n j} z_j(n-1) - \theta_{a_n} \right) \neq z(n-1)$$

This means that $z(n-1) = +1 \implies \sum_j w_{a_n j} z_j(n-1) - \theta_{a_n} \leq 0$, and: $z(n-1) = -1 \implies \sum_j w_{a_n j} z_j(n-1) - \theta_{a_n} > 0$. By proposition 2 this implies

$$H(z(n)) = H(\hat{z}^{(a_n)}(n-1)) < H(z(n-1))$$

□

Remark: The separate discussion of the exceptional case $z(0) \in \mathcal{E}$ in all above considerations can be avoided by replacing f in the definition of the dynamics by $\tilde{f}_{z(0)}$ defined by

$$\tilde{f}_{z(0)}(\lambda_k) = \begin{cases} 1 & \lambda_k > 0 \\ z_k(0) & \lambda_k = 0 \\ -1 & \lambda_k < 0 \end{cases}$$

This is discussed and explained in Ay (1996).

Theorem 3: Consider the Hopfield model with an a_n -synchronous dynamics. Then for any $z(0) \in E$ there exists a unique $n_{z(0)} \in \mathbb{N}$ s. t. in $\{z(0), \dots, z(n_{z(0)})\}$ only $z(n_{z(0)})$ is stable.

Proof: If $z(0)$ is stable then $n_{z(0)} = 0$. If $z(0)$ is not stable, we consider

$$M = \{m \in \mathbb{N} \mid z(m) \neq z(m-1)\}$$

Then $M \neq \emptyset$. For $m \in M$ we have

$$z(m) \neq z(m-1)$$

On the other hand $z(m) = \Phi_{as}^{(a)}(z(m-1))$, and thus by Theorem 2.

$$H(z(m)) < H(z(m-1)).$$

But since H is lower bounded, this implies that M is a finite set. Set $n_{z(0)} \equiv \max M$. Then

$$z(n) = z(n_{z(0)}) \quad \forall n > n_{z(0)}$$

by the definition of M and $n_{z(0)}$. This is however easily seen to be equivalent to $z(n_{z(0)})$ stable. We now prove that $z(0), \dots, z(n_{z(0)} - 1)$ are not stable. Assume ad absurdum that $n < n_{z(0)}$ and $z(n)$ is stable. Then

$$z(n) = z(n+1) = \dots = z(n_{z(0)})$$

By the definition of M it follows then that $n_{z(0)} \notin M$, which is a contradiction. \square

Define the map $\psi : E \rightarrow \mathcal{F}$ by $z \mapsto \psi(z) = z(n_z)$. Then ψ is the identity on \mathcal{F} . We introduce ψ -equivalence classes in E by saying $z \sim z'$ (z ψ -equivalent to z') iff $\psi(z) = \psi(z')$.

It is easily seen that this is an equivalence relation, hence we can introduce corresponding equivalence classes. Let $[z]$ by the equivalence class of z . To it there is bijectively associated $z(n_z)$, as the unique stable representative of $[z]$. It would be interesting to study in general the basin of attraction of the Hopfield model. We can determine it when w are chosen in a special Hebbian way, according to the following:

Theorem 4: Consider the Hopfield model with only one pattern ($p = 1$) and $\theta = 0$; $w_{ij} \equiv \begin{cases} \frac{1}{N}s_i s_j & i \neq j \\ 0 & i = j \end{cases}$, with $s = (s_1, \dots, s_N) \in E$ (“given pattern”). Then for any a -asynchronous dynamics this model has the patterns equal to $\pm s$ as the only stable points and attractors. The corresponding basins of attractions are described as follows: if $z(0) = z$ then

$$\begin{aligned} d(z, s) < \frac{N}{2} \rightarrow n_z &\equiv \text{Min}\{n \in \mathbb{N}_0 \\ z_i \neq s_i \rightarrow i \in \{a_1, \dots, a_n\} \} &\equiv n^+ \\ z(n_z) &= s \\ d(z, s) > \frac{N}{2} \rightarrow n_z &\equiv \text{Min}\{n \in \mathbb{N}_0 \\ z_i = s_i \rightarrow i \in \{a_1, \dots, a_n\} \} &\equiv n^- \\ z(n_z) &= -s \end{aligned}$$

$$d(z, s) = \frac{N}{2} \text{ if}$$

$$\begin{cases} z_{a_1} \neq s_{a_1} \\ z_{a_1} = s_{a_1} \end{cases} \quad \text{then} \quad n_z = \begin{cases} n^+ \\ n^- \end{cases} \quad z(n_z) = \begin{cases} s \\ -s \end{cases}$$

Proof: (sketch): That $\pm s$ are stable (for both synchronous and asynchronous dynamics) can easily be seen:

$$f(\sum_k w_{ik} s_k) = f\left(\frac{1}{N} \sum_k s_i s_k s_k\right) = f(s_i) = s_i$$

(where we used $s_k^2 = 1$ and $f = \text{sign}$). The rest follows by a detailed analysis, which is left as an exercise. \square

Exercise:

$$N = 4, \quad s = \begin{pmatrix} 1 \\ -1 \\ -1 \\ 1 \end{pmatrix}$$

In this case we see that by the above choice of w we get a “landing” of $z(o) = \begin{pmatrix} 1 \\ 1 \\ -1 \\ 1 \end{pmatrix}$ after only 1 step into s (“recognition of the pattern s in one step”).

We shall now present some results for the *case of p -patterns*

Let s^μ ; $\mu = 1, \dots, p$ be given patterns. Consider that Hopfield model with the Hebbian rule of the form:

$$w_{ij} = \begin{cases} \frac{1}{N} \sum_{\nu=1}^p s_i^\nu s_j^\nu & i \neq j \\ 0 & i = j \end{cases} \quad i, j = 1, \dots, N \quad (6)$$

\square

Exercise: Show that for $\theta = 0$, N even, p odd, one has $\sum w_{ij}z_j(t) \neq 0 \quad \forall t \in \mathbb{N}_0$, so in this case H has only isolated local minima i. e. isolated attractors for any asynchronous dynamics, under the above assumptions.

Remark: By the above Hebbian choice of w we have

$$\begin{aligned} s_i^\mu \sum_j w_{ij} s_j^\mu &= \frac{1}{N} \sum_j \sum_{\nu=1}^p s_i^\mu s_i^\nu s_j^\nu s_j^\mu - \frac{p}{N} \\ &= (1 - \frac{p}{N}) + \frac{1}{N} \sum_j \sum_{\nu=1, \nu \neq \mu}^p s_i^\mu s_i^\nu s_j^\nu s_j^\mu \end{aligned} \quad (7)$$

(the term $\frac{p}{N}$ coming from the $i = j$ contribution to the l. h. s. of the first equality; the contribution for $\nu = \mu$ on the r. h. s. of the first equality gives 1)

By (7) using the criterium for stability we easily get:

Theorem 5: For $\alpha \equiv \frac{p}{N} < 1$ and $s^\mu s^\nu = 0$, $\nu \neq \mu$ the Hopfield dynamics (with Hebbian rule (6) and $\theta = 0$) has s^μ as stable point ■

Remark: For α small and s^μ “almost orthogonal” to s^ν for $\nu \neq \mu$ one also expects stability of s^μ .

Exercise: Prove:

1. If there exists patterns s^μ , $\mu = 1, \dots, N$ with $s^\mu s^\nu = 0$, $\mu \neq \nu$, then all states are stable.
2. For $N \geq 5$, $p = 5$, $s_i^\mu = 1$, $i \neq \mu$, $s_\mu^\mu = -1$, the only stable states are

$$z_i = 1 \quad \forall i = 1, \dots, N$$

and

$$z_i = -1 \quad \forall i = 1, \dots, N.$$

Remark: Further results on the nature of the attractors in Hopfields and other models can be found e. g. in the books Amit (1989), Peretto (1992), and in Procesi & Tirozzi (1989), Newman (1988), Ay (1996), Talagrand (1996b).

2 Statistical Mechanical Methods

2.1 The Case of the Hopfield Dynamics at Temperature Zero

We consider again the Hopfield dynamics described in sect. 1, but now with the aim of exploiting the fact that in many applications the number N of neurons is big, so that taking the limit $N \rightarrow \infty$ can be expected to be a good approximation.

Let $\xi^\mu \equiv \{\xi_i^\mu\}$, $i = 1, \dots, N$, $\mu = 1, \dots, p$ be given “random patterns”, e. g. identically and independently distributed ± 1 -valued random variables (i. i. d.), each with Bernoulli symmetric $(\frac{1}{2}, \frac{1}{2})$ -distribution (i. e. $P(\xi_i^\mu = \pm 1) = \frac{1}{2}$) (we use the notation ξ^μ instead of the previous notation s^μ to underline the fact that the ξ^μ are random).

We assume the weight matrix $w = ((w_{ij}))$ is taken as before according to the Hebbian rule. We consider the Hopfield synchronous dynamics with $\theta = 0$, initial value $z(0) = \xi^\mu \varepsilon$, with $\varepsilon = (\varepsilon_i)$, $i = 1, \dots, N$ and $\varepsilon_i = \pm 1$ -valued Bernoulli $(1 - q, q)$ -distributed i. i. d. random variables, i. e. $P(\varepsilon_i = +1) = 1 - q$, $P(\varepsilon_i = -1) = q$, with $0 \leq q < \frac{1}{2}$.

A theorem of the following type can be proven in a simple way:

Theorem 6: If $p = p(N)$, $N \rightarrow \infty$ is such that

$$\sum_N \frac{p(N)^2}{N^2} < \infty,$$

then the solution $z(t)$ of the above Hopfield dynamics satisfies

$$\lim_{N \rightarrow \infty} z(1) = \xi^\mu \quad \text{a. s.}$$

Corollary: The given random patterns ξ^μ are stable points of the Hopfield dynamics and $z(t) \rightarrow \xi^\mu$ a. s. as $N \rightarrow \infty$ and then $t \rightarrow \infty$ (for more details see e. g. Tirozzi (1995) and references therein).

Sketch of the Proof: Consider e. g. the case $\mu = 1$ with dynamics given by f_{sign} (instead of f). The dynamics is thus given by

$$\begin{aligned} z_i(1) &= f_{\text{sign}} \left(\sum_{j \neq i} w_{ij} z_j(0) \right) \\ &= f_{\text{sign}} \left(\sum_{j \neq i} \frac{1}{N} \sum_\mu \xi_i^\mu \xi_j^\mu z_j(0) \right) \end{aligned} \tag{1}$$

Splitting the argument of f_{sign} into a contribution for $\mu = 1$ and one for $\mu \neq 1$ we obtain that the right hand side is equal $f_{\text{sign}}(A_i^{(N)} + R_i^{(N)})$, with

$$\begin{aligned} A_i^{(N)} &\equiv \frac{1}{N} \sum_{j \neq i} \xi_i^1 \xi_j^1 z_j(0) \\ R_i^{(N)} &\equiv \frac{1}{N} \sum_{j \neq i} \sum_{\mu \neq 1} \xi_i^\mu \xi_j^\mu z_j(0). \end{aligned}$$

But

$$R_i^{(N)} \xrightarrow[N \rightarrow \infty]{} 0 \quad \text{a. s.} \tag{2}$$

(since, e. g. $E(|R_i^{(N)}|^4) = 3 \left(\frac{p(N)^2}{N^2} + \frac{p(N)}{N^3} \right)$, by an easy calculation), hence, using the assumption on $p(N)$:

$$\sum_N E \left[|(R_i^{(N)})|^4 \right] < \infty;$$

(2) follows then by the Tschebycheff inequality and Borel-Cantelli's Lemma). Moreover, using $z_j(0) = \xi_j^1 \varepsilon_j$ we see that

$$A_i^{(N)} = \frac{1}{N} \xi_i^1 \sum_{j \neq i} \varepsilon_j \xi_j^1 \xi_j^1,$$

which, using $(\xi_j^1)^2 = 1$, yields

$$\frac{1}{N} \xi_i^1 \left[\sum_{j=1}^N \varepsilon_j - \varepsilon_i \right] \xrightarrow[N \rightarrow \infty]{} \quad (3)$$

$$\xi_i^1 E(\varepsilon_1) = \xi_i^1 (1 - 2q),$$

where in the convergence and limit we have used that the ξ_i are i. i. d. with the $(1 - q, q)$ -Bernoulli distribution. Thus from (1), (2), (3) using that f_{sign} is a continuous function, we get

$$z_i(1) \xrightarrow[N \rightarrow \infty]{} f_{\text{sign}}(\xi_i^1 (1 - 2q)),$$

a.s. Using $q < \frac{1}{2}$ and the definition of f we then get the statement in the theorem by a limiting argument. \square

Remark: The assumption on $\alpha(N) \equiv p(N)/N$ for $N \rightarrow \infty$ are not optimal. Moreover there exist estimates on the value of α such that the patterns are fixed points of the dynamics; see for example work by C. Newman (Newman (1988)) for $\frac{p(N)}{N} \leq \alpha_c$, $\alpha_c \geq 0.05$ and by D. Loukianova (Loukianova (1994a); Loukianova (1994b)), where $\alpha_c \geq 0.07$.

Feng & Tirozzi (1997) have found, using extreme value theory, a formula connecting the percent of errors in the retrieval process with the capacity α which coincides with the formula found by Amit, Gutfreund, Sompolinsky (see Amit (1989)) in the non-rigorous framework of the “replica trick”.

For further mathematical results see Malyshev & Spieksma (1997), Talagrand (1996b), Albeverio *et al.* (1997a) (and references therein).

Remark: The so called overlap parameter

$$m^\mu(t) \equiv \frac{1}{N} \sum_i \xi_i^1 z_i(t),$$

with ξ_i^μ the pattern nearest to $z(0)$, is useful for further discussions.

If $z_i(t) \xrightarrow[t \rightarrow \infty]{} \xi_i^\mu$, i. e. if “one has eventual recognition of the pattern ξ^μ ”, then $m^\mu(t) \xrightarrow[t \rightarrow \infty]{} 1$ (as seen from the definition of $m^\mu(t)$). m^μ plays the role of a “macroscopic parameter”. Later on (sect. 2.3, 2.4) we shall discuss a stochastic process $X = (X_t)_{t \geq 0}$ (“Monte Carlo or Glauber dynamics”) s. t.

$$E(X_t - m^\mu(t)) \xrightarrow[t \rightarrow \infty]{} 0$$

(with E meaning expectation).

Remark: Above theorem indicates that the “quality of recognition” depends on the parameter $\alpha \equiv \frac{p}{N}$.

2.2 Gibbs Measure for the Positive Temperature Hopfield Model

The basic idea to be described in this section is to extend the “deterministic zero-temperature dynamics” (discussed in 2.1) to a corresponding “positive temperature dynamics” (Monte Carlo or Glauber dynamics). The study of the latter dynamics together with its invariant (stationary) Gibbs measure is of interest in itself (and there are efficient statistical mechanical tools to perform such a study!) and yields also (new) results on the “temperature $T = 0$ dynamics” in the limit where the temperature T tends to 0.

Let H_N be the energy functional of the Hopfield models with N neurons (later on we shall study the limit $N \rightarrow \infty$) and Hebbian rule i. e.

$$H_N(\sigma) = -\frac{1}{2}\sigma \cdot w\sigma + \theta\sigma,$$

with

$$w = ((w_{ij})), \quad w_{ij} \equiv \begin{cases} \frac{1}{N} \sum_{\mu=1}^p \xi_i^\mu \xi_j^\mu & i \neq j \\ 0 & i = j \end{cases}$$

$\sigma \in E$, $\theta \in \mathbb{R}^N$, $\{\xi_i^\mu\}$ i.i.d. Bernoulli symmetrically distributed.

Definition 5: The Gibbs measure given by H_N and the temperature $T > 0$ is by definition the probability measure P_N on configuration space E given by:

$$P_N(\sigma) \equiv Z_N^{-1} e^{-\beta H_N(\sigma)},$$

where $\beta \equiv \frac{1}{T}$ and Z_N is the normalization constant ("partition function")

$$Z_N \equiv \sum_{\sigma \in E} e^{-\beta H_N(\sigma)}.$$

There is an interest in studying the *overlap parameter*

$$m^\mu(\xi, \sigma) \equiv \frac{1}{N} \sum_{i=1}^N \xi_i^\mu \sigma_i$$

as $N \rightarrow \infty$. Tools for this study are the control of $E_{P_N}(m^\mu)$ (with the general notation E_Q for the expectation with respect to a measure Q) and

$$E_\xi E_{P_N}(m^\mu) \equiv \mathbb{E}(m^\mu) = \frac{1}{N} \sum_{\xi_i^\mu = \pm 1} \frac{1}{2^{Np}} \xi_i^\mu E_{P_N}(\sigma_i) \quad \mu = 1, \dots, p \quad i = 1, \dots, N$$

(in the latter equality we have used that the ξ_i^μ are i. i. d. symmetrically Bernoulli distributed). If $E_{P_N}(m^\mu)$ turns out to be ≈ 0 for $\mu \neq \mu_0$, ≈ 1 for $\mu = \mu_0$ one says that "the pattern ξ^{μ_0} is well recognized".

Remark: Above Gibbs measure is similar to the one of well known models studied in classical statistical mechanics.

1. *Ising (-Lenz) model:* here the energy is

$$H_{\Lambda_N} \equiv -J \sum_{i,k: n. n.} \sigma_i \sigma_k - h \sum_i \sigma_i,$$

The sum being over nearest neighbours (n. n.) of a compact subset $\Lambda_N \subset \mathbb{Z}^d$ with N^d points. $h \in \mathbb{R}$ has the interpretation of external uniform magnetic field; $J > 0$ is a ferromagnetic parameter. For $d = 1$ and $T > 0$ one has just one phase, in the limit $N \rightarrow \infty$; for $T = 0$ one has a phase transition; for $d \geq 2$ one has more than one phase already for T small, $T \neq 0$; see e. g. Sinai (1982), Simon (1993), Baxter (1982).

2. *Mean field model:* here the energy is

$$H_{\Lambda_N} = -\frac{J}{N} \sum_{i,k} \sigma_i \sigma_k - h \sum_{i=1}^N \sigma_i$$

(as compared with the Ising model one has a "long range coupling" which is however weak for $N \rightarrow \infty$). This model is known to have a (second order) phase transition for $T = T_c = J$.

3. *Spin Glass model* (Sherrington-Kirkpatrick model) In this case the energy is defined similarly as for the Hopfield model but with w_{ij} replaced by J_{ij} , with $J_{ii} = 0$, J_{ij} for $i \neq j$ s. t. $J_{ij}, J_{i'j'}$ are independent for $(i, j) \neq (i', j')$, distributed with law the Gaussian normal distribution with mean 0 and variance $\frac{1}{N}$ (in the Hopfield model w_{ij} is independent of $w_{i'j'}$ only if $\{(i, j)\} \cap \{(i', j')\} = \emptyset$!). See e. g. Tirozzi (1995), Amit (1989), Talagrand (1996a), Talagrand (1996b), Pastur & Shcherbina (1991), Guerra (1995), Pastur & Figotin (1977) and Pastur & Figotin (1978).

For all these models tools of *equilibrium* statistical mechanics are available (see below for the case of Hopfield's model)

2.3 Stochastic Dynamics Associated with a Probability Measure

It is possible to relate the Gibbs measure description with a dynamical description, according to a general principle.

Given a system described by a probability measure μ on some state space E one looks for a stochastic Markov process $X = (X_t, t \in I)$ (I a certain "time set", e. g. \mathbb{R}_+ or \mathbb{N}_0) s. t. μ is the stationary measure for X_t i. e.

$$\text{Prob}(X_t \in A) = \mu(A) \quad \forall t \in I$$

for all measurable A .

If P_t is the corresponding Markov semigroup of transition probabilities, then, for $t_1 \leq \dots \leq t_n$:

$$\begin{aligned} \text{Prob}(X_{t_1} \in A_1, \dots, X_{t_n} \in A_n) = \\ \int_E \int_{A_1} \dots \int_{A_n} P_{t_n-t_{n-1}}(x_{n-1}, dx_n) \dots P_{t_1}(x_0, dx_1) \mu(dx_0) \end{aligned}$$

In general $\int_E P_t(x_0, A) \mu(dx_0) = \mu(A)$ expresses the fact that P_t has invariant (i. e. stationary) measure μ .

One says that X describes a Glauber or Monte-Carlo or "stochastic dynamics" associated with μ .

Remark: If P_t is s. t.

$$P_t(x, dy) \mu(dx) = P_t(y, dx) \mu(dy)$$

("detailed balance"), or equivalently, P_t is a symmetric semigroup in $L^2(\mu)$ then μ is an invariant measure for P_t .

If the state space is finite dimensional and $I = \mathbb{N}_0$ one has $P_t = (P_1)^t$, $(P_1)^t$ being the t -th power of P_1 . $p \equiv P_1$ is a stochastic matrix in the sense that $0 \leq p(\sigma, \sigma') \leq 1$, $\sum_{\sigma'} p(\sigma, \sigma') = 1$

It is well known that given a Markov semigroup P_t on some (suitable) space E (like e. g. our space $E = \{\pm 1\}$; in fact E polish is enough) there

exists a Markov process $X = (X_t)$ with transition semigroups P_t (and some “start measure” μ , which can be an invariant measure). In particular given a stochastic matrix p one gets a Markov semigroup $P_t = (p)^t$, $t \in \mathbb{N}_0$ and a Markov process with transition semigroup P_t . In the case where E is finite dimensional and $t \in I = \mathbb{N}_0$ one says that X is a Markov chain (see e.g. Iosifescu (1980)).

Remark: A general setting for these relations is given e. g. in Albeverio *et al.* (1997b) (and references therein).

2.4 The Monte-Carlo Dynamics for the Positive Temperature Hopfield Model

We shall now apply this general construction to the case of the positive temperature Hopfield model. We first define a *Markov chain* (matrix) P associated with the Gibbs measure $P_N^G \equiv Z_N^{-1} e^{-\beta H_N}$ of the Hopfield model: $p(\sigma, \sigma') = 0$ if $\sigma' \neq \hat{\sigma}^{(k)}$ $\forall k$ (where the notation $\hat{\sigma}^{(k)}$ corresponds to the one used in sect. 1.6, i. e. $\hat{\sigma}_i^{(k)} \equiv \sigma_i$ for $i \neq k$, $\hat{\sigma}_k^{(k)} \equiv -\sigma_k$) and

$$p(\sigma, \hat{\sigma}^{(k)}) \equiv \begin{cases} C & \text{if } \Delta H_N \leq 0 \\ Ce^{-\beta \Delta H_N} & \text{if } \Delta H_N > 0, \end{cases}$$

with

$$\Delta H_N \equiv H_N(\hat{\sigma}^{(k)}) - H_N(\sigma), \quad \sigma \in E$$

(with notations introduced in the previous chapter). C is a normalization (to make P a stochastic matrix).

The Markov process with transition probabilities constructed from p is by definition the *Monte-Carlo dynamics* associated with the Gibbs measure P_N^G .

Theorem 7: $\mu \equiv P_N^G$ is an invariant measure for the Monte Carlo dynamics of the Hopfield model defined above. The corresponding Markov semigroups P_t is μ -symmetric (i. e. detailed balance holds “in the mean” with respect to μ).

Proof: The proof is left as an exercise. □

We shall see that one can study the ergodic properties of the Monte-Carlo dynamics and these are connected with the statistical mechanical properties of P_N^G .

First however we would like to point out *the connection with the temperature zero dynamics*:

Theorem 8: If $(X_t, t \in \mathbb{N}_0)$ is the Markov process described by the above Monte Carlo dynamics, then

$$X_t \xrightarrow[T \rightarrow 0]{} \sigma(t)$$

(in the sense of weak convergences of processes), where $\sigma(t)$ ($= z(t)$) is the solution of the $T = 0$ Hopfield dynamics.

Proof (Sketch): By construction we have (with $X_k(t) \equiv (X_k)_t$) : $X_k(t-1) \rightarrow -X_k(t)$ with probability 1 if $\Delta H_N \leq 0$, $X_k(t-1) \rightarrow e^{-\beta \Delta H_N}$ if $\Delta H_N > 0$. But the latter converges to 0 as $T \rightarrow 0$.

On the other hand

$$\Delta H_N = 2\sigma_i \sum_{k \neq i} n_{ik} \sigma_i - 2\theta_i \sigma_i,$$

hence

$$\Delta H_N \leq 0 \leftrightarrow X_k(t) = f\left(\sum_l w_{kl} X_l(t-1) - \theta_k\right),$$

with $f \equiv \text{sign}$. So for $T \rightarrow 0$, $X(t)$ behaves like the solution $\sigma(t)$ of the “Hopfield $T = 0$ dynamics”.

2.5 Ergodicity of the Positive Temperature Dynamics

Here we need some basic notions of ergodic theory, see e.g. Arnold & Avez (1968), Sinai (1994). Consider a dynamical system with state space E , let $\varphi_t : E \rightarrow E$, $t \in I$ be a 1-parameter (semi-) groups of automorphisms, leaving the measure μ on E invariant. Let

$$f : E \rightarrow C, f \in L^1(\mu).$$

The individual ergodic theorem (of Birkhoff and Khinchine) gives sufficient conditions for

$$\langle f(z) \rangle_{\text{time}} \equiv \lim_{T \rightarrow \infty} \frac{1}{T} \int_0^T f(\varphi_t z) dt$$

to exist, μ -a.e. $z \in E$. In this case $\langle f \rangle_{\text{time}} \in L^1(\mu)$, is φ_t -invariant and one has

$$\int \langle f \rangle_{\text{time}} d\mu = \langle f \rangle_{\text{space}} \equiv \int f d\mu.$$

The system is called ergodic if

$$\langle f \rangle_{\text{time}} = \langle f \rangle_{\text{space}} \quad (\mu - \text{a.e.})$$

This is equivalent with the system being indecomposable in the sense that if A is φ_t invariant then $\mu(A) = 0$ or $\mu(A) = \mu(E)$.

We shall now apply these notion to the case of Markov chains $X = (X_t)$ and invariant measure μ . One says that X is time shift-ergodic if the mapping $\varphi_t : E \rightarrow E$ defined by $\varphi_t X_0 \equiv X_t$ is ergodic. In this case one has

$$\begin{aligned} \langle f \rangle_{\text{time}} &= \lim_{T \rightarrow \infty} \frac{1}{T} \int_0^T f(\varphi_t X_0) dt \\ &= \lim_{T \rightarrow \infty} \frac{1}{T} \int_0^T f(X_t) dt = \int f(X_0) d\mu = \text{const.}(\mu - a.e.) \end{aligned}$$

A sufficient condition for ergodicity is, e.g., $P^n > 0 \quad \forall n \geq n_0 > 0$ (see e.g. Iosifescu (1980)).

Theorem 9: The Monte-Carlo dynamics for the Hopfield model is ergodic.

Proof: The proof is left as an exercise (hint: one verifies that $P^n > 0$ for sufficiently large n). \square

Rem.: For more general results on ergodicity of the Monte-Carlo dynamics associated with a Gibbs measure see Albeverio *et al.* (1997b).

2.6 Equilibrium Statistical Mechanical Results for the Positive Temperature Hopfield Model

Let $H_N(\xi, \sigma) \equiv -\frac{1}{2}\sigma \cdot w(\xi)\sigma + \theta\sigma$, with w as in 2.2, be the energy for the Hopfield model, and let, as before T be a fixed temperature: $0 < T < \infty$. Set $\beta = \frac{1}{T}$ and consider the Gibbs measure

$$Z_N^{-1}(\xi) e^{-\beta H_N(\xi, \sigma)},$$

with

$$Z_N(\xi) \equiv \sum_{\sigma \in E} e^{-\beta H_N(\xi, \sigma)}.$$

Denote the corresponding *free energy* $f_N(\xi)$ by

$$f_N(\xi) \equiv -\frac{1}{\beta N} \ln Z_N(\xi).$$

We remark that

$$m_N^\mu(\xi) \equiv \frac{1}{N} \sum_{i=1}^N \xi_i^\mu \langle \sigma_i \rangle_{\text{Gibbs}} = \frac{\partial}{\partial \theta^\mu} f_N(\xi)$$

(with $\langle \cdot \rangle_{\text{Gibbs}}$ the expectation with respect to the Gibbs measure).

There is an interest in discussing the limit $N \rightarrow \infty$, in fact one has

Theorem 10: For all $T > 0$

$$f_N(\xi) \rightarrow E(f_N) \xrightarrow[N \rightarrow \infty]{} 0 \quad \text{in} \quad L^2(\mu) \quad \text{and} \quad \mu - a.e.$$

Remark: This fact expresses the so called “autoaveraging of the free energy”. It has been proven in Albeverio *et al.* (1992), Shcherbina & Tirozzi (1993) (where also the results on f_N and related quantities are given).

Theorem 11: For all $T > 0$

$$\lim_{N \rightarrow \infty} f_N(\xi) = -\frac{1}{\beta} \lim_{N \rightarrow \infty} \frac{1}{N} \ln \psi_N$$

with

$$\psi_N \equiv \int_{\mathbb{R}^p} \frac{dx}{(2\pi)^{\frac{p}{2}}} \exp \left[-\beta \frac{N}{2} |x|^2 - \frac{1}{N} \frac{1}{2^p} \sum_{\xi \in E} \ln \{2ch[\beta x \xi + h\xi]\} \right]$$

Proof (Sketch): By the previous theorem it suffices to consider $E f_N$ for $N \rightarrow \infty$. This is controlled by utilizing

$$\begin{aligned} Z_N(\xi) &= \sum_{\sigma} \exp(-\beta H_N(\sigma, \xi)) \\ &= \sum_{\sigma} \exp \left[\frac{\beta}{2N} \sum_{\mu} (\xi^{\mu} \sigma)^2 - pN \right], \end{aligned}$$

where we took $\theta = 0$ for simplicity. Using the fact that the ξ_i^{μ} are i.i.d. we see that the r.h.s. is equal to

$$e^{-\beta \frac{p}{2}} \sum_{\sigma} \prod_{\mu=1} e^{2 \frac{\beta}{N} (\xi^{\mu} \sigma)^2}$$

The proof is then carried through using the fact that $e^{\frac{\beta}{2N} (\xi^{\mu} \sigma)^2}$ is of the form

$$e^{\frac{a^2}{2}} = \int_{\mathbb{R}} \frac{dy}{\sqrt{2\pi}} e^{-\frac{y^2}{2} + ay}.$$

□

For the further discussion we distinguish 2 cases:

- A) p fixed, $N \rightarrow \infty$
- B) $\frac{p(N)}{N} = \alpha > 0$ fixed, $p(N)$, $N \rightarrow \infty$

Case A: In this case the formula for $\lim_{N \rightarrow \infty} f_N(\xi)$ in Theorem 11 together with a rigorous Laplace method to control the asymptotics for $N \rightarrow \infty$ yield

$T > 1 :$

$$\lim_{N \rightarrow \infty} m_N^\mu = 0 \quad (\text{a.s.}) :$$

“no retrieval takes place”

$T < 1 :$

$$\lim_{N \rightarrow \infty} m_N^\mu \neq 0 \quad (\text{a.s.}) :$$

“retrieval takes place”

(in this case the limit is described in term of the stationary points of the above Laplace method)

$T = 1 :$ there exists a phase transition.

A reference for these results is Albeverio *et al.* (1992) (who also give asymptotic expansions in powers of N)

Case B: In the case $T = 0$ a simple consideration yields that for a given pattern the noise from the other patterns is of order $\sqrt{\alpha}$, so for small α and small $T > 0$ one can also expect some retrieval. In fact one has the following results:

Theorem 12: As $p(N) \rightarrow \infty$, $N \rightarrow \infty$ so that $\frac{p(N)}{N} = \alpha = \text{const}$ one has

$$\lim(E_{\text{Gibbs}} m^\mu - E_\xi E_{\text{Gibbs}} m^\mu) = 0$$

(for all $\alpha > 0, T > 0$)

References for the proof of this theorem are Shcherbina (1997), Shcherbina & Tirozzi (1993), Talagrand (1996b).

Theorem 13: Given $T > 0$ there exists $\alpha(T) > 0$ s.t. as $N \rightarrow \infty$, $p(N) \rightarrow \infty$ s.t. $\alpha(T) > \alpha \equiv \frac{p(N)}{N} > 0$ remains constant, we have (a.s.)

$$\lim_{N \rightarrow \infty} f_N(\xi) = \lim_{N \rightarrow \infty} Ef_N,$$

the r. h. s. being given by the well known “replica symmetry expression” derived heuristically e.g. in Amit (1989) (based on work by Amit, Gutfreund and Sompolinsky).

For the proof see Pastur *et al.* (1994) and Pastur *et al.* (1996) (see also Pastur & Shcherbina (1991), Talagrand (1996a) and Talagrand (1996b)).

Remark: There also exist estimates on $\alpha(T)$ and formulae for m^μ . In part the well known $\alpha - T$ picture described e.g. in Amit (1989) is thus rigorously established in above references.

Conclusion: We hope to have given an introduction and an idea of what type of rigorous mathematical results have been established in the study of neural networks, particularly for Hopfield networks. This however only covers a small portion of the work done, in a very active area of research, for more information we refer to Bovier & Gayrard (1992), Bovier & Gayrard (1997), Bovier & Gayrard (1995), Bovier *et al.* (1994), Scacciatelli & Tirozzi (1992), Shcherbina (1997), Albeverio *et al.* (1997a).

Acknowledgements

It is a great pleasure for the first named author to thank Prof. Dr. P. L. Garrido and Prof. Dr. J. Marro for their kind invitation to a most exciting Summer School.

Many stimulating discussions with them, colleagues and students at the School are also gratefully acknowledged. Dorothea Henn, Markus Debort and Jan Micheel should be thanked for their skillful setting of the paper.

References

- Amit D. (1989): *Modeling brain function*, Cambridge Univ. Press.
- Albeverio S., Feng J. and Tirozzi B. (1997): *Rigorous results in neural networks*, book in preparation.
- Albeverio S., Kondratiev Yu. and Röckner M. (1997): J. Funct. Anal. **144**, 394-423.
- Arnold V.I. and Avez A. (1968): *Ergodic Problems of Classical Mechanics*, Benjamin, New York.
- Albeverio S., Tirozzi B. and Zegarlinski B. (1992): Comm. Math. Phys. **150**, 337-373.
- Ay N. (1996): *Ein kombinatorisch geometrischer Zugang zum Hopfield-Modell*, Diplomarbeit, Bochum.
- Baxter R.J. (1982): *Exactly solvable models in statistical mechanics*, Academic Press, London.
- Bovier A. and Gayrard V. (1992): J. Stat. Phys. **69**, 597-627.
- Bovier A. and Gayrard V. (1997): *On the retrieval states of the Hopfield Model*, Prob. Theory. relat. Fields to appear.
- Bovier A. and Gayrard V. (1995): *An Almost Sure Large Deviation Principle for the Hopfield Model*, Preprint **146**, Weierstrasse Institute, Berlin.
- Bovier A., Gayrard V. and Picco P. (1994): Probab. Theory Related Fields **100**, 329-363.
- Feng J. and Tirozzi B. (1997): *Capacity of the Hopfield Model* J. of Physics A in press.
- Guerra F. (1995): *About the overlap distribution in mean field spin glass models* preprint.
- Hopfield J.J. (1982): Proc. Natl. Acad. Sci. USA **79**, 1554-2558.
- Hecht-Nielsen R. (1990): *Neurocomputing* Addison- Wesley, Reading.
- Iosifescu M. (1980): *Finite Markov Processes and their application*, Wily, Chihertzer.
- Kinnebrock W. (1992): *Neuronale Netze*, Oldenbourg, München.

- Loukianova D. (1994): *Two rigorous bounds in the Hopfield model of associative memory* Manuscript.
- Loukianova D. (1994): *Capacité de mémoire dans le modèle de Hopfield*, C. R. Acad. Sci. Paris, 318, Ser. I, 157-160.
- Malyshev V. and Spieksma F.M. (1997): *Dynamics in neural networks with a finite number of patterns*, to appear in Math. Phys. Electr. J.
- Newman C. (1988): *Memory capacity in neural network models. Rigorous bounds*, Neural Networks 1, 223-238.
- Peretto P. (1992): *An introduction to the modeling of neural networks*, Cambridge University Press.
- Pastur L. and Figotin A. (1977): Sov. J. Low Temp. Phys. 3 378-383.
- Pastur L. and Figotin A. (1978): Theor. Math. Phys. 35, 403-414.
- Pastur L. and Shcherbina M. (1991): J. Stat. Phys. 621, 1-19.
- Pastur L., Shcherbina M. and Tirozzi B. (1994): J. Stat Phys. 74, 1161-1183.
- Pastur L., Shcherbina M. and Tirozzi B. (1996): *Disordered systems: self averaging and replica solutions*, WIAS Workshop on "Mathematics of random interactions", Berlin, 21-24 August 1996.
- Procesi C. and Tirozzi B. (1989): Int. J. Mod. Phys., 13 4, 143-159.
- Ritter H., Martinez Th. and Schulten K. (1994): *Neurale Netze*, Addison, Bonn.
- Rojas R. (1993): *Theorie der neuronalen Netze*, Springer.
- Rosenblatt F. (1980): *Principles of Neurodynamics*, Spartina, New York.
- Scacciatelli E. and Tirozzi B. (1992): J. Stat. Phys. 67, 981-1008.
- Shcherbina M. (1997): *On the replica symmetric solution for the Sherrington-Kirkpatrick model*, to appear in Helv. Phys. Acta.
- Shcherbina M. and Tirozzi B. (1993): J. Stat. Phys. 72, 113-125.
- Simon B. (1993): *The statistical mechanics of lattice gases*, Princeton University.
- Sinai Ya. G. (1982): *Model Theory of Phase transitions: Rigorous results*, Oxford.
- Sinai Ya. G. (1994): *Topics in ergodic theory*, Princeton University Press.
- Tirozzi B. (1995): *Modelli Matematici di Reti Neurali*, CEDAM, Padova.
- Talagrand M. (1996): *The Sherrington-Kirkpatrick model: A challenge for mathematicians*, Paris, Preprint.
- Talagrand M. (1996): *Rigorous results for the Hopfield model with many patterns*, Paris VI, Preprint.
- Taylor J.G. ed. (1993): *Mathematical approaches to neural networks*, North Holland, Amsterdam.

The Statistical Mechanics of Absorbing States

G. Grinstein¹ and M.A. Muñoz²

¹ IBM Research Division, T.J. Watson Research Center, Yorktown Heights, New York 10598, U.S.A.

² Dipartimento di Fisica, Università di Roma “La Sapienza”, P.le A. Moro 2, I-00185 Roma, Italy.

1 Introduction

Many noisy nonequilibrium systems, among them chemical reactions, directed percolation problems, and spreading forest fires or epidemics possess one or more “absorbing states” – configurations which persist forever, and in which all nontrivial dynamics ceases. In these lectures we investigate the statistical mechanics of such systems, with particular emphasis on the continuous phase transitions connecting absorbing phases to “active” phases with nontrivial dynamics and correlations. Two common universality classes into which such transitions fall – the directed percolation and multiplicative noise classes – are analyzed through the use of Langevin equations and renormalization group methods.

2 Absorbing States and Directed Percolation

2.1 Introduction

Any configuration in which a system becomes trapped forever with no possibility of escape is said to be an “absorbing” configuration or state (Deutsher *et al.* 1980, Marro & Dickman 1997) of that system. Though they seldom receive much attention in courses on statistical mechanics, such states abound in physics, chemistry, biology, and other disciplines.

Particularly intuitive (if menacing), examples include the spread of epidemics (Cardy 1983, Cardy & Grassberger 1985, Janssen 1985) through a population, or fire (Chen *et al.* 1990) through a forest. If all stricken individuals in the first example happen to recover or die without infecting any of their fellows, then the disease disappears, and the disease-free state persists forever. This state is therefore absorbing. In the second example, the state wherein all fire has died out is likewise absorbing, at least on time scales short compared to the interval before the next electrical storm (or overly relaxed marijuana-smoking hiker) arrives. We will consider less threatening examples from, *inter alia*, catalysis and autocatalytic chemical reactions later, but these two should suffice to make the main point: Absorbing states occur in

situations where some quantity of interest can proliferate or die out, but cannot be generated spontaneously.

The essential physics is the competition between the proliferation and death of the quantity in question. When the former predominates, one typically reaches a steady state with a nonzero density of the quantity; this is the so-called “active” phase of the system. When the latter predominates, one falls, with unit probability in the long-time limit (Broadbent & Hammersley 1957, Harris 1974, Liggett 1985), into the absorbing state, and so is said to be in the absorbing phase. As the control parameter, roughly defined as the ratio between the rates of proliferation and death, decreases, one can expect a transition from the active to the absorbing phase. It is primarily with elucidating the properties of such phase transitions, and identifying the different universality classes (i.e., distinct sets of critical exponents characterizing the transitions), that these lectures are concerned.¹

It is important to note that systems with absorbing states are explicitly out of equilibrium. This is particularly easy to see if one defines stochastic equilibrium systems very loosely² as those satisfying detailed balance at some nonzero temperature T for some underlying Hamiltonian \mathcal{H} . Since the transition rate out of an absorbing state is zero, such states cannot fulfill the detailed balance requirement with any other state for any conceivable \mathcal{H} , thus making the system a nonequilibrium one. In studying the critical behavior of systems with absorbing states, therefore, we will be working in the growing subfield of nonequilibrium critical phenomena. The goal of this subfield, viz., the classification of continuous transitions into universality classes, is the extension to nonequilibrium systems of the program implemented so laboriously and successfully for equilibrium critical phenomena (Ma 1976, Binney *et al.* 1992).

Broad experience with equilibrium systems has shown that the most effective tool for analyzing universality classes is renormalization group (RG) (Wilson & Kogut 1975) analysis of classical field-theoretic models. That is, coarse-grained Ginzburg-Landau-Wilson Hamiltonians (Wilson & Kogut 1975) (or, more correctly, free-energy functionals), are far simpler to analyze for genericity, and for the symmetry properties that largely determine universality classes, than are microscopic models (Onsager 1944). Having understood the symmetry of such a free energy functional \mathcal{H} , and studied its critical behavior through the RG – even if only in an expansion near the upper critical dimension d_c above which mean-field theory (MFT) becomes

¹ In our consideration of multiplicative noise in Section 5, we shall see that the active and absorbing phases themselves have unusual properties in the vicinity of the critical point, so more than just asymptotic critical behavior is of interest.

² Although this definition is usually quite sensible, it fails miserably for certain odd special cases. There are, e.g., systems that satisfy detailed balance for underlying Hamiltonians, yet nonetheless succeed in producing temporally periodic phases rather than stationary ones (Vichniac 1986).

valid (Wilson & Kogut 1975) – one is in a strong position to classify many seemingly unrelated microscopic models as having phase transitions described by \mathcal{H} .

While nonequilibrium systems do not have free energy functionals, they can often be described on the coarse-grained level by phenomenological Langevin equations (van Kampen 1981), i.e., stochastic partial differential equations. Such equations are good nonequilibrium analogues of free-energy functionals, in that their symmetry properties are simple to understand, and their critical behavior is usually straightforward to analyze with the RG, at least in certain limits. Thus they form a natural formalism around which to build a universality class structure analogous to that for equilibrium problems. It is on this formalism that we will rely in analyzing the critical properties of systems with absorbing states.

The rest of this lecture is devoted to a review of the phenomenology of the directed percolation (DP) problem, a discussion of several of the many other microscopic models that have unique absorbing states and belong to the DP universality class, and a quick and dirty derivation of the Langevin equation that characterizes this class. In section 3 we demonstrate desperately poor judgement, by attempting a schematic summary of the RG technique, in the context of analyzing the Langevin equation for DP. The section 4 deals with systems possessing multiple absorbing states, and their relation to the DP problem. In the section 5, we discuss a quite different set of systems with absorbing states, namely, those with multiplicative noise.

2.2 Directed Percolation and Related Problems

Let us first review the venerable microscopic model of directed percolation (Broadbent & Hammersley 1957, Deutsher *et al.* 1980, Marro & Dickman 1997). This model is often defined somewhat fancifully as describing the systematic dripping of water (or, in the truly fanciful up-scale version, oil), through a lattice with randomly occupied bonds. Consider, e.g., the semi-infinite square lattice of sites illustrated in Fig. 1. The only bonds that we allow on this lattice are those linking the site (i, t) to the sites $(i - 1, t + 1)$, $(i, t + 1)$, and $(i + 1, t + 1)$, where t and i label the rows and columns of the lattice, respectively. (Note that only the bond between (i, t) and $(i, t + 1)$ is a nearest-neighbor bond of the square lattice, the other two being next-nearest-neighbor bonds.) Imagine further that each of these allowed bonds is present with probability p , and absent with probability $1 - p$. Next imagine that a fixed fraction of the lattice sites in the top row, chosen randomly, is occupied by drops of water, while the rest of the sites in that row and elsewhere on the lattice are dry. At the first (discrete) time step, water is imagined to drip down from each wet site in the top row along any occupied bond connected to it, thereby wetting every site in the second row connected to a wet site in the top row by at least one occupied bond. At the next time step, the dripping process is repeated, this time from the second to the third row, and so on. In

principle, then, after t time steps there may be wet sites in all rows down to and including the $(t + 1)^{st}$. In practice, however, whether water succeeds in dripping arbitrarily far down the lattice depends on p : If p is too small, there is insufficient connectivity in the lattice to sustain the cascade of water, and all rows of sites below some finite level remain completely dry in perpetuity. (Note that the probability of a given wet site (i, t) “dying,” i.e., failing to produce any wet offspring at level $t + 1$, is $(1 - p)^3$.) Since a given wet site at level t can, however, produce as many as *three* wet sites at level $t + 1$, then for sufficiently large p the flow of water down the lattice can be sustained forever. (The probability of a given wet site “proliferating,” i.e., producing more than one wet offspring, is $3p^2 - 2p^3$.) In this case, the system achieves a kind of steady state wherein the density n of wet sites in layer t approaches a constant value as $t \rightarrow \infty$. It follows that there must be a critical value, p_c , of p , separating these distinct “dry” and “wet” phases of the system. This intuitive picture of the phase structure of the model has been demonstrated rigorously in certain cases (Broadbent & Hammersley 1957, Harris 1974, Liggett 1985, Bezuidenhout & Grimmett 1992), and verified in staggering numbers of computer simulations,³ at immense cost to the taxpayers of the world.

This struggle between death and proliferation sounds very much like the general scenario that we outlined above for systems with absorbing states. Moreover, the dripping-water model does have something like an absorbing state, in the sense that if water fails to penetrate to some particular level (say t), then clearly all levels below t remain completely dry as well, and all interesting dynamics ceases. To make this situation fall more precisely into our definition of absorbing states, we need only think of the vertical direction in Fig. 1 as representing time rather than space, so that the system has only one space dimension (i.e., consists of a single chain of sites). Then the $(t + 1)^{st}$ row of the lattice depicts the state of that chain after t time steps, the first row representing the initial state of the chain. The time evolution of this one-space, one-time (i.e., (1+1)-dimensional) system is described as follows: Any wet site, say i , along the chain at time t can (as in Fig. 1), result in any of the $(i - 1)^{st}$, i^{th} , or $(i + 1)^{st}$ sites being wet at time $t + 1$, depending on whether the bonds connecting site i at time t to sites $i - 1$, i , or $i + 1$ at time $t + 1$ are occupied or not. It is clear that in this (1+1)-dimensional representation, the totally dry state is an absorbing one: If the chain has no wet sites at some time t , then it cannot possibly have any at time $t + 1$, since water (or, even more tragically, oil), can at most spread in time from site i to site $i - 1$ and $i + 1$, but cannot be produced spontaneously.

Viewed as a (1+1)-dimensional chain, the dripping-water model is just a one-dimensional (1d) cellular automaton (CA) and can readily be generalized to (d+1) dimensions. The competition between proliferation and death

³ See Jensen (1992) and references therein; see also Grassberger & de la Torre (1979).

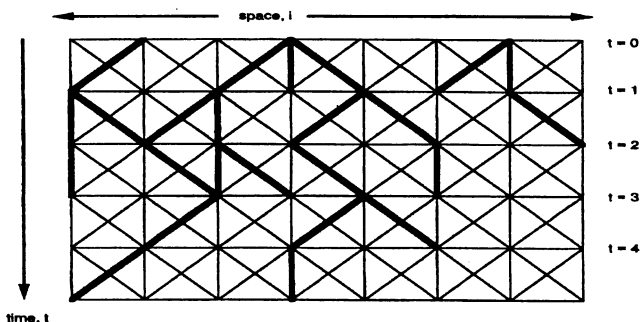


Fig. 1. Directed percolation defined on a square lattice of sites. Allowed bonds link site (i,t) to sites $(i-1,t+1)$, $(i,t+1)$, and $(i+1,t+1)$, and are shown as thin lines. A fraction p of the allowed bonds are actually present (shown as thick lines). Water drips down from any wet site along any present bond connected to that site.

that it captures is so common in nature that we should not be surprised to see variations of this model in many different contexts. To give a couple of concrete examples:

(1) The so-called “contact process” (Harris 1974, Liggett 1985, Durrett 1988, Marro & Dickman 1997) was concocted as a simple lattice model for the spread of epidemics, diseased and healthy sites being represented by the respective presence or absence of a particle. Particles can create (with probability p), new particles at randomly chosen vacant near-neighbor sites, or can simply disappear into thin air (with probability $1-p$). When this process takes place in discrete time steps, then the model is a CA which is obviously very close to the directed percolation problem described above; but it can of course equally well be defined in continuous time.

(2) Autocatalytic reaction-diffusion equations for the production of some chemical species, X say, have much the same character. For example, Schlögl’s so-called “first model” (Schlögl 1972) describes the reactions $X \rightleftharpoons{} 2X$ and $X \rightleftharpoons{} 0$.⁴ If the rate of the reaction $0 \rightarrow X$, wherein X is produced spontaneously from the vacuum (i.e., 0), is zero, then the vacuum state with no X ’s

⁴ Other models of catalytic reactions exhibiting an absorbing state can be found in Kohler & ben-Avraham (1991) and ben-Avraham & Kohler (1992).

is absorbing, and the model describes the competition between proliferation ($X \rightarrow 2X$) and death ($2X \rightarrow X$ and $X \rightarrow 0$). Reaction-diffusion models are typically described in a spatio-temporal continuum, by partial differential equations with a diffusion term that keeps the concentration of X from becoming too high in any given region. The basic physics is, however, essentially identical to that of directed percolation, and discrete lattice versions of Schlögl's first model look very similar to the contact process.

(3) Elementary models of heterogeneous catalysis are another much studied realization. Consider, for example, the Ziff-Gulari-Barshad (ZGB) (Ziff *et al.* 1986) model for the catalytic oxidation of poisonous carbon monoxide gas, CO , to harmless carbon dioxide, CO_2 : $2CO + O_2 \rightarrow 2CO_2$. Anyone with a car, a garage, and a taste for grade B American movies, has at some point given this process thought, however obliquely. The ZGB model is defined on a lattice representing the surface of an appropriate catalytic material, such as platinum. We consider a 2d square lattice here, for purposes of illustration. A gas composed of CO and O_2 molecules, with fixed molecular concentrations of y and $1 - y$ respectively, is imagined to be in contact with the surface. Each lattice site can either be empty, occupied by a CO molecule, or occupied by an O atom. The system evolves according to the following rules: (i) A CO molecule will fill any vacant site with probability γy per unit time, where γ is an arbitrary rate constant. (ii) With probability $\gamma(1 - y)$ per unit time, each member of any nearest-neighbor pair of vacant sites will become occupied by a single O atom, produced by the dissociation of an O_2 pair from the gaseous atmosphere. (iii) A CO molecule and an O atom on neighboring sites react instantaneously, producing a CO_2 molecule that leaves the surface at once, and is imagined removed from the system. Thus, no two neighboring sites are ever occupied by a $CO - O$ pair.

These rules make clear that the two uniform ("poisoned") states wherein all sites are either filled by CO molecules or filled by O atoms are both absorbing. Computer simulations (Ziff *et al.* 1986, Meakin & Scalapino 1987) show that these two absorbing phases occur for sufficiently large and small y respectively, and are separated by an active phase (Fig. 2), that exists over some modest range of intermediate y values. The transitions from the active phase into the O -poisoned and CO -poisoned phases are respectively continuous and first order. In either case, the transition is governed by the competition between proliferation and death of vacant sites surrounded by sites all filled with O atoms (or all filled with CO molecules).

Some years ago, Grassberger (1982) conjectured that the critical exponents characterizing the transition into the absorbing phase in the DP problem also govern the transitions in all of these other models. Indeed, he hypothesized that a unique set of critical exponents, i.e., a single universality class, describes all continuous transitions into absorbing phases consisting of a unique absorbing configuration, in systems with single-component order parameters. This universality class, the broadest and most ubiquitous one

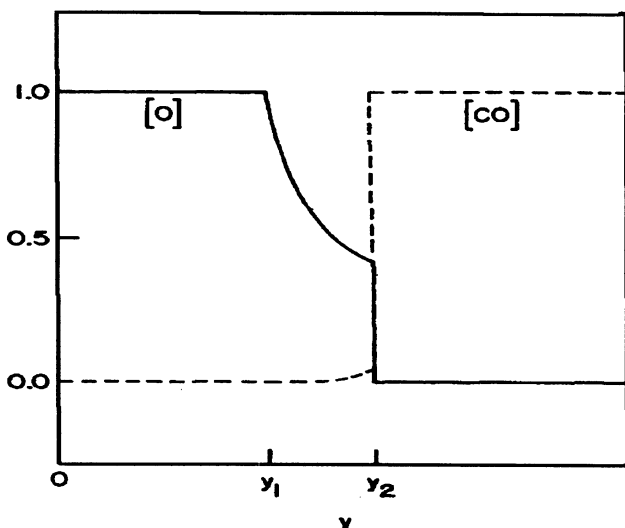


Fig. 2. Schematic phase diagram for the ZGB model catalysis of CO . Concentrations of O (solid line), and CO (dashed line), on the catalytic surface, are shown as functions of the concentration, y , of CO in the gas. Transitions into the O -poisoned phase at y_1 and the CO -poisoned phase at y_2 are of second and first order, respectively. This is Fig. 1 of Grinstein et al. 1989.

in the absorbing-state business, is often simply referred to as the “directed percolation” universality class, in honor of its earliest, and arguably most famous, member. Lest things be too clear, however, it is also frequently called the “Reggeon field theory” (RFT) class, in honor of the particular field theory – known as Reggeon field theory (Gribov 1967, Abarbanel *et al.* 1975) – that captures the macroscopic (and hence critical) behavior of all of the class’s diverse members. We will not discuss RFT here, since our vehicle for discussing RG notions about critical properties and universality will be the Langevin equation. The Langevin formalism allows one to justify and extend Grassberger’s conjecture in a simpler, more intuitive way than through RFT, which can readily be derived from the Langevin equation. It also provides a compact framework for placing problems with absorbing states in the broader context of classical statistical mechanics. Let us then take a few minutes briefly to summarize the central ideas of the Langevin approach.

2.3 The Langevin Equation

The Langevin equation for a single-component field $\psi(\mathbf{x}, t)$ takes the following form (van Kampen 1981), the generalization to several components being

fairly obvious:

$$\partial\psi(\mathbf{x}, t)/\partial t = f_x(\{\psi\}) + g_x(\{\psi\})\eta(\mathbf{x}, t) , \quad (1)$$

where f_x and g_x are functionals of ψ , typically taken to be local, i.e., to depend only on $\psi(\mathbf{x}', t')$ for (\mathbf{x}', t') in the vicinity of (\mathbf{x}, t) ; η is a Gaussian random variable with zero mean, whose only nonvanishing correlations are $\langle \eta(\mathbf{x}, t)\eta(\mathbf{x}', t') \rangle = D\delta(\mathbf{x} - \mathbf{x}')\delta(t - t')$.

Since the Langevin equation is a coarse-grained representation intended to capture the physics of microscopic models on large length and time scales, f_x and g_x^2 are typically taken to be⁵ analytic functions of $\psi(\mathbf{x}, t)$ and its spatial derivatives. In other words, the coarse graining is imagined to smooth out any nonanalyticities in the underlying microscopic dynamical rules. This enormous simplification is very much in the spirit of the analyticity assumption at the core of the Ginzburg-Landau-Wilson free-energy-functional representation for equilibrium systems (Wilson & Kogut 1975, Landau & Lifshitz 1980).

Since Eq. (1) is designed to describe low-frequency, small-wavenumber phenomena (such as critical properties), it is purely first order in time. The point is that each time derivative corresponds to a factor of frequency, ω , in Fourier space. For low frequencies, therefore, the second derivative term, $\partial^2\psi/\partial t^2$, representing the inertial properties of the system, is down by a factor of ω relative to the dissipative term, $\partial\psi/\partial t$. Thus dissipation dominates the low-frequency physics, where inertia becomes negligible.

Even after these simplifications, it remains to decide which of the infinite number of possible analytic terms in ψ and its space derivatives one should include on the right hand side of Eq. (1) if one is faithfully to represent the macroscopic physics of a given microscopic model. The solution was provided by Landau, in his pioneering work on phase transitions (Landau & Lifshitz 1980). He postulated that symmetry considerations suffice to determine the infinite set of terms that constitute $f_x(\{\psi\})$ and $g_x(\{\psi\})$: Every analytic term consistent with the symmetry of the microscopic problem at issue *must* in principle be included in these functionals, and no term with lower symmetry can appear. The coefficients of these various terms are taken as unknown parameters satisfying whatever constraints are necessary to make the Langevin equation well behaved – to keep the values of ψ from increasing without bound, for example. In principle, the values of these coefficients can be determined by performing the coarse-graining operation that produces the Langevin equation from the microscopic model (e.g., Garrido *et al.* 1996). In practice, however, this difficult, thankless procedure is seldom carried out. Rather one takes the coefficients as unknown constants, to be determined phenomenologically through experiments, real and/or numerical.

⁵ As averages over the noise variables η , all physical observables of the system are functions of g_x^2 . Hence the analyticity assumption implies only that g_x^2 , rather than g_x , be analytic in ψ and its derivatives.

As we shall see, the reason one can afford to be so cavalier about this point is that RG methods demonstrate that a typical phase transition is characterized by a set of universal quantities such as critical exponents, which do not depend on the precise values of parameters. Changing coefficients changes certain nonuniversal features of the transition, notably the value of the control parameter (e.g., the temperature), where the transition occurs. The universal quantities remain invariant, however, being determined only by the symmetry of the problem and the number of spatial dimensions. The same RG arguments also show that all but a very few of the lowest order terms in ψ and its derivatives in equations like (1) likewise do not influence universal properties at all, and so can be omitted. This is an enormous simplification, since it allows one to ignore infinite numbers of symmetry-allowed terms, and concentrate on a small, finite number of them.

We are now in a position to identify two main categories of statistical-mechanics problems, according to the behavior of their noise amplitude functionals $g_x(\{\psi\})$ in the limit of small ψ :

(i) Systems Without Absorbing States: In the first and most common situation, $g_x(\{\psi\})$ approaches a constant (which, without loss of generality, can be taken to be unity), in this limit. Typically, then, all higher powers of ψ and its derivatives in g_x can be shown through RG arguments to be irrelevant for the computation of universal critical properties, and so can be neglected. Thus one arrives at a general category of Langevin equations with simple “additive” Gaussian noise of constant amplitude.

This class of equations is appropriate only for describing systems *without* absorbing states. To see this, assume that $f_x(\{\psi\})$ vanishes for some particular function $\psi(\mathbf{x}) = \psi_a(\mathbf{x})$, which therefore is potentially an absorbing state. Since the additive noise is independent of ψ , however, there is always a nonzero probability of its kicking the system out of the state $\psi_a(\mathbf{x})$, meaning that $\psi_a(\mathbf{x})$ is not in fact absorbing. Equations with additive noise will therefore not be of direct interest to us for the remainder of these lectures. It is nonetheless worth mentioning that the additive-noise class includes classical equilibrium systems as a special case, as well as a vast collection of important nonequilibrium problems. We illustrate this now with two examples:

(a) Uhlenbeck and Ornstein (1930) showed more than half a century ago that whenever the functional $f_x(\{\psi\})$ can be written as the functional derivative, $f_x = -\Gamma \delta \mathcal{H}(\{\psi\}) / \delta \psi(\mathbf{x})$ of some new functional $\mathcal{H}(\{\psi\})$ (with Γ a constant), then the Langevin theory with additive noise describes the approach to equilibrium of a system described by the Hamiltonian (or more precisely, free-energy functional⁶), $\mathcal{H}(\{\psi\})$. Uhlenbeck and Ornstein (1930) showed that in the long-time limit the probability distribution function $P(\{\psi\})$ approaches the stationary Boltzmann distribution proportional to $e^{-\mathcal{H}/k_B T}$,

⁶ Since we are dealing with coarse-grained variables, free-energy functional is the more appropriate term.

where k_B is Boltzmann's constant, and the effective temperature T is defined by $k_B T = D/2\Gamma$. The Langevin equation is often referred to as a "time-dependent Ginzburg-Landau" equation under these circumstances (Hohenberg & Halperin 1977).

To cite what is surely the best known example of this scenario: If $f_x(\{\psi\})$ can be written

$$f_x(\{\psi\}) = \Gamma(\nabla^2\psi - r\psi - u\psi^3) , \quad (2)$$

for constants r and u , then it is the functional derivative of the free energy functional

$$\mathcal{H}(\{\psi\}) = \int d\mathbf{x}[(\nabla\psi)^2/2 + r\psi^2/2 + u\psi^4/4] , \quad (3)$$

the famous Ginzburg-Landau-Wilson free-energy functional for the Ising model and its many, diverse physical realizations. Naturally, in this case the Langevin equation has the global up-down symmetry, $\psi(\mathbf{x}) \rightarrow -\psi(\mathbf{x})$, characteristic of Ising systems in zero field. RG arguments show that higher order terms such as ψ^5 , that possess this symmetry and hence ought to appear on the right hand side of (2), can be neglected since they do not affect universal critical properties.

(b) Though the special case of time-dependent Ginzburg-Landau equations for equilibrium systems is the most familiar example, it is important to keep in mind that Langevin equations with additive noise describe a wealth of equally important nonequilibrium systems, for which f_x cannot be expressed as a functional derivative. One of the most celebrated examples in modern statistical mechanics is the KPZ equation, introduced in 1986 by Kardar, Parisi, and Zhang (1986) to model the behavior of moving interfaces with no overhangs.⁷ (To have a concrete picture in mind, think of the interface between water flowing through a large-bore pipe and the air which it displaces.) In interfacial systems, $\psi(\mathbf{x}, t)$ represents the height at time t , measured from an arbitrarily chosen zero plane, of a point on the interface at position \mathbf{x} in the plane (Fig. 3). If, as is often the case, gravity can be neglected in the interface motion, then the problem is invariant under uniform translations of the interface in the direction perpendicular to its plane. Thus the appropriate Langevin equation must be invariant under the global transformation $\psi(\mathbf{x}, t) \rightarrow \psi(\mathbf{x}, t) + C$, where C is an arbitrary constant. The right hand side of the Langevin equation can then depend only upon spatial derivatives of ψ , not upon ψ itself. In *et al.* (1986) it was shown that the functional f_x that captures the large-scale physics of moving interfaces under a wide variety of conditions is $f_x = c\nabla^2\psi + \lambda(\nabla\psi)^2$, for constants c and λ , producing the KPZ equation

$$\partial\psi/\partial t = c\nabla^2\psi + \lambda(\nabla\psi)^2 + \eta(\mathbf{x}, t) . \quad (4)$$

⁷ For a general review, see Barabási & Stanley (1995).

Again, higher terms in $\nabla\psi$ are all irrelevant (Kardar *et al.* 1986) for computing universal asymptotic properties of interfaces, and so can be ignored in writing Eq. (4).

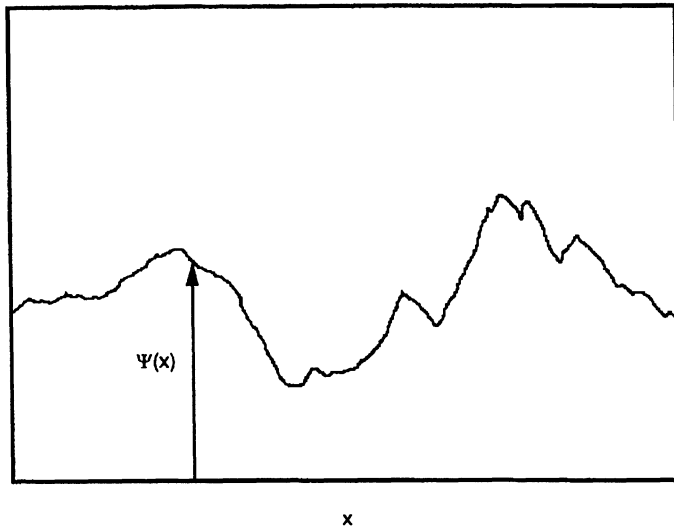


Fig. 3. Instantaneous configuration of an interface, showing height $\psi(x)$, as a function of the lateral coordinate x .

Enormous effort has been devoted to the study of the KPZ model, about which a great deal is known. In this purely cultural summary, let us mention only its most remarkable property: Owing to its translational symmetry, the KPZ model is always scale invariant, i.e., correlation functions such as $\langle (\psi(\mathbf{x}, t) - \psi(\mathbf{0}, t))^2 \rangle$ behave asymptotically like power laws of their arguments (e.g., $\langle (\psi(\mathbf{x}, t) - \psi(\mathbf{0}, t))^2 \rangle \sim x^{2\chi}$, where χ is the so-called roughness exponent).

(ii) Systems with Absorbing States: In the second class of Langevin equations, the noise amplitude functional $g_x(\{\psi\})$ vanishes with ψ , implying that the state $\psi(\mathbf{x}) = 0$ is an absorbing state for any functional f_x which has no constant piece, and hence also vanishes with ψ . Typically g_x vanishes like ψ^α for small ψ . The analyticity condition on g_x^2 implies that α can assume only positive integer or half-odd-integer values. With very rare exceptions, $\alpha = 1/2$ and $\alpha = 1$ are the only cases of interest in practice.⁸ Thus we

⁸ Since only g_x^2 , not g_x alone, appears in any perturbative expansion for quantities of physical interest, one need not be concerned about the formal problems

can think of the absorbing-state category of Langevin theories dividing into two subclasses: $\alpha = 1/2$ and $\alpha = 1$. Most of the rest of these lectures will be devoted to the study of these two subclasses, the first of which, as we shall see, includes the directed percolation problem, and the second of which includes the multiplicative-noise problem.

2.4 Langevin Representation of Directed Percolation

Let us now endeavor to apply the dry, academic principles of Langevin technology to the living, breathing problem of directed percolation. The first, relatively easy, question is precisely what the field $\psi(\mathbf{x}, t)$ in the Langevin representation of DP is supposed to represent. The obvious candidate is a coarse-grained version of the density of wet sites, which is the quantity of central interest or “order parameter”⁹ of the problem.

The next issue to be confronted – what to choose for the deterministic functional $f_x(\{\psi\})$ and the noise-amplitude functional $g_x(\{\psi\})$ – is slightly more subtle, though still hardly a great intellectual challenge: Since in DP the totally dry state, $\psi(\mathbf{x}) = 0$, must be absorbing, $f_x(\{\psi\})$ and $g_x(\{\psi\})$ must both vanish as $\psi \rightarrow 0$, so neither can contain a term independent of ψ .

Let us first decide the form of f_x . Slavishly following Landau’s general principle described above, we ask “What are the symmetries of the problem?” and are pleased to find that there are none, except for those of the lattice on which we imagine the DP problem to be defined. Thus any analytic term in ψ and its derivatives consistent with the symmetry of the lattice in question should, and in fact *must*,¹⁰ appear in f_x . Assuming that the lattice is (inversion) symmetric under $\mathbf{x} \rightarrow -\mathbf{x}$, so that terms like $\nabla\psi$ are forbidden, we can write the few lowest allowed terms in ψ and its derivatives as

$$f_x(\psi) = c\nabla^2\psi(\mathbf{x}, t) - r\psi(\mathbf{x}, t) - u\psi^2(\mathbf{x}, t) + \dots , \quad (5)$$

where c , r , and u are constants whose connection with the occupation probability p of the underlying microscopic DP model is at present unknown, but

associated with defining $\psi^{1/2}$ for negative ψ .

⁹ Strictly speaking, an order parameter should be zero on symmetry grounds and nonzero only in ordered phases, where the symmetry is spontaneously broken. Problems with absorbing states are unusual from this standpoint, in that typically there is no symmetry that forces any quantity to vanish in the absorbing phase. Likewise, the active phase does not typically require a broken symmetry. So when we refer to the average density of wet sites in DP as an “order parameter,” we use the term very loosely, solely to avoid trotting out pompous and irritating phrases such as “the quantity of central interest in the problem.”

¹⁰ The principle that every term allowed by symmetry must be included is often concisely summarized as “everything not forbidden is compulsory.” The authors advise against applying this rule too generally outside of science. Both have occasionally lost sight of this point, with predictably disastrous results.

will be roughly inferred below. This rough correspondence will turn out to be good enough.

It transpires that the three terms displayed in (5) are the only variables relevant for the computation of universal critical properties, at least near the so-called upper critical dimension (Wilson & Kogut 1975), $d_c = 4$. (Since the terms in which the lattice symmetry is manifest involve higher order derivatives of ψ , and so are irrelevant, critical exponents are independent of lattice structure.) We shall have more to say about this later; for the moment, let us just savor the relief of not having to treat the full infinite set of higher powers and derivatives of ψ . Note, however, that if we throw out all higher terms in f_x , then we must assume $u > 0$ to avoid having ψ grow without bound under evolution of the Langevin equation.

Finally, let us deal with g_x . Here, as mentioned above, the only relevant term is the lowest order one in ψ , viz., ψ^α , meaning that all we need do is choose the value, 1/2 or 1, of the exponent α . The following elementary argument, presented here for DP, but valid for most problems with a microscopic stochastic element, shows that the correct choice is $\alpha = 1/2$: Consider the microscopic DP model viewed in the $(d+1)$ -dimensional representation, and imagine that the system is in steady state, deep in the active phase, where the average density of occupied sites is $\langle \psi \rangle = n$. Obviously there will be stochastic fluctuations in the occupation of any site. Viewed on a scale so coarse that the correlations between different sites are negligible, however, these fluctuations can be accounted for by saying that any given site is occupied or empty with probability n or $1 - n$, respectively. This gives a mean square deviation $\langle \psi^2 \rangle_c \equiv \langle \psi^2 \rangle - \langle \psi \rangle^2 = n - n^2$, which goes like n for small n .

Let us now try to match this bit of physics with what emerges from the Langevin representation:

$$\partial\psi/\partial t = c\nabla^2\psi - r\psi - u\psi^2 + \psi^\alpha\eta . \quad (6)$$

In steady state, the expectation value of the right hand side must vanish, yielding $r \langle \psi \rangle = -u \langle \psi^2 \rangle$. Expanding ψ around its mean value n , through $\delta\psi \equiv \psi - n$, then yields, to linear order in $\delta\psi$, $n = -r/u$ (implying that $r < 0$ for the active phase), and

$$\partial\delta\psi/\partial t \sim c\nabla^2\delta\psi - un\delta\psi + n^\alpha\eta . \quad (7)$$

Given the Gaussian nature of η , fourier transformation then yields $\langle \delta\psi^2 \rangle \sim Dn^{2\alpha} \int d^dk \int d\omega / (\omega^2 + (ck^2 + un)^2)$, which has a term proportional to $n^{2\alpha}$ for small n . In order to make this term match the behavior found in the microscopic model, i.e., to go like n , requires $\alpha = 1/2$.

2.5 The Langevin Equation and Universality

Prosaic Remarks: Thus we have arrived, aided by a great waving of hands, at a prospective Langevin equation – Eq. (6) with $\alpha = 1/2$ – for the DP

problem. So little seems to have gone into the derivation that one might feel one has gotten something for nothing. This is typical of the construction of Ginzburg-Landau free energies or Langevin equations. Landau's insights about analyticity and symmetry, supported by RG notions of irrelevant variables, are deceptively powerful, getting one rapidly to the stage where one can obtain useful results from fairly standard manipulations. This point has significant implications for universality: Though nominally we have been deriving a Langevin equation for DP, nothing about directed percolation other than the existence of a single absorbing state and the absence of other symmetries (except lattice symmetries) was used in the derivation. The analysis therefore applies equally well to *all* systems with these properties, including the explicit examples we introduced earlier. Since, as we shall see, the critical exponents of the Langevin model (6) are unique, it follows that all of the microscopic models with a unique absorbing state, single-component order parameter, and no extra symmetries, belong in the DP universality class characterized by (6). This reasoning provides an intuitive demonstration of the remarkable robustness of the DP universality class postulated by Grassberger (1982) through a more formal “Fock-space” construction.

Mean-Field Analysis of the Langevin Model for DP: Let us now see whether the Langevin model in fact produces sensible predictions for DP and related problems. To get a crude feel for the physics of Eq. (6), we first consider MFT, the approximation in which spatial fluctuations and noise are neglected. This is most easily implemented by neglecting the noise and gradient terms of (6), and replacing the field $\psi(\mathbf{x}, t)$ by the spatial constant $\psi(t)$, thereby obtaining the deterministic ordinary differential equation

$$d\psi/dt = -r\psi - u\psi^2 . \quad (8)$$

This equation obviously has two stationary solutions in the long-time limit, respectively representing the absorbing and active phases: $\psi = 0$, and $\psi = -r/u$. These solutions are stable for $r > 0$ and $r < 0$ respectively. Roughly speaking, therefore, r plays the role of the probability p in the microscopic model: decreasing r from ∞ to $-\infty$ corresponds to increasing p from 0 to 1. In MFT, the critical value of r is $r_c = 0$, and the critical exponent β governing the decay of the average density, $\langle \psi \rangle \sim |r - r_c|^\beta$, as r_c is approached from the active phase, is unity. It is encouraging to see that this value is independent of any parameters of the model. Well advised to quit while we're ahead, we will press recklessly onward, beyond MFT, in the next lecture.

3 Critical Behavior of DP from Impressionistic RG Analysis

At the mean-field level, the qualitative physics of Eq. (6) seems consistent with our expectations for DP. To make further progress we must treat the fluctuations left out in MFT, which means employing the RG. While it is hopeless in the available time to give a satisfactory account of RG methods, in this lecture we will foolishly attempt to provide enough background to give those in the audience not familiar with the technique the illusion that they understand how it works. (Smoke and mirrors will be the crucial elements of this effort, which should at least succeed in eliciting fond recollections of Don Quixote.) Here goes:

3.1 A Brief Technical Digression: RG on the (Very) Cheap

The essence of the RG is of course coarse graining, i.e., viewing a problem on progressively larger length scales, and monitoring the associated evolution of the parameters. For differential equations like (6), this can be done straightforwardly by Fourier transforming the equation in space, and solving for the modes, $\tilde{\psi}(\mathbf{k}, t)$, of ψ with wavenumbers $|\mathbf{k}|$ greater than Λ/b , in terms of those with wavenumbers less than Λ/b . Here $b(> 1)$ is the factor by which lengths are rescaled, and Λ the high-momentum cutoff that embodies the existence of a shortest distance – the lattice spacing a – in the model; hence $\Lambda = 2\pi/a$. This cutoff guarantees that all momentum integrals converge in the ultraviolet.¹¹

Substituting these solutions back into the equations gives a new set of equations, similar to the original ones, for the remaining small- \mathbf{k} modes, $\tilde{\psi}(\mathbf{k}, t)$, where $0 \leq |\mathbf{k}| \leq \Lambda/b$. One then rescales the values of x , t , and $\psi(\mathbf{x}, t)$ (or, equivalently, \mathbf{k} , t , and $\tilde{\psi}(\mathbf{k}, t)$), to make the new equations look as much as possible like the originals. In particular, the rescaled \mathbf{x} variable, \mathbf{x}' , is always chosen to make the new high-momentum cutoff, Λ/b , look the same as the original, Λ , i.e., $\mathbf{x}' = \mathbf{x}/b$. This of course corresponds precisely to increasing the scale of distances in the problem by b . The rescalings of t and ψ are typically written as $t' = t/b^z$, and $\psi'(\mathbf{x}', t') = \psi(\mathbf{x}, t)/b^\zeta$, where the exponents z and ζ turn out to be critical exponents of the theory. We shall see how these exponents are chosen in a very simple example below.

First, however, note that terms not in the original equations may be generated by the elimination of the high- \mathbf{k} (short-distance) modes. For example, starting with Eq. (6), one generates higher terms in ψ and its derivatives, such as ψ^3 , $\partial^2\psi/\partial t^2$, etc. In principle, any term consistent with the symmetry of the original equations will be generated by the rescaling procedure.

¹¹ In condensed matter physics, the presence of a lattice spacing or some other short-distance cutoff is almost invariably assumed. Fields like ψ are therefore typically taken to consist of Fourier components $\tilde{\psi}(\mathbf{k})$ with all $|\mathbf{k}|$ values less than some upper (ultraviolet) cutoff Λ .

Since the new equations have exactly the same information in them as the originals, however, terms not obeying the symmetry can never be produced. This is just the RG justification of Landau's dictum that all terms allowed by symmetry must in principle be included from the beginning. If they are not, then they will be generated under the RG anyhow. So what gives us the right to claim that it is OK to ignore all but the few lowest order terms in constructing the Langevin theory? The answer is as follows: Suppose one starts with a Langevin equation consisting of the complete infinite set of symmetry-allowed terms, each with its own coefficient. After performing a RG rescaling operation, we will obtain an equation identical in form with the original, but with different coefficients for all of the terms. The crucial point is that all but a very few of those renormalized coefficients will have values *smaller* than their original ones. Thus if one repeats the RG transformation many times, the coefficients of these terms will decrease progressively, eventually becoming so small as to be totally negligible. Viewed on the longest length scales that are of interest to us, then, these terms can safely be ignored, in which case one might as well omit them from the beginning. It is this line of argument that is tacitly applied to legitimize the brutal truncation of the complete Langevin theory for DP to produce the more manageable form (6). We will see an explicit example of this shortly.

A Simple Illustration: Recursion Relations and Fixed Points from Pure Rescaling: To acquire a more concrete sense of how this works, and how the spatial dimension d enters the picture, let us perform a RG rescaling on Eq. (6) in the simplest possible limit, i.e., for d sufficiently large that MFT is valid. To do so, we replace x , t , and $\psi(\mathbf{x}, t)$ in (6) by $b\mathbf{x}'$, $b^z t'$, and $b^\zeta \psi'(\mathbf{x}', t')$ respectively, obtaining the rescaled equation

$$b^{\zeta-z} \partial \psi' / \partial t' = b^{\zeta-2} c \nabla'^2 \psi' - b^\zeta r \psi' - b^{2\zeta} u \psi'^2 + b^{\zeta/2} \psi'^{1/2} \eta' . \quad (9)$$

In deriving this equation, all we have done is perform a trivial rescaling, neglecting all nontrivial contributions resulting from the integration of the high- $|\mathbf{k}|$ modes. Ignoring this problem for the moment in the vain hope that it will go away, we divide through by $b^{\zeta-z}$, and cast the rescaled equation in the same form as the original:

$$\partial \psi' / \partial t' = c' \nabla'^2 \psi' - r' \psi' - u' \psi'^2 + \psi'^{1/2} \eta' . \quad (10)$$

Here $c' = b^{z-2} c$, $r' = b^z r$, $u' = b^{\zeta+z} u$, and $\eta'(\mathbf{x}', t') = b^{z-\zeta/2} \eta(\mathbf{x}, t)$. Defining the renormalized noise strength D' through $\langle \eta'(\mathbf{x}', t') \eta'(\mathbf{0}, 0) \rangle = D' \delta(\mathbf{x}') \delta(t')$ turns this last equation into $D' = b^{z-d-\zeta} D$. These equations for c' , r' , u' , and D' are recursion relations or flow equations, showing how parameters in the rescaled equation are related to those of the original. By considering arbitrarily small expansions in length scale generated by writing $b = e^{dl}$, where dl is an infinitesimal, we can write these recursion relations in a more convenient differential form:

$$\frac{dc}{dl} = (z - 2)c \quad (11)$$

$$\frac{dr}{dl} = zr \quad (12)$$

$$\frac{du}{dl} = (\zeta + z)u \quad (13)$$

$$\frac{dD}{dl} = (z - d - \zeta)D . \quad (14)$$

This shows directly how the coefficients change or flow with increasing (logarithmic) length scale l . The question is: What happens to them in the $l \rightarrow \infty$ limit? With very rare exceptions, flows ultimately terminate in fixed points, i.e., sets of values of the coefficients (c^* , r^* , u^* , and D^* in our case), which make the right hand sides of all the flow equations vanish.¹²

As most readers of this article are doubtless aware, fixed points come in two varieties: critical and noncritical, respectively corresponding to correlation lengths that are infinite or zero. This is easy to see from the scaling of lengths under the RG: Suppose the correlation length of an arbitrary system specified by parameters $\{u_i\}$ for $i = 1, 2, 3, \dots$ is $\xi(\{u_i\})$. At a fixed point, $\{u'_i\} = \{u_i\} = \{u_i^*\}$, the parameters do not change under length rescaling, so the correlation length, which obeys $\xi(\{u_i\}) = b\xi(\{u'_i\})$ in general, satisfies $\xi(\{u_i^*\}) = b\xi(\{u_i^*\})$. Obviously, $\xi = 0$ and $\xi = \infty$ are the only solutions of this equation.

Critical fixed points describe critical points or surfaces, which are defined as places in parameter space where correlation lengths diverge and correlations decay algebraically. Critical exponents and other universal properties are controlled by such fixed points. (Phases of systems in which correlations everywhere decay algebraically, with exponents that vary continuously with parameters, are typically described by lines of critical fixed points. The Kosterlitz-Thouless phase of the classical equilibrium 2d XY model and its many physical realizations (Kosterlitz & Thouless 1973) is the best known example.)

Noncritical fixed points, on the other hand, describe entire (non-algebraic) phases¹³ of a system, where correlation lengths are finite and correlations decay exponentially. The point is that as a system with finite correlation length is viewed on progressively longer scales, the effective correlation length

¹² For certain classes of equilibrium problems, one can argue (Wallace & Zia 1974) that limit cycles, chaotic behavior, or other behaviors of RG flows more exotic than termination in fixed points will not occur. We are not aware of such results for nonequilibrium systems, but the typical expectation is for fixed points there as well. For one thing, the physical interpretation of coupling constants trapped in a limit cycle or chaotic trajectory is usually unclear. (Hierarchical models for spin glasses have nonetheless been shown to give rise to chaotic RG flows (McKay *et al.* 1982, Berker & McKay 1984).)

¹³ Noncritical fixed points also control first order phase transitions, where correlation lengths are also finite.

shrinks by the factor b each time, vanishing at the fixed point, which is reached only on the infinite length scale.

Critical Dimension, d_c : Let us return to our approximate recursion relations (11)-(14) for the DP problem, to try to extract something – anything – useful. The search for fixed points is simple: Clearly c and u achieve finite, nonzero fixed point values if and only if $z = 2$ and $\zeta = -z = -2$. These choices reduce the r and D equations to $dr/dl = 2r$ and $dD/dl = (4-d)D$. The first of these equations reaches a finite fixed point (at $r^* = 0$) only if $r = 0$. Otherwise r will flow off to either positive or negative infinity, depending on its initial sign. There is sensible physics in this result: We have already seen in MFT that we have to adjust r to zero to find the DP critical point. Thus the fixed point at $r^* = 0$ must be the critical fixed point. An initial positive (negative) value of r then corresponds to being in the absorbing (active) phase, which is evidently governed by a noncritical fixed point at $r^* = \infty$ ($-\infty$). As for D , clearly if $d > 4$ it evolves to the fixed point value $D^* = 0$. This vanishing of the noise on large scales means that MFT should be valid, from which we conclude that the critical fixed point at $c^* = c$, $u^* = u$, $r^* = 0$, and $D^* = 0$, with $\zeta = -z = -2$, should give rise to mean field exponents. If this is so (which we will verify in just a second), then the stability of this fixed point for $d > 4$ implies that $d_c = 4$ is the so-called “upper critical dimension” – the dimension above which MFT is valid. For $d < 4$, however, the fixed point at $D^* = 0$ is unstable, and the D equation flows off to arbitrarily large values of D . This means that noise, and hence fluctuations, are so strong on large scales that they cannot be neglected, implying that MFT is invalid. The fixed point at $D^* = \infty$ is impossible to analyze, so no information about the DP transition can be extracted from Eqs. (14) for $d < d_c = 4$.

Critical Exponents from Fixed Points: As a long-overdue sanity check, let’s now establish that the fixed point at $D^* = 0$ indeed gives rise to mean-field exponents. This will also serve as a lightning review of how critical exponents are calculated from fixed points. We first consider the correlation length exponent ν , which we didn’t bother calculating in the direct MFT formulation earlier. Since all lengths, ξ included, rescale like $x = bx'$, it follows that $\xi(r) = b\xi(r') = b\xi(b^z r)$. Since both sides of this equation must be independent of b , this yields $\xi \sim r^{-\nu}$ with $\nu = 1/z = 1/2$, the correct mean-field result. Note for future reference that in more general problems, where the critical value of the control parameter r_c is not zero, one typically uses $\delta r \equiv r_c - r$, rather than simply r , as the argument of ξ and other quantities of interest. Moreover, the recursion relation for δr is almost universally written as $\delta r' = b^{1/\nu} \delta r$, which, together with $x = bx'$, immediately gives $\xi \sim \delta r^{-\nu}$, the conventional definition of the correlation length exponent. In our mean-field approximation, it turns out that $1/\nu = z$, so the r recursion relation (Eq. (12)), involves z rather than ν . But in general this relation between z

and ν does not hold, whereas writing $\delta r' = b^{1/\nu} \delta r$ always correctly implies $\xi \sim \delta r^{-\nu}$.

In similar style, let us now show that the exponent z as we defined it is the conventional dynamical exponent, in this problem and quite generally. To do so, note that the typical relaxation time τ characterizing the response of the system near the critical point is expected to diverge as $r \rightarrow r_c$. Being a time, τ scales like $\tau(\delta r) \sim b^z \tau(\delta r') \sim b^z \tau(b^{1/\nu} \delta r)$, whereupon $\tau(\delta r) \sim \delta r^{-z\nu} \sim \xi^z$. This relation between τ and ξ is the standard definition of the dynamical exponent z , so our original use of the letter z for the time-rescaling exponent was not inappropriate. Note too that $z = 2$ is the correct mean-field value of the dynamical exponent.¹⁴

Flogging this dead horse one last time, let us now consider the order parameter exponent β , defined via $M(\delta r) \equiv \langle \psi(0,0) \rangle \sim \delta r^\beta$, as r_c is approached from the active phase. Using the rescalings $\psi = b^\zeta \psi'$, and $\delta r' = b^{1/\nu} \delta r$ we have $M(\delta r) = b^\zeta M(b^{1/\nu} \delta r)$, immediately implying $M(\delta r) \sim \delta r^{-\zeta\nu}$, or $\beta = -\zeta\nu$, a result which holds very generally. For the specific fixed point we consider here, $\zeta = -2$ and $\nu = 1/2$, giving $\beta = 1$, the correct mean-field result. (Recall that $r_c = 0$ here, making everything particularly simple.)

Neglect of “Irrelevant” Terms: So far we have just done a rather trivial RG rescaling, ignoring the terms in the recursion relations coming from the high-momentum degrees of freedom integrated out as part of the RG transformation process. Before sketchily remedying this omission, however, let us make two points of more general conceptual significance. The first concerns the neglect of all the higher powers of ψ and its derivatives in the Langevin equation. We are finally in position to justify this, at least loosely. Imagine including on the right hand side of Eq. (6) a term such as $u_{ps} \nabla^p \psi^s$, for any positive integers p and s and some coefficient u_{ps} . Rescaling the equation as before, we obtain, with little effort, the differential recursion relation $du_{ps}/dl = (z - p + (s-1)\zeta)u_{ps}$. Recalling that $\zeta = -z = -2$ at the mean-field fixed point, we see that for $s > 2$ and *any* $p \geq 0$, or for $s = 2$ and $p > 0$, the coefficient of u_{ps} on the right-hand side of this equation is negative. In these cases, then, u_{ps} will flow to the fixed point value $u_{ps}^* = 0$ as $l \rightarrow \infty$. Thus the term $u\psi^2$ (note $u_{02} \equiv u$), is the only nonlinearity that need be treated. We lose nothing by setting these higher u_{ps} 's to zero from the outset. On the large scales that matter, they will disappear anyhow.

This result, which is readily seen to hold even when the contributions from the integrated small- k modes are included, is really nothing more than dimensional analysis. One can see this directly, by rescaling ψ , x , and t in the Langevin equation (6) by factors chosen to keep the coefficient of $\partial\psi/\partial t$ unity, while simultaneously making the rescaled diffusion constant, c , and the rescaled noise strength, D , unity as well. The reader is encouraged to convince

¹⁴ In DP literature, the correlation length and time exponents, ν and νz , are often referred to as ν_\perp and ν_\parallel , respectively.

him or herself that this choice gives the rescaled field ψ the dimension of Λ^{d-2} , where Λ is a momentum. Of course the operator ∇ has the dimension of Λ . This means that for $d > 2$ each power of ψ or ∇ brings with it increased powers of momentum. In the small-momentum limit that interests us for critical phenomena, therefore, terms become progressively less important as they contain higher powers of ψ and/or ∇ . The dimension of the coefficient, $u_{02} \equiv u$, of the lowest order nonlinearity, ψ^2 , is Λ^{4-d} . Since every term in the perturbation expansion in u for any quantity of interest must have the same dimension, it follows that the algebraic expression multiplying the factor of u^n in the n th order of perturbation theory must have dimension $\Lambda^{n(d-4)}$ for large n . Thus for $d > 4$ ($d < 4$), higher orders of perturbation theory become, for the small momenta of interest in critical phenomena, progressively *less* (*more*) important as n increases. One therefore concludes that $d_c = 4$. Such dimensional considerations are probably the simplest way of inferring the upper critical dimension of any problem. Note that all higher nonlinear coefficients, u_{ps} have *negative* momentum dimensions for d near 4, implying their *irrelevance* for affecting universal critical behavior.

Ruminations on Universality: The second general point concerns universality – the fact that critical exponents are independent of parameters in the Langevin equation. As eigenvalues of recursion relations linearized around critical fixed points, exponents are properties of these fixed points. Since the fixed points in turn are properties of the recursion relations, and hence of the general structure of the Langevin equation, spatial dimension, etc., rather than of specific parameters, the celebrated indifference of critical exponents to parameter values, lattice type, and other details follows immediately. Since we have already argued on symmetry grounds that many different microscopic models are characterized by a single Langevin equation (such as that for DP), the universality of exponents across many apparently diverse microscopic systems is thereby justified.

Having established these grand principles, let us return to earth and study the effect of the terms coming from the high-momentum degrees of freedom integrated out as part of the RG transformation process. We have blithely ignored these terms up to now. Though such terms can be generated through standard diagrammatic perturbation theory, time does not permit us to summarize that calculation. Rather, we just state the result, leaving it as an exercise to the reader to verify the following recursion relations, correct to one-loop order for Eq. (6):

$$dc/dl = (z - 2 + A_4 u D/8)c \quad (15)$$

$$dr/dl = (z - A_4 u D/4)r + \Lambda^2 A_4 u D/2 \quad (16)$$

$$du/dl = (\zeta + z - 3A_4 u D/4)u \quad (17)$$

$$dD/dl = (z - 4 + \epsilon - \zeta - A_4 u D/2)D . \quad (18)$$

Here $\epsilon \equiv 4 - d$, and A_4 is a constant equal to $1/4\pi^4$ times the volume of the unit hypersphere in four dimensions. It is simple to check from these equations that for $\epsilon < 0$ (i.e., $d > 4$), the mean-field fixed point with $r^* = u^* = D^* = 0$ remains the only stable critical fixed point. (Again, it is reached only when the control parameter r is adjusted to a critical value r_c , which is of $O(u)$ for small u .) This demonstrates that 4 remains the upper critical dimension, even when diagrammatic corrections are included.¹⁵ For $\epsilon > 0$, the mean field fixed point is unstable, but a new stable, non-trivial, critical fixed point, located at $r^* \sim -\Lambda^2\epsilon/6$ to order ϵ , emerges. Critical exponents can of course be calculated in standard fashion, by linearizing the recursion relations around this new fixed point. A modest calculation (again, left to the long-suffering audience), shows that to order ϵ : $\nu = (1 + \epsilon/8)/2$, $z = 2 - \epsilon/12$, and $\zeta = -2 + 7\epsilon/12$, whereupon the general scaling relation $\beta = -\zeta\nu$ gives $\beta = 1 - \epsilon/6$.

Scaling Relations and Functions: At this point, we understand much of the basic critical behavior of the DP universality class, at least on a crude level. It is not that the ϵ expansion produces reliable values of exponents in the physically sensible dimensions $d = 1, 2$, and 3 , even when it is extended beyond lowest order. Numerics remain a better bet for generating accurate numbers, provided one can continue to count on the largesse of scientific funding agencies for computer support.¹⁶ But the RG provides a conceptual framework for unifying the many members of a universality class, and predicting which quantities should be universal, and hence are worth computing. In this context, it is worth emphasizing the scaling laws relating critical exponents that follow naturally from the RG formulation, reducing the number of independent exponents that need be computed. An example will suffice to make the point: Suppose one wishes to calculate the behavior of the connected, steady-state, two-point correlation function $C_c(\mathbf{x}, t, \delta r) \equiv \langle \psi(\mathbf{x}, t)\psi(\mathbf{0}, 0) \rangle - M^2$ in the active phase of any system with absorbing states. Rescaling of ψ , \mathbf{x} , and t in the by-now familiar way yields

$$C_c(\mathbf{x}, t, \delta r) = b^{2\zeta} C_c(\mathbf{x}/b, t/b^z, \delta r b^{1/\nu}) . \quad (19)$$

The only way for the right hand side of this equation to be independent of b (as it must be, since the left hand side doesn't contain b), is for C_c to have the form

$$C_c(\mathbf{x}, t, \delta r) = x^{2\zeta} c_c(x/\xi, t/\tau) , \quad (20)$$

¹⁵ We shall argue in Section 5 that inclusion of diagrammatic corrections can sometimes shrink the basin of attraction of the mean field fixed point even *above* d_c , producing a “strong-coupling” fixed point which is stable in the region where the mean field one is not.

¹⁶ Some numerical values for DP critical exponents can be found in Cardy & Sugar (1980), Jensen & Dickman (1991), Jensen & Dickman (1993a), Jensen (1992), Essam *et al.* (1986), Essam *et al.* (1988), Brower *et al.* (1978).

where, as usual, the correlation length ξ and characteristic time τ diverge like $\delta r^{-\nu}$ and $\delta r^{-\nu z}$ respectively, as $\delta r \rightarrow 0$. Here c_c is a so-called *scaling function*. Such functions occur ubiquitously in critical phenomena, and, apart from overall multiplicative factors, can often be shown to be universal (Domb & Green 1976). For our modest purposes, however, it is important mostly to note that in c_c , lengths x and times t are expressed in units of ξ and τ respectively. This is very typical of critical phenomena, where near the critical point a single characteristic length (ξ) and time (τ) set the scale for the decay of all correlation functions.

For simplicity, let us now restrict attention to the equal-time correlator, where $t = 0$. Suppose we go right to the critical point, $\delta r = 0$. Our treatment of C_c has actually been perfectly general thus far, applying equally well to systems with absorbing states and to more conventional critical phenomena, such as occur in, e.g., the ferromagnetic Ising model (Ma 1976, Domb & Green 1976, Binney *et al.* 1992). Let us now imagine we are dealing with a problem of the latter type, where, even right at the critical point, the correlation function remains finite and nonzero. In this case the scaling function $c_c(y, 0)$ must simply approach a nonzero constant as its argument $y \rightarrow 0$, implying that $C_c(\mathbf{x}) \sim x^{2\zeta}$ at the critical point. Now the decay of C_c at criticality is conventionally written $C_c(\mathbf{x}) \sim x^{-d+2-\eta}$, which really defines the critical exponent η . This definition implies $2\zeta = -(d - 2 + \eta)$. Since we saw just above that $\zeta = -\beta/\nu$, however, we arrive at the (legendary) scaling relation for systems without absorbing states, viz.,

$$2\beta = \nu(d - 2 + \eta) . \quad (21)$$

In other words, only two of the exponents β , ν , and η are truly independent, the third being derivable from Eq. (21). This serves, *inter alia*, as a useful consistency check on experimental and numerical determinations of exponents.

Turning now to systems such as DP that do have absorbing states, we observe that, at the critical point, $\psi(\mathbf{x}, t)$ is identically zero in steady-state, whereupon C_c must clearly vanish. So, although Eq. (20) continues to hold, the scaling function $c_c(y, 0)$ must now vanish, presumably like some power of y , y^ρ say, as criticality is approached, i.e., as $y \rightarrow 0$. We conclude that $C_c(\mathbf{x}, \delta r) \sim \delta r^{\nu\rho} x^{2\zeta+\rho}$ as $\delta r \rightarrow 0$ for fixed x . Defining $\Delta \equiv \nu\rho$, we can rewrite this equation as

$$C_c(\mathbf{x}, \delta r) = \delta r^\Delta x^{-d+2-\eta} , \quad (22)$$

where the scaling law relating β , η , and ν now reads (Grinstein *et al.* 1996)

$$2\beta = \Delta + \nu(d - 2 + \eta) . \quad (23)$$

For systems with absorbing states, therefore, an extra exponent, Δ , is required to characterize the phase transition. It turns out that in DP, a straightforward graphical argument shows that the exponent Δ is simply equal to β ,

whereupon the scaling relation (22) becomes simply $\beta = \nu(d - 2 + \eta)$. Those insomniacs still awake for the final lecture, however, will see that this does not hold for the multiplicative noise problem where, so far as is known, Δ is a genuinely new, independent exponent.

3.2 Seed Initial Conditions

Before ending this section, let us briefly study one last useful characterization of the physics of absorbing states, viz., the proliferation of active sites starting from a seed initial condition. Consider DP as an example, and imagine starting the system off from an initial state consisting of a single wet site (or “seed”), in a lattice that is otherwise dry. Since wet sites cannot be produced spontaneously from dry ones, the only way for them to appear in the initially dry background is to spread outward from the wet seed. (In systems without absorbing states, where wet sites or their analogues can be created spontaneously, seed initial conditions are not terribly useful.) The systematics of this spreading process at and near the critical point constitute a useful diagnostic for the system’s critical properties, and are particularly amenable to numerical simulation. The critical spreading is typically characterized by the following three quantities, all of which are found to behave algebraically at the critical point, and so are characterized by critical exponents (Grassberger & de la Torre 1979):

- (1) The linear extent, $R(t)$, of the wet region surrounding the seed at time t , grows like $R^2(t) \sim t^{\tilde{z}}$ for large t .
- (2) The average probability $P_s(t)$ that there remains at least one surviving wet site in the system after time t decays like $P_s(t) \sim t^{-\delta}$ for large t .
- (3) The total number of wet sites, $N(t)$, in the system after time t , grows like $N(t) \sim t^{\tilde{\eta}}$ at large t .

The word “average” in these definitions means an average over many different trials, all starting from the same seed initial condition. Of course in any given trial, even in the active phase, there is a nonzero probability that all wet sites simply die out after some length of time; this is quantified by the average survival probability $P_s(t)$.

Note that in the literature on systems with absorbing states, the exponents z and η are defined without tildes. Since, as we have seen, the symbols z and η are conventionally used as exponents for the steady-state behavior of the correlation time τ and the correlation function $C_c(x)$ respectively, this is confusing. It is to alleviate this confusion that we have given the seed exponents tildes. In fact it turns out that, at least for DP, the seed exponents are not new, but can be derived from the steady-state ones. In particular, $z = 2/\tilde{z}$, while $2\eta = 4 - d - z\tilde{\eta}$. There is, moreover, a scaling relation $(d+1)\tilde{z} = 4\delta + 2\tilde{\eta}$, which determines δ as a function of z and η as well. Time does not permit us to derive these various relations here (except to note that since characteristic lengths behave like characteristic times raised to the power $1/z$, the relation between z and \tilde{z} is obvious). The other relations are less trivial, and their

derivation is suggested as an worthwhile exercise for readers with masochistic inclinations. Broad hints can be found in Grassberger & de la Torre (1979), Cardy & Sugar (1980), Janssen (1981) and Takayasu & Tretyakov (1992).

Needless to say, one can generate reams of scaling relations involving the quantities $R(t)$, $P_s(t)$, and $N(t)$ in the active phase rather than at criticality. To give one example: $P_s(t, \delta r) \sim t^{-\delta} p_s(t/\tau)$, where $\tau \sim \delta r^{-\nu z}$, and $p_s(y)$ is a scaling function. Again, readers are encouraged to make sure they understand the origin of such relations, and to infer the behavior of scaling functions such as $p_s(y)$ in the limits $y \rightarrow 0$ and $y \rightarrow \infty$.

We will see at the end of the next lecture that not all sailing on the seas of seed initial conditions is as smooth as it is in DP. In systems with multiple absorbing states, e.g., there is numerical evidence to suggest that the exponents $\tilde{\eta}$, δ , and sometimes \tilde{z} are nonuniversal.

4 Multiple Absorbing States

In this section, faithful (and even less-than-faithful) readers will get the chance to apply techniques for constructing and analyzing Langevin equations to models that are newer, more complex, and far less well understood than DP: those which in the thermodynamic limit contain infinite numbers of absorbing states. Can we endure the excitement?

4.1 Motivation: Models of Catalysis

$2H_2 + O_2 \rightarrow 2H_2O$: The systems of interest occur naturally in many of the same contexts as do realizations of DP, such as in the spread of epidemics and in toy models of heterogeneous catalysis. We motivate the discussion by considering a simple model for the catalytic oxidation of hydrogen on a metal surface. First introduced by a participant at this meeting, Ezequiel Albano, in 1992, this so-called “dimer-dimer” model (Albano & Maltz 1992, Maltz & Albano 1992) is similar in spirit to the ZGB model for the oxidation of carbon monoxide described in section 2. It involves the catalytic facilitation of the chemical reaction $2H_2 + O_2 \rightarrow 2H_2O$. The rules are as follows:

The metal surface, taken for simplicity to be a d-dimensional hypercubic lattice, is immersed in an atmosphere consisting of a mixture of the diatomic molecules O_2 and H_2 . With a probability proportional to p (or $1 - p$) per unit time, each nearest-neighbor pair of unoccupied lattice sites adsorbs a hydrogen (or oxygen) molecule, simultaneously dissociating the molecule so that one of the atoms occupies each of the sites in question. If an oxygen and a hydrogen atom find themselves sitting in nearest neighbor positions, the hydrogen atom moves onto the oxygen site instantaneously, forming an OH complex. If such a complex finds itself neighboring another hydrogen atom, a reaction occurs, instantaneously producing an H_2O molecule that leaves the surface, freeing up the two sites for further participation in the reaction.

If two OH complexes find themselves in nearest-neighbor positions, they react, instantaneously producing an H_2O molecule that leaves the surface, and an O atom that remains adsorbed. Individual hydrogen atoms diffuse freely through the unoccupied sites of the lattice with some diffusion constant.

Computer simulations (Albano & Maltz 1992, Maltz & Albano 1992) show that as a function of the parameter p , this model has a phase diagram consisting of three phases: two absorbing phases at low and high p , separated by an intermediate active phase. Both transitions are apparently continuous. In the absorbing phase at high p , the lattice, not surprisingly, becomes hydrogen-poisoned, i.e., completely filled with hydrogen atoms. The transition from this phase into the active phase is, according to the principles so brutally elaborated in the previous two sections, doubtless in the DP universality class: ho hum. The absorbing phase at small p , however, is more interesting, consisting of a mixture of OH complexes, O atoms, and single vacancies whose near neighbor sites are all occupied. It is clear that there are many different possible configurations with this character, each of which is a perfectly legitimate absorbing state of the system. Indeed, the number of distinct absorbing states of this type obviously increases exponentially with increasing system size, diverging in the thermodynamic limit. This multiplicity raises the possibility that the continuous transition from this phase into the active one might belong in a universality class distinct from DP. The earliest computer simulations (Albano & Maltz 1992, Maltz & Albano 1992) of the dimer-dimer system suggested that this might possibly be the case. Identifying this universality class analytically thus seems an interesting challenge.

A Simpler Abstraction – the PCP: Rather than undertaking the analysis of the dimer-dimer model, with its three different adsorbed species and hence its daunting geometrical complexity, we are well advised first to tackle a simpler, if less physical, abstraction, whose absorbing phase likewise consists of exponentially diverging numbers of absorbing configurations. Just such a model was concocted (Jensen 1993) by Iwan Jensen in 1993. Called the “pair contact process” (PCP), it consists of particles and empty sites on a lattice, and is an elementary generalization of the ordinary contact process we discussed in section 2. As in the contact process, the rules are extremely simple. All of the dynamics involves nearest neighbor pairs of particles, such pairs therefore constituting the “order parameter.” Any nearest neighbor pair of particles can do one of two things: With probability p per unit time, it simply disappears, leaving two vacant sites behind; and with probability $1 - p$ per unit time, it creates another particle at a randomly chosen vacant site neighboring either of the members of the original pair. It follows at once that any state without nearest neighbor pairs of particles is absorbing. The immense freedom available in choosing the positions of the isolated particles in such a state means that the number of absorbing configurations grows exponentially

large with system size. Moreover, simulations show that it undergoes a continuous transition from an active phase at small p to this highly degenerate absorbing phase. (The critical value, p_c , of p , is roughly 0.08.) Thus from all points of view, the PCP seems an ideal subject for our analytical attention. The next section summarizes the Langevin analysis of this model presented in Muñoz *et al.* (1996, 1996b).

4.2 Langevin Analysis of the Prototypical PCP Model

Coupled Langevin Equations: The first step, obviously, is to identify a set of fields appropriate for the coarse-grained description of the phase transition. Vacant sites clearly constitute the background, and need not be treated explicitly. Isolated near neighbor pairs of particles drive all of the dynamics. Their coarse-grained density, $n_2(\mathbf{x}, t)$, is thus the system's "order parameter," whose vanishing defines the absorbing phase. However, the coarse-grained density, $n_1(\mathbf{x}, t)$, of isolated particles must also be accounted for if the dynamics is to be faithfully represented. In principle, we must also worry about occupied clusters of three, four, five sites, and so on. However, it is straightforward to show that such higher clusters can be regarded as composed of combinations of single particles and occupied pairs, the difference between the true cluster and this approximate version being irrelevant for the computation of universal critical properties. This point is discussed in a paper (Grinstein *et al.* 1989) on the ZGB model for the reaction $2CO + O_2 \rightarrow 2CO_2$ of section 2, in which clusters of CO or O atoms must also be accounted for. The argument establishing the irrelevance of these higher clusters for the critical behavior of this model (which is in the DP universality class), should apply equally well to the present problem. We refer the interested reader to Grinstein *et al.* 1989 for the details, and simply take for granted here that $n_1(\mathbf{x}, t)$ and $n_2(\mathbf{x}, t)$ suffice to describe the oxidation of H_2 .

The next step is the construction of the Langevin theory, in this case two coupled Langevin equations for n_1 and n_2 . Again this task is simplified by the absence of any symmetries other than those of the lattice, which occur in higher order, presumably irrelevant, derivative terms. Thus we need only write down the lowest order terms in n_1 , n_2 , and their derivatives, consistent with the absorbing-state constraint that all dynamics must vanish when the field n_2 is identically zero. Each term on the right hand sides of both equations must therefore contain at least one factor of n_2 , whereupon the following theory results:

$$\begin{aligned} \frac{\partial n_1(\mathbf{x}, t)}{\partial t} &= [r_1 + c_1 \nabla^2 - u_1 n_2(\mathbf{x}, t) - w_1 n_1(\mathbf{x}, t)] n_2(\mathbf{x}, t) + \dots + n_2^{1/2} \eta_1(\mathbf{x}, t); \\ \frac{\partial n_2(\mathbf{x}, t)}{\partial t} &= [r_2 + c_2 \nabla^2 - u_2 n_2(\mathbf{x}, t) - w_2 n_1(\mathbf{x}, t)] n_2(\mathbf{x}, t) + \dots \\ &\quad + n_2^{1/2} \eta_2(\mathbf{x}, t). \end{aligned} \quad (24)$$

Here the c_i , r_i , u_i , and w_i are all constants, assumed to have the signs required to keep the fields n_1 and n_2 bounded. The noise terms are taken to have Gaussian correlations given by

$$\langle \eta_i(\mathbf{x}, t) \eta_j(\mathbf{x}', t') \rangle = D_{ij} \delta(\mathbf{x} - \mathbf{x}') \delta(t - t') , \quad (25)$$

for $i = 1, 2$, where the D_{ij} are the noise strengths. As usual, the ellipsis in (24) represents the infinite set of higher order terms which we sincerely hope will prove irrelevant near the transition.

Nonlocal Interactions in Time: These sinister coupled equations are not likely to win any beauty contests. Before panicking, however, let us step back and see if we can facilitate the analysis by solving the n_1 equation for n_1 in terms of n_2 , and substituting the result into the n_2 equation, thereby producing a single equation for n_2 that is hopefully more manageable. This task is greatly simplified by first dropping the $\nabla^2 n_2$, $r_1 n_2$, and $n_2^{1/2} \eta_1$ terms in the n_1 equation. But isn't that cheating? What gives us the right simply to eliminate some of the very terms whose necessity we have been emphasizing with solemn invocations of Landau's name? The answer is that the truncated model remains generic, since the omitted terms will be generated under RG iteration anyway. This is easy to check via standard diagrammatic RG methods, but can be understood less formally as a consequence of the fact that all symmetry-allowed terms in the problem are generated under RG iteration. This certainly applies to the terms we propose to drop from the bare equations. We conclude that the critical behavior of model (24) is the same as that of our proposed truncated version.

It is a straightforward matter of algebra to solve the truncated n_1 equation for $n_1(\mathbf{x}, t)$ and substitute it back into the n_2 equation, with the result

$$\begin{aligned} \partial n_2 / \partial t &= c_2 \nabla^2 n_2 + (r_2 - w_2 r_1 / w_1) n_2 - u_2 n_2^2 \\ &\quad + w_2 (r_1 / w_1 - n_1(\mathbf{x}, t = 0)) n_2 e^{-w_1 \int_0^t n_2(\mathbf{x}, s) ds} + n_2^{1/2} \eta_2 . \end{aligned} \quad (26)$$

Here $n_1(\mathbf{x}, 0)$ is the initial condition of the n_1 field, and all of the other symbols have already been defined. This equation is hardly a thing of great beauty and simplicity either. In fact, it has a nasty, unanticipated complication: The exponential term is *nonlocal* in time, involving values of the field $n_2(\mathbf{x}, s)$ for all times s from the initial time 0 to the present time, t . Before deciding how to deal with this monstrosity, we should understand its physical origins, which lie in the fact that the dynamics of the n_1 field ceases in the absence of n_2 , the density of occupied pairs. Imagine, then, that we are in the active phase close to the transition, where the density of such pairs is very small. The configuration of single particles (and vacancies) in any region devoid of pairs is frozen, until such time as a pair wanders into the region from somewhere else. The pair produces dynamics that will in general alter

this configuration in the region, before it wanders off again, or disappears, once more leaving the region fixed in time. A trace of the history of the pair thus remains frozen in the configuration of single particles and vacancies that its appearance produced. Hence when another pair enters the region at some arbitrarily later time, it can feel the effect of the earlier pair in this still unchanged configuration. This is the basic physics underlying the long-range interaction in time or “memory” effect in equation (26).

For those who prefer a more concrete mathematical explanation of the nonlocality, the structure of the n_1 equation when $n_2 \rightarrow 0$ provides the answer: The response function (Hohenberg & Halperin 1977) in Fourier space derived for this equation when $n_2 = 0$ is simply $g(\mathbf{k}, \omega) = 1/(-i\omega)$. The long-time (or low-frequency) behavior of this quantity is extremely singular. The nonlocal interactions in the n_2 equation are a direct consequence of this singularity.

Steady-State Analysis and DP: Now we must face up to dealing with the nonlocality. Fortunately, that turns out to be surprisingly easy, at least for steady-state properties in the active phase, where most of the action is. To see this, recall that the active phase is characterized by a nonzero expectation value $M_2 \equiv \langle n_2(\mathbf{x}, t) \rangle$ in the large- t limit. We write $n_2(\mathbf{x}, t) = M_2 + \delta n_2(\mathbf{x}, t)$, where the field δn_2 , whose expectation value is zero, represents the deviation of n_2 from its mean value. The integral $\int_0^t \delta n(\mathbf{x}, s) ds$ must grow more slowly than t for asymptotically large t , since otherwise $\langle \delta n(\mathbf{x}, s) \rangle$ would be nonzero. It follows immediately that $\int_0^t n_2(\mathbf{x}, s) ds$ behaves like $M_2 t$ for large t , whereupon the nonlocal term $e^{-w_1 \int_0^t n(x, s) ds}$ decays exponentially fast – like $e^{-w_1 M_2 t}$ – in the long-time limit. We conclude that in steady-state, which is achieved only for asymptotically large t , this term is negligibly small, and can be ignored.

We hope that by now readers will recognize what remains in Eq. (26) when the nonlocality is removed as nothing more or less than the Langevin equation for ordinary DP, with the coefficient of the linear term in n_2 given by $r_2 - w_2 r_1 / w_1$. Thus when all the nonlocal smoke has cleared, the steady-state properties of the generic problem with infinite numbers of absorbing states lie in the DP universality class.

Some Dynamical Properties: Let us see if we can go further, and determine whether some universal *dynamical* features are likewise described by DP. In particular, suppose we start the system off with an initial average density of particles, $M_2(t = 0) \equiv \langle n_2(\mathbf{x}, t = 0) \rangle$, and monitor its evolution. Right at the critical point, $M_2(t)$ presumably decays to zero like a power of t ; the exponent governing the decay is usually called θ : $M_2(t) \sim t^{-\theta}$. Here it should be understood that at any time t we can write $\langle n_2(\mathbf{x}, t) \rangle = M_2(t) + \delta n_2(\mathbf{x}, t)$, where $\langle \delta n_2(\mathbf{x}, t) \rangle$ vanishes for all t .

To compute θ , we must analyze Eq. (26) in the case where we cannot simply replace $n_2(\mathbf{x}, s)$ in the integral in the argument of the exponential by a constant M_2 , as we could in the steady-state situation. We can, however, try to see whether DP provides a self-consistent solution of the equation right at the critical point. To do so, let's assume that $\langle n_2(\mathbf{x}, s) \rangle$ decays like $s^{-\theta}$ at r_c , for asymptotically large s . Then $\int_0^t n_2(s)$ grows like $t^{1-\theta}$, provided $\theta < 1$, whereupon the nonlocal term in (26) decays like the stretched exponential $e^{-A_1 t^{1-\theta}}$, for some constant A_1 . Though it is slower than a pure exponential, this decay is still fast enough to make the nonlocal term negligible with respect to the other terms of (26) at long times. But tossing out the exponential leaves us with the DP equation, and therefore gives the DP value, θ_{DP} , for the exponent θ . This result is then self-consistent if and only if $\theta_{DP} < 1$. Let us therefore appeal to the ϵ -expansion and to numerical results for θ . The appeal is simplified by the observation that standard RG scaling arguments allow one to express θ in terms of more familiar exponents. The point is simply that in the active phase $M_2(t)$ must behave like

$$M_2(t, \delta r) \sim |\delta r|^\beta m(t/\tau) , \quad (27)$$

where $m(y)$ is a scaling function, and $\tau \sim |\delta r|^{-\nu z}$ is the usual characteristic time. In the active state, where $\delta r > 0$, $m(y)$ must approach a constant for large y (i.e., large t), consistent with M_2 vanishing like $|\delta r|^\beta$ with δr . As $\delta r \rightarrow 0$ for fixed t , however, the only way that $M_2(t, \delta r = 0)$ can achieve a finite, nonzero limit is for $m(y)$ to diverge like $y^{-\beta/\nu z}$ for small y . This yields $M_2(t) \sim t^{-\beta/\nu z}$, and hence the scaling relation

$$\theta = \beta/\nu z . \quad (28)$$

The results of the ϵ -expansion for β , ν , and z in DP then give $\theta_{DP} \sim 1 - \epsilon/4 + O(\epsilon^2)$, while numerical estimates for θ_{DP} in $d = 1, 2$, and 3 are 0.1598(3) (Jensen & Dickman 1991, Jensen & Dickman 1993a), 0.46(2) (Cardy & Sugar 1980), and 0.73(3) (Jensen 1992), respectively. Thus in 1d, 2d, 3d, and close to 4d, θ_{DP} is always less than unity, whereupon the self-consistency of the hypothesis that $\theta = \theta_{DP}$ for the multiple-absorbing-state problem is established.

4.3 Numerical Tests

Homogeneous Initial Conditions: Of course “self-consistent” does not necessarily mean correct, so it behooves us to check this conclusion numerically. Fortunately, this has already been done: Jensen and Dickman (1993b, Jensen 1994a, Jensen 1993) have carried out careful numerical studies of both static and dynamical properties of various microscopic models with infinite numbers of absorbing states in 1d. Their data constitute compelling evidence for θ having its DP value of around 0.16 in this case. In Fig. 4 we reproduce a figure from Jensen (1993), showing $M_2(t)$ vs. t for the PCP on

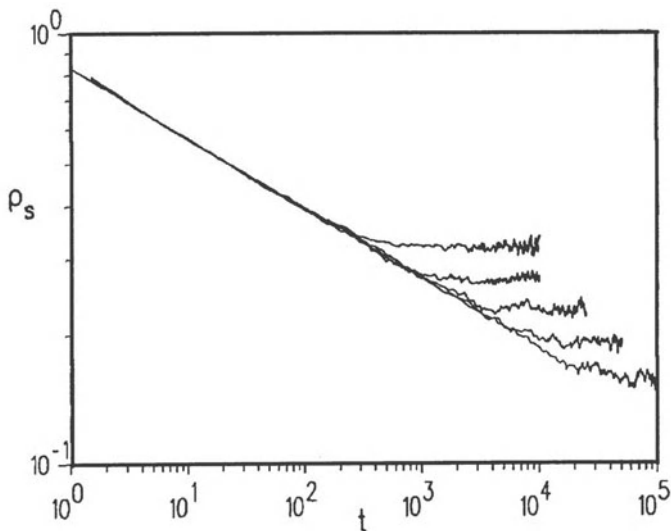


Fig. 4. Average number of pairs, ρ_s , in surviving samples of the 1d PCP model, as a function of time t at $p = 0.0771$, for (from top to bottom), system size $L = 128, 256, 512, 1024$, and 2048 . This is Fig. 2 of Jensen 1993.

a log-log scale. At the critical point, the well-defined straight line over more than four decades has a slope of $0.160(5)$, which compares very well with the number $0.1598(3)$ quoted by the authors as the best θ value for DP. As an illustration of how well the steady-state critical behavior of systems with multiple absorbing states is observed to fall into the DP universality class, we reproduce in Fig. 5 another figure from Jensen 1993, showing the steady-state concentration of M_2 vs. δr for the PCP in 1d, on the proverbial log-log plot. From this graph the exponent value $\beta = 0.28(1)$ is estimated, again in excellent agreement with the DP value of $0.2769(2)$.

Seed Initial Conditions: Before declaring victory in the struggle to understand the critical behavior of systems with multiple absorbing states, we should mention one set of intriguing numerical results for which there is not yet a satisfactory explanation (Mendes *et al.* 1994, Jensen & Dickman 1993b, Dickman 1996). These concern the evolution of the system from seed initial conditions, as discussed at the end of the previous lecture. Numerical results on the PCP in 1d (Jensen & Dickman 1993b) show strong indications of nonuniversal behavior of the exponents $\tilde{\eta}$ and δ , respectively describing the growth of the total number of active sites, and the decay of the survival probability. The point is that, in preparing an initial condition consisting of

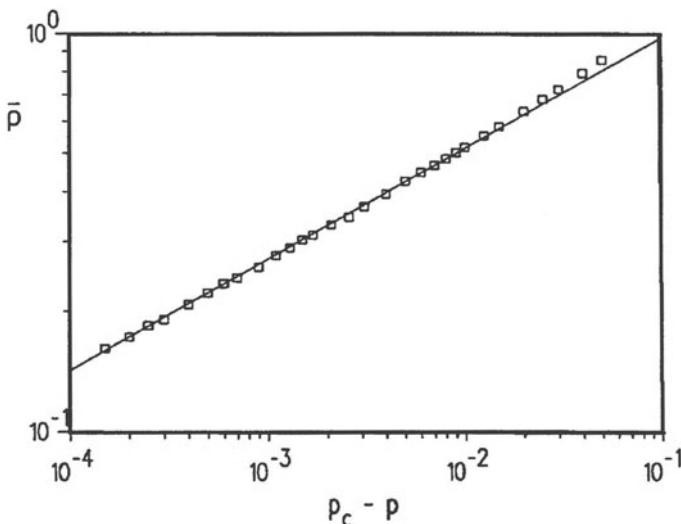


Fig. 5. Steady-state concentration of pairs, $\bar{\rho}$, in the 1d PCP model with $p_c = 0.0771$, plotted against $p_c - p$ (i.e., δr), on a log-log scale. Slope of the line is $\beta \sim 0.277$. This is Fig. 4 of Jensen (1993).

a localized active region immersed in a sea of the absorbing phase, one has considerable freedom to choose the absorbing phase in systems with multiple absorbing states. In the PCP, e.g., one can vary from 0 to 1 the average density, $\langle n_1(t=0) \rangle$, of singly occupied sites surrounding the single occupied pair which serves as the active seed in the initial state. The numerics indicate that the exponents $\tilde{\eta}$ and δ change with $\langle n_1(0) \rangle$. (The exponents nonetheless continue to satisfy a generalized scaling relation (Mendes *et al.* 1994).) In order to achieve DP values for these exponents, one must use a “natural” absorbing initial condition, i.e., one prepared as follows: Take a lattice of modest size, L_t , and start the system with a random initial condition right at its critical point. Eventually (i.e., after a time that grows with L_t like L_t^z), the system reaches an absorbing configuration. Replicate this absorbing configuration many times, to form a large lattice consisting of many copies of the original small absorbing configuration. Place a seed, i.e., a nearest neighbor pair of particles, at the center of this large lattice, isolating the pair by removing any particles that happen to border it. The subsequent evolution from this “natural” starting point produces DP exponent values for $\tilde{\eta}$ and δ , whereas other choices (such as placing the seed in an otherwise empty lattice), typically do not.

Similar nonuniversality holds in other 1d microscopic models with large numbers of absorbing states, notably in the “dimer reaction” model (Jensen

& Dickman 1993b, Mendes *et al.* 1994). Interestingly, however, the value of \tilde{z} and the location of the critical point seem to be unique in all of these 1d problems. Any initial condition of the seed type seems to yield the same critical value of the control parameter as does the steady-state behavior. This is almost as mysterious as the apparent nonuniversality.

To end this section on a note of even greater confusion, we mention that simulations in 2d that start from seed initial conditions in a model with an infinite number of absorbing states – the so-called “second neighbor reaction” model – also show evidence of nonuniversality (Dickman 1996). Indeed, the nonuniversal behavior is if anything more pronounced than in 1d. Not only do $\tilde{\eta}$, and δ vary, as in 1d, with the details of the environment surrounding the initial seed, but the exponent \tilde{z} and the location of the critical point vary as well. An interesting challenge is to see whether all of these results can be derived from the Langevin equation (26), or whether (heaven forfend!) they are too subtle to be captured by the Langevin representation. In any event, these unanswered questions should prevent our success in deriving the DP behavior of certain critical properties from making us complacent.

4.4 Non-DP Behavior in Conserving Systems

To emphasize the importance of symmetry in determining critical properties, we conclude this lecture by briefly mentioning a class of systems with unique absorbing states whose phase transitions nonetheless do *not* belong in the DP universality class. The original member of this class is a cellular automaton introduced by Grassberger (Grassberger *et al.* 1984, Grassberger 1989). Other members subsequently identified include the interacting monomer-dimer model (Kim & Park 1994), certain nonequilibrium kinetic Ising models with competing dynamics (Menyhard 1994), and the so-called branching annihilating random walk (BAW) with an even number of offspring (Takayasu & Tretyakov 1992, Jensen 1994b). Numerical calculations of critical exponents for these systems strongly suggest that they belong in a single universality class, which differs from that of DP.¹⁷

The feature that is common to all these models and is believed to distinguish them from DP is a locally conserved quantity: In each of them the number of particles (or in some cases the number of kinks), is conserved, modulo-2; i.e., the parity is conserved.

Though time does not permit us to discuss this class of systems here, it is worth mentioning that no satisfactory Langevin equation description of them exists at present. A very recent calculation (Cardy & Täuber 1996) of the critical properties of BAW’s is based on the Fock-space formalism, which is reviewed in, e.g., Lee (1994).

¹⁷ In particular a rather complete set of exponents has been obtained for the BAW; see Jensen (1994b) for a review of its scaling laws and the numerical values of the exponents.

5 Multiplicative Noise

5.1 An Example from Chemical Reactions

In section 2, we pointed out that Langevin equations describing systems with absorbing states must have noise amplitude functionals $g_x(\{\psi\})$ that vanish with ψ . The analyticity requirement of a coarse-grained Langevin model, moreover, constrains the power α with which g_x vanishes as $\psi \rightarrow 0$ to be an integer or half-odd integer. We have already seen that DP-like problems and their generalization to systems with infinite numbers of absorbing states give rise to $\alpha = 1/2$. In this lecture we deal with a second important class of absorbing-state problems – those with $\alpha = 1$. Such systems are often referred to as having “multiplicative noise (MN).”

Multiplicative noise occurs in microscopic problems where the dominant stochastic processes are external. The simplest and most frequently cited example (Schenzle & Brand 1979) concerns the following autocatalytic chemical reactions, designed to produce some chemical substance X , say:



Here A , B , and C are three other chemical species in which we have no interest except insofar as they influence the production of X . Note that the first reaction can proceed in both the forward and backward directions, with rate constants k_1 and k_2 respectively, whereas the second reaction proceeds in the forward direction only, with rate constant k_3 . (In practice this means that the rate of the reverse reaction is so small as to be negligible.) This makes the state without any X molecules absorbing.

We imagine that the chemicals A , B , C , and X are mixed together in a vessel to form a chemical soup whose ingredients diffuse about, reacting stochastically, when they come together, according to Eqs. (29–30). Standard modeling of such a reaction-diffusion system (Kuramoto 1984) involves writing rate equations, looking much like the deterministic parts of Langevin equations, for the coarse-grained density $n_X(\mathbf{x}, t)$, of X , the other densities, n_A , n_B , and n_C entering in an obvious way:

$$\partial n_X / \partial t = \nabla^2 n_X + k_1 n_A n_X - k_3 n_B n_X - k_2 n_X^2 . \quad (31)$$

Each of the three allowed reactions in (29–30) is represented by one of the last three terms in (31). For example, the $k_1 n_A n_X$ term represents the reaction $A + X \rightarrow 2X$. Since it requires the presence of both an A and an X molecule to proceed, it is proportional to n_A and to n_X , the rate constant k_1 governing the reaction speed; the positive sign reflects the fact that this reaction adds one extra X molecule to the system. Note that the coefficient of

the diffusive term $\nabla^2 n_x$ can always be made unity by rescaling the distances \mathbf{x} .

Now suppose that the chemists overseeing this process try to control the densities of A , B , and C externally to keep the reactions bubbling along in some desired fashion. Imagine that their intention is to keep $n_A(\mathbf{x}, t)$, $n_B(\mathbf{x}, t)$, and $n_C(\mathbf{x}, t)$ everywhere fixed at the constant values n_A^0 , n_B^0 , and n_C^0 , respectively. Despite their best efforts, however, local fluctuations $\delta n_i(\mathbf{x}, t)$ for $i=A, B$, and C will arise in the n_i : i.e., $n_i(\mathbf{x}, t) = n_i^0 + \delta n_i(\mathbf{x}, t)$, where the space and/or time averages of all the δn_i are zero. Substituting this equation for the n_i in (31) immediately yields the result

$$\partial n_X / \partial t = \nabla^2 n_X - rn_X - un_X^2 + n_X \eta , \quad (32)$$

where $r \equiv k_3 n_B^0 - k_1 n_A^0$, $u \equiv k_2$, and $\eta(\mathbf{x}, t) \equiv k_1 \delta n_A(\mathbf{x}, t) - k_3 \delta n_B(\mathbf{x}, t)$ is a noise variable with zero mean, which we can take to be Gaussian random. Thus we have arrived at a Langevin equation whose noise amplitude is proportional to the first power of the order parameter, so that $\alpha = 1$, as advertised.

It is important, however, to take a skeptical view of this derivation. The dedicated follower of these lectures (admittedly an outrageous concept), will be disturbed by our abandonment of the sacred symmetry principles on which we based our earlier derivations of Langevin equations, in favor of an intuitive but vaguely-defined pseudo-microscopic approach that fails to produce the standard noise term with $\alpha = 1/2$. After all, there is a stochastic element in the reactions themselves, since no two molecules react with unit probability even if they are in spatial contact. Thus there is internal randomness, in addition to the “external” randomness in the concentrations of n_A and n_B that produced $\alpha = 1$ in (32). That internal stochasticity ought to give rise to a noise term whose coefficient is proportional to $n_X^{1/2}$, just as it did in DP-like problems, and as the symmetry approach demands. Since the RG shows that the lowest power of n_X in the noise term is the dominant one at large distances, then the $n_X^{1/2}$ term should actually dominate on the longest length scales, placing the chemical reaction example in the DP universality class. One can nonetheless imagine situations where the external noise is so much larger in amplitude than the internal noise as to make the $n_X^{1/2}$ term negligible until one gets immeasurably close to the critical point. In such circumstances, the linear multiplicative noise term governs the physics for all practical purposes, the ultimate crossover to DP-like behavior being inaccessible. This is the spirit in which model (32) should be viewed. Schenzle and Brand (1979) provide several other physical problems with absorbing states, mostly in the area of quantum optics, which purportedly fall in the $\alpha = 1$ category,¹⁸ but our cautionary remarks about a possible ultimate

¹⁸ See also, e.g., Horsthemke & Lefever (1984), Garcia Ojalvo *et al.* (1993), Ramírez Piscina *et al.* (1993), Van den Broeck *et al.* (1994a, 1994b), Ramswamy *et al.* (1995) and Shapiro (1993).

crossover to DP-like behavior should be applied to those situations as well.

Having unburdened ourselves of this weighty issue of conscience, let us press ahead to analyze the simple, generic multiplicative noise problem that emerges from the chemical reaction problem:

$$\partial n / \partial t = \nabla^2 n - rn - un^2 + n\eta ; \quad (33)$$

here η is a Gaussian noise variable of strength D .¹⁹

5.2 Analysis of the Multiplicative Noise Problem

Mean Field Theory: The only difference between Eq. (33) and the Langevin equation (6) for DP lies in the coefficient of the random variable. Since noise is neglected in constructing MFT, the two models are therefore identical at the mean-field level. Thus in MFT, Eq. (33) exhibits a transition from the absorbing phase to the active phase as r is decreased through the critical value $r_c = 0$. In the active phase, $\langle n \rangle = -r/u$, giving the critical exponent $\beta = 1$, just as for DP.

Critical Dimension and Phase Diagrams: Beyond MFT, however, the two problems differ substantially. Let us perform the same trivial rescaling of \mathbf{x} , t , and n as for DP, ignoring for the moment any perturbative corrections arising from integration of the high-wavenumber modes. Substituting $\mathbf{x} = b\mathbf{x}'$, $t = b^z t'$, and $n = b^\zeta n'$ into (33), we readily arrive at the renormalized equation

$$\partial n' / \partial t' = b^{z-2} \nabla'^2 n' - b^z r n' - b^{z+\zeta} u n'^2 + b^z n' \eta . \quad (34)$$

To beat this into precisely the same form as (33) requires taking $z = 2$, $r' = b^z r$, $u' = b^{z+\zeta} u$, and $\eta' = b^z \eta$. Defining the renormalized noise strength D' as before, through $\langle \eta'(\mathbf{x}', t') \eta'(\mathbf{0}, 0) \rangle = D' \delta(\mathbf{x}') \delta(t')$, then yields $D' = b^{z-d} D$. Since $z = 2$, this implies that for $d > 2$ the noise strength decreases with increasing length scale, disappearing on the largest scales relevant for critical phenomena. We conclude that fluctuations induced by the noise play no role for $d > 2$, meaning that MFT should be valid. For $d > 2$, the choices $\zeta = -z = -2$ and $r = r_c = 0$ place the system at the critical fixed point $r^* = 0$, $u^* = u$, $D^* = 0$, whose critical properties are precisely what one gets in the mean-field approximation.

Thus the upper critical dimension is $d_c = 2$. Since this conclusion is based on the neglect of perturbative corrections arising from the nonlinearity, it can, as noted earlier, only be trusted for small values of D . It is, however,

¹⁹ It is easy to show that no noise term with a coefficient proportional to $n^{1/2}$ is generated when one applies the RG to model (33). Note too that the MN problem defined with a *cubic* nonlinearity, n^3 , gives results qualitatively the same as those derived here for the quadratic nonlinearity. See Grinstein *et al.* (1996), Tu *et al.* (1996).

straightforward to compute the first nontrivial perturbative corrections to the recursion relations for r , u , and D in $d = 2 + \epsilon$ dimensions, the result being (Grinstein *et al.* 1996)

$$r' = b^z r \quad (35)$$

$$u' = b^{z+\zeta} u(1 + A_d D) \quad (36)$$

$$D' = b^{-\epsilon} D(1 + A_d D) ; \quad (37)$$

here $A_d = 1/4\pi + O(\epsilon)$ is a positive, d -dependent constant.

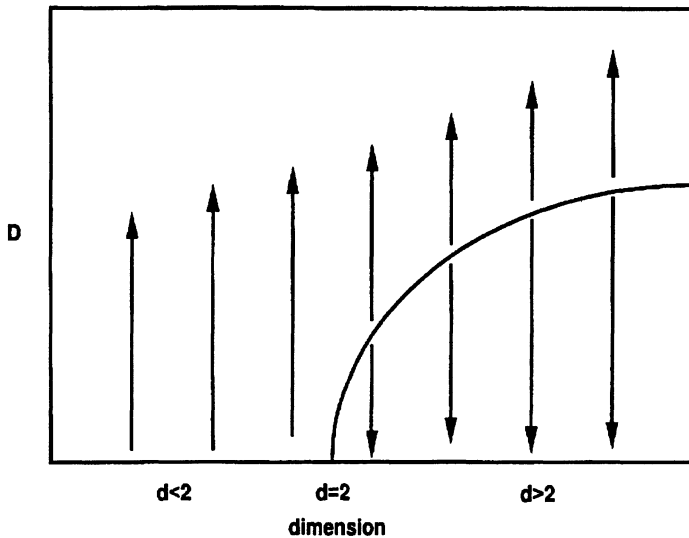


Fig. 6. Schematic RG flow diagram for the noise strength D in Eq. (37), as a function of dimension d . For $D > D_c$, flows run off to large values of D , while for $D < D_c$, flows lead to the MFT fixed point $D^* = 0$. For $d \leq d_c = 2$, $D_c = 0$, so flows always run off.

For $\epsilon > 0$ ($d > 2$), the D equation has two finite fixed points, one at $D^* = 0$ corresponding to MFT, and one at $D^* = \epsilon/A_d$, which is readily seen to be unstable: It is accessible only when D is tuned to the critical value $D_c \equiv D^*$. Eq. (37) makes clear that starting with $D < D_c$ or $D > D_c$ respectively leads to the MFT fixed point, or a runaway flow to arbitrarily large values of D where perturbative RG analysis is of no use. We assume that the behavior in this regime is controlled by an inaccessible “strong-coupling” fixed point. For $\epsilon \leq 0$, i.e., for $d \leq 2$, the Gaussian fixed point at $D^* = 0$ is simply unstable,

and one gets a runaway flow to large D , starting from any $D > 0$. Thus strong coupling behavior is impossible to avoid in this case. The schematic RG flow diagram of Fig. 6 illustrates these results.

These findings can also be summarized in the schematic phase diagrams of Fig. 7. For $d > 2$, a line of mean field (“weak coupling”) transitions occurs at $r = r_c = 0$, so long as $D < D_c$. When $D > D_c$, a line of strong-coupling transitions occurs at negative values of r_c . A multicritical point at $r = 0$ and $D = D_c$ separates the weak- and strong-coupling regimes. For $d < 2$, only the line of strong-coupling transitions occurs.

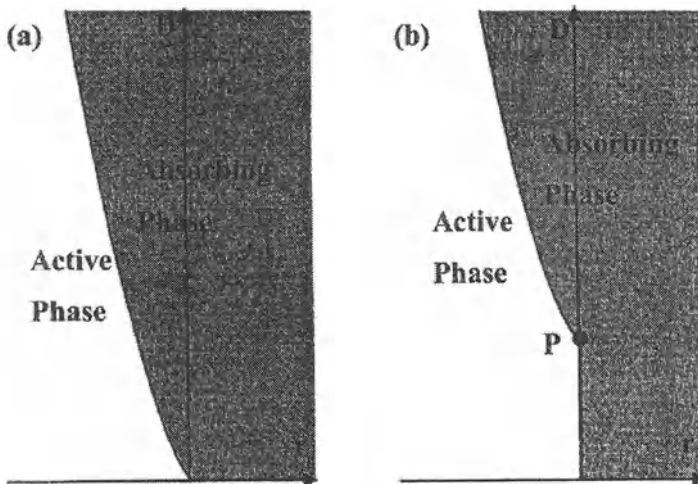


Fig. 7. Schematic phase diagrams for the multiplicative noise problem in the Ito representation. For (a) $d \leq 2$, only a strong-coupling transition between the active and absorbing phases occurs; for (b) $d > 2$, mean-field and strong-coupling transitions occur for D respectively below and above the multicritical point, P . Uniform susceptibility is infinite in the regions of the absorbing phases where $r < 0$. This is Fig. 1 of Grinstein *et al.* (1996).

The shift of r_c away from zero is a characteristic feature of the strong coupling transition, and has received much attention in the literature. Becker and Kramer (1994) have shown for 1d and 2d that (in the Ito representation²⁰),

²⁰ To define stochastic equations like (33) uniquely, one must specify how to integrate the noise term in time. The two standard prescriptions for doing this are due to Ito (1951) and Stratonovich (1989). In practice they differ only by a trivial redefinition of the coefficient r in (33): All results for the Ito repre-

r_c becomes *negative*, as indicated in the figure. We will not take the time to reproduce their arguments here. Suffice it to say that the result is achieved by mapping the problem onto that of finding the lowest bound state energy of a quantum mechanical potential given by the spatial correlation function of the noise, viz., $D\delta(\mathbf{x} - \mathbf{x}')$. Their analysis can readily be extended to $d > 2$, where it is well known that the depth of a potential well has to exceed a d -dependent critical value, D_c , in order for there to be a bound state. The existence of a bound state for $D > D_c$ implies that the critical value of r is shifted to $r_c < 0$, corresponding to the strong-coupling fixed point. When $D < D_c$ there is no bound state, which corresponds to the weak-coupling fixed point, where r_c is not shifted away from 0.

We note incidentally that standard RG calculations of the type described so painstakingly (or at least painfully), in the second lecture enable one to compute critical exponents for the multicritical point at $D = D_c$ when $d > 2$. One finds, e.g., $z = 2$, $\nu = 1/2$, and $\beta = (2 + \epsilon)/2$; the new exponent Δ (which is 2 in mean-field theory), takes the value $2 + \epsilon/2$ at the multicritical point. The relation $\Delta = \beta$ that holds for DP thus fails at the MN multicritical point. So far as we know, Δ is a new independent exponent in the MN problem, at both the strong-coupling and multicritical fixed points.

Diverging Susceptibility Near Critical Point: A most unusual feature of the behavior of model (33) in the vicinity of its critical point can be deduced as an almost trivial consequence of the phase diagrams of Fig. 7. This concerns the behavior of the response function $G(\mathbf{x}, t)$, defined as (Hohenberg & Halperin 1977) $G(\mathbf{x} - \mathbf{x}', t - t') \equiv \delta \langle n(\mathbf{x}, t) \rangle / \delta H(\mathbf{x}', t')|_{H=0}$, where $H(\mathbf{x}, t)$ is a source term added to the right hand side of Eq. (33), and which is set to zero after the functional differentiation is performed. Physically, then, $G(\mathbf{x} - \mathbf{x}', t - t')$ represents the change in the average density $\langle n(\mathbf{x}, t) \rangle$ induced by the introduction of an infinitesimal source of particles at the point \mathbf{x}' at some earlier time t' . The Fourier transform $\chi(\mathbf{k}, \omega)$ of $G(\mathbf{x}, t)$ is of course simply the wave-number (\mathbf{k}) and frequency (ω)-dependent susceptibility of the system. In equilibrium systems, χ is related to the Fourier transform of the connected correlation function C_c through the fluctuation-dissipation theorem (Hohenberg & Halperin 1977), but in nonequilibrium systems the two functions are generally independent.²¹

Sadly (or perhaps mercifully), time does not permit us to embark on a cogent discussion of diagrammatic perturbation theory for the MN model

smentation can be expressed in the Stratonovich representation by making the substitution $r \rightarrow r - D/2$. This technical point is clearly explained in van Kampen (1981), so we will not elaborate further here. It is worth noting, however, that the Stratonovich representation is presumably the appropriate one for describing the physics of the autocatalytic chemical reactions used to motivate Eq. (33).

²¹ Under special conditions, nonequilibrium systems can satisfy a fluctuation dissipation theorem; the 1d KPZ equation (Kardar *et al.* 1986) is a familiar example.

(33). However, once one understands how to compute various quantities of interest perturbatively (something which is straightforward to do and is described in some generality in Hohenberg & Halperin 1977), it is easy to convince oneself that *in the absorbing phase of the MN theory*, $\tilde{G}(\mathbf{k}, t)$, the spatial fourier transform of G , is given exactly by the zeroth order result $\tilde{G}(\mathbf{k}, t - t') = \theta(t - t')e^{-(r+k^2)(t-t')}$, with no corrections whatsoever arising from the nonlinearity. (Verifying this claim is left as an exercise for the much-abused reader.) Fourier transforming this result in time yields a uniform susceptibility $\chi(\mathbf{k} = \omega = 0)$ which is $1/r$ for $r > 0$, and which diverges for $r < 0$ (all in the Ito representation). Thus the uniform susceptibility is infinite in the absorbing phase whenever r is negative. But Fig. 7 shows that, both for $d \leq 2$ and for $d > 2$ when $D > D_c$, the absorbing phase (again, in the Ito representation), indeed extends into the regime of negative r . In this entire region of the phase diagram then, $\chi(\mathbf{k} = \omega = 0) = \infty$. This result is an unexpected one, since in systems without a continuous symmetry or quenched randomness,²² susceptibilities normally diverge only on critical surfaces, and not throughout whole volumes of parameter space.

5.3 The Single-Variable Multiplicative Noise Problem

To check this rather striking prediction and try to understand it better, it is useful to consider the single-variable, or 0d, MN problem defined by the ordinary differential equation $dn(t)/dt = -rn - un^2 + n\eta + H$. Here H is a constant source field, included to allow the computation of the uniform susceptibility, and all other symbols have their usual meanings. For $H = 0$, there exists an exact solution (Schenzle & Brand 1979, Graham & Schenzle 1982) of the 0d problem, in which the shift of r_c to negative values (Fig. 7) can be seen explicitly, and critical exponents calculated exactly. It is a relatively straightforward matter to extend this solution to the case where $H \neq 0$. Standard techniques (van Kampen 1981) can be used to write the Fokker-Planck equation for the time evolution of the probability distribution function $P_t(n)$ of the variable n at time t , in the Ito representation: $\partial P_t(n)/\partial t = \partial((rn + un^2 - H)P)/\partial n + \frac{1}{2}\partial^2(n^2P)/\partial n^2$.

The steady-state solution at $t = \infty$ is readily found to be $P_\infty(n) = n^{-2r/D-2}e^{-2H/Dn-2un/D}/Z$, with Z a constant chosen to normalize $\int_0^\infty dn P_\infty(n)$ to unity. Setting H to zero in this formula, one straightforwardly recovers the exact results of Schenzle & Brand (1979), Graham & Schenzle (1982), notably the critical value $r_c = -D/2$ for r . From the complete expression for nonzero H , one can calculate $\langle n \rangle = \int_0^\infty dnnP_\infty(n)$, and hence obtain

²² The Kosterlitz-Thouless phase (Kosterlitz & Thouless 1973) of the 2d XY model is the best known example of a phase of a system with continuous symmetry wherein the susceptibility is everywhere divergent. Frustrated systems such as spin glasses can have infinite susceptibilities even when their symmetries are discrete (Fisher & Huse 1988).

an explicit expression for the uniform susceptibility $\chi(H) \equiv \partial < n > / \partial H$. One finds that $\chi(H) \sim H^{\gamma(r)-1}$ with $\gamma(r) = |2r/D + 1|$ for small H , so that $\chi(H \rightarrow 0)$ approaches a finite limit provided $|2r/D + 1| > 1$. When $|2r/D + 1| < 1$, however, $\chi(H)$ diverges as $H \rightarrow 0$. Thus the susceptibility at $H = 0$ is infinite throughout the portion of the absorbing phase where $r < 0$, i.e., whenever $r_c < r < 0$, in perfect accord with our expectations. Our general arguments did not predict, however, that the susceptibility would remain infinite in the active phase just below the critical point, viz., in the range $2r_c < r < r_c$. It is hard to determine analytically whether this divergence of χ in the active phase is special to the 0d problem, or whether it persists in higher dimensions as well. We shall see shortly, however, that numerics strongly suggest that a region in the active phase with $\chi = \infty$ also occurs in 1d.

An interesting aspect of the divergence of $\chi(H)$ as $H \rightarrow 0$ in 0d is that the exponent $\gamma(r) - 1$ governing the divergence changes continuously with r . Such behavior is characteristic of the presence of a *line* of critical fixed points in the RG formulation, and suggests that perhaps a sufficiently sophisticated RG treatment of the MN problem, at least for $d > 0$, would show the occurrence of a fixed line. (Readers who dimly recall the mysterious parenthetical remark on the subject of fixed lines in lecture II will remember that the 2d XY model and its physical realizations, such as the 2d melting problem (Nelson & Halperin 1979), are the most illustrious examples of fixed-line behavior.)

A final noteworthy element of the exact results in 0d concerns the topic of multiscaling (Jensen *et al.* 1991) (or anomalous scaling), a mainstay of the grueling, never-ending struggle to understand turbulence. Though terminology seems to be used loosely and nonuniformly in the literature, we can safely define anomalous scaling in the MN problem to mean that the exponent β_p governing the decay of the p^{th} moment of the field n as the critical point is approached from the active phase is not a linear function of p . To be more explicit, if, asymptotically, $< n^p >$ vanishes like δr^{β_p} as $\delta r \rightarrow 0$, then unless $\beta_p = p\beta_1$ for all positive integers p , then the system is said to exhibit multiscaling. (In turbulence, the typical quantities of interest are the so-called structure functions, $S_p(\mathbf{r}) \equiv < |v(\mathbf{r}) - v(\mathbf{0})|^p >$, where $v(\mathbf{r})$ is a component of the velocity field at point \mathbf{r} . In the inertial subrange, where turbulent systems are scale invariant, $S_p(\mathbf{r}) \sim |\mathbf{r}|^{\zeta_p}$, where the exponents ζ_p are observed both experimentally (Herweijer & van de Water 1995) and numerically (Cao *et al.* 1996) to deviate from a simple linear dependence on p , the deviations often being referred to as “intermittency corrections.”)

In linear or Gaussian theories, where correlations factorize, β_p clearly grows linearly with p , but at nontrivial fixed points with nonvanishing nonlinear terms, one should expect this linear relationship to break down, i.e., one should anticipate multiscaling. The MN transition in 0d presents one of the rare situations where one can study the multiscaling in an explicit calculation. Things are made even rosier by the fact that the general p^{th} moment

has already been calculated in Schenzle and Brand (1979) and Graham & Schenzle (1982), so all we need do is quote their results: $\beta_p = \beta_1 = 1$, where $\beta_1 \equiv \beta$ in the standard notation. Thus all moments vanish with the same exponent at r_c – a rather extreme form of multiscaling. An obvious question is whether this result persists in higher dimension as well. While the answer is unknown in general, we show numerical evidence below for $\beta_p = \beta$ for $p = 2$ and $p = 3$ in 1d.

Before leaving the safety of the solvable 0d problem, we note that all the standard critical exponents have been computed exactly in Schenzle & Brabd (1979) and Graham & Schenzle (1982). One can, in particular, infer from Graham & Schenzle (1982) the following results, in addition to $\beta = 1$: $\nu z = 2$; $(d - 2 + \eta)/z = 1/2$; and $\Delta = 1$. These numbers can be used as a nontrivial check of the validity of the general scaling relation proposed in Eq. (22): $2\beta = \Delta + \nu(d - 2 + \eta)$.

5.4 Strong Coupling Exponents: Connection to KPZ

Having understood the upper critical dimension and phase diagrams, we should now try to calculate the strong coupling exponents if possible. For this purpose, the Hopf-Cole change of variable (van Kampen 1981) $n = e^h$, which transforms Eq. (33) into

$$\partial h(\mathbf{x}, t) / \partial t = -r + \nabla^2 h + (\nabla h)^2 + \eta(\mathbf{x}, t) - ue^h , \quad (38)$$

is extremely helpful (Pikovsky & Kurths 1994, Grassberger 1995). The first thing to note is that by dropping the last term of this equation one recovers the KPZ equation we discussed briefly in the first lecture (with the coefficients, c and λ , of the $\nabla^2 h$ and $(\nabla h)^2$ terms equal to unity). Though the constant r was zero in that earlier version of KPZ, r has no significant effect on correlations in the KPZ model. This can be seen through the change of variable $h(\mathbf{x}, t) = \tilde{h}(\mathbf{x}, t) - rt$, which produces a KPZ equation with $r = 0$ for \tilde{h} .

However, r does control one basic piece of phenomenology in the KPZ equation, viz., it determines whether the interface described by the equation moves up or down. Inspection of (38) with $u = 0$ makes clear that for sufficiently large r the average value of $h(\mathbf{x}, t)$ *decreases* with time, so the interface moves down, whereas for sufficiently large negative r , h *increases*. Obviously, then, there is a special value, r_c , of r that separates the upward-moving and downward-moving regions. At r_c , the interface maintains a constant average position in space. More importantly, recall from the first lecture that for any value of r the KPZ equation exhibits scale-invariance, i.e., has correlation functions that behave like power laws in space and/or time. This is a consequence of the invariance of the equation under uniform translations: $h \rightarrow h + \text{constant}$.

Let us now restore the dreaded exponential term ue^h in Eq. (38). Obviously this term breaks the translational symmetry and so can safely be expected to destroy the scale invariance, producing a finite correlation length, ξ , and exponential decays of correlations for distances $x \gg \xi$. This is just what we would expect, since Eq. (38) is just a transformed version of Eq. (33), which has exponential correlations in the active phase in steady state, becoming algebraic only at the critical point. Clearly, however, when $x \ll \xi$, i.e., at distances short enough that the nonlinearity ue^h can be neglected, the fluctuations in the MN system continue to be controlled by the pure KPZ equation.

Let us now identify the phases of the MN problem in the h representation: For r sufficiently large and positive, the interface obviously still moves down without bound, the ue^h term serving only to increase the downward velocity. In this case, therefore, $\langle h \rangle$ reaches $-\infty$ as $t \rightarrow \infty$, so that $n = e^h$ reaches 0, meaning that the system is in the absorbing phase, as expected. For r sufficiently negative, however, the interface will clearly start moving upward. When $\langle h \rangle$ becomes large enough, however, the $-ue^h$ term will grow rapidly, eventually producing a strong negative contribution to $\partial h / \partial t$ that opposes the upward contributions from $-r$ and from $(\nabla h)^2$. The net result is that the interface finds a fixed average position where these competing tendencies just balance. In steady state, then, $\langle h \rangle$ achieves a constant, finite value, as does $\langle n \rangle$. This, obviously, is the active phase. As r increases in the active phase, the steady-state value of $\langle h \rangle$ decreases monotonically, eventually diverging to $-\infty$ at the critical value r_c , where $\langle n \rangle$ first becomes zero in the large- t limit.

The crucial thing to observe about this h -representation is that in steady state for $r = r_c$, we have $h = -\infty$, whereupon $n = e^h$ vanishes, and hence so does the troublesome ue^h term in Eq. (38). Thus the steady-state fluctuations in h right at r_c are controlled simply by the KPZ equation. It follows that any critical exponent that can be defined right at the critical point must have its KPZ value. In particular, the dynamical exponent z , which relates the characteristic decay time τ_l , for disturbances of wavelength l right at r_c , to l , via $\tau_l \sim l^z$, can be defined right at r_c . We conclude that z for the MN problem takes its KPZ value. It is worth recalling (Kardar *et al.* 1986) that in 1d the KPZ value of z is known to be precisely 3/2.

Let us now see whether the KPZ analogy can be used to predict the values of strong-coupling critical exponents that can only be defined by approaching r_c from the active phase. Choose a value of r in this phase (i.e., with $r < r_c$), and take expectation values of Eq. (38) in steady state, using $n = e^h$ to get:

$$-r + \langle (\nabla h)^2 \rangle - u \langle n \rangle = 0 . \quad (39)$$

Now right at the critical point, $r = r_c$ and $\langle n \rangle = 0$, whereupon $-r_c + \langle (\nabla h)^2 \rangle_c = 0$, the subscript c indicating that the expectation value is to be taken at r_c . Subtracting these two equations, and using $\langle n \rangle \sim B\delta r^\beta$ for

small δr and some positive constant B , one obtains

$$\langle (\nabla h)^2 \rangle_c - \langle (\nabla h)^2 \rangle = \delta r - Bu\delta r^\beta . \quad (40)$$

The first thing to note about this equation is that the fluctuations in ∇h are larger at the critical point than in the active phase, where they are suppressed by the finite correlation length. Thus the left hand side of Eq. (40) is positive. Given that $B > 0$, this implies that $\beta \geq 1$, in order that the right hand side likewise be positive for small δr . Thus the KPZ representation immediately provides a nontrivial bound on the exponent β . It does more than that, however, since the quantity $\langle h^2 \rangle$, which measures the interfacial roughness, is well known to behave like $L^{2\chi}$ in rough phases of the KPZ theory. Equivalently (Krug & Meakin 1990), $\langle (\nabla h)^2 \rangle \sim L^{2\chi-2}$. (Recall from lecture I that χ is the roughness exponent.) Standard RG scaling then implies that when, as in the active phase of the MN problem, the KPZ theory has an extra term that makes the correlation length ξ finite, $\langle h^2 \rangle \sim L^{2\chi} f_h(\xi/L)$. Here $f_h(y)$ is a scaling function which approaches a constant at the critical point, where $y = \xi = \infty$. Since, in the active phase, where ξ is finite, $\langle h^2 \rangle$ must remain finite as $L \rightarrow \infty$ (i.e., as $y \rightarrow 0$), $f_h(y)$ must vanish like $y^{2\chi}$ for small y . Hence $\langle h^2 \rangle$ scales like $\xi^{2\chi}$ in the active phase near the critical point, whereupon $\langle (\nabla h)^2 \rangle \sim \xi^{2\chi-2}$. Since χ is known to be less than unity in the KPZ model in any dimension (i.e., the width of a KPZ interface is always less than its length), the power $2\chi - 2$ is always negative. Thus to be more precise, one should write $\langle (\nabla h)^2 \rangle \sim C_1 - C_2 \xi^{2\chi-2}$, where C_1 and C_2 are positive constants, C_1 being the value of $\langle (\nabla h)^2 \rangle_c$. Finally, then, we conclude that $\langle (\nabla h)^2 \rangle_c - \langle (\nabla h)^2 \rangle \sim C_2 \xi^{2\chi-2}$, whereupon Eq. (40) yields the result we have been looking for:

$$\xi \sim \delta r^{-1/(2-2\chi)} . \quad (41)$$

Thus the correlation length exponent ν in the strong-coupling MN problem is given by $1/(2-2\chi)$, where χ is the roughness exponent of the strong-coupling KPZ problem in the same dimension.

There is a well-known scaling relationship for the KPZ exponents χ and z , $\chi + z = 2$, that follows from the Galilean invariance of an advancing KPZ interface (Kardar *et al.* 1986). This equation implies that the exponents z and ν for the strong-coupling MN problem are not in fact independent (as they almost always are in critical phenomena), but rather obey the identity $z - 1/(2\nu) = 1$. Thus in fact, as in the infinite-absorbing-state problem, three exponents (say ν , β , and Δ), suffice to characterize the transition into the absorbing phase, rather than the four that we postulated in lecture II on general grounds. It would obviously be nice to be able to complete this characterization by computing β and Δ for the strong-coupling transition, but as things stand we will have to assign this unsolved problem as an exercise for the reader.

5.5 Numerical Verification

It remains to be seen whether the highfalutin theory presented in this section stands up to numerical testing. Here, we briefly discuss the results of a numerical study (Tu *et al.* 1996) of Eq. (33) in 1d, discretized in space and time.²³ The short, happy summary is that our predictions seem fairly convincingly confirmed by the numerics. In particular:

(1) The most striking qualitative prediction – the infinite susceptibility in an entire region of the absorbing phase – is clearly demonstrated by the 1d data. As in 0d, moreover, χ is seen numerically to diverge on *both* sides of the critical point, not just in the absorbing phase. Furthermore, the exponent $\gamma(r) - 1$ controlling the divergence of χ as the external source field H is sent to zero (recall $\chi \sim H^{\gamma(r)-1}$), is found to vary with r , again exactly as our calculations predicted, and as was observed in 0d. These features can be seen in Fig. 8, which shows a plot of the exponent $\gamma - 1$, versus r . Here the critical point occurs at approximately $r_c = -2.18$, while χ diverges (i.e., $\gamma < 1$) in the range $-5.9 < r < 3.2$. Finally, the numerics confirm that the region in which χ diverges in the absorbing phase is bounded above by $r = 0$, in the Ito representation. (This is not apparent from Fig. 8, which was not carried out in the Ito representation for model (33).)

(2) As far as critical exponent values go, the best estimates from the numerical data are $\beta = 1.70 \pm 0.05$, $\eta = 2.65 \pm 0.07$, $z = 1.53 \pm 0.07$, and $\Delta = 1.7 \pm 0.07$. Note that the value for z is consistent with the prediction $z = 3/2$ coming from the KPZ analogy. The scaling relation $2\beta = \Delta + \nu(d - 2 + \eta)$ yields the numerical value 1.03 ± 0.05 for ν , again consistent with the $\nu = 1$ prediction from KPZ. An independent measurement of ν from the finite-size scaling²⁴ of r_c with system size L , while not accurate to more than about 10%, is fully consistent with $\nu = 1$. Together with the measured values of β , η , and Δ , this number for ν serves as a consistency check for the scaling relation, written just above, that connects the four exponents.

(3) Finally, measurements on β_2 and β_3 in 1d show that these exponents are equal to β within the numerical accuracy. This suggests that the 0d result on multiscaling, viz., β_p being independent of p , might well hold in 1d as well. Some theoretical insight into this question would evidently be welcome. Consider this the final exercise for the reader.

²³ In discretizing Eq. (33) in time, one encounters the difficulty that the order parameter $n(\mathbf{x}, t)$ can become negative at some points (\mathbf{x}, t) , even if it is everywhere positive at $t = 0$; this phenomenon cannot occur in the continuum equation. In the numerics summarized here, this difficulty has been circumvented by setting $n(\mathbf{x}, t)$ to zero at each (\mathbf{x}, t) point where it has gone negative.

²⁴ The well-known result used implicitly here is that the variation of r_c with L satisfies $r_c \sim L^{-1/\nu}$. Convincing oneself that this is true is an instructive and not too demanding exercise in the manipulation of simple RG scaling relations. For help, see Privman (1990).

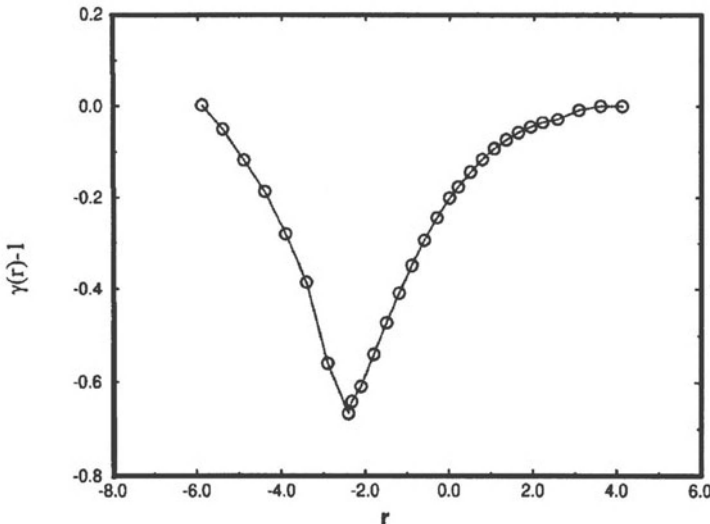


Fig. 8. The exponent $\gamma - 1$ as a function of r for the discretized 1d multiplicative noise model described in text. Susceptibility $\chi \sim H^{\gamma-1}$ diverges as $H \rightarrow 0$, for all $\gamma < 1$. This is Fig. 4b of Tu et al. 1996.

Acknowledgements: We are grateful to our faithful collaborators, Ron Dickman, Roberto Livi, and Yuhai Tu, for teaching us much about systems with absorbing states. Conversations with Nianzheng Cao, John Cardy, Shiyi Chen, Peter Grassberger, Terry Hwa, C. Jayaprakash, Juan Parrondo, and Arkady Pikovsky are also gratefully acknowledged. The gracious hospitality of the organizers, Pedro L. Garrido and Joaquín Marro, during the course of this meeting, is much appreciated.

References

- Abarbanel H.D.I. *et al.* (1975): Phys. Rep. **21C**, 120.
- Albano, E.V. (1992): J. Phys. A **25**, 2557.
- Barabási A.L. and Stanley H.E. (1995): *Fractal Concepts in Surface Growth* (Cambridge University Press, Cambridge).
- Becker A. and Kramer L. (1994): Phys. Rev. Lett. **73**, 955.
- ben-Avraham D. and Kohler J. (1992): J. Stat. Phys. **65**, 839.
- Berker A.N. and McKay S.R. (1984): J. Stat. Phys. **36**, 787.
- Bezuidenhout C. and Grimmett G. (1990): Ann. Prob. **18**, 1462.
- Binney J.J., Dowrick N.J., Fisher A.J. and Newman M.E.J. (1992): *The Theory of Critical Phenomena* (Clarendon Press, Oxford).
- Broadbent S.R. and Hammersley J.M. (1957): Proc. Camb. Philos. Soc. **53**, 629.

- Brower R.C., Furman M.A. and Moshe M. (1978): Phys. Lett. **76B**, 213.
- Cao N., Chen S. and She Z.-S. (1996): Phys. Rev. Lett. **76**, 3711.
- Cardy J.L. (1983): J. Phys. A **16**, L709
- Cardy J.L. and Grassberger P. (1985): J. Phys. A **18**, L267.
- Cardy J.L. and Sugar R.L. (1980): J. Phys. A **13**, L423.
- Cardy J. and Täuber U.C. (1996): *Theory of Branching and Annihilating Random Walks*, preprint.
- Chen K., Bak P., and Jensen M.H. (1990): Phys. Lett. **A 149**, 207.
- Deutsher G., Zallen R. and Adler J., eds. (1980): *Percolation Structures and Processes*, Annals of the Israeli Physical Society, Vol. 5 (Hiler, Bristol).
- Dickman R. (1996): Phys. Rev. E **53**, 2223.
- Domb C. and Green M.S., eds. (1976): *Phase Transitions and Critical Phenomena*, Vol. 6 (Academic, London).
- Durrett R. (1988): *Lecture Notes on Particle Systems and Percolation* (Wadsworth, Pacific Grove, CA).
- Essam J.W. et al. (1986): Phys. Rev. B**33**, 1986.
- Essam J.W., Guttmann A.J. and De'Bell K. (1988): J. Phys. A **21**, 3815.
- Fisher D.S. and Huse D.A. (1988): Phys. Rev. B**38**, 373.
- Garcia Ojalvo J., Hernandez Machado A. and Sancho J.M. (1993): Phys. Rev. Lett. **71**, 1542.
- Garrido P.L., de los Santos F. and Muñoz M.A. (1996): *A New Langevin Equation for Driven Diffusive Systems*, preprint.
- Graham R. and Schenzle A. (1982): Phys. Rev. A **25**, 1731.
- Grassberger P. (1982): Z. Phys. B **47**, 365.
- Grassberger P. (1989): J. Phys. A **22**, L1103.
- Grassberger P. (1995): *Directed Percolation: Results and Open Problems*, preprint.
- Grassberger P. and de la Torre A. (1979): Ann. Phys.(N.Y.) **122**, 373.
- Grassberger P., Krause F. and von der Twer T. (1984): J. Phys. A **17**, L105.
- Gribov V.N. (1967): Zh. Eksp. Teor. Phys. **53**, 654 [Sov. Phys. JETP **26**, 414 (1968)].
- Grinstein G., Lai Z.-W. and Browne D.A. (1989): Phys. Rev. A**40**, 4820.
- Grinstein G., Muñoz M.A. and Tu Y. (1996): Phys. Rev. Lett. **76**, 4376.
- Harris T.E. (1974): Ann. Prob. **2**, 969.
- Herweijer J. and van de Water W. (1995): Phys. Rev. Lett. **74**, 4651.
- Hohenberg P.C. and Halperin B.I. (1977): Rev. Mod. Phys. **49**, 435.
- Horsthemke W. and Lefever R. (1984): *Noise-Induced Transitions* (Springer, Berlin).
- Ito K. (1951): Mem. Amer. Math. Soc. **4**, 288.
- Janssen H.K. (1981): Z. Phys. **B42**, 151.
- Janssen H.K. (1985): Z. Phys. **B58**, 311.
- Jensen I. (1992): Phys. Rev. A**45**, R563.
- Jensen I. (1993): Phys. Rev. Lett. **70**, 1465.
- Jensen I. (1994a): Int. J. Mod. Phys. B**8**, 3299.
- Jensen I. (1994b): Phys. Rev. E **50**, 3623.
- Jensen I. and Dickman R. (1991): Phys. Rev. Lett. **67**, 2391.
- Jensen I. and Dickman R. (1993a): J. Stat Phys. **71**, 89.
- Jensen I. and Dickman R. (1993b): Phys. Rev. E**48**, 1710.
- Jensen M.H., Paladin G., Vulpiani A. (1991): Phys. Rev. Lett. **67**, 208.

- Kardar M., Parisi G., Zhang Y.C. (1986): Phys. Rev. Lett. **56**, 889.
- Kim M.H. and Park H. (1994): Phys. Rev. Lett. **73**, 2579.
- Kohler J., ben-Avraham D. (1991): J. Phys. A **24**, L621.
- Kosterlitz J.M. and Thouless D.J. (1973): J. Phys. **C6**, 1181.
- Krug J. and Meakin P. (1990): J. Phys. A **23**, L987.
- Kuramoto Y. (1984): *Chemical Oscillations, Waves and Turbulence* (Springer-Verlag, Berlin).
- Landau L.D. and Lifshitz E.M. (1980): *Statistical Physics*, 3rd Edition, Part 1 (Pergamon, Oxford).
- Lee B.P. (1994): J. Phys. A **27**, 2633.
- Liggett T.M. (1985): *Interacting Particle Systems* (Springer-Verlag, New York).
- Ma S.-K. (1976): *Modern Theory of Critical Phenomena* (Benjamin, NY).
- Maltz A. and Albano E.V. (1992): Surf. Sci. **277**, 414.
- Marro J. and Dickman R. (1997): *Nonequilibrium Phase Transitions and Critical Phenomena* (Cambridge University Press, Cambridge)
- McKay S.R., Berker A.N. and Kirkpatrick S. (1982): Phys. Rev. Lett. **48**, 767.
- Meakin P. and Scalapino D.J. (1987): J. Chem. Phys. **87**, 731.
- Mendes J.F.F., Dickman R., Henkel M. and Marques M.C. (1994): J. Phys. A **27**, 3019.
- Menyhard N. (1994): J. Phys. A **27**, 6139.
- Muñoz M.A., Grinstein G., Dickman R. and Livi R. (1996): Phys. Rev. Lett. **76**, 451.
- Muñoz M.A., Grinstein G., Dickman R. and Livi R. (1996): to appear in Physica D.
- Nelson D.R. and Halperin B.I. (1979): Phys. Rev. B **19**, 2457.
- Onsager L. (1944): Phys. Rev **65**, 117.
- Pikovsky A. and Kurths J. (1994): Phys. Rev. E **49**, 898.
- Privman V. ed. (1990): *Finite Size Scaling and Numerical Simulation of Statistical Systems* (World Scientific, Singapore).
- Ramaswamy S., Pandit R. and Lahiri R. (1995): Phys. Rev. Lett. **75**, 4786.
- Ramírez Piscina L., Sancho J.M., Hernandez Machado A. (1993): Phys. Rev. B **48**, 125.
- Schenzle A. and Brand H. (1979): Phys. Rev. A **20**, 1628.
- Schlögl F. (1972): Z. Phys. B **253**, 147.
- Shapiro V.E. (1993): Phys. Rev. E **48**, 109.
- Stratonovich R.L. (1989): in *Topics in the Theory of Random Noise*, Vols. 1, 16 (Cambridge University Press, Cambridge).
- Takayasu H. and Tretyakov A. Yu. (1992): Phys. Rev. Lett. **68**, 3060.
- Tu Y., Grinstein G. and Muñoz M.A. (1996): to appear in Phys. Rev. Lett.
- Uhlenbeck G.E. and Ornstein L.S. (1930): Phys. Rev. **36**, 823.
- Van den Broeck C., Parrondo J.M.R., Armero J. and Hernandez Machado A. (1994a): Phys. Rev. E **49**, 2639.
- Van den Broeck C., Parrondo J.M.R. and Toral R. (1994b): Phys. Rev. Lett. **73**, 3395.
- van Kampen N.G. (1981): *Stochastic Processes in Chemistry and Physics* (North Holland, Amsterdam).
- Vichniac G. (1986): private communication.
- Wallace D.J. and Zia R.K.P. (1974): Phys. Lett. **48A**, 325.

- Wilson K.G. and Kogut J. (1975): Phys. Rep **12**, 74.
Ziff R.M., Gularí E. and Barshad Y. (1986): Phys. Rev. Lett. **56**, 2553.

On the Self-organization of Migrating Individuals

E. Albano

Instituto de Investigaciones Fisicoquímicas Teóricas y Aplicadas, (INIFTA),
Facultad de Ciencias Exactas, Universidad Nacional de La Plata.

Sucursal 4, Casilla de Correo 16, (1900) La Plata - ARGENTINA.

FAX : 0054-21-254642. E-mail: ealbano@isis.unlp.edu.ar

1 Introduction

This lecture is concerned with a simple model aimed to describe the self-organized displacements of self-driving individuals. Processes such as growth, death, survival, self-propagation, competition and communication are considered. Starting from either small colonies or a randomly distributed population, the system evolves towards a stationary state where the population density is conserved. It is shown that the stationary state exhibits self-organized critical behavior.

It is known that a variety of biological objects frequently exhibit tendency to clustering and migration (herds of quadrupeds, flocks of birds, bacterial growth, etc.). Motivated by this observation, Vicsek *et al.* 1995, Csahók *et al.* 1995 and Toner *et al.* 1995 have very recently presented models aimed to describe the collective motion of living individuals. These models are quite simple but they retain basic facts characteristic of biological objects exhibiting collective behavior : i) the individuals are self-driven, i.e. transforming energy gained from food into mechanical energy they are able to perform displacements. ii) The motion of an individual is, on the one hand, perturbated by environmental conditions and on the other hand, conditioned by communications among their neighbours Vicsek *et al.* 1995, Csahók *et al.* 1995.

The aim of this work is to further extend these models in order to account for two relevant facts characteristic of the actual cooperative behaviour of the individuals : the first one is to allow the onset of self-organization via communications between neighboring individuals, while the second one is to explicitly consider the dynamic evolution of the population.

2 Definition of the Model

The model is based on the following rules :

Rule 1 : *The displacements.* All individuals have the same absolute velocity $|v|$. At each time step all individuals assume the average direction

of motion of the neighboring individuals within a range R with some random perturbation added. So, the location of the j -th individual is updated according to

$$\mathbf{x}_j(t+1) = \mathbf{x}_j(t) + \mathbf{v}_j \Delta t. \quad (1)$$

The direction of motion is given by the angle $\theta_j(t+1)$ according to

$$\theta_j(t+1) = <\theta_j(t)>_R + \pi Q N_R^{-\alpha}, \quad (2)$$

where the first term of eq.(2) is the average direction of the velocities of the N_R individuals (including the j -th one) within a circle of radii R surrounding the j -th individual. The second term introduces a random noise, where Q is a random number in the interval $(-1, 1)$ and α is an exponent. So, neighboring individuals may self-organize in order to minimize the noise being α a measure of the strength of such ability. This rule implies communications between the individuals (e.g. via sensing of chemicals, visual, verbal, etc.).

Rule 2 : The population dynamics. A live individual such as $N_R > N_3$ will die in the next step (decease by overcrowding). Also, a live individual will die in the next step if $N_R \leq N_1$ (decease by isolation). Individuals survive if the neighborhood is not too crowded ($N_2 \leq N_R \leq N_3$) and birth also occurs if N_R satisfies some stringent constraints ($N_1 < N_R < N_2$). This rule, inspired on Life (Berlekamp *et al.* 1982), allows the population to self-regulate its density.

The model is simulated in a two dimensional off-lattice cell of linear size L with periodic boundary conditions. All individuals are updated simultaneously at each time step (cellular automata updating). Simulations are made taking $|\mathbf{v}| = 0.03$, $R = 1$, $N_1 = 2$, $N_2 = 6$, and $N_3 = 9$.

3 Results and Discussion

3.1 Dynamics of Population Spreading

Population spreading is studied starting, at $t = 0$, with a small colony of N_o individuals placed in the center of the lattice. Then the colony is allowed to evolve according to the rules of the model and the following quantities are computed: (i) The average number of living individuals $N(t)$ and (ii) the survival probability $P(t)$ (i.e. the probability that the system had not evolved to extinction at time t). Figure 1 shows plots of $P(t)$ vs t obtained for lattices of different size and $\alpha = 0$. For large lattices ($L \geq 8$) the average survivability of the colonies is of about 70%, while in smaller lattices ($L = 5$) the system evolves to extinction. The insert of figure 1, which shows plots of $N_S(t) = N(t)/P(t)$ vs t , indicates that after same transient period, the population of the surviving colonies becomes stabilized, i.e. the systems reach a stationary state of constant density of living individuals.

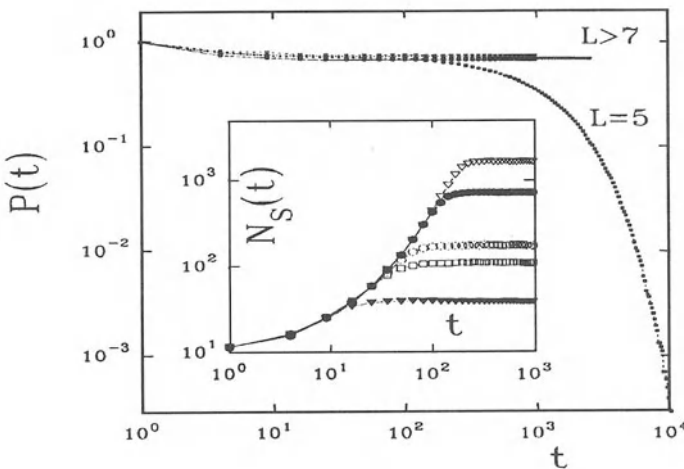


Fig. 1. Log-log plots of $P(t)$ vs t . The insert shows the corresponding plots of $N_S(t)$ vs t , obtained for lattices of size (from top to bottom) $L = 30, 20, 10, 8$ and 5 .

Figure 2 shows plots of $N_S(t)$ vs t obtained for lattices which are large enough so that the spreading colonies never reach the boundary. In the asymptotic regime the behavior $N_S(t) \propto t^\eta$ is found to hold, with $\eta = 2.13 \pm 0.03$, independent of α and N_o .

3.2 The Stationary State

Starting either from a random distribution of living individuals or due to the spreading of small colonies, it is found that the system evolves towards a stationary state (SS). The global density (ρ_g) is defined as the number of individuals over the total area of the sample. Also, the local density (ρ_l) is measured within the neighborhood (circle of radii R) of each individual. In the SS the system self-organizes in order to keep both the global and the local density constant independent of α , $\rho_g \cong 1.825(8)$ and $\rho_l \cong 2.511(8)$, respectively. The observed enhancement of the local density reflects a tendency to clustering (“flocking behavior”). This behavior is mostly due to the dynamics of the population, but it is not a consequence of the operation of an attractive potential as observed in most physical systems. However, the behaviour of the clusters (“flocks”) as a whole, depends on α . In fact, using the absolute value of the normalized average velocity $|\langle v \rangle|$ as a measure of the flocking behavior, the crossover between two distinct regimes is observed : for larger α values (e.g. $\alpha \geq 4$) one has $|\langle v \rangle| \rightarrow 1$, that is individuals self-organize in

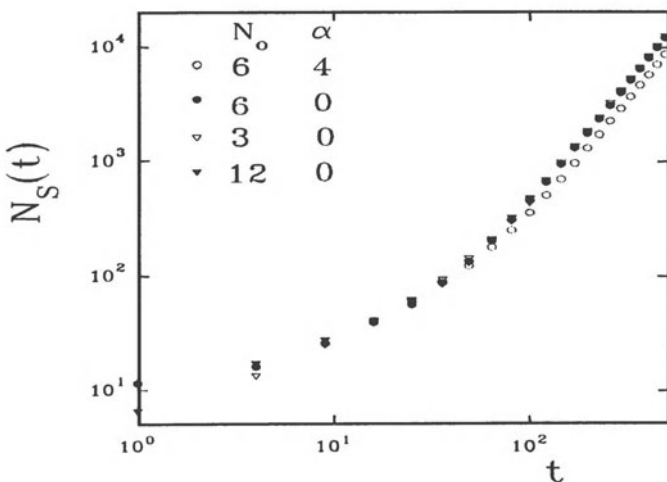


Fig. 2. Log-log plots of $N_S(t)$ vs t .

a single flock with a well defined direction of migration; however for $\alpha \rightarrow 0$ also $|\langle v \rangle| \rightarrow 0$, that is many flocks move in random directions.

A relevant feature of the SS is that it exhibits **self-organized criticality (SOC)** behavior. SOC is a concept proposed by Bak *et al.* 1987-88 to describe the dynamics of a class of non-linear spatio-temporal systems, which evolve spontaneously toward a critical state (i.e. without having to tune a control parameter). Systems exhibiting SOC have attracted much attention since they might explain part of the abundance of $1/f$ noise, fractal structures and Lévy distributions in Nature (Bak *et al.* 1987-88), for examples of systems exhibiting SOC see also Bunde *et al.* 1995. In order to test for SOC behavior, the stationary state is perturbed by randomly adding a single individual. The evolutionary change triggered by this small perturbation is called an avalanche. The fate of the added individual depends on the environment: some individuals may die while others may succeed to survive and reproduce generating avalanches of all sizes, i.e. a highly complex branching process. The life-time of an avalanche t is defined as the time elapsed between the introduction of the perturbation and the extinction of the perturbative individual itself and all its descendants. The size of the avalanche (s) is then computed by counting the number of descendants originated by the perturbative individual during the life-time of the avalanche.

For the stationary state to be SOC the distributions of life-time ($D(t)$) and size ($D(s)$) must exhibit power law behavior, i.e. $D(t) \propto t^{-a}$ and $D(s) \propto s^{-b}$

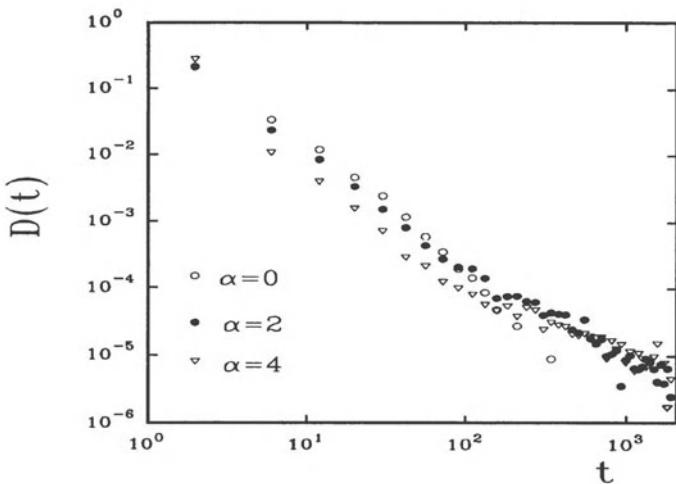


Fig. 3. Log-log plots of the distribution of life-time $D(t)$ vs t of the avalanches within the SOC regime. $L = 30$, results averaged over 2×10^4 avalanches.

(see e.g. figure 3). The estimates for the exponents are $a \cong 1.7 \pm 0.1$ and $b \cong 1.6 \pm 0.1$, respectively. Due to the highly complex non-linear branching process involved in the present model, one expects $a \neq b$ and the scaling relationship $t \propto s^x$, with $x = (b-1)/(a-1)$, holds. Measurements give $x = 0.82 \pm 0.1$ in agreement with the scaling value obtained from the exponents a and b , i.e. $x \approx 0.86$.

It has to be stressed that, while the flocking behaviour of the individuals strongly depends on α (i.e. single flock behaviour for large α and random displacements of individuals for $\alpha \rightarrow 0$), all power laws describing the distribution of avalanches and spatial correlations are independent of α ; pointing out that the model exhibits robust critical behaviour which is achieved spontaneously without the necessity of tuning any external parameter, i.e. SOC.

4 Conclusions

A model which describes the self-organized cooperative displacement of self-driving and self-replicating individuals is proposed and studied. The spreading of small colonies in an otherwise empty landscape is investigated. If the available space for spreading is large enough, the colonies have a high average survivability (roughly 70%) while extinction, which takes place at early times, is mostly due to unfavorable initial conditions. In finite spaces, however, a stationary state is achieved such as the population self-organize to

keep constant both, the local and the global density. The addition of an individual (i.e. a small perturbation) in the stationary state triggers avalanches of all sizes, i.e. the system lacks of any characteristic time- and size-scale. This behavior is the signature that the system self-organize in a critical state. So, the emergency of a very rich and complex critical behaviour at global scale, originated in simple local rules, is observed.

ACKNOWLEDGEMENTS. This work was financially supported by the CONICET (Argentina), the National University of La Plata and the Commission of European Communities under contract ITDC-122.

References

- Bak P., Tang C. and Wiesenfeld K. (1987): Phys. Rev. Lett. **59**, 381;(1988): Phys. Rev. A. **38**, 364.
Berlekamp E. R., Conway J. H. and Guy R. K. (1982): *Winning Ways for your Mathematical Plays*. Vol. 2, Academic.
Bunde A. and Havlin S. (Eds) (1995): in *Fractals in Science*, (Springer Verlag), Berlin.
Csahók Z. and Vicsek T. (1995): Phys. Rev. E., **52**, 5295.
Toner J. and Tu Y. (1995): Phys. Rev. Lett., **75**, 4326.
Vicsek T., et al. (1995): Phys. Rev. Lett. **75**, 1226.

Recent Progress in the Study of Irreversible Transitions in Reaction Systems

E. Albano

Instituto de Investigaciones Fisicoquímicas Teóricas y Aplicadas, (INIFTA),
Facultad de Ciencias Exactas, Universidad Nacional de La Plata.
Sucursal 4, Casilla de Correo 16, (1900) La Plata - ARGENTINA.
FAX : 0054-21-254642. E-mail: ealbano@isis.unlp.edu.ar

1 Introduction

In this lecture I present two studies in the field of irreversible transitions in reaction systems. On the one hand, the influence of long-range interactions, generated via Lévy exchanges, on the irreversible critical behavior of the contact process is studied, showing that the critical exponents are tunable functions of the Lévy exponent. On the other hand, the displacement of poisoned states by the reactive stationary state, in narrow channels, is investigated using a dimer-monomer reaction model which mimics the catalytic oxidation of carbon monoxide.

In thermodynamic phase transitions the behavior of the system under consideration changes qualitatively when a certain control parameter (e.g. pressure or temperature) passes through a critical point. Analogously, surface catalyzed reaction processes may change, between a stationary reactive state and an inactive state (without reaction), when the control parameter (e.g. the partial pressures of the reactants) is finely tuned through a critical value. These irreversible phase transitions (IPT's) are in contrast to thermally driven transitions which are reversible. The study of IPT's in reaction systems, collectively known as *interacting particle systems* Liggett 1985, is an important problem in many branches of physics, chemistry, biology, etc.; for a recent review see Albano (1996a), for instance.

One of the simplest system undergoing an IPT is the contact process (CP), as proposed by Harris 1974, which describes the propagation of an epidemic. The CP is a *single-component* system which evolves according to a Markov process with *local* and intrinsically irreversible rules. Such rules involve the spontaneous annihilation of particles with probability p independent of the state of the others sites, and autocatalytic creation of particles at rate $1-p$ at a randomly chosen nearest neighbor site (provided it is vacant). As there is no spontaneous creation of particles the state with all vacant sites is irreversibly inactive. Also, if the annihilation rate is sufficiently small, there is a non-trivial active state with non-zero average density of particles. So, the CP

exhibits an IPT between the active and the vacuum state. In Section 2 the CP is generalized to account for long range interactions between particles.

Among *multi-component* reaction systems, one of the best studied is the ZGB model proposed by Ziff *et al.* 1986, which mimics the catalytic oxidation of CO , $2A + B_2 \rightarrow 2AB$, i.e. A is CO , B_2 is O_2 and AB is CO_2 . It is assumed that the reaction proceeds according to Langmuir-Hinshelwood mechanism, so the computer implementation of the ZGB model is as follows : i) A or B_2 molecules are selected randomly with relative probabilities Y_A and Y_B , respectively. These probabilities are the relative impingement rates of both species, which are proportional to their partial pressures. Due to the normalization, $Y_A + Y_B = 1$, the model has a single parameter, i.e. Y_A . If the selected species is A , one surface site is selected at random, and if that site is vacant, A is adsorbed on it. Otherwise, if that site is occupied, the trial ends and a new molecule is selected. If the selected species is B_2 , a pair of nearest neighbor sites is selected at random and the molecule is adsorbed on them only if they are both vacant. ii) After each adsorption event, the nearest neighbors of the added molecule are examined in order to account for the reaction; for additional details see Ziff *et al.* (1986). The ZGB model exhibits two IPT's between an active regime with AB -production and poisoned states with B - and A -species. These IPT's are of second (first) order and lie close to $Y_{1A} = 0.3905$ ($Y_{2A} = 0.5256$), respectively. In Section 3 the invasion of the reactive state to poisoned phases is studied.

2 The Contact Process with Long Range Correlations

It has been demonstrated, in the field of reversible phase transitions, that random exchange via Lévy flights can effectively generate long range interactions, see e.g. Bergersen & Rácz 1991. The Lévy flight (Lévy 1937, Mandelbrot, 1982) is a random walk in which the step length (l) is a random variable with a probability distribution given by $P(l) \propto l^{-d-\sigma}$, where d is the spatial dimension and the parameter σ is the dimension of the walker. For $\sigma < 1$ the walker exhibits superdiffusive behavior, while for $\sigma = 1$ one recovers ordinary diffusion. The generalization of the CP to account for long range interactions (i.e. the CPLRI) is straightforward : a randomly selected empty site evolves according to the rules of the CP, however a randomly chosen occupied site may either evolve according to the rules of the CP with probability $1 - \tau$ or undergo a Lévy exchange with other site with probability τ . We carried out Monte Carlo simulations of the CPLRI process in one dimension for $\tau = 1/2$ and $0 \leq \sigma \leq 11$.

Test runs of the CPLRI model shown that the system reaches an active stationary state for small enough values of p , while increasing p causes the system to irreversibly evolve into a vacuum state. The IPT's are of second order and the critical values of p at which such transitions take place depend on σ . In order to determine the critical points and some relevant critical

exponents time dependent simulations also known as epidemic analysis are performed. The general idea behind epidemic simulations is to start from a configuration which is very close to the inactive state, and follow the averaged time evolution of this configuration by generating a large ensemble of independent realizations. So, one starts, at $t = 0$, with two occupied nearest neighbor sites, placed in the center of the lattice, in an otherwise empty sample. Then the configuration is allowed to evolve according to the rules of the model. The time evolution of the sites is monitored and the following quantities are computed: (i) The average number of occupied sites $N(t)$, (ii) the survival probability $P(t)$ (i.e. the probability that the system had not entered in the inactive state at time t), and the average mean square distance of spreading from the center of the lattice $R^2(t)$. At criticality, the following scaling behavior is expected to hold (Grasberger & de la Torre 1979): $P(t) \propto t^{-\delta}$, $N(t) \propto t^\eta$, and $R^2(t) \propto t^z$, where δ , η and z are dynamic critical exponents.

At criticality, log-log plots of $P(t)$, $N(t)$ and $R^2(t)$ versus t give straight lines, while upward and downward deviations occur even slightly off-criticality. This behavior allow us a precise determination of both the critical points and the critical exponents, as e.g. it is shown in figure 1 for $\sigma = 0.75$. Figure 2 shows log-log plots of $N(t)$ versus t taken for different values of σ . Here the change in the asymptotic slope can clearly be observed. The obtained exponents are listed in Table I.

Model	σ	p_c	η	δ	z
DP	--	--	0.308	0.160	1.265
CPLRI	11	0.4235(5)	0.305(5)	0.161(3)	1.257(5)
CPLRI	2	0.4380(5)	0.304(5)	0.166(3)	1.261(5)
CPLRI	1.50	0.4490(5)	0.306(5)	0.166(3)	1.260(5)
CPLRI	1	0.4710(5)	0.306(5)	0.165(3)	1.260(5)
CPLRI	0.75	0.4890(5)	0.328(5)	0.159(3)	1.262(5)
CPLRI	0.50	0.5137(3)	0.352(5)	0.145(3)	1.265(5)
CPLRI	0.25	0.5463(3)	0.367(5)	0.14(1)	1.28(2)
CPLRI	0.0	0.5868(3)	0.403(8)	0.12(1)	1.30(2)

Table 1. Critical points and critical exponents of CPLRI and directed percolation (the latter taken from Grassberger *et al.* (1979)).

From Table I it follows that within the range of Lévy exponents ($\sigma \geq 1$) which corresponds to standard diffusion the obtained critical exponents reveal that the CPLRI model belongs to the universality class of directed percolation. This finding is in agreement with well established concepts of univer-

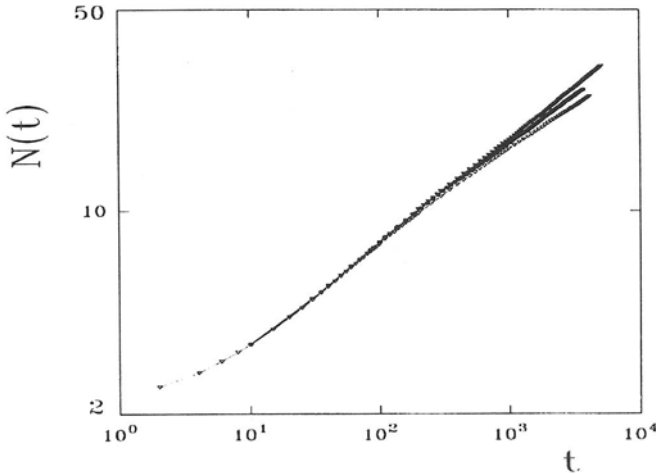


Fig. 1. Log-log plots of $N(t)$ vs t obtained for $\sigma = 0.75$ and different values of p : $p = 0.4885$ upper curve (supercritical), $p = 0.4890$ medium curve (critical) and $p = 0.4895$ lower curve (subcritical).

sal behavior: since exchanges are restricted to short distances, the diverging correlation length remains as the only relevant length scale. However, for smaller σ values, when superdiffusive behavior is observed, the exchanges are not longer restricted to short distances and additional long-range correlations can effectively been established. So, in these cases, one observes departure from the standard directed percolation behavior and the critical exponents depend on σ ; in other words they can be tuned varying σ .

3 The Invasion of the Reactive State to Poisoned Phases in the ZGB Model

The displacement of B - and A -poisoned phases by the reactive regime is simulated in narrow channels using the ZGB model on the square lattice with rectangular geometries of sides $L \times M$ ($L \ll M$), where L is the width of the channel and M its length. Free boundary conditions are taken along the channel while the opposites ends are in contact with A and B sources, respectively. This geometry mimics the experimental setup used by Haas *et al.* (1995). Basic information on the invasion of the reactive phase to the poisoned one is obtained from the concentration profiles of the reactants; $\theta_A(x)$ and $\theta_B(x)$; which are measured along the length of the channel x in

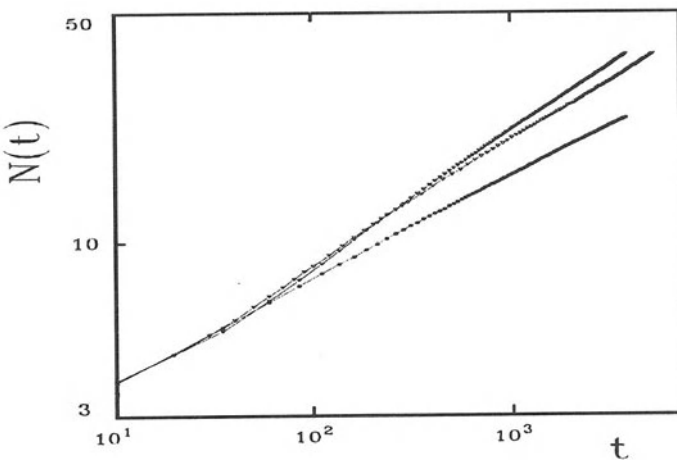


Fig. 2. Log-log plots of $N(t)$ vs t obtained at criticality for different values of σ : $\sigma = 2$ (upper curve), $\sigma = 0.25$ (medium curve) and $\sigma = 0$ (lower curve).

the M -direction and averaged over each column of lattice sites of length L . After determining smooth profiles, averaged over 10^4 different samples, one can get insight on the propagation behavior measuring the moments of n -th order of the profiles which are given by

$$\langle x^n \rangle_\theta = \frac{\sum x^n [\theta(x+1) - \theta(x)]}{\sum [\theta(x+1) - \theta(x)]}. \quad (1)$$

The propagation velocity is then obtained from the first moment, i.e. $V = \frac{d\langle x \rangle}{dt}$. Figure 3 shows plots of the propagation velocities of A and B -profiles vs Y_A . Notice that these velocities correspond to the invasion of the reactive regime to the B and A -poisoned phases, respectively. These results and others obtained for channels of different width ($3 \leq L \leq 30$), can be summarized as follows : a) two critical pressures $Y_A^{c1}(L)$ and $Y_A^{c2}(L)$, which depend on the width of the channel, at which the displacement of the poisoned phases stop are found; b) within these critical values A - and B -poisoned phases are displaced; and c) The displacement of the A -poisoned phase is faster than that of the B -poisoned one. All these observations appear in qualitative agreement with the experimental results reported in figure 2(a) of Haas *et al.* (1995). However, the underlaying physics is different: in the simulations the displacement of a poisoned phase by the invading reactive phase takes place within a range of pressures where the later is unstable while

the former is stable. In contrast the experiment may show the propagation of coexisting phases within a bistable regime.

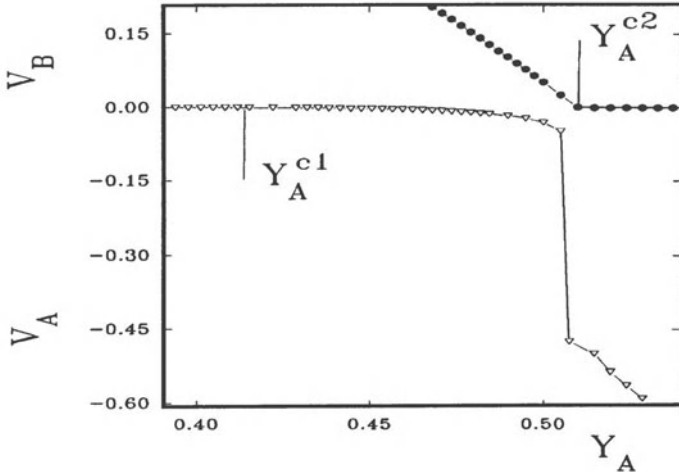


Fig. 3. Plots of the propagation velocities of A and B -profiles *vs* Y_A obtained in channels of width $L = 10$. The lines show the location of the critical probabilities at which propagation stops.

Simulations also show a jump in the propagation velocity of A -profiles which occurs close to $Y_A^{c2}(L)$ (see figure 3). This discontinuity simply reflects the first order A -poisoning transition of the ZGB model at Y_{2A} and the fact that propagation within the poisoned phase must be faster than within the reactive phase. Figure 4 shows that plots of $Y_A^{c1}(L)$ and $Y_A^{c2}(L)$ *vs* L^{-1} converge, in the asymptotic limit, to Y_{1A} and Y_{2A} , respectively. So, the critical pressures at which the displacement of the poisoned states stops can be identified with the poisoning transitions of the ZGB model.

4 Conclusions

The influence of long-range interactions in the critical behavior of IPT's has received little attention, presumably due to the huge computational effort required to obtain reliable results. It is shown that this shortcoming can be avoided since long-range interactions can effectively generated via long-range Lévy exchanges. The IPT of the CP in presence of long-range exchanges

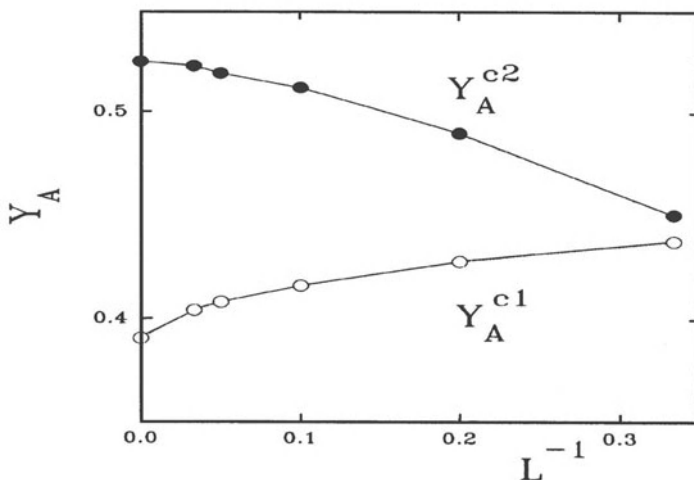


Fig. 4. Plots of the critical probabilities $Y_A^{c1}(L)$ and $Y_A^{c2}(L)$ vs L^{-1} . The points for $L = \infty$ are Y_{1A} and Y_{2A} , respectively.

remains second order, but the relevant critical exponents become tunable functions of the Lévy exponent. The new set of tunable exponents define a generalized universality class of directed percolation with long-range interactions. This conjecture is also supported by simulations of branching annihilating Lévy walkers Albano 1996b. In a related context of the study of IPT, it is shown that the ZGB model is suitable for the study of the displacement of poisoned phases during the catalytic oxidation of CO . In narrow channels, the critical points at which the displacements stop exhibit marked finite-size effects, however, extrapolating to $L \rightarrow \infty$ the critical points of the ZGB model are recovered. Simulation results have many points of qualitative agreement with experimental findings of front propagation, a fact which gives further support to many theoretical studies based on the ZGB model. It is expected that more elaborate models, e.g. including diffusion, surface reconstruction, etc., will improve the description.

ACKNOWLEDGEMENTS. This work was financially supported by the CONICET (Argentina), the National University of La Plata and the Commission of European Communities under contract ITDC-122.

References

- Albano E. V. (1996): *Het. Chem. Rev.*, in press.
Albano E.V. (1996): *Europhys. Lett.*, in press.
Bergeren B. and Rácz Z. (1991): *Phys. Rev. Lett.* **67**, 3047.
Grassberger P. and de la Torre A. (1979): *Ann. Phys. (N. Y.)*, **122**, 373.
G. Haas *et al.* (1995): *Phys. Rev. Lett.*, **75**, 3560.
Harris T. E. (1974): *Ann. Probab.* **2**, 969.
Lévy P. (1937): *Theorie de l'addition des variables aleatoires*, (Paris, Gauthier-Villars).
Liggett T. M. (1985): *Interacting particle Systems* (Springer, Berlin, Heidelberg).
Mandelbrot B. B. (1982): *The Fractal Geometry of Nature*, (San Francisco, Freeman).
Ziff R., Gulari E. and Barshad Y. (1996): *Phys. Rev. Lett.*, **56**, 2553.

Part II

Contributions

Critical Behavior of an Evolution Model

S. Clar, R.A. Monetti, and F. Schwabl

Technische Universität München, James-Franck-Str., D-85747 Garching, Germany

We study a variant of the Bak-Sneppen (B-S) evolution model by introducing random mixing of particles after each time step. The scaling behavior is found to be that of directed percolation or Reggeon Field Theory (RFT).

We modify the B-S evolution model by randomly mixing the positions of all particles at each time step. The dynamics of the model are studied by simulating a branching process with branching probability x_{min} , starting from a single particle in the vacuum state. Thus, we have a tunable control parameter. We compute the average number of particles $N(t)$, the survival probability of the avalanche $P(t)$, and the average spreading distance $R(t)$. Time is defined to increase by an amount $1/N(t)$ at each update. At criticality, we expect $N(t) \propto t^\eta$, $P(t) \propto t^{-\delta}$ and $R(t) \propto t^{z/2}$. Figure 1 show log-log plots of $N(t)$ and $P(t)$ for different values of x_{min} .

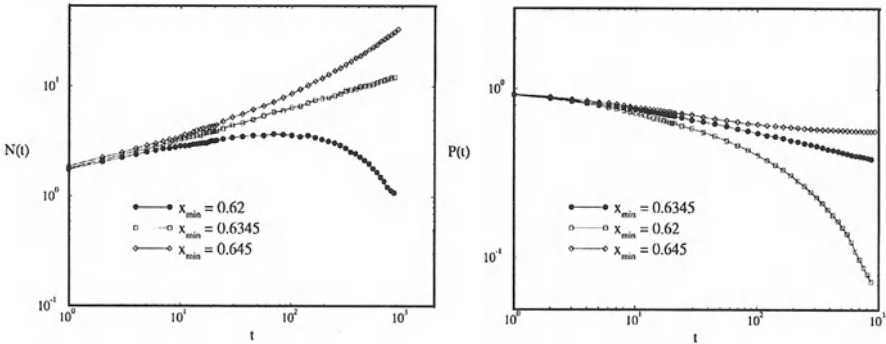


Fig. 1. Plots of $N(t)$ vs. t and $P(t)$ vs. t respectively

Criticality is achieved for $x_{min} = 0.6345(2)$. The values $\eta = 0.301$, $\delta = 0.158$ and $z = 0.632$ are in excellent agreement with the RFT universality class. We expect that the system displays a crossover between the B-S fixed point and RFT when the range of mixing is varied via a temperature like parameter. This model is very similar to "model 3" of Jovanovic et al., where it was not clear whether or not the model belongs to the RFT universality class.

References

- Bak P. and Sneppen K. (1993): *Punctuated Equilibrium and Criticality in a Simple Model of Evolution*, Phys. Rev. Lett. **71**, 4083
- Jovanovic B., Buldyrev S.V., Havlin S. and Stanley H.E. (1994): *Punctuated Equilibrium and "History-dependent" Percolation*, Phys. Rev. E **50**, R2403

Simulation of Phase Behavior of Fluids in Gels

R. Salazar¹, R. Toral^{1,2}, and A. Chakrabarti³

¹ Departament de Física, Universitat de les Illes Balears, Espanya

² Instituto Mediterráneo de Estudios Avanzados (IMEDEA, UIB-CSIC), 07071 Palma de Mallorca, España

³ Physics Department, Kansas State University, Manhattan, Kansas 66505, U.S.A.

It is found experimentally that the coexistence region of a vapor–liquid system is substantially narrowed when the fluid is confined in a silica aerogel with a high degree of porosity (e.g., of the order of 95%). A Hamiltonian model for this system has been recently introduced. This is the usual Ginzburg–Landau model for a scalar concentration field $m(\mathbf{r})$ used in binary phase–transitions plus the inclusion of an additional term representing the superficial stress in the neighborhood of the gel:

$$\begin{aligned}\mathcal{H} = & \int_V dV \left[-\frac{\theta}{2}m^2(\mathbf{r}) + \frac{\chi}{4}m^4(\mathbf{r}) - Hm(\mathbf{r}) + \frac{1}{2}|\nabla m(\mathbf{r})|^2 \right] \\ & + \oint_S ds \left[-H_1 m(\mathbf{r}) - \frac{g}{2}m^2(\mathbf{r}) \right]\end{aligned}$$

Volume V is the available volume for the fluid and the surface S is the set of fluid points in contact with the gel. We perform Monte–Carlo simulations of the above Hamiltonian in order to find the phase diagram. We consider a three-dimensional lattice with periodic boundary conditions. The gel sites in this lattice form a periodic fractal structure generated by diffusion–limited–cluster–aggregation process.

To find the phase diagram for a defined value of the surface field H_1 , the surface enhancement parameter g and the width of the coexistence curve χ , we use the following scheme: for each reduced temperature θ , we compute the hysteresis loop and the Gibbs free–energy (evaluated by integration of the ensemble average order parameter $\bar{M}(H)$ from $H = \pm\infty$) for several values of total field H . The two minima of the free–energy identify the two coexisting phases and indicate the actual location of the transition causing the hysteresis loop, i.e., the actual value H_0 of the total field H such that the two phases have the same value for the free–energy. We find in this way the function $H_0 = H_0(\theta)$ which allows us to compute the phase diagram. This is qualitatively similar to that observed experimentally: the coexistence region in the presence of gel is narrowed and shifted with respect to the non–gel situation. However, it is difficult to perform simulations near the critical point and, hence, we have not been able yet to obtain an accurate value for the critical exponents of the model.

References

- Donley J. and Liu A. (1996): *Phase Behavior of Near-Critical Fluids Confined in Periodic Gels*, preprint.
- Wong A. and Chan M. (1990): Phys. Rev. Lett. **65**, 2567–2570.
- Falicov A. and Berker A. (1995): Phys. Rev. Lett. **74**, 426–429.
- Nakanishi H. and Fisher M. (1983): J. Chem. Phys. **78**, 3279–3293.

Mesoscopic Descriptions of Fluids

M. Serrano, P. Español, and I. Zúñiga

Departamento de Física Fundamental, Universidad Nacional de Educación a Distancia, Apartado 60141, 28080 Madrid, España

Molecular Dynamics simulations of hydrodynamics require an overwhelming computational effort. This motivates the development of *mesoscopic descriptions* in which the relevant hydrodynamic behavior appears with a number of particles much smaller than those required in conventional Molecular Dynamics. Dissipative Particle Dynamics (DPD) is an attempt for such a mesoscopic approach. The crucial idea behind is that the point particles describing the fluid interact through conservative, dissipative and random forces. In a previous paper we have derived from first principles the DPD for a 1D harmonic chain. Starting from a microscopic description of the harmonic chain in terms of the positions and momenta of the atoms of the chain, we have deduced the equations of motion for a coarse-grained chain constructed by grouping the atoms in clusters of size n . Making use of a projection operator technique we found, in the limit of very long chains and large groupings, that the clusters interact elastically and dissipatively. They are also subject to random delta-correlated forces that take into account the eliminated degrees of freedom. This is how *dissipation* and *noise* come out naturally.

We attempt a similar approach for a fluid system. Analytical results are difficult to obtain and a numerical Molecular Dynamics scheme is proposed. We define clusters of fluid in a way that resembles the Voronoi tessellation: seeding a number of points randomly in the box, we associate to each of these points a cluster of microscopic particles belonging to its neighborhood. Through the simulation, the clusters move according to Newton's law. We are interested in extracting the law of force between these clusters. To this end, we have calculated the radial distribution function from which the potential of mean force can be extracted. We have studied the dependence of the fitted potential's parameters with the cluster length λ_c and have found (in the asymptotic limit of large cluster size M_c) a purely repulsive potential, "soft-drop like", quite similar to that first used by Hoogerbrugge and Koelman. The next step to be performed is the introduction of dissipative forces and thermal noise in order to complete a realistic dynamic description of the fluid.

References

- Hoogerbrugge P.J. and Koelman J.M.V.A. (1992): *Europhys. Lett.*, **19**, 155.
Koelman J.M.V.A. and Hoogerbrugge P.J. (1993): *Europhys. Lett.*, **21**, 363.
Español P. and Warren P. (1995): *Europhys. Lett.* **30**, 191.

Español P. (1995): Phys. Rev. E. **52**, 2.

Español P., Zúñiga I. and Serrano M. (1997): Submitted to Int. J. Mod. Phys. C.

Description of Growth Models with Density Equations

C. López¹ and P.L. Garrido^{1,2}

¹ Instituto Carlos I de Física Teórica y Computacional, Facultad de Ciencias, Universidad de Granada, E-18071-Granada, España.

² Departamento de Física Moderna, Facultad de Ciencias, Universidad de Granada, E-18071-Granada, España.

We define growth models through a stochastic bulk dynamics. In this way shadowing effects and interfacial overhangs are naturally taken into account. The model is initially defined by means of a master equation. From it, we derive its corresponding Langevin mesoscopic description. In this way, the influence of the microscopic dynamics into the Langevin equation is shown explicitly. Finally, we relate our density equations with the better known interfacial equations. Several examples are commented and in particular, we show the way to obtain the Euclidean-invariant Kardar-Parisi-Zhang equation with a particular election of the bulk dynamics.

References

- López C. and Garrido P.L. (1997): submitted to Phys. Rev. E.
Marsili M., Maritan A., Toigo F. and Banavar J.R. (1996): to appear in Rev. Mod. Phys. (cond-mat/9606026).

Langevin Approach to Synthetic Turbulence and Applications

A.C. Martí¹, J.M. Sancho¹, and F. Sagués²

¹ Universitat de Barcelona, Departament d'Estructura i Constituents de la Matèria, Diagonal 647, E-08028 Barcelona, España.

² Universitat de Barcelona, Departament de Química Física, Diagonal 647, E-08028 Barcelona, España

We present an analytic scheme, easily implemented numerically, to generate synthetic Gaussian turbulent flows by using a linear Langevin equation, where the noise term acts as a stochastic stirring force. The characteristic parameters of the velocity field are well introduced, in particular the kinematic viscosity and the spectrum of energy. As an application, we study the dynamics of reaction-diffusion systems convected by a turbulent velocity field. It is shown how the propagation velocity and the front roughness are affected by the fluid motion. We also consider phase separation processes under the influence of turbulent stirring.

References

- Careta A., Sagués F. and Sancho J.M. (1993): Phys. Rev. E **46**, 2279–2287
Martí A.C., Sagués F. and Sancho J.M. (1996): preprint
Sagués F., Sancho J.M. and Martí A.C. (1996): *Synthetic Random Flows: Generation and Applications* to appear in Lectures on Stochastic Dynamics edited by L. Schimansky-Geier and T. Pöschel (Springer, Berlin, Heidelberg).

Irreversible Adsorption of Colloidal Particles

J. Faraudo and J. Bafaluy

Departament de Física, Universitat Autònoma de Barcelona, 08193 Bellaterra (Barcelona), España

A (1+1)-dimensional adsorption model has been analyzed to investigate the influence of diffusion and sedimentation on the structure of monolayers of particles irreversibly adsorbed on a line (Faraudo & Bafaluy 1996). The relative influence of both effects is measured by the dimensionless particle radius defined as $R^* \equiv R ((4\pi g \Delta \rho)/(3k_B T))^{1/4}$. For $R^* \gg 1$ the motion is deterministic, whereas if $R^* \ll 1$ brownian motion predominates. We focus our attention on the dependence of the radial distribution function $g(r)$ and the saturation coverage θ_∞ on R^* . First, we study the adsorption probability onto an available interval using approximate solutions of the transport equation and brownian dynamics simulations. In these simulations, the particle motion is discretized in time, and at every time step the particle performs sequentially the deterministic motion (sedimentation) and the random displacement (from a Gaussian distribution) corresponding to brownian motion. If a collision with an adsorbed particle occurs during the deterministic displacement, the incoming particle rolls over the pre-adsorbed one. The collision rule for the Brownian motion is a perfect reflection of the particle trajectory. The simulation results agree with our approximate solutions and with numerical solutions (Choi 1995) of the transport equation. The predicted scaling behavior for the probability of adsorption when $R^* \gg 1$ is shown to hold for R^* larger than ~ 2.3 . Combining our results with an approximate general formalism, we obtain θ_∞ and the gap density at the jamming limit. In this calculation we neglect the interaction with third neighbors, which plays a minor role, as shown by control simulations. The saturation coverage has also been obtained, as well as $g(r)$, performing 10^3 simulations for each R^* with lines of length $200R$ with periodic boundary conditions. For $R^* \leq 1$, $\theta_\infty(R^*)$ and $g(r)$ are close to the $R^* = 0$ form ($\theta_\infty \simeq 0.751$). For $R^* \geq 1$, $\theta_\infty(R^*)$ grows quickly with R^* . The peaks in $g(r)$ increase and are steeper when R^* grows reflecting the tendency of large particles to pack closer than smaller ones due to the increasing effect of the rolling mechanism. For large gravity, θ_∞ approaches the ballistic limit ($\theta_\infty^{BD} = 0.808\dots$) following a power law, $\theta_\infty^{BD} - \theta_\infty(R^*) \propto (R^*)^{-8/3}$, which is independent of the system dimension, as has been observed in simulations (Ezzeddine *et al.* 1995).

References

- Faraudo J. and Bafaluy F.J. (1996): Phys. Rev. E **54** 3725.
Choi H.S. (1995): Ph. D. Thesis, Purdue University.
Ezzeddine R., Schaaf P., Voegel J.C. and Senger B. (1995): Phys. Rev E **51**, 6286.

Probability Distribution Function for the Random Sequential Adsorption of Aligned and Unaligned Hard-Squares

F.L. Román, J.A. White, and S. Velasco

Departamento de Física Aplicada, Facultad de Ciencias, Universidad de Salamanca,
37008 Salamanca, España

The distributions of the number of aligned (or parallel) and unaligned hard squares deposited in a small subvolume of a finite flat surface with periodic boundaries through a random sequential adsorption (RSA) process are obtained from computer simulations. These distributions are compared with a hypergeometric model where the effects of mutual exclusion between squares are incorporated by a coverage dependent effective *volume* per square.

The statistical distribution of aligned and unaligned hard squares (AHS and UHS, respectively) deposited on a subvolume of a flat surface through a RSA mechanism has been examined by computer simulation. For large enough adsorbing surfaces, the associated relative fluctuation depends on the coverage θ , the relative size of the total adsorbing surface respect to the size of the subvolume ($\epsilon = V_0/V$), and on the relative size of one adsorbed square respect to the subvolume size (v/V). The distributions obtained from computer simulation have been compared with a binomial distribution and a hypergeometric distribution. The hypergeometric distribution incorporates a coverage dependent effective volume per particle $\nu(\theta)$. Analytical expressions for $\nu(\theta)$, written as a sum of three contributions proportional to $(v/V)^0$, $(v/V)^{1/2}$ and (v/V) , respectively, are proposed for the RSA of both AHS and UHS. We have found that the hypergeometric distribution reproduces the simulated distributions with excellent agreement for low and intermediate coverages, whereas this agreement is a bit worse for coverages close to the jamming limit.

This work was supported by the Dirección General de Investigación Científica y Técnica (DGICYT) of Spain under Grant No. PB 95-0934.

References

- Senger B., Schaaf P., Voegel J.C., Wojtaszczyk P. and Reiss H. (1994): *Proc. Natl. Acad. Sci.* **91**, 10029.
Schaaf P., Wojtaszczyk P., Mann E.K., Senger B., Voegel J.C. and Bedeaux D. (1995): *J. Chem. Phys.* **102**, 5077.
Román F.L., White J.A. and Velasco S. (1996): *Physica* (in press).
Román F.L., White J.A. and Velasco S. (1997): *J. Chem. Phys.* (submitted).

Resonance Phenomena Induced by Correlated Parametric Noise

J.L. Cabrera, J. Gorroñogoitia, and F.J. de la Rubia

Departamento de Física Fundamental, U.N.E.D., Apdo. 60141, 28080 Madrid, España

The phenomenon of stochastic resonance (SR) has been of broad interest in many different fields and has been observed experimentally in different areas going from physics to biology. Standard SR is the result of the co-operative effect of noise and a periodic driving force acting upon a bistable system, in which the response of the system is enhanced for a particular value of the noise strength. Recently it has been proved numerically that SR can also occur in the absence of an external periodic force as a consequence of the intrinsic dynamics of the nonlinear system. In this work we study the free external force discrete system $X_{n+1} = p_n X_n (1 - X_{n-1})$ where the control parameter is subject to a parametric noise $p_n = p + \zeta_n$ being ζ_n an Ornstein-Uhlenbeck process with zero mean and exponential correlation, τ . In the vicinity of a Hopf bifurcation ($p > p_H$) the system shows an stochastic resonancelike SNR response, but this appears as a function of τ instead of the usually considered noise intensity, σ . There is a particular correlation time, τ_r , for which the signal to noise ratio (SNR) shows a maximum. It is observed that for τ_r the frequency of the system's time series is as similar as possible to the corresponding deterministic frequency ($\omega_d(p)$). This noise induced stochastic enhancement is observed when p is close to the bifurcation value and is not obtained when the SNR response is studied as a function of σ . This resonant behavior is qualitatively understood as determined by the time of permanence of the system around the limit cycle which imposes a compromise between τ and the deterministic convergence time to the stable oscillatory state. Our results show that there is a particular τ for which this coherence is optimized, indicating that the system selects in mean a particular orbit. This idea is reinforced by the results obtained for $p > p_H$ in which τ_r appear shifted towards smaller values as also happens with the deterministic convergence time. We think that this behavior could be observed in other systems where a multiplicative colored random perturbation moves the control parameter through a Hopf bifurcation region. Preliminary results indicate the same kind of resonant response in other nonlinear discrete systems.

References

- Moss F., Bulsara A. and Shlesinger F. (1993): *Proceedings of the NATO Advanced Workshop on Stochastic Resonance in Physics and Biology*, J. Stat. Phys. **70**.
Gang H., Ditzinger T., Ning C. Z. and Haken H. (1993): Stochastic Resonance without External Periodic Force, Phys. Rev. Lett. **71**, 807-810.

Magnetic Relaxation via Competing Dynamics

J.A. Vacas and J. Marro

Instituto Carlos I de Física Teórica y Computacional, Facultad de Ciencias, Universidad de Granada, Spain

We study the magnetic relaxation of a system of finite identical non-interacting particles after a small applied magnetic field is reversed. We consider a "particle" consisting of N Ising spins, $\sigma_i = \pm 1$ at the sites of a square lattice with free boundaries. All the particles are in a completely ordered state at the beginning. When the magnetic field is reversed, the system is in a metastable state and the demagnetization starts due to the *superposition of two processes*: with probability p , there is a random spin-flip; with probability $1 - p$ we perform the flip according to the Metropolis' rule at a temperature T . The preliminary results show that the demagnetization at low temperatures could occurs via avalanches for any $p \neq 0$. The distribution of the sizes of this avalanches seems to follow a power law. The demagnetization shows, in a certain range, a lineal behavior with $\ln(t)$, defining a slope ν for each T . The value of ν becomes constant below a certain T_Q . This T -independent behavior has been reported before in experimental measurements from the demagnetization of real magnetic particles, associated to the quantum tunneling of magnetic vectors between two minima, in quantum coherence phenomena.

References

- Tejada J., Zhang X.X. and Balcells L. (1993): J. Appl. Phys. **73**, 6709.
Chudnovsky E.M. (1994): Phys. Rev. Lett. **72**, 3433.
Marro J. and Vacas J.A. (1997): submitted to Euro. Phys. Lett.

Atomic Dynamics in Liquid Alkali Metals. A Theoretical Study

J. Casas, L.E. González, and D.J. González

Departamento de Física Teórica, Universidad de Valladolid, 47011 Valladolid, España

This paper reports a theoretical study on some dynamical properties of the liquid alkali metals at thermodynamic conditions near their triple point. It is shown that by resorting to simple mode-coupling concepts it is possible to obtain, within a self-consistent approach, a good description for the dynamics of the motion of single particles.

Basically, we focus on the velocity autocorrelation function (VACF), $Z(t)$, of a tagged particle, along with the diffusion coefficient D . The VACF is determined by its associated memory function, $K(t)$, through the generalized Langevin equation (Hansen & McDonal 1986), $\tilde{Z}(z) = \{z + [\tilde{K}_B(z) + \tilde{K}_{MC}(z)]\}^{-1}$, where $\tilde{Z}(z)$ is the Laplace transform of $Z(t)$ and the memory function is split into a binary part, $K_B(t)$, which represents all the fast decay channels and a mode-coupling part, $K_{MC}(t)$, which incorporates the contribution from the collective processes associated with multiple collisions. Within a self-consistent scheme developed by the authors (Gonzalez *et al.* 1996), $K(t)$ can be evaluated from the knowledge of the equilibrium static properties of the liquid metal. In this work we have used a neutral pseudo atom method (Gonzalez *et al.* 1993) to obtain the interatomic pair potential and a variational modified hypernetted chain theory of liquids (Gonzalez *et al.* 1992) to obtain the liquid static structure. This combination results into a theoretical scheme in which the only input data needed for the calculation of the dynamic properties are the atomic number of the system and its thermodynamic state. Once $Z(t)$ has been evaluated, the diffusion coefficient is readily obtained by a straightforward integration (Hansen & McDonal 1986). Among the results obtained we mention the theoretical values for D ($\text{\AA}^2/\text{ps}$): 0.726(Li), 0.53(Na), 0.47(K), 0.32(Rb) and 0.23(Cs), which show a nice agreement with the experimental ones (0.69, 0.44, 0.37, 0.26 and 0.22 respectively). Moreover, it is found that the theoretical VACFs show a universal form when they are properly scaled.

References

- Hansen J.P. and McDonald I.R. (1986): *Theory of Simple Liquids* (Academic, London).
- Gonzalez L.E., Gonzalez D.J. and Canales M. (1996): Z. Phys. B **100**, 601.
- Gonzalez L.E., Gonzalez D.J., Silbert M. and Alonso J.A. (1993): J. Phys: Cond. Matter **5**, 4283.

Gonzalez L.E., Gonzalez D.J. and Silbert M. (1992): Phys. Rev. A **45**, 3803.

Electronic Structure of Delta-Doped Quantum Well as a Function of Temperature

L.M. Gaggero-Sager¹ and R. Pérez-Alvarez²

¹ Departamento de Física de los Materiales, U. N. E. D., Senda del Rey s/n, 28040 Madrid, España

² Facultad de Física, Universidad de La Habana. Ciudad Habana 10400, Cuba

Modern semiconductor growth techniques have provided great possibilities to create thin doping layers with a thickness of a few atomic layers (δ doping). The localization of ionized dopants in a δ -doped layer creates a strong electric field, which in turn results in the energy band bending, and forms a δ -doped quantum well. Up to now, the effect of temperature on the electronic structure in these systems has not been studied. In principle there is a reason to neglect temperature effects when $k_B T$ is small compared to the relevant energies of the well. We question such issue.

We work as in Gaggero-Sager & Pérez-Alvarez 1996 in a two band approximation (heavy hole (hh) and light hole (lh)) and we consider them as independent and isotropic in a Hartree approximation. If p_{2D} is the bidimensional impurity concentration, ρ_e is the free charge density in the well region, $F_i^j(z)$ is the z dependent envelope function, E_F is the Fermi level, j labels the bands ($j = 1$ for the hh band and $j = 2$ for the lh band). E_i^j is the i -th energy level of j -th band, and n_j is the occupation number for the j -th band. Charge neutrality requires, $e p_{2D} = - \int_{-\infty}^{\infty} \rho_e(\chi) d\chi$, and the Fermi level is given implicitly by:

$$e p_{2D} = \sum_{j=1}^2 \frac{em_j^* k_B T}{\pi \hbar^2} \sum_{i=1}^{n_j} \ln \left[1 + \exp \left(\frac{E_F - E_i^j}{k_B T} \right) \right] . \quad (1)$$

For non vanishing temperatures in principle all levels are occupied. Nevertheless, if the system is locally neutral, then the continuous part of the spectrum may be considered empty.

We have made a selfconsistent calculation of a δ -doped quantum well taking into account the temperature effects in the statistical distribution of charge Gaggero-Sager & Pérez-Alvarez 1997. We concluded that: i) when temperature is less than 60 K, its effect could be negligible; ii) when T takes values over 80 K, its effect is essential to describe the structure of the levels; iii) temperature is completely irrelevant to describe the charge concentration of the first levels.

Levels	$T = 0K$	$T \approx 300K$	p_i^j/p_{2D}	$T = 0K$	$T \approx 300K$
E_0^{hh}	274.3	343.8	p_0^{hh}/p_{2D}	0.6595	0.6540
E_1^{hh}	64.2	127.2	p_1^{hh}/p_{2D}	0.1532	0.1368
E_2^{hh}	16.1	67.9	p_2^{hh}/p_{2D}	0.0364	0.0344
E_3^{hh}	1.2	34.8	p_3^{hh}/p_{2D}	0.0006	0.0108
E_4^{hh}		18.9	p_4^{hh}/p_{2D}		0.0058
E_5^{hh}		7.8	p_5^{hh}/p_{2D}		0.0037
E_6^{hh}		2.4	p_6^{hh}/p_{2D}		0.0030
E_0^{lh}	197.1	264.6	p_0^{lh}/p_{2D}	0.1456	0.1424
E_1^{lh}	7.0	52.0	p_1^{lh}/p_{2D}	0.0045	0.0062
E_2^{lh}		19.6	p_2^{lh}/p_{2D}		0.0018
E_3^{lh}		2.6	p_3^{lh}/p_{2D}		0.0009
E_F	1.0	73.0			
$V(0)$	533.0	605.1			

Table 1. Energy levels, Fermi level, depth of the well and the relative occupation (p_i^j/p_{2D}) for δ -doped QW of B in Si ($p_{2D} = 9 \times 10^{13} \text{ cm}^{-2}$). The energies are given in meV.

References

- Gaggero-Sager L.M. and Pérez-Alvarez R. (1996): Phys. Stat. Sol.(B) **197**, 105.
 Gaggero-Sager L.M. and Pérez-Alvarez R. (1997): to appear in Appl. Phys. Lett. **70**.

Neural Networks with Fluctuating Synapses

J.J. Torres, P.L. Garrido, and J. Marro

Instituto Carlos I de Física Teórica y Computacional, Facultad de Ciencias, Universidad de Granada, E-18071- Granada, España

The Hopfield-like models for associative memory [1, 2] consist of a set of N binary *neurons*, $s_{\mathbf{x}} = \pm 1$, whose activity state evolves with time by some either deterministic or stochastic process. The neurons interact with each other according to the Hebb's rule $J_{xy} = N^{-1} \sum_{\mu=1}^P \xi_x^\mu \xi_y^\mu$, for instance, where $\{\xi_x^\mu = \pm 1; \mathbf{x} \in \Lambda_d\} \equiv \xi^\mu$ represent $\mu = 1, \dots, P$ *memorized* patterns. This is assumed to represent the case in which the intensities J_{xy} have been fixed in a previous learning process, independent from the process in which the neurons evolve with time. Motivated by the situation in biology systems, we argue that neglecting time variations of the synapses further than those during the learning process is not realistic. We report on a neural-network model that, in addition to learning *plasticity*, involves relatively fast local fluctuations of the synapse intensities, which vary randomly with time in such a way that its average over the characteristic time for the evolution of the neurons has the value corresponding to the involved learning rule [3]. The influence on emergent properties of such fluctuations happens to be interesting. For specific distributions for the fluctuations we obtain some exact results, namely, effective Hamiltonians for both symmetric or asymmetric couplings. We use the replica trick formalism to obtain explicit results from these effective Hamiltonians. The most general description is provided by a kinetic mean-field approach, which reveals a varied behavior. We show explicitly that allowing for fluctuations amounts to introduce an extra noise that significantly affects the property of associative memory. In particular, the occurrence of the spin-glass phase at finite temperature is substantially restricted in the model, and it does not appear at zero temperature above a critical value for the number of stored patterns. On the other hand, this version of the model is not critically affected by the *Almeida-Thouless line* or limit of stability for the replica symmetry solution. We also show that an appropriate choice for the synaptic fluctuation distribution may significantly improve the retrieval process for a finite number of patterns.

References

- Hopfield J. J. (1982): *Neural networks and physical systems with emergent collective computational abilities*, Proc. Natl. Acad. Sci. **79**, 2554–2558.
Peretto P. (1992): *An introduction to the Modeling of Neural Networks* (Cambridge University Press, Cambridge).
Torres J. J., Garrido P. L. and Marro J. (1997): preprint.

Local Field Distribution in Attractor Neural Networks: Effect of the Stimulus

E. Korutcheva¹ and K. Koroutchev²

¹ Departamento de Física Teórica, Universidad Autónoma de Madrid, Canto Blanco, 28049 Madrid, España

² Instituto de Ingeniería del Conocimiento, Universidad Autónoma de Madrid, Canto Blanco, 28049 Madrid, España

We investigate the distribution of the local fields in attractor neural networks using a simple model similar to that studied by Amit and Brunel (1993). This model consists of two layers of neurons: input layer and recurrent layer. The stimulus of the input layer, by means of feed-forward connections, creates receptive fields on the neurons of the recurrent layer. We discuss the dynamic properties and the basins of attraction of the network and propose a procedure to stabilize the system, driving it into a basin of attraction, without introducing explicitly inhibitory subnetwork. We also investigate the effect of the stimulus applied on the attractor network and propose a criterium of learnability of new patterns. The proposed techniques can be applied to more complex topologies of linked recurrent networks and could be used for designing hardware realizations with application to neurocomputers.

References

- Amit A. and Brunel N. (1993): *Adequate input for learning in attractor neural network*, Network **4**, 177.
Korutcheva E. and Koroutchev K. (1996): *On the local-field distribution in attractor neural networks*, Int. J. Mod. Phys. C **7**, 463.

A Field Theoretical Study of a Lattice Gas in Two Planes

F. de los Santos and P.L. Garrido

Instituto Carlos I de Física Teórica y Computacional, Universidad de Granada,
España

Appealing to *universality* the critical exponents of a lattice system can be calculated considering a continuum version easier to deal with. Algebraic manipulations and *renormalization group* arguments enables one to find out such a simpler model. However, this is not a straightforward procedure, in general, and technical problems can arise. In this spirit we have performed a field-theoretic approach to the two-layer lattice gas system with total particle density, ϱ , conserved (Achahbar 1993). Particles can hop from one lattice to the other, but there is no interaction between particles in different planes. The system undergoes a second order Ising like phase transition for $\varrho = 1/2$, and a discontinuous one if $\varrho \neq 1/2$. After a Gaussian transformation of the lattice partition function and a renormalization group discussion of the operators relevance, one gets an $O(M)$ continuous symmetric Lagrangian with an additional term with cubic symmetry, so it possesses two coupling constants which are known functions of the temperature and ϱ . A *one-loop expansion* for the free energy gives us a flow pattern of the couplings constants with four fixed points and runaway trajectories, *i.e.*, trajectories that do not flow to any of the fixed points and which are a reflection of a first order phase transition. In order to match these results with our problem we have to set ϱ and the temperature values as initial conditions for the flow trajectories to find out which critical theory corresponds to our original parameters. We thus find for $\varrho = 1/2$ that the system belongs to the Ising universality class, as expected. If $\varrho \neq 1/2$, there is no trace of a first-order phase transition, but a Heisenberg like continuous transition occurs. This is in disagreement with the exact solution, and some explanation is required. We think the irrelevant operators that were neglected on the basis of renormalization group arguments can produce a shift of the bare parameters. Finally we discuss the use of this formalism to study first-order phase transitions.

References

- Achahbar A. (1993): PhD Thesis. Universidad de Granada
Amit D.J. (1984): *Field Theory, the Renormalization Group, and Critical Phenomena*. World Scientific

A Regularization of the Nonstationary Two-Body Problem Under the Maneff Perturbing Potential

I. Aparicio and L. Floría

Grupo de Mecánica Celeste I, E. T. S. de Ingenieros Industriales, Universidad de Valladolid, Paseo del Cauce s/n, E-47 011 Valladolid, España

Within the framework of classical mechanics, the Maneff model of gravitational potential constitutes a nonrelativistic modification of Newton's gravitational law which can be successfully used to accurately account for the secular motion of the pericentre of some celestial bodies, at least in the Solar System (e.g. the advance of the perihelion of the inner planets, or the motion of the perigee of the Moon.) We are concerned with the two-body problem as contemplated in classical celestial mechanics, and concentrate on the so-called *Gylden systems*, say two-body problems with *variable Keplerian parameter* $\mu(t)$. On such systems, we superimpose perturbing effects emanating from a *Maneff*-type nonrelativistic gravitational potential, and we intend to arrive at regularized equations of motion for the resulting dynamical system.

Mioc & Stoica (1995) discussed regularization of the equations of relative motion of a Kepler problem perturbed by the Maneff potential. After formulation in plane polar coordinates, they solved the regularized equations. Special emphasis was put on the equation for the relative distance.

On the stage of extended-phase-space Hamiltonian mechanics (Stiefel & Scheifele 1971, §30), we consider regularization by combining (weakly) canonical transformations of the redundant dependent variables and reparametrizations of motion in terms of other independent variables instead of time (Stiefel & Scheifele 1971, §34 and 37), so as to create second-order differential equations for the spatial-like variables.

We investigate the reduction of the equations of motion of a *Maneff* two-body problem with a time-dependent Keplerian parameter into the form of second-order differential equations resembling those of a (perturbed) 4-dimensional oscillator. To this end, we consider the framework of linear and regular celestial mechanics (Stiefel & Scheifele 1971). Recently, Deprit *et al.* (1994) have refined the approach to linearizing transformations and put the question in a more rigorous, modern and advanced mathematical context.

Use is made of the (canonical or weakly canonical) transformations studied in Deprit *et al.* (1994, §4) along with reparametrizing transformations introducing new fictitious time variables (of the type of a generalized true-like anomaly.)

References

- Deprit A., Elipe A. and Ferrer S. (1994): *Linearization: Laplace vs. Stiefel*, Celest. Mech. **58**, 151-201.
- Mioc V. and Stoica C. (1995): *Discussion et résolution complète du problème des deux corps dans le champ gravitationnel de Maneff (I et II)*, C. R. Acad. Sci. Paris, Sér. I, **320**, 645-648; **321**, 961-964.
- Stiefel E.L. and Scheifele G. (1971): *Linear and Regular Celestial Mechanics* (Springer, Berlin, Heidelberg, New York).

Pattern Formation in Catalytic Processes: Phase–Field Model

M.N. Kuperman¹, A.S. Mikhailov², and H.S. Wio¹

¹ Centro Atómico Bariloche (C.N.E.A.) and Instituto Balseiro (U.N.C.) 8400 - San Carlos de Bariloche, Rio Negro, Argentina

² Fritz-Haber Institut, M.P.G., Faradayweg 6, Berlin, Germany.

We present a first step towards the modeling of adsorption and desorption of CO in empty sites during its catalytic oxidation on a Pt monocrystalline surface ($2 \text{ CO} + \text{O}_2 \rightarrow 2 \text{ CO}_2$). After a diffusion process on the Pt surface, the CO and O reacts at the moment of their encounter in the same site. The crystalline structure of the surface suffers a phase transition that governs the dynamics of the problem, turning from a cubic 2-D lattice, when occupied by CO to an hexagonal one after desorption.

In this work we consider the simplest situation of only one *adsorbate*, with a lateral attractive interaction whose concentration is described by a scalar field, that is coupled to the phase transition process occurring on the surface. We model in a phenomenological way the processes associated with this scalar field that corresponds to:

- adsorption,
- desorption, including a local bounding associated to the lateral interaction,
- diffusion,
- a flux induced by the lateral interaction,
- reaction (modeled as a simple annihilation process).

Together with these aspects, we must also consider those related with the phase transition on the surface. This phenomenon, that must be dynamically coupled to the scalar field, is described using a Ginzburg-Landau functional for an order parameter associated to the phase on the surface. This coupled system resembles an activator-inhibitor one, but have additional characteristics associated to the flux induced by the lateral interaction.

We have established the phenomenological constraints that allows the existence of “bubbles” with a high density of the adsorbate, immersed in an extended low density region. These conjectures have been tested, solving numerically the coupled set of equations for the density and the order parameter. The adopted numerical scheme was based in a path integral procedure that allows to transform the original set of partial differential equations into a set of selfconsistent integral equations. The same procedure was exploited to analyze the propagation of fronts and test the analytical results obtained via a singular perturbation approach.

Subject Index

- 1/f noise 274
- absorbing state 223, 226, 245
- activator-inhibitor system 174, 181, 192
- active phase 224
- adiabatic elimination 144, 153
- adiabatic regime 27, 48, 50
- adsorption model 295
- albedo boundary condition 165
- algorithm 93
- Amdahl's law 69, 79
- anomalous scaling 262
- Arrhenius law 159
- artificial intelligence 57, 79
- associative memory 197
- asymptotically stable 141
- attractor 138, 202
- autocatalytic chemical reaction 255, 260
- autonomous system 137
- avalanches 299
- axon 198
- Büsse balloon 168
- Bénard's convection 125
- Bak-Sneppen evolution model 287
- balance equations 111–113
- ballast resistor 169, 172, 180
- basin of attraction 141
- BBGKY hierarchy 110
- Belousov-Zhabotinskii reaction 175
- BGK equation
- exact normal solution 115
- bifurcation 142
- binary transfer function 199
- binding energy 7
- blackboard hints 69, 74, 76
- Bloch condition 6
- Bloch states 7, 9, 11, 13–15, 48
- Bloch superposition 7
- Boltzmann's equation 83, 103
- Grad's solution 106
- Boltzmann-Grad limit 83
- brain 197
- branching annihilating random walk 254
- Brownian motion 152
- CBT
- see *complete binary tree* 91
- chaotic RG flows 239
- Chapman-Enskog method 84
- Chapman-Kolmogorov equation 151
- clustering and migration 271
- coherent state product 12
- collective motion of living individuals 271
- collision frequency 100
- collision rate 100
- collisional transport 94
- committee of agents 69
- complete binary tree 91
- complex systems 163
- computational ecology 55
- computer science 57
- computer simulation
- strategy 88
- conservative system 138
- constitutive equations 85, 112
- constraint satisfaction problems 68
- contact process 227, 277
- long range interactions 278
- control parameters 137
- cooperation 55, 56, 68, 77, 79, 80, 271
- cooperative search 79

- chess 57
- heuristics 58
- hints 58–60
- performance 61
- pruning effectiveness 59
- robot navigation 58
- correlations 96, 97
- Couette flow 114, 115
- CPLRI
 - see contact process: long range interactions 278
- critical exponent 239, 266, 279
- crossing a cell wall 90
- cryptarithmetic 68, 78
- damped anharmonic oscillator 144
- Davidov Ansatz state 42
- Debye-Waller factor 16
- delocalized framework 11, 13, 50
- delocalized state 12
- delta rule 199
- demagnetization 299
- density
 - measure of 94
- diffusion in a field 154
- dimer reaction model 253
- dimer-dimer model 246
- directed percolation 225, 227, 234, 279, 287
- displaced oscillator transformation 7
- dissipative structures 149, 163
- dissipative system 138
- distribution
 - lognormal 56, 80
 - of finishing times 71
 - of national income 56
 - of performance 56
- diversity 56, 77
- of methods 79
- DNLS
 - see *nonlinear Schrödinger equation, discrete* 42
- DP
 - see *directed percolation* 225
- DP critical point 240
- DP universality class 229, 243, 250, 256
- dripping-water model 225, 226
- dynamical flow
 - classification 148
 - dynamical system
 - effect of noise 178
 - dynamics of solitons 44
- Eckhaus instability 168
- effective conductivity 125, 126, 129, 132
- effectiveness of a heuristic 66
- effectiveness of cooperation 78
- effectiveness of hints 72
- electronic structure
 - effect of temperature on 302
- energy density 111
- Enskog's equation 83, 104
- epidemic analysis 279
- ergodic theorem 216
- Euler's hydrodynamics 85
- event driven 89, 90
- exact results 6
 - numerical computation of 19
- excitable medium 163
- exciton 3
 - amplitude 23, 33, 46
 - nonlocal couplings 4
 - wave vectors 5
- exciton-phonon interaction 50
- expert system 57
- extremum principle 135
- FEL
 - see *future event list* 91
- Fermi golden rule 152
- finite size effects 131, 283
- fire through a forest 223
- first passage times 159
- fixed point 138, 139
- flocking behavior 273
- fluctuation-dissipation theorem 260
- fluctuations 136
 - quantum 135
 - stochastic 136
 - thermal 136
- fluid model 87
- flux 94
 - measure of 94
- flux vector 94, 101, 102, 112
- Fokker-Planck equation 155, 157, 261
- Fourier's law 96, 102

- Franck-Condon factor 17
 free energy 217
 free-energy functional 231
 – Ginzburg-Landau-Wilson 230, 232
 free-exciton energy band 10, 38, 39
 free-exciton limit 8
 free-phonon limit 8
 friction coefficient 153
 front propagation 283
 front wave 173
 future event list 91
- gas with strain flow 114
 genetic algorithm 57
 Gibbs measure 213
 Ginzburg-Landau model 289
 GL
 – see *global-local method* 16
 GL Ansatz state 16
 global correlations 15
 global stability 146, 179
 global-local method 16, 24, 40, 48
 Graham's potential 179
 Grassberger conjecture 228
 Green-Kubo formulas 114
 Green-Kubo method 114
 growth models with stochastic bulk dynamics 293
- Hamming distance 204
 hard disk 95, 116
 – equation of state 95
 hard rods 96
 hard self-excitation 144
 heat flux 121
 Heaviside function 199
 Hebbian rule 199
 heterogeneous catalysis 228, 246
 hierarchical search 62
 hints 70
 Holstein Hamiltonian 4
 Hopf bifurcation 144, 298
 Hopfield dynamics 205
 – fixed points 203
 Hopfield model 197, 201, 208
 – energy function 204
 – positive temperature dynamics 212
 – temperature zero dynamics 215
 Hopfield network 304
- hot-spot model 169
 hydrodynamic equations 112
 hydrodynamic velocity 98
 hydrodynamics 83, 291
- integrated flux 94
 interacting particle systems 277
 interesting event 94
 invariant manifolds 138
 IPT
 – see *irreversible phase transitions* 277
 irreversible phase transitions 277
 Ising model 213, 244
 Ising models with competing dynamics 254
- kinetic theory 83
 kinetic transport 94
 Kosterlitz-Thouless phase 239, 261
 KPZ equation 232, 260, 263, 264
 Kramers' formula 159
 Kramers-Moyal expansion 154
 Kubo function 46
- Lagrangian 185
 Langevin equation 153, 225, 229, 232, 235, 254, 255
 – additive Gaussian noise 231
 Langevin force 153
 Langmuir-Hinshelwood mechanism 278
 large polaron regime 28, 33
 large polaron state 13
 leafnode 91
 learning rules 199
 limit cycle 141
 linear stability theory 139
 Liouville equation 138
 Lipschitz conditions 139
 liquid alkali metals 300
 local correlations 15
 local equilibrium 83
 local minimum event 91
 localized framework 10, 13, 50
 localized state 10
 logical threshold elements 199
 lognormal distribution 60
 Lyapunov function 146, 148, 178

- Lévy flight 278
- Maneff model 307
- MAPPLE 118
- marginally stable 141
- Markov chain 215
- markovian processes 150
- master equation 152, 154
- mathematical neurons 199
- Maxwell's distribution 84, 98
- MD
- see *molecular dynamics* 85
- mean free path 100
- mean-field theory 62
- Merrifield Ansatz state 16
- Merrifield method 12, 24, 29, 40, 48
- mesoscopic description of a fluid 291
- metastable state 299
- MN
- see *multiplicative noise* 255
- model of screened ions and electrons 106
- molecular dynamics 85, 86
- momenta of distribution 98
- momentum balance equation 126
- monomer-dimer model 254
- moving interfaces 232
- multicritical fixed points 260
- multilayer configurations 200
- multiple absorbing states 246, 251, 252
- multiplicative noise 255, 257, 259, 264
- Navier-Stokes equations 85
- numerical solutions 129
- neighborhood of a particle 90
- neural network 57, 197, 304, 305
- neurons
- number of 198
- Newton's law of viscous flow 102
- NLS
- see *nonlinear Schrödinger equation, continuous* 42
- non-adiabatic limit 7
- non-adiabatic regime 9, 26, 48, 50
- nonequilibrium critical phenomena 224
- nonequilibrium potential 155, 179, 182, 185, 187, 188, 191
- nonequilibrium steady states 304
- nonequilibrium systems 225
- nonlinear Schrödinger equation
- continuous 42
 - discrete 42
- nonlocality 250
- nonrelaxational flow 178
- nonuniversality 253, 254
- normal modes 140
- numerical convergence 21
- one-exciton state 15
- one-phonon band 10
- optimal polaron states 4
- Ornstein-Uhlenbeck process 155
- overlap parameter 212
- pair contact process 247
- parallel computers 197
- pattern formation 135, 309
- pattern recognition 197
- peculiar velocity 98
- perceptron model 200
- performance 93
- phase space 137
- phase transition
- in overall agent performance 63
 - in tree searches 64
- phonon displacement 23, 33
- phonon wave vectors 5
- poisoned state 228
- polaron band 10, 11, 18, 39
- polaron effective mass 40
- polaron energy band 39
- variational estimate 6
- polaron Hamiltonian 41
- polaron problem 3, 47
- polaron state 18
- polaron structure 6, 14
- polaron Wannier states 47, 51
- populaton dynamics 272
- porosity 289
- propagator-inhibitor system 176
- quality of recognition 212
- quantum tunneling 299
- radial distribution function 95

- random sequential adsorption process 297
- RD
 - see *reaction-diffusion* 135
- reaction-diffusion 135
- reaction-diffusion model 164, 180, 228, 255
- Reggeon field theory 229, 287
- relaxation techniques 19
- relaxational flow 178
- relaxational gradient flow 147
- renormalization group 224
- replica trick 211
- reversible computation 20
- Reynolds number 118
- RG
 - see *renormalization group* 224
- RG fixed points 239, 240
- RG flow 258
- RG transformation 237, 238, 241
- roughness exponent 233
- round-off errors 21
- saddle point 140
- satisficing search 65, 67
- scaling relation 244, 245, 251, 279
- Schlögl model 165, 170, 227
- scientific productivity 56
- SDE
 - see *stochastic differential equation* 150
- second neighbor reaction model 254
- self-organization phenomena 163, 271
- self-organized criticality 274
- self-trapping transition 19, 30, 31, 37, 49
- separatrices 141
- shear viscosity 113
- signal-to-noise ratio 162
- singular points 138
- small polaron energy band 38
- small polaron regime 22, 26, 33, 48
- small polaron state 7, 12, 20
- SNR
 - see *signal-to-noise ratio* 160
- SOC
 - see *self-organized criticality* 274
- soft self-excitation 144
- solitary waves 172
- soliton theory 42, 43, 50
- solitons 42
- spatio-temporal patterns 149, 274
- specific heat 96
- spin glass 200, 214
- spiral 176
- spread of colonies 275
- spread of epidemics 223, 227
- spread of population 272
- SR
 - see *stochastic resonance* 160
- SS
 - see *stationary state* 273
- stable focus 140
- stable node 140
- stochastic differential equation 150
- stochastic dynamics 214
- stochastic equilibrium system 224
- stochastic process 149, 153
- stochastic resonance 160, 187, 298
- stochastic stirring force 294
- strong coupling region 23
- subcritical bifurcation 144
- super-linear speed-up 69, 77
- supercritical bifurcation 144
- susceptibility 262, 266
- symmetry 234
- symmetry breaking 146
- synapses 198
- temperature field 98
- thermal conductivity 102, 113, 124, 125, 132
- thermal diffusion 96
- thermal expansion coefficient 96
- thermal slip 107
- thermal velocity 100
- thermodynamic branch 142
- time-dependent Ginzburg-Landau equation 232
- total crystal momentum 5
- Toyozawa method 14, 16, 24, 40, 48
- transition
 - from exponential to polynomial time 56
- transport coefficients
 - size independent 114
- traveling salesman problem 65
- travelling waves 173

- turbulence 262
 - Turing instability 168
 - two-layer lattice gas: field theory 306
 - universality 56, 242, 280
 - universality class 224, 225, 231, 282
 - upper critical dimension 235, 240, 257
 - vapor-liquid coexistence in gels 289
 - variational calculation 48
 - variational principle 10
 - Verlet's algorithm 93
 - virial coefficients 95
 - viscosity 102, 123
 - wall effects 87
 - weak coupling limit 8
 - weak coupling regime 26
 - white noise 153
 - Wiener process 156
 - Wiener-Khinchin theorem 162
- ZGB
– see *Ziff-Gulari-Barshad model* 228
- Ziff-Gulari-Barshad model 228, 229,
278
- zig-zag instability 168

Springer and the environment

At Springer we firmly believe that an international science publisher has a special obligation to the environment, and our corporate policies consistently reflect this conviction.

We also expect our business partners – paper mills, printers, packaging manufacturers, etc. – to commit themselves to using materials and production processes that do not harm the environment. The paper in this book is made from low- or no-chlorine pulp and is acid free, in conformance with international standards for paper permanency.



Springer

Lecture Notes in Physics

For information about Vols. 1–455
please contact your bookseller or Springer-Verlag

- Vol. 456: H. B. Geyer (Ed.), Field Theory, Topology and Condensed Matter Physics. Proceedings, 1994. XII, 206 pages. 1995.
- Vol. 457: P. Garbaczewski, M. Wolf, A. Weron (Eds.), Chaos – The Interplay Between Stochastic and Deterministic Behaviour. Proceedings, 1995. XII, 573 pages. 1995.
- Vol. 458: I. W. Roxburgh, J.-L. Masnou (Eds.), Physical Processes in Astrophysics. Proceedings, 1993. XII, 249 pages. 1995.
- Vol. 459: G. Winnewisser, G. C. Pelz (Eds.), The Physics and Chemistry of Interstellar Molecular Clouds. Proceedings, 1993. XV, 393 pages. 1995.
- Vol. 460: S. Cotsakis, G. W. Gibbons (Eds.), Global Structure and Evolution in General Relativity. Proceedings, 1994. IX, 173 pages. 1996.
- Vol. 461: R. López-Peña, R. Capovilla, R. Garcí'a-Pelayo, H. Waelbroeck, F. Zertuche (Eds.), Complex Systems and Binary Networks. Lectures, México 1995. X, 223 pages. 1995.
- Vol. 462: M. Meneguzzi, A. Pouquet, P.-L. Sulem (Eds.), Small-Scale Structures in Three-Dimensional Hydrodynamic and Magnetohydrodynamic Turbulence. Proceedings, 1995. IX, 421 pages. 1995.
- Vol. 463: H. Hippelein, K. Meisenheimer, H.-J. Röser (Eds.), Galaxies in the Young Universe. Proceedings, 1994. XV, 314 pages. 1995.
- Vol. 464: L. Ratke, H. U. Walter, B. Feuerbach (Eds.), Materials and Fluids Under Low Gravity. Proceedings, 1994. XVIII, 424 pages. 1996.
- Vol. 465: S. Beckwith, J. Staude, A. Quetz, A. Natta (Eds.), Disks and Outflows Around Young Stars. Proceedings, 1994. XII, 361 pages. 1996.
- Vol. 466: H. Ebert, G. Schütz (Eds.), Spin – Orbit-Influenced Spectroscopies of Magnetic Solids. Proceedings, 1995. VII, 287 pages. 1996.
- Vol. 467: A. Steinchen (Ed.), Dynamics of Multiphase Flows Across Interfaces. 1994/1995. XII, 267 pages. 1996.
- Vol. 468: C. Chiuderi, G. Einaudi (Eds.), Plasma Astrophysics. 1994. VII, 326 pages. 1996.
- Vol. 469: H. Grosse, L. Pittner (Eds.), Low-Dimensional Models in Statistical Physics and Quantum Field Theory. Proceedings, 1995. XVII, 339 pages. 1996.
- Vol. 470: E. Martínez-González, J. L. Sanz (Eds.), The Universe at High-z, Large-Scale Structure and the Cosmic Microwave Background. Proceedings, 1995. VIII, 254 pages. 1996.
- Vol. 471: W. Kundt (Ed.), Jets from Stars and Galactic Nuclei. Proceedings, 1995. X, 290 pages. 1996.
- Vol. 472: J. Greiner (Ed.), Supersoft X-Ray Sources. Proceedings, 1996. XIII, 350 pages. 1996.
- Vol. 473: P. Weingartner, G. Schurz (Eds.), Law and Prediction in the Light of Chaos Research. X, 291 pages. 1996.
- Vol. 474: Aa. Sandqvist, P. O. Lindblad (Eds.), Barred Galaxies and Circumnuclear Activity. Proceedings of the Nobel Symposium 98, 1995. XI, 306 pages. 1996.
- Vol. 475: J. Klamut, B. W. Veal, B. M. Dabrowski, P. W. Klamut, M. Kazimierski (Eds.), Recent Developments in High Temperature Superconductivity. Proceedings, 1995. XIII, 362 pages. 1996.
- Vol. 476: J. Parisi, S. C. Müller, W. Zimmermann (Eds.), Nonlinear Physics of Complex Systems. Current Status and Future Trends. XIII, 388 pages. 1996.
- Vol. 477: Z. Petru, J. Przystawa, K. Rapcewicz (Eds.), From Quantum Mechanics to Technology. Proceedings, 1996. IX, 379 pages. 1996.
- Vol. 479: H. Latal, W. Schweiger (Eds.), Perturbative and Nonperturbative Aspects of Quantum Field Theory. Proceedings, 1996. X, 430 pages. 1997.
- Vol. 480: H. Flyvbjerg, J. Hertz, M. H. Jensen, O. G. Mouritsen, K. Sneppen (Eds.), Physics of Biological Systems. From Molecules to Species. X, 364 pages. 1997.
- Vol. 481: F. Lenz, H. Grießhammer, D. Stoll (Eds.), Lectures on QCD. VII, 276 pages. 1997.
- Vol. 482: X.-W. Pan, D. H. Feng, M. Vallières (Eds.), Contemporary Nuclear Shell Models. Proceedings, 1996. XII, 309 pages. 1997.
- Vol. 483: G. Trottet (Ed.), Coronal Physics from Radio and Space Observations. XVII, 226 pages. 1997.
- Vol. 484: L. Schimansky-Geier, T. Pöschel (Eds.), Stochastic Dynamics. XVIII, 386 pages. 1997.
- Vol. 485: H. Friedrich, B. Eckhardt (Eds.), Classical, Semi-classical and Quantum Dynamics in Atoms. VIII, 341 pages. 1997.
- Vol. 486: G. Chavent, P. C. Sabatier (Eds.), Inverse Problems of Wave Propagation and Diffraction. XV, 379 pages. 1997.
- Vol. 487: E. Meyer-Hofmeister, H. Spruijk (Eds.), Accretion Disks – New Aspects. XIII, 356 pages, 1997.
- Vol. 488: B. Apagyi, G. Endrédi, P. Lévay (Eds.), Inverse and Algebraic Quantum Scattering Theory. XV, 385 pages. 1997.
- Vol. 489: G. M. Simnett, C. E. Alissandrakis, L. Vlahos (Eds.), Solar and Heliospheric Plasma Physics. VIII, 278 pages, 1997.
- Vol. 491: O. Boratav, A. Eden, A. Erzan (Eds.), Turbulence Modeling and Vortex Dynamics. XII, 245 pages, 1997.
- Vol. 493: P. L. Garrido, J. Marro (Eds.), Fourth Granada Lectures in Computational Physics. XIV, 316 pages. 1997.

New Series m: Monographs

- Vol. m 1: H. Hora, *Plasmas at High Temperature and Density*. VIII, 442 pages. 1991.
- Vol. m 2: P. Busch, P. J. Lahti, P. Mittelstaedt, *The Quantum Theory of Measurement*. XIII, 165 pages. 1991. Second Revised Edition: XIII, 181 pages. 1996.
- Vol. m 3: A. Heck, J. M. Perdang (Eds.), *Applying Fractals in Astronomy*. IX, 210 pages. 1991.
- Vol. m 4: R. K. Zeytounian, *Mécanique des fluides fondamentale*. XV, 615 pages. 1991.
- Vol. m 5: R. K. Zeytounian, *Meteorological Fluid Dynamics*. XI, 346 pages. 1991.
- Vol. m 6: N. M. J. Woodhouse, *Special Relativity*. VIII, 86 pages. 1992.
- Vol. m 7: G. Morandi, *The Role of Topology in Classical and Quantum Physics*. XIII, 239 pages. 1992.
- Vol. m 8: D. Funaro, *Polynomial Approximation of Differential Equations*. X, 305 pages. 1992.
- Vol. m 9: M. Namiki, *Stochastic Quantization*. X, 217 pages. 1992.
- Vol. m 10: J. Hoppe, *Lectures on Integrable Systems*. VII, 111 pages. 1992.
- Vol. m 11: A. D. Yaghjian, *Relativistic Dynamics of a Charged Sphere*. XII, 115 pages. 1992.
- Vol. m 12: G. Esposito, *Quantum Gravity, Quantum Cosmology and Lorentzian Geometries*. Second Corrected and Enlarged Edition. XVIII, 349 pages. 1994.
- Vol. m 13: M. Klein, A. Knauf, *Classical Planar Scattering by Coulombic Potentials*. V, 142 pages. 1992.
- Vol. m 14: A. Lerda, Anyons. XI, 138 pages. 1992.
- Vol. m 15: N. Peters, B. Rogg (Eds.), *Reduced Kinetic Mechanisms for Applications in Combustion Systems*. X, 360 pages. 1993.
- Vol. m 16: P. Christe, M. Henkel, *Introduction to Conformal Invariance and Its Applications to Critical Phenomena*. XV, 260 pages. 1993.
- Vol. m 17: M. Schoen, *Computer Simulation of Condensed Phases in Complex Geometries*. X, 136 pages. 1993.
- Vol. m 18: H. Carmichael, *An Open Systems Approach to Quantum Optics*. X, 179 pages. 1993.
- Vol. m 19: S. D. Bogan, M. K. Hinders, *Interface Effects in Elastic Wave Scattering*. XII, 182 pages. 1994.
- Vol. m 20: E. Abdalla, M. C. B. Abdalla, D. Dalmazi, A. Zadra, *2D-Gravity in Non-Critical Strings*. IX, 319 pages. 1994.
- Vol. m 21: G. P. Berman, E. N. Bulgakov, D. D. Holm, *Crossover-Time in Quantum Boson and Spin Systems*. XI, 268 pages. 1994.
- Vol. m 22: M.-O. Hongler, *Chaotic and Stochastic Behaviour in Automatic Production Lines*. V, 85 pages. 1994.
- Vol. m 23: V. S. Viswanath, G. Müller, *The Recursion Method*. X, 259 pages. 1994.
- Vol. m 24: A. Ern, V. Giovangigli, *Multicomponent Transport Algorithms*. XIV, 427 pages. 1994.
- Vol. m 25: A. V. Bogdanov, G. V. Dubrovskiy, M. P. Krutikov, D. V. Kulginov, V. M. Strelchenya, *Interaction of Gases with Surfaces*. XIV, 132 pages. 1995.
- Vol. m 26: M. Dineykhan, G. V. Efimov, G. Ganbold, S. N. Nedelko, *Oscillator Representation in Quantum Physics*. IX, 279 pages. 1995.
- Vol. m 27: J. T. Ottesen, *Infinite Dimensional Groups and Algebras in Quantum Physics*. IX, 218 pages. 1995.
- Vol. m 28: O. Piguet, S. P. Sorella, *Algebraic Renormalization*. IX, 134 pages. 1995.
- Vol. m 29: C. Bendjaballah, *Introduction to Photon Communication*. VII, 193 pages. 1995.
- Vol. m 30: A. J. Greer, W. J. Kossler, *Low Magnetic Fields in Anisotropic Superconductors*. VII, 161 pages. 1995.
- Vol. m 31: P. Busch, M. Grabowski, P. J. Lahti, *Operational Quantum Physics*. XI, 230 pages. 1995.
- Vol. m 32: L. de Broglie, *Diverses questions de mécanique et de thermodynamique classiques et relativistes*. XII, 198 pages. 1995.
- Vol. m 33: R. Alkofer, H. Reinhardt, *Chiral Quark Dynamics*. VIII, 115 pages. 1995.
- Vol. m 34: R. Jost, *Das Märchen vom Elfenbeinernen Turm*. VIII, 286 pages. 1995.
- Vol. m 35: E. Elizalde, *Ten Physical Applications of Spectral Zeta Functions*. XIV, 228 pages. 1995.
- Vol. m 36: G. Dunne, *Self-Dual Chern-Simons Theories*. X, 217 pages. 1995.
- Vol. m 37: S. Childress, A.D. Gilbert, Stretch, Twist, Fold: *The Fast Dynamo*. XI, 410 pages. 1995.
- Vol. m 38: J. González, M. A. Martín-Delgado, G. Sierra, A. H. Vozmediano, *Quantum Electron Liquids and High-T_c Superconductivity*. X, 299 pages. 1995.
- Vol. m 39: L. Pittner, *Algebraic Foundations of Non-Commutative Differential Geometry and Quantum Groups*. XII, 469 pages. 1996.
- Vol. m 40: H.-J. Borchers, *Translation Group and Particle Representations in Quantum Field Theory*. VII, 131 pages. 1996.
- Vol. m 41: B. K. Chakrabarti, A. Dutta, P. Sen, *Quantum Ising Phases and Transitions in Transverse Ising Models*. X, 204 pages. 1996.
- Vol. m 42: P. Bouwknegt, J. McCarthy, K. Pilch, *The W-Algebra. Modules, Semi-infinite Cohomology and BV Algebras*. XI, 204 pages. 1996.
- Vol. m 43: M. Schottenloher, *A Mathematical Introduction to Conformal Field Theory*. VIII, 142 pages. 1997.
- Vol. m 44: A. Bach, *Indistinguishable Classical Particles*. VIII, 157 pages. 1997.
- Vol. m 45: M. Ferrari, V. T. Granik, A. Imam, J. C. Nadeau (Eds.), *Advances in Doublet Mechanics*. XVI, 214 pages. 1997.
- Vol. m 46: M. Camenzind, *Les noyaux actifs de galaxies*. XVIII, 218 pages. 1997.
- Vol. m 48: P. Kopietz, *Bosonization of Interacting Fermions in Arbitrary Dimensions*. XII, 259 pages. 1997.
- Vol. m 49: M. Zak, J. B. Zbilut, R. E. Meyers, *From Instability to Intelligence, Complexity and Predictability in Nonlinear Dynamics*. XIV, 552 pages. 1997.